frontiers | Research Topics

Brain patterns of pain processing and non-pharmacological treatments

Edited by
Jin Cao, Jixin Liu, Lei Lan, Lu Liu and Lingmin Jin

Published in
Frontiers in Neurology

ISSN 1664-8714
ISBN 978-2-8325-3311-6
DOI 10.3389/978-2-8325-3311-6

About Frontiers

Frontiers is more than just an open access publisher of scholarly articles: it is a pioneering approach to the world of academia, radically improving the way scholarly research is managed. The grand vision of Frontiers is a world where all people have an equal opportunity to seek, share and generate knowledge. Frontiers provides immediate and permanent online open access to all its publications, but this alone is not enough to realize our grand goals.

Frontiers journal series

The Frontiers journal series is a multi-tier and interdisciplinary set of open-access, online journals, promising a paradigm shift from the current review, selection and dissemination processes in academic publishing. All Frontiers journals are driven by researchers for researchers; therefore, they constitute a service to the scholarly community. At the same time, the *Frontiers journal series* operates on a revolutionary invention, the tiered publishing system, initially addressing specific communities of scholars, and gradually climbing up to broader public understanding, thus serving the interests of the lay society, too.

Dedication to quality

Each Frontiers article is a landmark of the highest quality, thanks to genuinely collaborative interactions between authors and review editors, who include some of the world's best academicians. Research must be certified by peers before entering a stream of knowledge that may eventually reach the public - and shape society; therefore, Frontiers only applies the most rigorous and unbiased reviews. Frontiers revolutionizes research publishing by freely delivering the most outstanding research, evaluated with no bias from both the academic and social point of view. By applying the most advanced information technologies, Frontiers is catapulting scholarly publishing into a new generation.

What are Frontiers Research Topics?

Frontiers Research Topics are very popular trademarks of the *Frontiers journals series*: they are collections of at least ten articles, all centered on a particular subject. With their unique mix of varied contributions from Original Research to Review Articles, Frontiers Research Topics unify the most influential researchers, the latest key findings and historical advances in a hot research area.

Find out more on how to host your own Frontiers Research Topic or contribute to one as an author by contacting the Frontiers editorial office: frontiersin.org/about/contact

Brain patterns of pain processing and non-pharmacological treatments

Topic editors

Jin Cao — Harvard Medical School, United States

Jixin Liu — Xidian University, China

Lei Lan — Chengdu University of Traditional Chinese Medicine, China

Lu Liu — Capital Medical University, China

Lingmin Jin — Guizhou University of Traditional Chinese Medicine, China

Citation

Cao, J., Liu, J., Lan, L., Liu, L., Jin, L., eds. (2023). *Brain patterns of pain processing and non-pharmacological treatments*. Lausanne: Frontiers Media SA.

doi: 10.3389/978-2-8325-3311-6

Table of contents

frontiers in Neurology

ORIGINAL RESEARCH
published: 18 January 2022
doi: 10.3389/fneur.2021.813723

Acupuncture Enhances Dorsal Raphe Functional Connectivity in Knee Osteoarthritis With Chronic Pain

Nan Gao[1†], Haiping Shi[2†], Sheng Hu[1,3], Bixiang Zha[2], Aihong Yuan[2], Jianhua Shu[3], Yinqiu Fan[2], Jin Bai[2], Hongyu Xie[2], Jingcheng Cui[4], Xiaoxiao Wang[1], Chuanfu Li[2], Bensheng Qiu[1] and Jun Yang[2*]*

[1] Center for Biomedical Imaging, University of Science and Technology of China, Hefei, China, [2] First Affiliated Hospital of Anhui University of Traditional Chinese Medicine, Hefei, China, [3] School of Medical Information Engineering, Anhui University of Chinese Medicine, Hefei, China, [4] Third People's Hospital of Hefei, Hefei, China

OPEN ACCESS

Edited by:
Lei Lan,
Chengdu University of Traditional Chinese Medicine, China

Reviewed by:
Liang Kang,
Chengdu Sport University, China
Hantong Hu,
Zhejiang Chinese Medical University, China
Mailan Liu,
Hunan University of Chinese Medicine, China

***Correspondence:**
Jun Yang
yangjunacup@126.com
Bensheng Qiu
bqiu@ustc.edu.cn

[†] These authors have contributed equally to this work and share first authorship

Specialty section:
This article was submitted to Headache and Neurogenic Pain, a section of the journal Frontiers in Neurology

Received: 12 November 2021
Accepted: 02 December 2021
Published: 18 January 2022

Citation:
Gao N, Shi H, Hu S, Zha B, Yuan A, Shu J, Fan Y, Bai J, Xie H, Cui J, Wang X, Li C, Qiu B and Yang J (2022) Acupuncture Enhances Dorsal Raphe Functional Connectivity in Knee Osteoarthritis With Chronic Pain. Front. Neurol. 12:813723. doi: 10.3389/fneur.2021.813723

Introduction: Knee osteoarthritis is a common disease in the elderly. Patients suffer from long-term chronic pain and reduced life quality. Acupuncture has been proven to be an effective treatment for KOA. However, the neural mechanism of acupuncture is unclear, so far. Periaqueductal gray (PAG) and raphe nuclei (RPN) are essential structures associated with chronic pain in human brains. This study aims to investigate functional connectivity (FC) changes of PAG and RPN in KOA to interpret the neural mechanism of acupuncture.

Methods: In 15 patients with KOA and 15 healthy controls (HC), we acquired Visual Analog Scale (VAS) scores and resting-state fMRI images of each participant before and after acupuncture stimulation on EX-LE5 acupoint. Then, PAG and RPN were selected as seeds to perform FC analysis based on resting-state fMRI images. Finally, we compared FC patterns of PAG and RPN between patients with KOA and HC, then between pre-acupuncture and post-acupuncture. Correlations between FC values and VAS scores were calculated as well.

Results: For PAG, FC of patients with KOA was lower in the right lingual gyrus at post-acupuncture compared with HC (p <0.001, uncorrected). For dorsal RPN, FC of patients with KOA was significantly higher in right putamen at post-acupuncture compared with HC (p <0.001, corrected with FDR), and FC changes were significant between pre-acupuncture and post-acupuncture in patients with KOA. Post-acupuncture FC values between dorsal RPN and right putamen were correlated with VAS scores. For medial RPN, FC of patients with KOA was lower in the right cerebellum at post-acupuncture compared with HC (p <0.001, uncorrected), but no significant FC changes were found between pre-acupuncture and post-acupuncture in patients with KOA. FC values between medial RPN and right cerebellum were not correlated with VAS scores at pre-acupuncture and post-acupuncture.

Discussion: Our study demonstrated that acupuncture enhanced FC between dorsal RPN and the right putamen in patients with KOA, which was associated with chronic pain intensity. This result suggests that acupuncture stimulation can enhance FC between dorsal raphe and striatum, illustrating a neural mechanism that acupuncture can drive the patients' brain, with KOA, to perceive pain.

Keywords: functional magnetic resonance imaging, chronic pain, acupuncture, functional connectivity, knee osteoarthritis

INTRODUCTION

Knee osteoarthritis is a common type of arthritis and prevalently affects the quality of life among the elderly (1). Chronic pain is the primary complaint associated with KOA, severely influencing the patients by physical dysfunction and muscular weakness (2, 3). Acupuncture is considered an effective therapy to relieve the chronic pain of KOA (4–6), but the mechanism underlying its clinical efficacy is still controversial. Previous studies have reported that chronic pain can induce changes in brain function (7–9), and acupuncture stimulation can mediate brain function to relieve chronic pain (10). Therefore, this study aims to explore the mechanism of acupuncture treatment by investigating how acupuncture induces the functional connectivity (FC) of brains in patients with KOA.

Periaqueductal gray and raphe nuclei, located in the brainstem, play a well-established pain responses because these structures have optimal anatomical positioning to integrate relevant contextual information, driving the central neural system to release pain-related neurotransmitters (11, 12). Recently, functional MRI (fMRI) studies have investigated how the activation of PAG and RPN contributes to neural mechanisms underlying chronic pain. Lee et al. applied the FC method to test the FC changes between patients with chronic migraine and with episodic migraine. They revealed that FC was enhanced, from PAG and RPN to cortical regions, in patients with chronic migraine (13). Notably, a recent study on the mouse model of OA has found that, in the early phase of OA pain, the PAG network, especially the connection between PAG and RPN, may contribute to the transition from acute to chronic OA pain (14). Another study demonstrated that dorsal RPN and ventral PAG have the potential to regulate pain by releasing dopamine and glutamate (15).

Acupuncture, one of the traditional Chinese treatment modalities, has a good therapeutic effect on chronic pain (16), that includes chronic migraine and chronic low back pain. Some previous studies reported that the possible mechanism of relieving pain by acupuncture stimulation was mediating through central pain modulation of the PAG and RPN in the brainstem (17, 18). Although some studies have supported that acupuncture is an efficient treatment tool for KOA pain, the neural mechanism underlying acupuncture treatment on KOA is unclear. Therefore, this study aimed to clarify the acupuncture neural mechanism on KOA by using fMRI. Considering the above, we speculated that acupuncture stimulation could alter FC of PAG and RPN in patients with chronic KOA pain, which is associated with pain-related clinical symptoms.

To test this hypothesis, we respectively calculated FC for patients with KOA and healthy controls (HC) at pre-acupuncture and post-acupuncture stimulation. The group differences between KOA and HC, and between pre-acupuncture and post-acupuncture, were evaluated, as well as the correlations between altered FC and the related clinical symptom were further calculated to assess how the FC changes through acupuncture stimulation have modulated chronic KOA pain.

MATERIALS AND METHODS

Participants

Fifteen patients with chronic KOA pain (mean age: 59.13 ± 10.27; eight females), whose pain lasts at least 4 months, were recruited from the First Affiliated Hospital of Anhui University of Chinese Medicine (AUCM), while 15 HC (mean age: 58.53 ± 8.15; 11 females) were recruited from the local community. The patients who presented with neurological or psychiatric diseases, poorly controlled hypertension, head injury, or any other conditions that might affect the study were excluded. All the participants had signed an informed consent before the study, which was approved by the Ethics Committee of the First Affiliated Hospital of AUCM (No. 2021AH-29).

KOA Diagnostic Criteria

The diagnostic criteria of KOA were determined according to the Chinese Guideline for Diagnosis and Treatment of Osteoarthritis (2021 edition) formulated by the Joint Surgery Branch of the Chinese Orthopedic Association (19). Patients with KOA were diagnosed by the results of both clinical and X-ray examinations, plus the following rules: (1) middle-aged and elderly people; (2) recurrent knee pain for nearly a month; (3) morning stiffness $\leq$ 30 min; and (4) bone frictions when physically exercising.

Pain Assessment

Pain intensity was evaluated by the Visual Analog Scale (VAS), a tool widely used to measure pain (20). The patients were asked to indicate their perceived pain intensity as a point along a 100-mm horizontal line, and the length from the left edge to this point was measured to acquire a VAS score. The VAS score ranges from 0 to 10, where VAS = 0 represents the patient feels no pain, VAS $<$ 3 indicates the patient feels mild but tolerable pain, $4 <$ VAS $<$ 6 means the patient feels pain and sleep is affected, and $7 <$ VAS < 10 depicts the patient feels severe pain, which is unbearable and already affects the sleep and appetite. Detailed information is presented in **Supplementary Table 1**.

Experiment Design

Pre-acupuncture resting-state fMRI data were acquired with 205 time points for 6 min 50 s before acupuncture stimulation. After that, acupuncture stimulation was performed at EX-LE5 acupoint, which is considered effective in treating KOA (21). When the participants received *de-qi* sensation (soreness, numbness, fullness, and heaviness) (22), task-state fMRI data with 205 time points were acquired for 6 min 50 s. Finally, after pulling out the acupuncture needles, post-acupuncture resting-state fMRI data acquisition of 205 time points was obtained for 6 min 50 s. The workflow is shown in **Supplementary Figure 2**. For the patients with KOA, VAS scores were acquired for assessment of pain intensity at both pre-acupuncture and post-acupuncture. In this study, we used the pre-acupuncture and post-acupuncture resting-state data and the VAS scores for analysis.

Image Acquisition

MRI data were acquired using a 3.0-Tesla MRI scanner (Discovery MR750, General Electric, USA), with an eight-channel high-resolution radio-frequency head coil. Sagittal 3D T1-weighted images were acquired using T1-3D BRAVO sequence with repetition time (TR)/echo time (TE): 8.16 ms/3.18 ms, flip angle (FA): 12°, matrix: 256 × 256, field of view (FOV): 256 × 256 mm, slice thickness: 1 mm, with 170 axial slices with no gap. Resting-state and task-state fMRI data were acquired using a gradient-echo single-shot echo planar imaging sequence with TR/TE: 2,000/30 ms, FOV: 220 × 220 mm, matrix: 64 × 64, FA: 90?, slice thickness: 3 mm, with 205 volumes. All the participants were instructed to lie down with their eyes closed, keep their minds relaxed, and not fall asleep during the scanning.

Data Preprocessing

For each participant, resting-state fMRI images were preprocessed using a combination of analysis packages, including FSL and AFNI. Functional images were preprocessed using the following steps: (1) the first 10 functional images were discarded to eliminate transients and account for T1 relaxation effects, followed by slice timing to compensate for acquisition delays across slices; (2) motion correction was performed by realigning all functional images to the middle image, and the data with head motion over 2 mm or 2° were excluded; (3) functional images were co-registered to the high-resolution anatomical images, and then normalized to Montreal Neurological Institute standard brain; (4) voxels were re-sampled to 2 × 2 × 2 mm^3 resolution; (5) images were spatially smoothed with a 6-mm full width at half-maximum (FWHM) Gaussian kernel; (6) the data were linearly detrended, and the residual signals were band-pass temporal filtered at.01–0.1 Hz; and (7) nuisance variable regression was performed to regress out the six head motion parameters, as well as the signals of white matter (WM) and cerebrospinal fluid (CSF).

Functional Connectivity Analysis

To evaluate FC changes of PAG and RPN, we first selected these two regions as seeds for FC analysis. Seed of PAG was structurally defined with the "atlas of the basal ganglia" (https://www.nitrc.org/projects/atag/), in which the nonlinear elderly atlas of PAG was selected for FC analysis. RPN was divided into dorsal and medial sub-regions, defined based on a previous study (23). The seeds of PAG and RPN are shown in **Figure 1**.

For each participant, the Pearson correlation coefficient between the mean time series of each seed and the time series

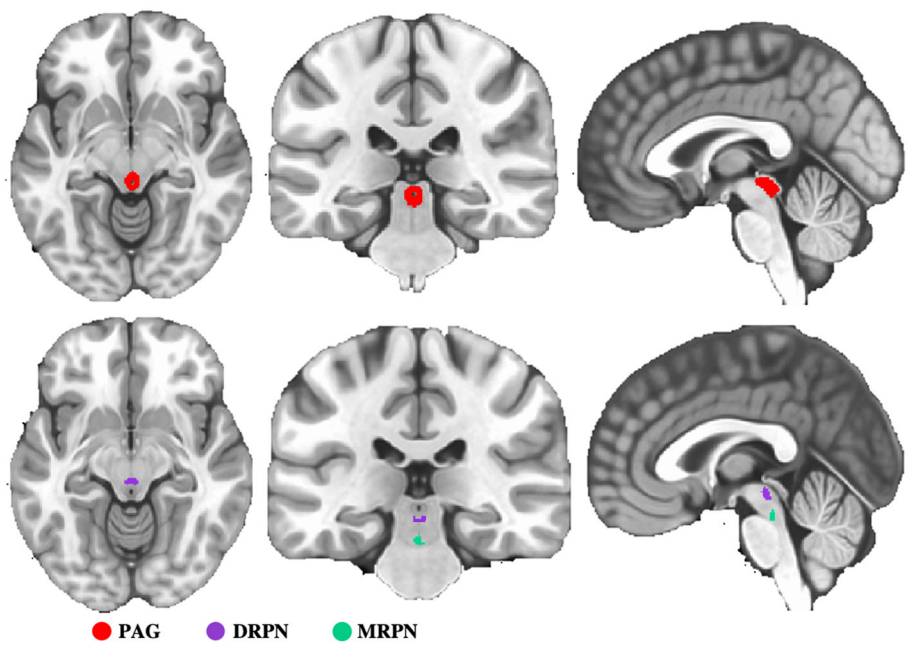

FIGURE 1 | Representation of seed regions. PAG, periaqueductal gray; DRPN, dorsal raphe nuclei; MRPN, medial raphe nuclei.

of each voxel across the whole brain was calculated. Then, the coefficients were converted to a z-value using Fisher r-to-z transformation to improve the normality.

Statistical Analysis

A paired two-sampled *t*-test was applied to both KOA and HC groups to compare FC changes between pre-acupuncture and post-acupuncture, uncovering how acupuncture mediates FC. An unpaired two-sampled *t*-test was used at both pre-acupuncture and post-acupuncture to compare FC changes between KOA and HC to investigate the group differences mediated by acupuncture. The results of group analysis were corrected using a false discovery rate (FDR) of $p < 0.001$.

TABLE 1 | Group differences of FC between KOA and HC at post-acupuncture.

Regions	MNI			Z Value	Voxel size
	x	y	z		
Periaqueductal gray					
Right Lingual Gyrus	4	−64	−2	−4.16	42
Dorsal Raphe					
Right Putamen	26	0	6	4.97	91
Medial Raphe					
Right Cerebellum	16	−72	−35	−4.65	41

FC between dorsal raphe and right putamen was corrected for FDR with $p < 0.001$, whereas FC between periaqueductal gray and right lingual gyrus, and also between medial raphe and right cerebellum were uncorrected with $p < 0.001$.

Correlation Analysis

We explored the relationships between FC values and the VAS scores in the patient group to identify how acupuncture affects chronic pain through mediating brain function. For all correlation analyses, we used partial correlations to factor out age and sex.

RESULTS

FC Changes of PAG

No FC changes of PAG were observed between pre-acupuncture and post-acupuncture in both patients with KOA and groups with HC. No FC differences of PAG were found between the two groups at pre-acupuncture. Lower FC of PAG in patients with KOA was found in right lingual gyrus at post-acupuncture compared with HC (**Supplementary Figure 1** and **Table 1**, $p < 0.001$, uncorrected).

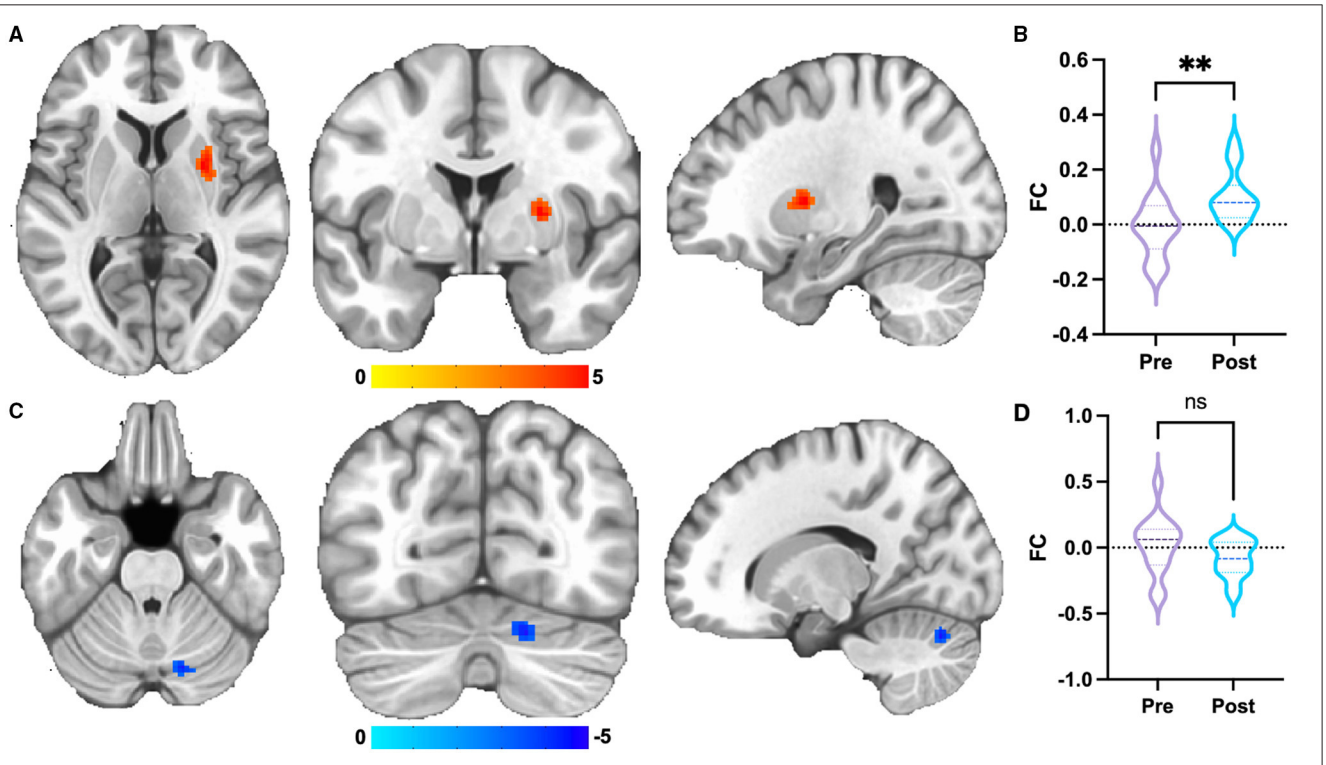

FIGURE 2 | Group differences of FC. **(A)** FC of dorsal RPN of patients with KOA enhanced at post-acupuncture compared with HC. The result was corrected for FDR with $p < 0.001$. **(B)** FC differences of right putamen between pre-acupuncture and post-acupuncture in KOA. **(C)** FC of medial RPN of patients with KOA decreased at post-acupuncture compared with HC. The result was uncorrected with $p < 0.001$. **(D)** FC differences of right cerebellum between pre-acupuncture and post-acupuncture in KOA. **: represents significant group difference with $p < 0.05$; ns: represents no significant group difference.

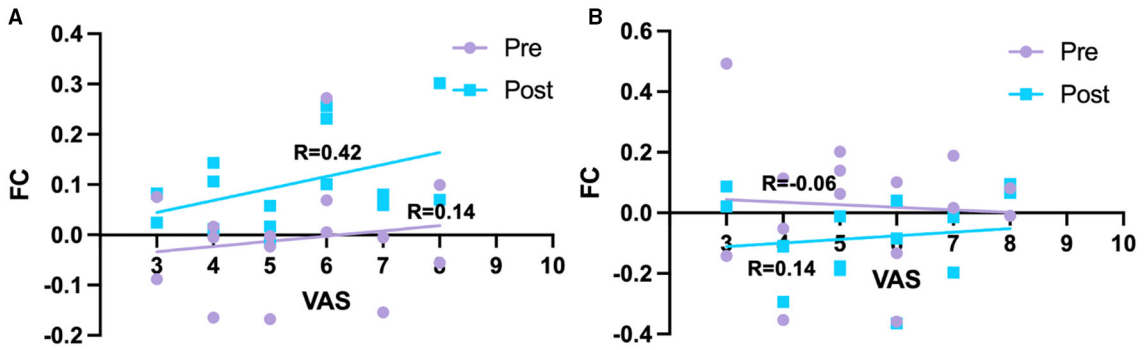

FIGURE 3 | Relationships between FC and pain intensity. **(A)** Correlation between FC of right putamen and pain intensity in KOA. **(B)** Correlation between FC of right cerebellum and pain intensity in KOA. Pre, pre-acupuncture; Post, post-acupuncture.

FC Changes of RPN

For dorsal RPN, no FC changes were observed between pre-acupuncture and post-acupuncture in two groups; no FC differences were found between patients with KOA and HC at pre-acupuncture, whereas FC in patients with KOA was significantly higher in right putamen at post-acupuncture compared with HC (**Figure 2A** and **Table 1**, p <0.001, corrected with FDR). The FC difference of right putamen was significant between pre-acupuncture and post-acupuncture in patients with KOA (**Figure 2B**). Post-acupuncture FC values of right putamen were correlated with VAS scores, while the pre-acupuncture FC values were not (**Figure 3A**).

For medial RPN, no FC changes were observed between pre-acupuncture and post-acupuncture of two groups; no FC differences were found between patients with KOA and HC at pre-acupuncture, whereas FC in patients with KOA was lower in right cerebellum at post-acupuncture compared with HC (**Figure 2C** and **Table 1**, p <0.001, uncorrected). FC difference of right cerebellum was not significant between pre-acupuncture and post-acupuncture in patients with KOA (**Figure 2D**). FC values of right cerebellum were not correlated with VAS scores at both pre-acupuncture and post-acupuncture (**Figure 3B**).

DISCUSSION

The brainstem involvement in relieving chronic pain has been investigated in previous studies, demonstrating a mediating role of PAG and RPN, as well as their interactions with cortical regions (24, 25). Therefore, we applied the resting-state fMRI to evaluate the neural mechanism underlying acupuncture, intervening in chronic KOA pain by investigating the FC changes of the PAG and RPN mediated by acupuncture. Our results suggested that acupuncture enhanced FC between dorsal RPN and the right putamen in patients with KOA, and enhanced FC is associated with chronic pain intensity.

Periaqueductal gray (PAG) plays a central role in the descending modulation of pain (26). Dysfunction of PAG is thought to contribute to dysregulation of pain, which is the main reason for chronic pain (24). Previous studies have demonstrated that FC between PAG and prefrontal cortex/anterior cingulate cortex in low back chronic pain (27) and chronic migraine (28) is enhanced after acupuncture treatment, associated with the relieving of pain symptoms (28). However, in our study, FC differences of PAG were not found between patients with KOA and HC. Acupuncture stimulation has also not induced PAG-related FC changes in patients with KOA with chronic pain. These results were inconsistent with previous studies. In this study, the patients also received several other medications in addition to acupuncture treatment, which possibly drove the FC of PAG close to the normal level. Previous studies have demonstrated that transient drug therapy could enhance the patients' brain function, whereas the patients were also accompanied by clinical symptoms (29, 30). This is the possible explanation why we did not observe the changes in PAG function in the patients with chronic KOA pain.

Previous studies have interpreted the neural mechanism of dorsal RPN in the regulation and the perception of pain from electrophysiology and neuroimaging, based on the fact that FC between dorsal RPN and cortical/subcortical regions was increased in patients with chronic pain after treatment (13, 16). The striatum receives serotonin innervation from the dorsal RPN, which implicates the behaviors of emotions, depression, and anxiety (31, 32). This evidence was further proved in a PET-fMRI study, revealing that dorsal RPN has strong functional connections with striatum (23). In present studies, FC between dorsal RPN and right putamen was enhanced after acupuncture stimulation rather than FC between medial RPN and right cerebellum. Moreover, the rising value of FC was associated with pain intensity. In summary, our results may explain that acupuncture stimulation induces the enhanced FC between dorsal RPN and striatum to drive the patients' brain with KOA to perceive the pain.

There were also several limitations in this study. The sample size of the participants was relatively small so that individual variation may affect the accuracy of the results. Moreover, considering the comfort and cooperation of the patients, short-term acupuncture stimulation was conducted in this research rather than typical acupuncture therapy, because the participants were lying in the bore of MRI equipment through the whole experiment. Our study pursued the instantaneous effect of

how the brain perceives the pain right after the acupuncture stimulation; not the neural mechanism of the acupunctural therapeutic effect. For further research, more participants will be recruited, and we will simultaneously study the effects of both the short-term acupuncture stimulation and long-term acupuncture therapy.

CONCLUSIONS

In conclusion, our results have demonstrated that acupuncture stimulation can enhance FC between dorsal raphe and striatum, illustrating a neural mechanism that acupuncture can drive the patients' brain, with KOA, to perceive pain.

DATA AVAILABILITY STATEMENT

The raw data supporting the conclusions of this article will be made available by the authors, without undue reservation.

ETHICS STATEMENT

The studies involving human participants were reviewed and approved by the Ethics Committee of the First Affiliated Hospital of Anhui University of Chinese Medicine. The patients/participants provided their written informed consent to participate in this study.

AUTHOR CONTRIBUTIONS

NG and HS wrote the first draft of the article, edited, and revised the article. BZ, AY, JS, and YF analyzed imaging data. JB, HX, and JC contributed to data acquisition. SH, XW, CL, BQ, and JY designed the study. All the authors contributed to and have approved the final version of the article.

FUNDING

This work was supported by the National Natural Science Foundation of China (No. 81873370), Ministry of Science and Technology of the People's Republic of China (No. 2018YFC170460-4), the Support Project of Natural Science Foundation for Distinguished Young Scholars of Anhui Province (No. gxyq2020016), and the Key Project of Natural Science Foundation of Anhui Province (No. KJ2020A0394).

SUPPLEMENTARY MATERIAL

The Supplementary Material for this article can be found online at: https://www.frontiersin.org/articles/10.3389/fneur.2021.813723/full#supplementary-material

REFERENCES

1. Sharma L, Kapoor D, Issa S. Epidemiology of osteoarthritis: an update. *Curr Opin Rheumatol.* (2006) 18:147–56. doi: 10.1097/01.bor.0000209426.84775.f8
2. Felson DT. The sources of pain in knee osteoarthritis. *Curr Opin Rheumatol.* (2005) 17:624–8. doi: 10.1097/01.bor.0000172800.49120.97
3. Shimura Y, Kurosawa H, Ishijima M, Liu L, Kaneko H, Futami I, et al. The sources of pain in knee osteoarthritis are changing dependent upon the progression of the disease. *Osteoarthr Cartilage.* (2013) 21:S262. doi: 10.1016/j.joca.2013.02.546
4. Lin LL, Tu JF, Wang LQ, Yang JW, Shi GX Li JL, et al. Acupuncture of different treatment frequencies in knee osteoarthritis: a pilot randomised controlled trial. *Pain.* (2020) 161:2532–8. doi: 10.1097/j.pain.0000000000001940
5. Tu JF, Yang JW, Shi GX Yu ZS Li JL, Lin LL, et al. Efficacy of intensive acupuncture versus sham acupuncture in knee osteoarthritis: a randomized controlled trial. *Arthritis Rheumatol.* (2021) 73:448–58. doi: 10.1002/art.41584
6. Wang M, Liu L, Zhang CS, Liao Z, Jing X, Fishers M, et al. Mechanism of traditional chinese medicine in treating knee osteoarthritis. *J Pain Res.* (2020) 13:1421–9. doi: 10.2147/JPR.S247827
7. Aytur SA, Ray KL, Meier SK, Campbell J, Gendron B, Waller N, et al. Neural mechanisms of acceptance and commitment therapy for chronic pain: a network-based fMRI approach. *Front Hum Neurosci.* (2021) 15:587018. doi: 10.3389/fnhum.2021.587018
8. Baliki MN, Geha PY, Jabakhanji R, Harden N, Schnitzer TJ, Apkarian AV. A preliminary fMRI study of analgesic treatment in chronic back pain and knee osteoarthritis. *Mol Pain.* (2008) 4:47. doi: 10.1186/1744-8069-4-47
9. Flodin P, Martinson S, Altawil R, Waldheim E, Lampa J, Kosek E, et al. Intrinsic brain connectivity in chronic pain: a resting-state fmri study in patients with rheumatoid arthritis. *Front Hum Neurosci.* (2016) 10:107. doi: 10.3389/fnhum.2016.00107
10. Cai RL, Shen GM, Wang H, Guan YY. Brain functional connectivity network studies of acupuncture: a systematic review on resting-state fMRI. *J Integr Med-Jim.* (2018) 16:26–33. doi: 10.1016/j.joim.2017.12.002
11. Behbehani MM. Functional-characteristics of the midbrain periaqueductal gray. *Prog Neurobiol.* (1995) 46:575–605. doi: 10.1016/0301-0082(95)00009-K
12. Wang QP, Nakai Y. The dorsal raphe - an important nucleus in pain modulation. *Brain Res Bull.* (1994) 34:575–85. doi: 10.1016/0361-9230(94)90143-0
13. Lee MJ, Park BY, Cho S, Kim ST, Park H, Chung CS. Increased connectivity of pain matrix in chronic migraine: a resting-state functional MRI study. *J Headache Pain.* (2019) 20:29. doi: 10.1186/s10194-019-0986-z
14. Da Silva JT, Tricou C, Zhang Y, Tofighbakhsh A, Seminowicz DA, Ro JY. Pain modulatory network is influenced by sex and age in a healthy state and during osteoarthritis progression in rats. *Aging Cell.* (2021) 20:e13292. doi: 10.1111/acel.13292
15. Li C, Sugam JA, Lowery-Gionta EG, McElligott ZA, McCall NM, Lopez AJ, et al. Mu opioid receptor modulation of dopamine neurons in the periaqueductal gray/dorsal raphe: a role in regulation of pain. *Neuropsychopharmacology.* (2016) 41:2122–32. doi: 10.1038/npp.2016.12
16. Lai HC, Lin YW, Hsieh CL. Acupuncture-analgesia-mediated alleviation of central sensitization. *Evid Based Complement Alternat Med.* (2019) 2019:6173412. doi: 10.1155/2019/6173412
17. Niddam DM, Chan RC, Lee SH, Yeh TC, Hsieh JC. Central modulation of pain evoked from myofascial trigger point. *Clin J Pain.* (2007) 23:440–8. doi: 10.1097/AJP.0b013e318058accb
18. Ma F, Xie H, Dong ZQ, Wang YQ, Wu GC. Effects of electroacupuncture on orphanin FQ immunoreactivity and preproorphanin FQ mRNA in nucleus of raphe magnus in the neuropathic pain rats. *Brain Res Bull.* (2004) 63:509–13. doi: 10.1016/j.brainresbull.2004.04.011
19. Association TJSBotCO. The Subspecialty Group of Osteoarthritis CAoOS, Disorders TNCRCfG, Orthopaedics EOoCJo. Chinese guideline for diagnosis and treatment of osteoarthritis (2021 edition). *Chin J Orthop*. (2021) 18:1291–314. doi: 10.3760/cma.j.cn121113-20210624-00424
20. Haefeli M, Elfering A. Pain assessment. *Eur Spine J.* (2006) 15:S17–24. doi: 10.1007/s00586-005-1044-x

21. Wu MX Li XH, Lin MN, Jia XR, Mu R, Wan WR, et al. Clinical study on the treatment of knee osteoarthritis of Shen-Sui insufficiency syndrome type by electroacupuncture. *Chin J Integr Med.* (2010) 16:291–7. doi: 10.1007/s11655-010-0513-1
22. Yuan H, Wang P, Hu N, Ma L, Zhu J, Yuan H, et al. A review of the methods used for subjective evaluation of De Qi. *J Tradit Chin Med.* (2018) 38:309–14. doi: 10.1016/j.jtcm.2017.03.001
23. Beliveau V, Svarer C, Frokjaer VG, Knudsen GM, Greve DN, Fisher PM. Functional connectivity of the dorsal and median raphe nuclei at rest. *Neuroimage.* (2015) 116:187–95. doi: 10.1016/j.neuroimage.2015.04.065
24. Yu W, Pati D, Pina MM, Schmidt KT, Boyt KM, Hunker AC, et al. Periaqueductal gray/dorsal raphe dopamine neurons contribute to sex differences in pain-related behaviors. *Neuron.* (2021) 109:1365–80 e5. doi: 10.1016/j.neuron.2021.03.001
25. Oliva V, Gregory R, Davies WE, Harrison L, Moran R, Pickering AE, et al. Parallel cortical-brainstem pathways to attentional analgesia. *Neuroimage.* (2021) 226:117548. doi: 10.1016/j.neuroimage.2020.117548
26. Fields H. State-dependent opioid control of pain. *Nat Rev Neurosci.* (2004) 5:565–75. doi: 10.1038/nrn1431
27. Yu RJ, Gollub RL, Spaeth R, Napadow V, Wasan A, Kong J. Disrupted functional connectivity of the periaqueductal gray in chronic low back pain. *Neuroimage-Clin.* (2014) 6:100–8. doi: 10.1016/j.nicl.2014.08.019
28. Li ZJ, Liu ML, Lan L, Zeng F, Makris N, Liang YL, et al. Altered periaqueductal gray resting state functional connectivity in migraine and the modulation effect of treatment. *Sci Rep-Uk.* (2016) 6 doi: 10.1038/srep 20298
29. Yu SY, Ortiz A, Gollub RL, Wilson G, Gerber J, Park J, et al. Acupuncture treatment modulates the connectivity of key regions of the descending pain modulation and reward systems in patients with chronic low back pain. *J Clin Med.* (2020) 9:1719. doi: 10.3390/jcm90 61719
30. Hu S, Wu Y, Li C, Park K, Lu G, Mohamed AZ, et al. Increasing functional connectivity of the anterior cingulate cortex during the course of recovery from Bell's palsy. *Neuroreport.* (2015) 26:6–12. doi: 10.1097/WNR.0000000000000295
31. Di Matteo V, Pierucci M, Esposito E, Crescimanno G, Benigno A, Di Giovanni G. Serotonin modulation of the basal ganglia circuitry: therapeutic implication for Parkinson's disease and other motor disorders. *Prog Brain Res.* (2008) 172:423–63. doi: 10.1016/S0079-6123(08)00921-7
32. Peyron C, Petit JM, Rampon C, Jouvet M, Luppi PH. Forebrain afferents to the rat dorsal raphe nucleus demonstrated by retrograde and anterograde tracing methods. *Neuroscience.* (1998) 82:443–68. doi: 10.1016/S0306-4522(97)00268-6

Conflict of Interest: The authors declare that the research was conducted in the absence of any commercial or financial relationships that could be construed as a potential conflict of interest.

Publisher's Note: All claims expressed in this article are solely those of the authors and do not necessarily represent those of their affiliated organizations, or those of the publisher, the editors and the reviewers. Any product that may be evaluated in this article, or claim that may be made by its manufacturer, is not guaranteed or endorsed by the publisher.

frontiers in Neurology

ORIGINAL RESEARCH
published: 20 January 2022
doi: 10.3389/fneur.2021.798969

Trigeminal Nerve White Matter Fiber Abnormalities in Primary Trigeminal Neuralgia: A Diffusion Spectrum Imaging Study

Si-ping Luo[1,2†], Fan-fan Chen[3†], Han-wen Zhang[2], Fan Lin[2], Guo-dong Huang[3*] and Yi Lei[2*]*

[1] College of Medicine, Shantou University, Shantou, China, [2] Department of Radiology, Shenzhen Second People's Hospital, The First Affiliated Hospital of Shenzhen University, Health Science Center, Shenzhen, China, [3] Department of Neurosurgery, Shenzhen Second People's Hospital, The First Affiliated Hospital of Shenzhen University, Health Science Center, Shenzhen, China

OPEN ACCESS

Edited by:
Lu Liu,
Capital Medical University, China

Reviewed by:
Danielle D. DeSouza,
Winterlight Labs, Canada
Peter Shih-Ping Hung,
University of Toronto, Canada

***Correspondence:**
Fan Lin
foxetfoxet@gmail.com
Guo-dong Huang
huangguodong@email.szu.edu.cn
Yi Lei
leiyisz2011@163.com

[†] These authors have contributed equally to this work and share first authorship

Specialty section:
This article was submitted to Headache and Neurogenic Pain, a section of the journal Frontiers in Neurology

Received: 20 October 2021
Accepted: 06 December 2021
Published: 20 January 2022

Citation:
Luo S-p, Chen F-f, Zhang H-w, Lin F, Huang G-d and Lei Y (2022) Trigeminal Nerve White Matter Fiber Abnormalities in Primary Trigeminal Neuralgia: A Diffusion Spectrum Imaging Study. Front. Neurol. 12:798969. doi: 10.3389/fneur.2021.798969

Objective: Diffusion spectrum imaging (DSI) was used to quantitatively study the changes in the trigeminal cistern segment in patients with trigeminal neuralgia (TN) and to further explore the value of acquiring DSI data from patients with TN.

Methods: To achieve high-resolution fiber tracking, 60 patients with TN and 35 healthy controls (HCs) were scanned with conventional magnetic resonance imaging (MRI) and DSI. The patients and the members of the control group were compared within and between groups. The correlations between quantitative parameters of DSI and the visual analog scale (VAS), and symptom duration and responsible vessel types were analyzed.

Results: Compared with unaffected side of patients in the TN group, the affected side showed significantly decreased quantitative anisotropy (QA) ($p < 0.001$), fractional anisotropy (FA) ($p = 0.001$), and general FA (GFA) ($p < 0.001$). The unaffected side exhibited significantly decreased QA ($p + 0.001$), FA ($p = 0.001$), and GFA ($p < 0.001$) and significantly increased axial diffusivity (AD) ($p = 0.036$) compared with the affected side of patients in the TN group and the average values of HCs. There were significantly decreased QA ($p = 0.046$) and FA ($p = 0.008$) between the unaffected side of patients and the average values of HCs. GFA can evidently distinguish arteries, veins, and features of unaffected side in TN patients.

Conclusion: Using high-resolution fiber tracking technology, DSI can provide quantitative information that can be used to detect the integrity of trigeminal white matter in patients with TN and can improve the understanding of the disease mechanism.

Keywords: trigeminal neuralgia, diffusion spectrum imaging, diffusion tensor imaging, fiber tractography, diffusion magnetic resonance image

INTRODUCTION

Trigeminal neuralgia (TN) is recurrent, unilateral, transient, and electric pain in the trigeminal nerve distribution area. It has been reported that the annual incidence is about 4–29/10 million person-years worldwide (1). The prevalence rate in women was higher than that in men (F:M = 3:2). With disease aggravation, pain attacks become more frequent, affecting basic human functions, such as speaking, eating, drinking, or touching the face, resulting in low quality of life (1).

The etiology of primary TN is unknown. At present, the generally accepted theory is neurovascular compression (NVC). This theory suggests that microvascular compression leads to demyelination of trigeminal nerve roots, causing TN. These vessels that compress the trigeminal nerve are called responsible vessels. Microvascular decompression (MVD), a minimally invasive interventional technique, is designed based on this etiological explanation and has been recognized as the most effective method for the treatment of TN (2, 3). MVD can identify the painful nerve and effectively isolate the responsible vessels that compress the trigeminal nerve root and brainstem to relieve compression and, repair nerve pain under the operating microscope and eliminate the source of trigeminal nerve pain (4).

As a non-invasive magnetic resonance imaging (MRI) technique to evaluate the integrity of white matter, diffusion tensor imaging (DTI) can indirectly reflect the integrity of nerve fiber bundles by measuring the diffusion movement of water molecules (5), thus providing new insights into the etiology of TN. Previous studies (6, 7) have shown that in patients with TN, DTI parameters such as fractional anisotropy (FA) decreased significantly and axial diffusivity (AD), radial diffusivity (RD), and mean diffusivity (MD) increased significantly. However, some studies (8, 9) argued different or even opposite opinions of the changes of DTI metrics values between affected and unaffected sides in patients and controls. In addition, the correlation between the degree of FA decrease and the degree of pain, symptom duration, and types of responsible vessels are controversial (8, 10, 11). Moreover, DTI needs larger sample sizes for standardization and the spatial resolution limits the further use of DTI in patients with TN.

Diffusion spectrum imaging (DSI) generalizes DTI by acquiring more directions in q-space, either by high-angular resolution diffusion imaging shells, a cube on a Cartesian grid, or Q-ball imaging, which has been used to non-invasively detect the complex structure of white matter bundles and fiber bundles in human brain (12). DSI reconstructs fiber bundles with higher resolution than traditional DTI and has been shown to accurately display crossing, winding, interruption, and small fibers (13, 14). DSI parameters include DTI parameters: FA, RD, MD, and AD as well as unique parameters: quantitative anisotropy (QA), general FA (GFA), restricted diffusion imaging (RDI), and isotropic diffusion component (ISO). The GFA value, which represents the direction consistency of water molecule diffusion and reflects the integrity of axon or myelin more accurately and sensitively than FA value, is the main quantitative parameter of DSI (15, 16). Generalized q-sampling imaging (GQI) (17) is one of the commonly used DSI data reconstruction models for calculating QA and ISO. RDI (18) is a model-free method to quantify the density of restricted diffusion given a diffusion displacement range. DSI has been used to study some mental diseases, such as autism (19) and schizophrenia (20), as well as neurodegenerative diseases, such as Alzheimer's disease (21) and multiple sclerosis (22). Recently, DSI has been increasingly used to study the brain nerve structure (23).

In this study, we used DSI technology to study and compare the changes in cistern segments between the affected side and the unaffected side of patients with TN, analyze the difference of DSI parameters between patients with TN and healthy controls (HCs), and the relationship between the degree of difference value and symptom duration, the degree of pain, and responsible vessels. We hypothesized that some of the identified white matter abnormalities exist in TN patients and would correlate with the degree of pain, symptom duration, and responsible vessel types, so as to further explore the value of utilizing DSI technology in patients with TN.

MATERIALS AND METHODS

Participants

This study collected patients with TN diagnosed in the Shenzhen Second People's Hospital from November 2019 to August 2021. They all underwent MRI and excluded: (1) TN secondary to other neurological conditions such as tumor growth or multiple sclerosis; (2) There are other known intracranial lesions including obvious trauma; (3) Previous history of craniocerebral surgery; and (4) Incomplete image data. After screening, a total of 60 patients were included in this study. By posting advertisements in several health management centers, 35 years of age and sex-matched participants without pain and any neurological diseases served as HCs. The protocol was approved by the Hospital Bioethics Committee. All the participants received a written informed consent prior to registration.

Magnetic Resonance Imaging Acquisition

Scanning was performed on a 3.0-T MRI system (Prisma, Siemens) using a 20-channel head coil. Comfortable and tight foam padding was used to limit head movement. All the patients were treated with three-dimensional time-of-flight magnetic resonance angiography (3D-TOF-MRA) and T2_SPC_TRA_ISO sequence before operation to check the relationship between blood vessels and nerves. The relevant parameters for the T2_SPC sequence were repetition time/echo time (TR/TE) = 1,000 ms/125 ms, field of view (FOV) = 82 mm × 160 mm, matrix = 320 × 164, 2 average, slice thickness = 0.5 mm, flip angle 100°, and scanning time: 3 min 46 s; 3D-TOF sequence: TR/TE = 20 ms/3.69 ms, FOV = 191 × 200 mm, matrix = 384 × 331, 1 average, slice thickness = 0.5 mm, flip angle 18°, and scanning time: 4 min 49 s.

Data were collected using MRI sequences including T1-weighted magnetization-prepared rapid acquisition gradient-echo (MPRAGE) for better anatomic reference and DSI using pulsed gradient twice-refocused spin-echo echo-planar imaging (EPI) sequences. T1-weighted sagittal images were obtained with 3D fast-field echo imaging. The following acquisition parameters were employed: repetition time, 2,300 ms; echo time, 3.55 ms; flip angle, 8°; slice thickness, 0.9 mm; number of sections, 192; FOV, 240 × 240 mm; matrix, 256 × 256; and voxel size, 0.9 × 0.9 mm. The acquisition parameters for DSI were as follows: repetition time, 6,300 ms; echo time, 71 ms; slice thickness, 2.2 mm; number of sections in the transverse plane, 60; FOV, 220 × 100 mm; matrix, 220 × 100; and voxel size, 2.2 × 2.2 × 2.2 mm. A total of 128 directions with the maximum diffusion sensitivity bmax = 3,000 s/mm^2 were sampled on the grid points in the 3D q-space. The grid sampling scheme sampled the diffusion

encoding space using a given grid, which consisted of 19 b-values of b = 200, 350, 400, 550, 750, 950, 1,100, 1,150, 1,500, 1,700, 1,850, 1,900, 2,050, 2,250, 2,400, 2,450, 2,600, 2,650, 3,000 s/mm^2 along 3, 2, 4, 4, 3, 12, 8, 4, 6, 15, 8, 4, 12, 4, 2, 10, 22, 2, and 3 directions, respectively.

Clinical Data

The clinical data of all the patients with TN including sex, age, symptom duration, and pain laterality (right or left pain) were obtained from medical records. The main results of pain intensity were evaluated by using the visual analog scale (VAS) (0: no pain; 10: the most serious possible pain). The pain perception of patients with TN was measured by a senior pain physician.

The judgment of the responsible vessel types shall be diagnosed by the surgeon doctors and radiologists. For patients undergoing MVD surgery, the type of responsible vessel can be obtained by querying the operation records. If MVD surgery is not performed or the operation records are unclear, two senior radiologists will diagnose the type of responsible vessel through pre-operative MRI examination. The types of responsible vessels are divided into artery and vein.

Tract Analysis

To analyze the microstructure integrity of white matter fiber bundles, we used the DSI Studio software (http://dsi-studio.Labsolver.org/) to reconstruct the fiber bundles of all the participants. The diffusion image was imported into the DSI Studio software, brain mask was set, and generalized q-sampling imaging (GQI) with diffusion sampling length ratio of 1.25 was used to reconstruct the model (17). Restricted diffusion was quantified using restricted diffusion imaging. The region of interest (ROI) is placed in the QA diagram, the volume sizes of the ROIs were 1.3 × 103 mm^3-2.0 × 103 mm^3 within the cisternal segment of the trigeminal nerve (24), and the trigeminal nerve can be seen in the brainstem area of bilateral trigeminal nerves. A deterministic fiber tracking algorithm is used to reconstruct the trigeminal nerve tracts (25). The quantitative anisotropy threshold was 0.20 ± 0.25 (subject dependent), the angular threshold was 60°, the step size was 1.2 mm, the smoothness was 0.80, the minimum length was 10 mm, and the maximum length was 200 mm. A total of 5,000 were calculated. Finally, the values of average GFA, QA, RDI, and ISO as well as the basic diffusion coefficients such as FA, MD, AD, and RD are calculated. Two radiologists with more than 10 years of neuroradiology experience tracked the seeds and targets, respectively, and obtained the average values of the above parameters.

Difference of Parameters

The average value of each parameter for HCs was obtained from the average value of the left and right sides of these participants. The difference value of each parameter = average parameter value of HCs—parameter value of the affected side. The difference scores of each parameter = (average parameter value of HCs)—(parameter value of the affected side)/(average parameter value of HCs) (10). The difference value and difference scores of each parameter on the affected side and unaffected side of patients with TN can be obtained. The above parameter value, including the parameter value of TN affected side, unaffected side and HCs, difference value, and difference scores were statistically were used. Correlation analysis and logistic analysis were carried out to investigate relationships among the parameter value and VAS scores, symptom duration, and responsible vessel types.

All the patients were assigned to either the short-duration (symptom duration < 4 years) or the long-duration (symptom duration ≥ 4 years) groups and their affected side parameters were compared. The threshold was set to the mean symptom duration of all the trigeminal patients in our cohort. The statistics analysis was performed with t-test.

Statistical Analysis

Continuous variables were summarized as means (±SD). For categorical variables, the percentages of patients in each category were calculated.

Statistical analyses were performed in the SPSS version 22.0 (IBM Corporation, Armonk, New York, USA). Differences between groups were assessed using the independent samples t-tests or the one-way ANOVA, whereas differences within groups were assessed using the paired-samples t-tests. Benjamini and Hochberg correction was used to correct the multiple comparisons of different groups. The Bonferroni correction was used to correct the multiple comparisons of intragroup comparison. Bivariate correlation and partial correlation analyses were used to identify the relationship between the DSI parameters that exhibited significant differences and clinical severity assessment. Normality of the data was assessed using the Shapiro–Wilk-test. For non-normally distributed variables, a non-parametric equivalent test was performed. If the data had unequal variances (determined by Levene's test for homogeneity of variances) and/or unequal sample sizes, Welch's t-test or Welch's ANOVA followed by Games–Howell *post-hoc* tests was performed. $p < 0.05$ was considered as statistically significant.

RESULTS

Demographic and Disease Characteristics of Participants

Table 1 shows 60 patients diagnosed with primary TN (age 57.45 ± 8.78 years; range 25–80 years; 22 men and 38 women) and 35 HC (age 54.6 ± 5.2 years; range 45–65 years; 20 men and 15 women). Sex and age were not significantly different between the two groups of subjects. Affected regions were more often observed on the right side than the on left. Responsible vessels are mainly arteries (73.3%) and veins (26.7%).

Diffusion Spectrum Imaging Analysis

In all the participants, we successfully completed high-definition fiber tractography of the trigeminal nerve in cistern segments and an instance of a patient's tractography is displayed in **Figure 1**. Two radiologists measured and calculated the parameters separately and the intraclass correlation coefficients (ICCs) of these measurements were $ICC_{QA} = 0.87$, $ICC_{ISO} = 0.96$, $ICC_{MD} = 0.93$, $ICC_{AD} = 0.95$, $ICC_{FA} = 0.86$, $ICC_{RD} = 0.92$, and $ICC_{GFA} = 0.83$. The parameters were averaged and analyzed.

TABLE 1 | Demographic and disease characteristics of participants.

	Patients ($n = 60$)	Controls ($n = 35$)	p-value
Age (mean ± SD, years)	57.45 ± 8.786	54.6 ± 5.259	0.085[a]
Sex (number, %)			
Male	22 (36.7%)	20 (57.1%)	0.058[b]
Female	38 (63.3%)	15 (42.9%)	
Disease duration (mean ± SD, years)	4.22 ± 4.04		
Short duration	35 (58.4%)	NA	NA
Long duration	25 (41.6%)		
Pain side (number,%)			
Right	38 (63.3%)	NA	NA
Left	22 (36.7%)	NA	
VAS (mean ± SD, score)	8.45 ± 0.72	NA	NA
Responsible vessels (number, %)			
Arteries	44 (73.3%)		
Superior cerebellar artery (SCA)	30 (50%)	NA	
Anterior inferior cerebellar artery (AICA)	10 (16.7%)		NA
Basilar artery	4 (6.6%)		
Veins	16 (26.7%)	NA	

VAS, visual analog scale; NA, not applicable.
[a]*p-values were calculated with the two-tailed t-tests.*
[b]*p-value was obtained using the chi-squared test.*

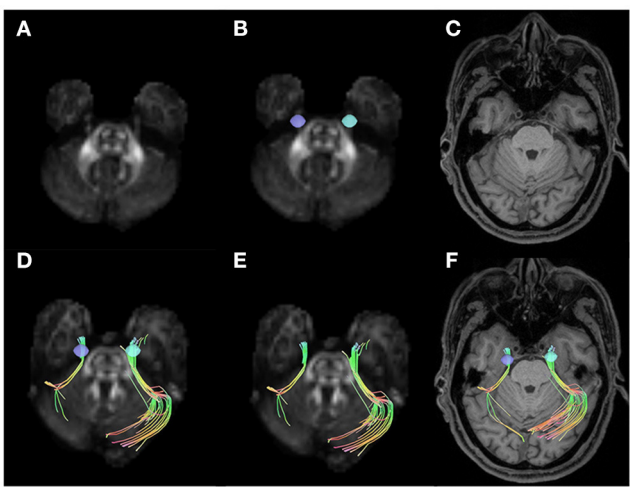

FIGURE 1 | Examples of volumes of interest, trigeminal nerve tracking, and trigeminal nerve reconstruction. **(A)** Shows the quantitative anisotropy (QA) diagram. **(B)** Shows the seeds placed on two sides of the cistern segments in trigeminal nerve (purple and blue). **(C)** Shows the T1-weighted image (T1WI) structural MRIs. The trigeminal nerve tractography for right side affected patients with trigeminal neuralgia (TN) in QA diagram **(D,E)** and T1WI MRI **(F)**.

After fiber tracking, DSI parameters were extracted for intragroup comparison. There was no significant difference in any parameters between the left and right sides of HCs. Compared with the unaffected side of patients in the TN group, the affected side showed significantly decreased QA ($p < 0.001$), FA ($p = 0.001$), and GFA ($p < 0.001$), as shown in **Table 2**.

The parameters of the patient's affected side and unaffected side were compared with the average parameter values of the HCs. In the affected side of patients in the TN group, significantly decreased QA ($p < 0.001$), FA ($p = 0.001$), and GFA ($p < 0.001$) and significantly increased AD ($p = 0.036$) were noted compared with the average values of HCs. In addition, there were significantly decreased QA ($p = 0.046$) and FA ($p = 0.008$) between the patient's unaffected side and the average parameter values of HCs, as shown in **Table 3** and **Figure 2**.

Difference of Parameters

The significantly different parameters discussed above were used to calculate the parameter difference scores and correlation analysis and logistic analysis were carried out between the difference scores and VAS scores and symptom duration, and responsible vessel types. There was a correlation between TN patient's' VAS scores and symptom duration and there was no significant correlation between the difference scores of each parameter and VAS scores and between the difference scores of each parameter and symptom duration. In the TN group, FA ($p = 0.028$) was significantly decreased between arteryies and veins in responsible vessel types. GFA showed artery ($p < 0.001$), followed by veins ($p = 0.017$), in the affected side had the most significant decreases, compared with measurements of the unaffected side, while FA showed no significant difference between the affected artery and unaffected side, these findings are depicted in **Table 4** and **Figure 3**.

For affected side of the TN group, patients in the long-duration (25, 41.6%) group showed significantly decreased ISO ($p = 0.021$) and RDI ($p = 0.021$) compared with patients in the short-duration group (35, 58.4%), as shown in **Table 5**.

TABLE 2 | Compared with the sides of the affected and unaffected patients and the healthy control group left and right.

	Patients ($n = 60$)		*p*-value	Healthy controls ($n = 35$)		*p*-value
	Affected	Unaffected		Left	Right	
QA	0.0665 ± 0.008	0.0837 ± 0.016	<0.001	0.0788 ± 0.013	0.0779 ± 0.011	0.7
FA	0.2678 ± 0.047	0.2764 ± 0.043	0.001	0.3159 ± 0.1159	0.3023 ± 0.0487	0.425
GFA	0.0627 ± 0.010	0.0713 ± 0.007	<0.001	0.0695 ± 0.0058	0.0700 ± 0.0064	0.744

QA, quantitative anisotropy; FA, fractional anisotropy; GFA, general FA.
p-values were calculated with the paired-samples t-tests.

TABLE 3 | Compared with patients and healthy controls.

	Patient-unaffected	Healthy control	*p*-value	Patient-affected	Healthy control	*p*-value
QA	0.08378 ± 0.0161	0.0783 ± 0.0099	0.046	0.0665 ± 0.0080	0.0783 ± 0.0099	<0.001
AD	0.00092 ± 0.0001	0.0008 ± 0.0001	0.059	0.00094 ± 0.0001	0.0008 ± 0.0001	0.036
FA	0.2764 ± 0.0435	0.3091 ± 0.0735	0.008	0.2678 ± 0.0469	0.3091 ± 0.0735	0.001
GFA	0.0713 ± 0.0071	0.0698 ± 0.0044	0.21	0.0627 ± 0.0102	0.0698 ± 0.0044	<0.001

QA, quantitative anisotropy; AD, axial diffusivity; FA, fractional anisotropy; GFA, general FA.
p-values were calculated with independent sample t-test.

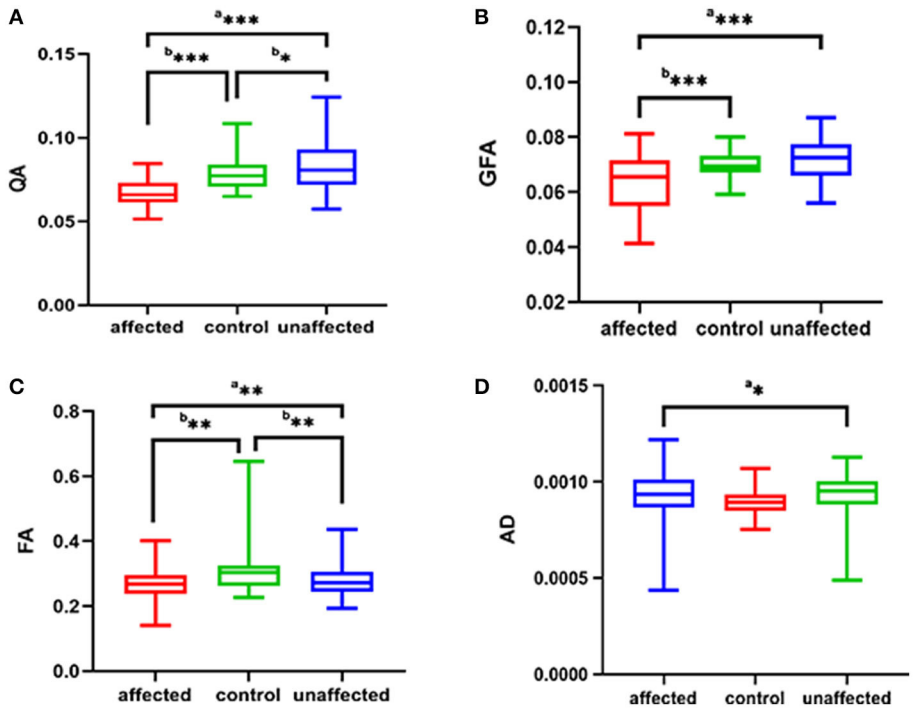

FIGURE 2 | The **(A–D)** respectively shows QA, GFA, FA, AD of the affected side and unaffected side of patient with TN were compared with those average of the HC group. ^{a}p was calculated with the paired-samples *t*-tests, ^{b}p was calculated with the independent samples *t*-tests (***$p < 0.001$; **$p < 0.01$; *$p < 0.05$). QA, quantitative anisotropy; GFA, generalized FA; FA, fractional anisotropy; AD, axial diffusivity; HC, healthy control.

DISCUSSION

In this study, we explored the DSI parameters of trigeminal nerve in patients with TN and HCs. The results showed that QA, FA, and GFA on the affected side of individuals in the TN group decreased significantly, compared with the values on the unaffected side. On the affected side of individuals in the TN group, QA, FA, and GFA were significantly decreased and AD was significantly increased compared with the average values of HCs. There were significantly decreased QA and FA in the

TABLE 4 | Compared responsible vessel types and the unaffected side in patients.

	FA	*p*-value	GFA	*p*-value
Arteries ($n = 44$)	0.25990 ± 0.0461	0.028	0.06150 ± 0.0105	0.12
Veins ($n = 16$)	0.28971 ± 0.0435		0.06617 ± 0.0089	
Arteries ($n = 44$)	0.25990 ± 0.0461	0.065	0.06150 ± 0.0105	<0.001
Unaffected side ($n = 60$)	0.27640 ± 0.0435		0.07133 ± 0.0071	
Unaffected side ($n = 60$)	0.28971 ± 0.0435	0.281	0.06612 ± 0.0089	0.017
Veins ($n = 16$)	0.27640 ± 0.0435		0.07133 ± 0.0071	

FA, fractional anisotropy; GFA, general FA.
p-values were calculated with independent sample t-test.

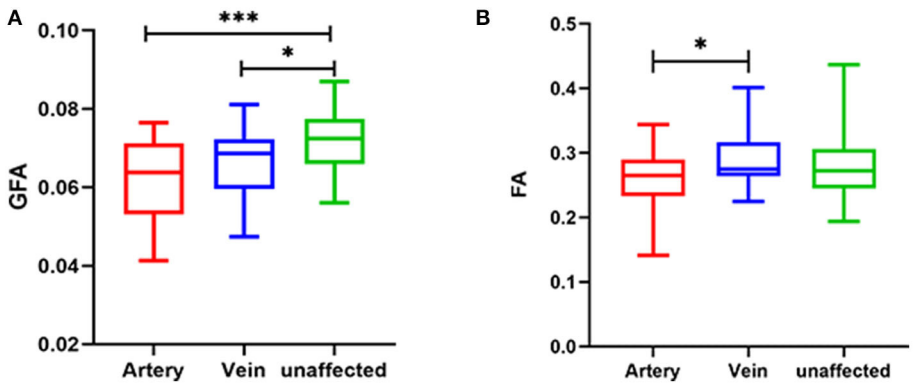

FIGURE 3 | Relationship between responsible vessel types and GFA value **(A)** and FA value **(B)** in TN patients (***$p < 0.001$; *$p < 0.05$). GFA, generalized FA; FA, fractional anisotropy; DSI, diffusion spectrum imaging.

TABLE 5 | Compare short-duration and long-duration groups.

	Patients ($n = 60$)		*p*-value
	Long duration ($n = 25$)	Short duration ($n = 35$)	
ISO	0.2766 ± 0.0494	0.3097 ± 0.0553	0.021
RDI	0.1625 ± 0.0345	0.1850 ± 0.0371	0.021

ISO, isotropic diffusion component; RDI, restricted diffusion imaging.
Short duration (symptom duration < 4 years), long duration (symptom duration ≥ 4 years).
p-values were calculated with independent sample t-test.

patient's unaffected side of patient than the average parameter values of HCs.

The etiology of primary TN is undefined. At present, the generally recognized theory is NVC. When the trigeminal nerve is compressed by blood vessels, the main cause of TN may be trigeminal nerve fiber bundle edema and demyelination (26). MVD well supports this theory. Routine MRI cannot suitably evaluate the integrity of trigeminal nerve white matter fiber bundle. Previous studies mostly used the traditional DTI method to study the white matter damage in patients with TN (27). Nevertheless, traditional DTI cannot accurately distinguish the cross fibers with limited angular resolution (28). In addition, DTI is affected by magnetic susceptibility artifact and partial volume average of complex fiber structure, which may lead to poor tracking (29).

In this study, we chose DSI instead of DTI to evaluate the damage of trigeminal nerve white matter fiber bundle. DSI has a longer acquisition time and provides more accurate quantitative details than DTI. DSI is a valuable tool for central nervous system imaging as it can be used to visualize the structural details of white matter bundles in multiple directions (14, 28–30). Similar to previous studies (6, 7), in our study, the FA value of trigeminal nerve on the affected side of TN patients was lower than that on the unaffected side and the decrease of FA value indicated that the integrity of white matter fiber bundle was damaged. However, in our study, AD, RD, and MD in the patient group did not increase significantly as previous studies. In this study,

we found that FA, QA, and GFA values of the affected side of TN patients were significantly lower than those of the unaffected side and HCs. GFA was sensitive to axonal properties such as the integrity of the axonal membrane and myelin (31), whereas Yeh et al. (25) suggested that QA was more robust to free water effect and partial volume of crossing fibers. In addition, QA is an anisotropy index similar to FA, but it is calculated for each orientation-distribution function peak in each voxel. The decrease of QA and GFA can both reflect the damage to white matter, similar to FA (25). In our study, the decrease of QA and GFA values in TN patients might have indicated incompleteness of axon structure.

Consistent with previous studies (6), our study found that the QA and FA values of the unaffected side of TN patients decreased compared with those of HCs. QA and FA decreased, indicating that the integrity of trigeminal nerve fibers on the unaffected side of TN patients was damaged. Therefore, there may be microstructural abnormalities in the trigeminal nervous system in individuals the TN group. TN patients may be sensitive to chronic pain due to pre-existing white matter abnormalities, which may explain why some people do not develop TN even if they have NVC. Because of the previous abnormalities of trigeminal nerve (such as high AD value and/or MD, RD value, and low FA value) (32), vascular compression is enough to cause TN, and there may be individual differences in susceptibility to chronic pain (6).

In our study, there were more patients with right TN than left TN, which was consistent with the results of previous studies (8, 26). The main responsible vessel type is the artery, especially the superior cerebellar artery (SCA), followed by the anterior inferior cerebellar artery (AICA) and the basilar artery, which is also consistent with the previous study (8, 26).

In the study of correlation with clinical symptoms, previous studies found that the decline rate of FA in DTI was significantly correlated with VAS scores, symptom duration, and responsible vessel types (11). Other studies showed that the decline of FA was negatively correlated with VAS and symptom duration (11). However, in this study, the difference scores of DSI parameters were not significantly correlated with VAS, symptom duration, and responsible vessel types. However, we found that artery GFA had the most significant decrease, followed by veins, compared with the unaffected side of individuals in the TN group. Previous studies have shown that trigeminal artery compression results in more obvious pain symptoms and more serious nerve injury than venous compression because the pulsation of the artery is better than that of the vein. Moreover, the calculation of GFA is based on the orientation distribution function (ODF), which accurately and sensitively reflects the integrity of axon or myelin sheath than FA value and is very sensitive to axon characteristics such as the integrity of axon membrane and myelin sheath (11). Regardless of the presence of artery or vein compression, the white matter fiber bundle of trigeminal nerve is damaged. The injury in fiber bundle might be minimally difference, but the edema caused by compression may be significantly different. Hence, FA might be showed different, while GFA is not divided. It might explain why GFA can evidently distinguish between arteries, veins, and the unaffected side in TN patients while FA not.

In our understanding, the longer the onset of pain symptoms takes, the longer the trigeminal nerve and vascular compression is. Then, damage to trigeminal nerve microstructure is more serious in patients with long symptom duration. However, our study showed that there was no significant difference in QA, GFA, and FA between the patients with long and short symptom duration. Previous animal studies (33) have proved that the supposed pulsatile nature of pathological vascular contact results in a process of demyelination and remyelination of the nerve root, rather than progressive demyelination. This process, together with the altered pain management threshold, is considered to be the cause of the typical paroxysmal rather than persistent pain syndrome in patients with TN. Based on this result, it can be assumed that the changes of parameters reflect the alternating process of demyelination and remyelination, rather than linear progressive demyelination.

Furthermore, our results showed that patients with long symptom duration had ISO and RDI decreased compared with that of patients with short symptom duration. The ISO is the minimum distribution value of an ODF. It represents background isotropic diffusion contributed from cerebrospinal fluid (CSF) or non-directional restricted diffusion (34). To separate restricted ISO from non-restricted ISO, a spectrum of RDI measures estimating restricted or non-restricted diffusion was used (18). We suggested that it was possibly caused by long-term microvascular compression, so that the intercellular space was smaller and the isotropic diffusion of water molecules was restricted. This finding may support NVC theory.

We acknowledge that our study has some limitations. First, there will be some differences in the results of manual tracking settings, including the position and size of ROIs, and the anisotropy threshold. Secondly, the sample size of a single center is relatively small, which may have limited the difference between groups of some parameters, thus hindering the realization of statistical significance to a certain extent. There are some methodological considerations in previous research, such as DTI vs. DSI, REZ vs. cisternal segment of nerve for the ROI placement, averaging control nerves vs. comparing to just one side etc. These methodological differences may also be a source of discrepancy between the current study and previous literature. The current study was a cross-sectional study. The longitudinal study of TN patients in the future will help to evaluate the prognosis of patients before operation and verify the accuracy of this study. In the future, we hope to include more samples for research.

CONCLUSION

We found that DSI parameters such as QA, GFA, FA decreased, and AD increased in TN patients. Moreover, GFA can evidently distinguish between arteries, veins, and the unaffected side in patients with TN. This findings reflects the change of trigeminal

nerve microstructure and fiber integrity, which helps us to better understand the mechanism of disease.

DATA AVAILABILITY STATEMENT

The raw data supporting the conclusions of this article will be made available by the authors, without undue reservation.

ETHICS STATEMENT

The studies involving human participants were reviewed and approved by Research Ethics Committee of the First Affiliated Hospital of Shenzhen University. The patients/participants provided their written informed consent to participate in this study.

AUTHOR CONTRIBUTIONS

S-pL, F-fC, FL, G-dH, and YL: manuscript editing. S-pL, F-fC, and FL: study conception/design, data analysis/interpretation and manuscript drafting, or revision for important intellectual content. S-pL and FL: literature research and data analysis. S-pL, F-fC, and H-wZ: data acquisition or clinical studies. All authors approval of final version of submitted manuscript and agrees to ensure any questions related to the work are appropriately resolved.

FUNDING

This study is supported by a grant from Basic Plan Program of Shenzhen, China (No. JCYJ20180228163333734).

REFERENCES

1. Lambru G, Zakrzewska J, Matharu M. Trigeminal neuralgia: a practical guide. *Pract Neurol.* (2021) 21:392–402. doi: 10.1136/practneurol-2020-002782
2. Sindou M, Brinzeu A. Topography of the pain in classical trigeminal neuralgia: insights into somatotopic organization. *Brain.* (2020) 143:531–40. doi: 10.1093/brain/awz407
3. Desouza D D, Hodaie M, Davis K D. Structural magnetic resonance imaging can identify trigeminal system abnormalities in classical trigeminal neuralgia. *Front Neuroanat.* (2016) 10:95. doi: 10.3389/fnana.2016.00095
4. Zhao G, Sun X, Zhang Z, Yang H, Zheng X, Feng B. Clinical efficacy of MVD combined with PSR in the treatment of primary trigeminal neuralgia. *Exp Ther Med.* (2020) 20:1582–8. doi: 10.3892/etm.2020.8871
5. Willsey MS, Collins KL, Conrad EC, Chubb HA, Patil PG. Diffusion tensor imaging reveals microstructural differences between subtypes of trigeminal neuralgia. *J Neurosurg.* (2019) 19:1–7. doi: 10.3171/2019.4.JNS19299
6. Desouza DD, Hodaie M, Davis KD. Abnormal trigeminal nerve microstructure and brain white matter in idiopathic trigeminal neuralgia. *Pain.* (2014) 155:37–44. doi: 10.1016/j.pain.2013.08.029
7. Chen ST, Yang JT, Weng HH, Wang HL, Yeh MY, Tsai YH. Diffusion tensor imaging for assessment of microstructural changes associate with treatment outcome at one-year after radiofrequency Rhizotomy in trigeminal neuralgia. *BMC Neurol.* (2019) 19:62. doi: 10.1186/s12883-019-1295-5
8. Lutz J, Thon N, Stahl R, Lummel N, Tonn JC, Linn J, et al. Microstructural alterations in trigeminal neuralgia determined by diffusion tensor imaging are independent of symptom duration, severity, and type of neurovascular conflict. *J Neurosurg.* (2016) 124:823–30. doi: 10.3171/2015.2.JNS142587
9. Lutz J, Linn J, Mehrkens JH, Thon N, Stahl R, Seelos K, et al. Trigeminal neuralgia due to neurovascular compression: high-spatial-resolution diffusion-tensor imaging reveals microstructural neural changes. *Radiology.* (2011) 258:524–30. doi: 10.1148/radiol.10100477
10. Chen F, Chen L, Li W, Li L, Xu X, Li W, et al. Pre-operative declining proportion of fractional anisotropy of trigeminal nerve is correlated with the outcome of micro-vascular decompression surgery. *BMC Neurol.* (2016) 16:106. doi: 10.1186/s12883-016-0620-5
11. Wu M, Qiu J, Jiang X, Li M, Wang SD, Dong Q, et al. Diffusion tensor imaging reveals microstructural alteration of the trigeminal nerve root in classical trigeminal neuralgia without neurovascular compression and correlation with outcome after internal neurolysis. *Magn Reson Imaging.* (2020) 71:37–44. doi: 10.1016/j.mri.2020.05.006
12. Jin Z, Bao Y, Wang Y, Li Z, Zheng X, Long S, et al. Differences between generalized Q-sampling imaging and diffusion tensor imaging in visualization of crossing neural fibers in the brain. *Surg Radiol Anat.* (2019) 41:1019–28. doi: 10.1007/s00276-019-02264-1
13. Hodgson K, Adluru G, Richards LG, Majersik JJ, Stoddard G, Adluru N, et al. Predicting motor outcomes in stroke patients using diffusion spectrum MRI microstructural measures. *Front Neurol.* (2019) 10:72. doi: 10.3389/fneur.2019.00072
14. Leng B, Han S, Bao Y, Zhang H, Wang Y, Wu Y, et al. The uncinate fasciculus as observed using diffusion spectrum imaging in the human brain. *Neuroradiology.* (2016) 58:595–606. doi: 10.1007/s00234-016-1650-9
15. Basser PJ. Inferring microstructural features and the physiological state of tissues from diffusion-weighted images. *NMR Biomed.* (1995) 8:333–44. doi: 10.1002/nbm.1940080707
16. Fritzsche KH, Laun FB, Meinzer HP, Stieltjes B. Opportunities and pitfalls in the quantification of fiber integrity: what can we gain from Q-ball imaging? *Neuroimage.* (2010) 51:242–51. doi: 10.1016/j.neuroimage.2010.02.007
17. Yeh FC, Wedeen VJ, Tseng WY. Generalized q-sampling imaging. *IEEE Trans Med Imaging.* (2010) 29:1626–35. doi: 10.1109/TMI.2010.2045126
18. Yeh FC, Liu L, Hitchens TK, Wu YL. Mapping immune cell infiltration using restricted diffusion MRI. *Magn Reson Med.* (2017) 77:603–12. doi: 10.1002/mrm.26143
19. Lin HY, Perry A, Cocchi L, Roberts JA, Tseng WI, Breakspear M, et al. Development of frontoparietal connectivity predicts longitudinal symptom changes in young people with autism spectrum disorder. *Transl Psychiatry.* (2019) 9:86. doi: 10.1038/s41398-019-0418-5
20. Wu CH, Hwang TJ, Chen PJ, Chou TL, Hsu YC, Liu CM, et al. Reduced structural integrity and functional lateralization of the dorsal language pathway correlate with hallucinations in schizophrenia: a combined diffusion spectrum imaging and functional magnetic resonance imaging study. *Psychiatry Res.* (2014) 224:303–10. doi: 10.1016/j.pscychresns.2014.08.010
21. Lin YC, Shih YC, Tseng WY, Chu YH, Wu MT, Chen TF, et al. Cingulum correlates of cognitive functions in patients with mild cognitive impairment and early Alzheimer's disease: a diffusion spectrum imaging study. *Brain Topogr.* (2014) 27:393–402. doi: 10.1007/s10548-013-0346-2
22. Romascano D, Meskaldji DE, Bonnier G, Simioni S, Rotzinger D, Lin YC, et al. Multicontrast connectometry: a new tool to assess cerebellum alterations in early relapsing-remitting multiple sclerosis. *Hum Brain Mapp.* (2015) 36:1609–19. doi: 10.1002/hbm.22698
23. Zhang Y, Zhang Z, Jia X, Guan X, Lyu Y, Yang J, et al. Imaging parameters of the ipsilateral medial geniculate body may predict prognosis of patients with idiopathic unilateral sudden sensorineural hearing loss on the basis of diffusion spectrum imaging. *AJNR Am J Neuroradiol.* (2021) 42:152–9. doi: 10.3174/ajnr.A6874
24. Yoshino M, Abhinav K, Yeh FC, Panesar S, Fernandes D, Pathak S, et al. Visualization of cranial nerves using high-definition fiber tractography. *Neurosurgery.* (2016) 79:146–65. doi: 10.1227/neu.0000000000001241
25. Yeh FC, Verstynen TD, Wang Y, Fernández-Miranda JC, Tseng WY. Deterministic diffusion fiber tracking improved by quantitative anisotropy. *PLoS ONE.* (2013) 8:e80713. doi: 10.1371/journal.pone.0080713

26. Chai W, You C, Zhang W, Peng W, Tan L, Guan Y, et al. Diffusion tensor imaging of microstructural alterations in the trigeminal nerve due to neurovascular contact/compression. *Acta Neurochir (Wien).* (2019) 161:1407–13. doi: 10.1007/s00701-019-03851-2
27. Moon HC, You ST, Baek HM, Jeon YJ, Park CA, Cheong JJ, et al. 7.0 Tesla MRI tractography in patients with trigeminal neuralgia. *Magn Reson Imaging.* (2018) 54:265–70. doi: 10.1016/j.mri.2017.12.033
28. Wedeen VJ, Wang RP, Schmahmann JD, Benner T, Tseng WY, Dai G, et al. Diffusion spectrum magnetic resonance imaging (DSI) tractography of crossing fibers. *Neuroimage.* (2008) 41:1267–77. doi: 10.1016/j.neuroimage.2008.03.036
29. Bao Y, Wang Y, Wang W, Wang Y. The superior fronto-occipital fasciculus in the human brain revealed by diffusion spectrum imaging tractography: an anatomical reality or a methodological artifact? *Front Neuroanat.* (2017) 11:119. doi: 10.3389/fnana.2017.00119
30. Wu Y, Sun D, Wang Y, Wang Y, Wang Y. Tracing short connections of the temporo-parieto-occipital region in the human brain using diffusion spectrum imaging and fiber dissection. *Brain Res.* (2016) 1646:152–9. doi: 10.1016/j.brainres.2016.05.046
31. Tuch DS. Q-ball imaging. *Magn Reson Med.* (2004) 52:1358–72. doi: 10.1002/mrm.20279
32. Holliday KL, Mcbeth J. Recent advances in the understanding of genetic susceptibility to chronic pain and somatic symptoms. *Curr Rheumatol Rep.* (2011) 13:521–7. doi: 10.1007/s11926-011-0208-4
33. Apfelbaum RI. Neurovascular decompression: the procedure of choice? *Clin Neurosurg.* (2000) 46:473–98.
34. Li TY, Chen VC, Yeh DC, Huang SL, Chen CN, Chai JW, et al. Investigation of chemotherapy-induced brain structural alterations in breast cancer patients with generalized q-sampling MRI and graph theoretical analysis. *BMC Cancer.* (2018) 18:1211. doi: 10.1186/s12885-018-5113-z

Conflict of Interest: The authors declare that the research was conducted in the absence of any commercial or financial relationships that could be construed as a potential conflict of interest.

frontiers in Neurology

ORIGINAL RESEARCH
published: 17 March 2022
doi: 10.3389/fneur.2022.835050

Alterations of the White Matter in Patients With Knee Osteoarthritis: A Diffusion Tensor Imaging Study With Tract-Based Spatial Statistics

Shirui Cheng[1†], Xiaohui Dong[1†], Jun Zhou[1†], Chenjian Tang[2], Wenhua He[3], Yang Chen[1], Xinyue Zhang[1], Peihong Ma[4], Tao Yin[1], Yimei Hu[5], Fang Zeng[1], Zhengjie Li[1] and Fanrong Liang[1*]*

[1] The Acupuncture and Tuina School, Chengdu University of Traditional Chinese Medicine, Chengdu, China, [2] The First Affiliated Hospital, Chengdu University of Traditional Chinese Medicine, Chengdu, China, [3] The Second Affiliated Hospital of Shanxi, University of Traditional Chinese Medicine, Taiyuan, China, [4] Acupuncture and Moxibustion Department, Beijing University of Chinese Medicine, Beijing, China, [5] Clinical Medical School, Chengdu University of Traditional Chinese Medicine, Chengdu, China

Background: Functional and structural alterations in the gray matter have been observed in patients with knee osteoarthritis (KOA). However, little is known about white matter changes in KOA. Here, we evaluated fractional anisotropy (FA), mean diffusivity (MD), axial diffusivity (AD), and radial diffusivity (RD) to investigate potential alterations in the white matter of patients with KOA.

Methods: A total of 166 patients with KOA, along with 88 age- and sex-matched healthy controls were recruited and underwent brain magnetic resonance imaging (MRI). Diffusion tensor imaging (DTI) data were collected and analyzed using tract-based spatial statistics (TBSS). Statistical significances were determined at $p < 0.05$ and were corrected by the threshold-free cluster enhancement (TFCE) method. Then, we evaluated potential correlations between FA, MD, AD, RD values and disease duration, Western Ontario and McMaster Universities Osteoarthritis Index (WOMAC) scores, and visual analog scale (VAS) scores.

Results: FA values for the body of corpus callosum, splenium of corpus callosum, bilateral superior longitudinal fasciculus, cingulum, bilateral superior corona radiata, and right posterior corona radiata were significantly higher in patients with KOA than in healthy controls ($p < 0.05$, TFCE corrected). Compared with healthy controls, patients with KOA also had significantly lower MD, AD, and RD values of the genu of corpus callosum, body of corpus callosum, splenium of corpus callosum, corona radiata, right posterior thalamic radiation, superior longitudinal fasciculus, and middle cerebellar peduncle ($p < 0.05$, TFCE corrected). Negative correlations were detected between WOMAC scores and AD values for the body of the corpus callosum and the splenium of the corpus callosum ($p < 0.05$, FDR corrected).

Edited by:
Lingmin Jin,
Guizhou University of Traditional Chinese Medicine, China

Reviewed by:
Yuanqiang Zhu,
Fourth Military Medical University, China
Shaoqiang Han,
First Affiliated Hospital of Zhengzhou University, China
Kai Yuan,
Xidian University, China

***Correspondence:**
Zhengjie Li
lzjbenjamin@163.com
Fanrong Liang
acuresearch@126.com

[†] These authors have contributed equally to this work and share first authorship

Specialty section:
This article was submitted to Headache and Neurogenic Pain, a section of the journal Frontiers in Neurology

Received: *14 December 2021*
Accepted: *24 January 2022*
Published: *17 March 2022*

Citation:
Cheng S, Dong X, Zhou J, Tang C, He W, Chen Y, Zhang X, Ma P, Yin T, Hu Y, Zeng F, Li Z and Liang F (2022) Alterations of the White Matter in Patients With Knee Osteoarthritis: A Diffusion Tensor Imaging Study With Tract-Based Spatial Statistics. Front. Neurol. 13:835050. doi: 10.3389/fneur.2022.835050

Conclusion: Patients with KOA exhibited extensive white matter alterations in sensorimotor and pain-related regions. Longitudinal observation studies on the causation between abnormalities in the white matter tracts and KOA is needed in the future.

Keywords: knee osteoarthritis (KOA), diffusion tensor imaging, white matter, tract-based spatial statistics, neuroimaging

INTRODUCTION

Osteoarthritis (OA) is a common cause of pain and disability in the elderly (1) and predominantly affects the knee joint (2). Knee osteoarthritis (KOA) affects at least 15–18% of people globally (3), reduces multiple facets of the quality of life (QOL), and induces an enormous healthcare burden in industrialized societies (4). The risk factors for developing knee osteoarthritis are age, obesity, and articular malalignment (2). According to clinical guidelines, the first therapeutic principle for is to relieve knee pain (5). However, the pathology of KOA is not well-understood, thus restricting the development of specific therapeutic protocols for clinical practice.

It is generally believed that the key factor underlying KOA is inflammation due to the breakdown of joint tissues from mechanical loading, aging, or other factors (6, 7). However, these peripheral abnormalities do not fully account for the intensity of pain in patients with chronic musculoskeletal pain (8) because substantial discordance exists between radiographic OA of the knee when compared to knee pain (9, 10). With the development of neuroimaging techniques, researchers have found that the central neural system plays a key role in KOA (11). For example, several recent studies reported abnormal functions of the gray matter in the lateral prefrontal cortex, parietal lobule, anterior cingulate cortex, insula and limbic cortical, which were involved in altered pain processing in KOA patients (12–14). These findings were further validated by the observation of structural changes in the gray matter in other neuroimaging studies (15, 16). Given that the observed alterations in the structure and function of the gray matter arise from the adaption or maladaption of the brain to certain conditions such as prolonged nociceptive input from chronic knee pain, it is reasonable to hypothesize that the white matter could also be affected by this condition. However, little is known about white matter alterations in patients with KOA.

Diffusion tensor imaging (DTI) can provide significant insight into the diffusion of water molecules and thus quantify microstructural alterations within the white matter (17, 18). Tract-based spatial statistics (TBSS) is the most common method used to analyze DTI data (19) and includes four metrics: fractional anisotropy (FA), axial diffusivity (AD), radial diffusivity (RD), and mean diffusivity (MD). FA, as a marker of axonal membrane circumference and packing density, reflects the orientation and distribution of the random movements of water-molecules (20). AD can reflect diffusional directionality along axons and is related to the degree of myelination in the white matter (21). RD can characterize the diffusional directionality perpendicular to axons and is related to the beginning of demyelination (22) or axonal damage (20). MD reflects the diffusion magnitude; this is related to inflammation and edema in the white matter tracts (20). DTI and TBSS have been used wildly for detecting abnormal white matter in various disorders, such as schizophrenia spectrum disorders (23), chronic back pain (24), osteoarthritis (13, 14), and fibromyalgia syndrome (FMS) (25). In this study, we used the whole-brain TBSS method to investigate potential differences in the white matter tracts of patients with KOA and compared data with that derived from healthy controls (HCs). We also correlated abnormal FA, MD, AD, and RD values with clinical variables in patients with KOA to assess the clinical meaning of our findings.

MATERIALS AND METHODS

Participants

Patients with a diagnosis of KOA at three hospitals (The First Affiliated Hospital of Chengdu University of Traditional Chinese Medicine, the Third Affiliated Hospital of Chengdu University of Traditional Chinese Medicine, and the Orthopedic Hospital of Sichuan Province) were enrolled from September 2016 to September 2021. Brain magnetic resonance imaging (MRI) scans were obtained on a GE 3.0T MRI scanner (GE 3.0T MR750, Wauwatosa, WI) using a 16-channel head coil in Chengdu, China. Age- and sex-matched HCs were also recruited. This study was carried out in accordance with the Declaration of Helsinki and was approved by the Institutional Review Board and Ethics Committees of the First Affiliated Hospital of Chengdu University of Traditional Chinese Medicine (No. 2016KL-017).

The diagnostic symptoms and signs of KOA patients were assessed by two experienced orthopedists according to the American College of Rheumatology (ACR) criteria (26). Patients with KOA were recruited if they met the following inclusion criteria: (a) aged from 38 to 70 years and right-handed; (b) were diagnosed with KOA; (c) had a pain intensity >3 on a

Abbreviations: 3DT1, three-dimensional T1-weighted; ACC, anterior cingulate cortex; ACR, American College of Rheumatology; AD, axial diffusivity; BET, brain extraction tool; BMI, body mass index; CC, corpus callosum; CRPS, chronic complex regional pain syndrome; DTI, diffusion tensor imaging; FA, fractional anisotropy; FDR, false discovery rates method; FDT, FMRIB's diffusion toolbox; FMS, fibromyalgia syndrome; FOV, field of view; GMV, gray matter volume; HC, healthy control; IBS, irritable bowel syndrome; KOA, knee osteoarthritis; LPFC, lateral prefrontal cortex; MD, mean diffusivity; MITN, midline and intralaminar thalamic nuclei; MRI, magnetic resonance imaging; OA, osteoarthritis; OFC, orbital frontal cortex; PFC, prefrontal cortex; QOL, quality of life; RD, radial diffusivity; TR, repetition time; SAS, self-rating anxiety scale; SDS, self-rating depression scale; SLF, superior longitudinal fasciculus; TBSS, tract-based spatial statistics; TE, echo time; TFCE, threshold-free cluster enhancement; VAS, visual analogue scale; WOMAC, Western Ontario and McMaster Universities Osteoarthritis Index.

10-point numeric scale; (d) had a knee joint radiological degree on the Kellgren-Lawrence scale of 0-II (27); and (e) had signed a written and informed consent form. Patients with KOA were excluded if they (a) had other major painful, psychiatric, or neurological diseases; (b) had drug or alcohol addiction; (c) had contraindications for MRI scans; (d) had taken any pain killer medicine or complementary and alternative therapies within the previous month; or (e) were pregnant or lactating.

HCs were recruited if they met the following inclusion criteria: (a) aged from 38 to 70 years and right-handed; (b) were free from any pain disorders; and (c) signed the written and informed consent form. HCs were excluded if they met the following exclusion criteria: (a) accompanied by rheumatoid arthritis, high blood pressure, diabetes, or psychiatric or neurological diseases; (b) had drug or alcohol addiction; (c) had contraindications for MRI scans; (d) had taken any medicine or complementary and alternative therapies within the previous month; or (e) were pregnant or lactating.

Clinical Data Acquisition

A range of data were collected for each patient, including age, gender, height, weight, education level, and disease duration. The average intensity of pain over the previous 2 weeks was also obtained from all KOA participants using the visual analog scale (VAS). The Western Ontario and McMaster Universities Osteoarthritis Index (WOMAC) was used to assess the symptoms and QOL of the KOA patients. Anxiety and depression were evaluated in the KOA patients by using the validated Chinese version of the self-rating anxiety scale (SAS) and self-rating depression scale (SDS). The VAS, WOMAC, SAS, and SDS assessments were administered on the same day when the MRI scan was performed.

Image Acquisition

Brain MRI scanning sequences including three-dimensional T1-weighted (3DT1) MRI scans and diffusion-weighted DTI sequence with single-shot echo-planar imaging were performed for all participants at baseline. The parameters of the 3DT1 scans were as follows: repetition time (TR) = 6.008 ms, echo time (TE) = 1.7 ms, data matrix = 256 × 256, field of view (FOV) = 256 × 256 mm^2, and voxel size = 1.0 × 1.0 × 1.0 mm^3. The parameters of DTI scans were: FOV = 256 × 256 mm^2, TR = 8,500 ms, echo time = minimum, matrix = 128 × 128, number of diffusion-encoding directions = 64, slice thickness 2 mm, layer spacing = 0, and gradient values b = 0 s/mm^2 and b = 1,000 s/mm^2.

Diffusion Data Process

DTI data preprocessing and statistical analysis were conducted using the FMRIB software library (FSL; http://www.fmrib.ox.ac.uk/fsl/) (28). Data preprocessing steps included correction for eddy current effects and head motion using FDT (FMRIB's Diffusion Toolbox), extraction of the brain mask with FSL's brain extraction tool (BET), and the calculation of diffusion tensors by the DTIFIT program. After preprocessing, tract-based spatial statistical analysis was performed, including non-linear registration of each participant's FA image to a 1 × 1 × 1 mm^3 standard space of the FMRIB58-FA template. These images were affine co-registered to the MNI152 standard space, and tracts were averaged to create a mean FA skeleton, extracting the FA skeleton, and projecting each participant's aligned FA image back onto the mean FA skeleton with a 0.2 FA threshold. The MD, AD, and RD images of individual participants were also projected onto the mean FA skeleton.

Statistical Analysis

Statistical comparison of the clinical data between patients with KOA and HCs was performed using SPSS Statistics version 22.0 (IBM Corp., Armonk, NY). Age and body mass index (BMI) were compared between the two groups using a non-parametric test. Gender distribution was analyzed between the two groups using the *chi*-squared test.

Voxel-brain skeletal FA, MD, AD, and RD analysis was performed between the KOA patients and HCs using a general linear model through the FSL randomize toolkit. Age, gender, and BMI were used as covariates. A 5,000-repetition permutation test was conducted between the KOA patients and HCs, and significant clusters were corrected by the threshold-free cluster enhancement method (TFCE, $p < 0.05$). After correction, only clusters with voxel size >100 were reported (29). JHU ICBM-DTI-81 White-Matter Labels in FSL were used to identify white matter tracts showing significant alterations. Spearman's correlation analysis was conducted between the FA, MD, AD, and RD values of significant clusters and a range of clinical characteristics including disease duration, VAS scores, and WOMAC scores, which were corrected by the false discovery rates method (FDR, $p < 0.05$).

RESULTS

Clinical Characteristics

A total of 166 patients with a diagnosis of KOA (125 females, age range: 39–67 years, mean ± SD: 52.87 ± 5.23 years) and 88 HCs (56 females, age range: 42–62 years, mean ± SD: 53.76 ±

TABLE 1 | Clinical and demographic characteristics of KOA and HC.

Items	KOA (n = 166)	HS (n = 88)	P-value
Age (years)	52.87 ± 5.23	53.76 ± 4.82	0.110
Gender (female/male)	125/41	56/32	0.051
BMI (kg/m^2)	23.95 ± 2.85	23.85 ± 2.80	0.843
Duration (months)	45.95 ± 50.18	–	–
WOMAC	35.73 ± 28.63	–	–
VAS	4.31 ± 1.31	–	–
SAS	35.96 ± 8.03	–	–
SDS	30.97 ± 5.83	–	–

Data were expressed as the Mean ± SD. BMI, body mass index; HC, health control; KOA, knee osteoarthritis; SAS, self-rating anxiety scale; SDS, self-rating depression scale; VAS, visual analog scale; WOMAC, Western Ontario and McMaster Universities Osteoarthritis Index.

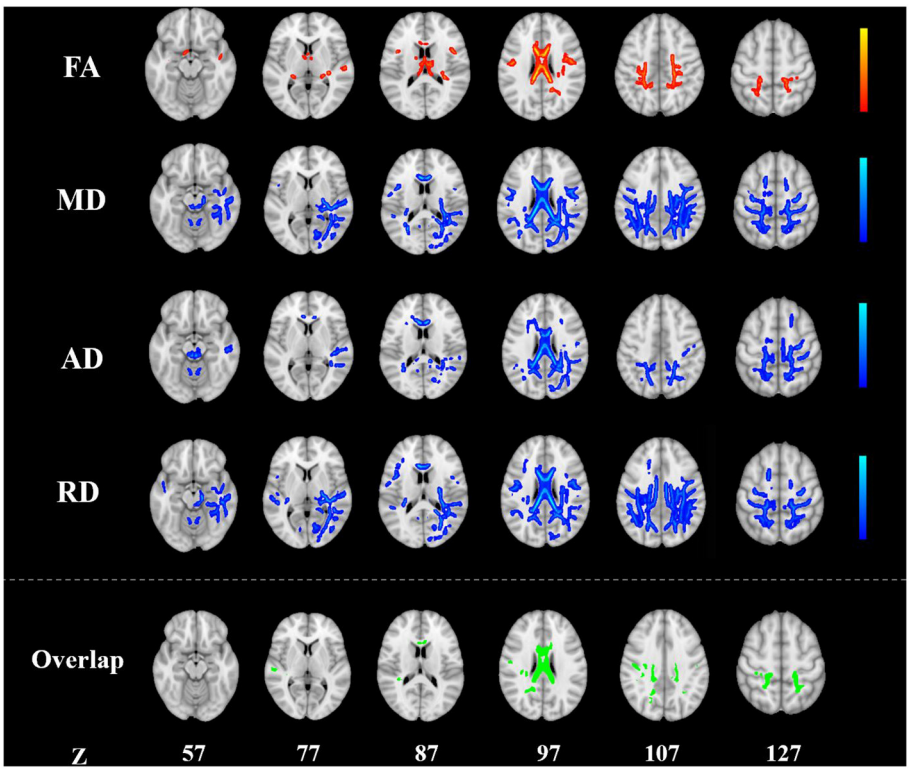

FIGURE 1 | Alterations in TBSS parameters in patients with KOA. White matter regions showing increased FA and decreased MD, AD, and RD values in patients with KOA compared to healthy controls. White matter regions showing overlapping FA, MD, AD, and RD values in the body, the splenium of the corpus callosum ($p < 0.05$, TFCE corrected). AD, radial diffusivity; FA, fractional anisotropy; KOA, knee osteoarthritis; MD, mean diffusivity; RD, radial diffusivity; TBSS, tract-based spatial statistics; TFCE, threshold-free cluster enhancement.

4.82 years) were recruited in this study. There were no significant differences between the two groups in terms of age, gender, and BMI ($p > 0.05$). The mean duration of patients with KOA was 45.95 ± 50.18 months (range: 1–241 months) and the mean WOMAC and VAS scores of patients with KOA were 35.73 ± 28.63 and 4.31 ± 1.31, respectively. The demographic and clinical data of the KOA patients and HCs are summarized in **Table 1**.

Tract-Based Spatial Statistics Analysis

Compared with HCs, patients with KOA showed a significant increased FA in the body of the corpus callosum (CC), splenium of CC, bilateral superior corona radiata, right posterior corona radiata, bilateral superior longitudinal fasciculus (SLF), left cingulum (cingulate gyrus), and bilateral fornix/stria terminalis ($p < 0.05$, TFCE corrected; **Figure 1**; **Table 2**).

The MD was significantly reduced in the middle cerebellar peduncle, genu of CC, body of CC, splenium of CC, right cerebral peduncle, right posterior limb of internal capsule, right retrolenticular part of the internal capsule, bilateral superior corona radiata, bilateral posterior corona radiata, right posterior thalamic radiation, right sagittal stratum, right external capsule, left cingulum (cingulate gyrus), right cingulum (hippocampus), and bilateral SLF in KOA patients ($p < 0.05$, TFCE corrected; **Figure 1**; **Table 2**).

KOA patients had a reduced AD in the middle cerebellar peduncle, pontine corticospinal tract, genu of CC, body of CC, splenium of CC, right corticospinal tract, bilateral medial lemniscus, bilateral inferior cerebellar peduncle, bilateral superior cerebellar peduncle, left anterior corona radiata, right superior corona radiata, bilateral posterior corona radiata, right posterior thalamic radiation, and right SLF ($p < 0.05$, TFCE corrected; **Figure 1**; **Table 2**).

The RD of the middle cerebellar peduncle, genu of CC, body of CC, splenium of CC, right cerebral peduncle, right posterior limb of internal capsule, bilateral retrolenticular part of the internal capsule, bilateral superior corona radiata, bilateral posterior corona radiata, right posterior thalamic radiation, right sagittal stratum, right external capsule, bilateral cingulum (cingulate gyrus), right cingulum (hippocampus), right fornix/stria terminalis, and bilateral SLF was also significantly reduced in patients with KOA ($p < 0.05$, TFCE corrected; **Figure 1**; **Table 2**).

The overlapping white matter tracts of the FA, MD, AD, and RD were the body of CC and splenium of CC (**Figure 1**; **Table 2**). Using education level, SAS and SDS scores as covariates for further analysis did not change these results above with respect to only age, gender, and BMI as covariates.

TABLE 2 | Regions with significantly increased FA and decreased MD, AD, and RD in patients with KOA.

WM (JHU WM)		Cluster size				
		FA	MD	AD	RD	Overlap
Middle cerebellar peduncle		–	905	1,068	1,179	–
Pontine crossing tract (a part of MCP)		–	–	202	–	–
Genu of corpus callosum		–	396	511	258	–
Body of corpus callosum		1,469	2,764	1,882	2,532	953
Splenium of corpus callosum		156	1,113	995	867	119
Fornix (column and body of fornix)		152	–	–	–	–
Corticospinal tract	R	–	–	131	–	–
Medial lemniscus	R	–	–	177	–	–
Medial lemniscus	L	–	–	108	–	–
Inferior cerebellar peduncle	R	–	–	154	–	–
Inferior cerebellar peduncle	L	–	–	161	–	–
Superior cerebellar peduncle	R	–	–	115	–	–
Superior cerebellar peduncle	L	–	–	131	–	–
Cerebral peduncle	R	–	203	–	283	–
Posterior limb of internal capsule	R	–	349	–	361	–
Retrolenticular part of internal capsule	R	–	641	–	661	–
Retrolenticular part of internal capsule	L	–	–	–	189	–
Anterior corona radiata	L	–	–	152	–	–
Superior corona radiata	R	146	566	143	601	
Superior corona radiata	L	139	141	–	318	–
Posterior corona radiata	R	151	736	493	524	
Posterior corona radiata	L	–	443	161	378	–
Posterior thalamic radiation (include optic radiation)	R	–	745	152	773	–
Sagittal stratum (include inferior longitudinal fasciculus and inferior fronto-occipital fasciculus)	R	–	264	–	232	–
External capsule	R	–	113	–	137	–
Cingulum (cingulate gyrus)	R	–	–	–	180	–
Cingulum (cingulate gyrus)	L	233	104	–	386	–
Cingulum (hippocampus)	R	–	113	–	180	–
Fornix (cres) / Stria terminalis	R	223	274	–	249	–
Fornix (cres) / Stria terminalis	L	143	–	–	–	–
Superior longitudinal fasciculus	R	516	1,170	296	1,073	–
Superior longitudinal fasciculus	L	100	292	–	558	–

$p < 0.05$, TFCE corrected. AD, radial diffusivity; FA, fractional anisotropy; JHU WM, JHU ICBM-DTI-81 White-Matter Labels; KOA, knee osteoarthritis; L, left; MCP, middle cerebellar peduncle; MD, mean diffusivity; R, right; RD, radial diffusivity; WM, white matter.

Correlations Between White Matter Tracts and Clinical Characteristics

For the KOA group, AD values of the body of CC ($r = -0.249$, $p = 0.0098$; FDR corrected) and the splenium of CC ($r = -0.201$, $p = 0.0489$; FDR corrected) were correlated with WOMAC scores (**Figure 2**). None of the FA, MD, and RD metrics in any of the brain tracts was related with WOMAC, VAS scores, disease duration, SAS, or SDS ($p > 0.05$, FDR corrected).

DISCUSSION

This study featured a large sample size and used TBSS analysis to investigate alterations in the white matter of patients with KOA. Several regions in patients with KOA showed increased FA, and decreased MD, AD, and RD values when compared with HCs, including the CC, corona radiata, longitudinal fasciculus, cingulum, and thalamic radiation (**Figure 1**; **Table 2**). In patients with KOA, the AD values of the body of CC and splenium of CC were both correlated with WOMAC scores (**Figure 2**). These results reflected global white matter alterations in the KOA patients. To our knowledge, this is the first DTI study to detect alterations in the white matter of neural pathways in patients with KOA.

Functional changes in the regions of the brain responsible for perception, affection, and cognition have been detected in OA patients (12–14). These alterations in functional plasticity are often accompanied by gray matter remodeling

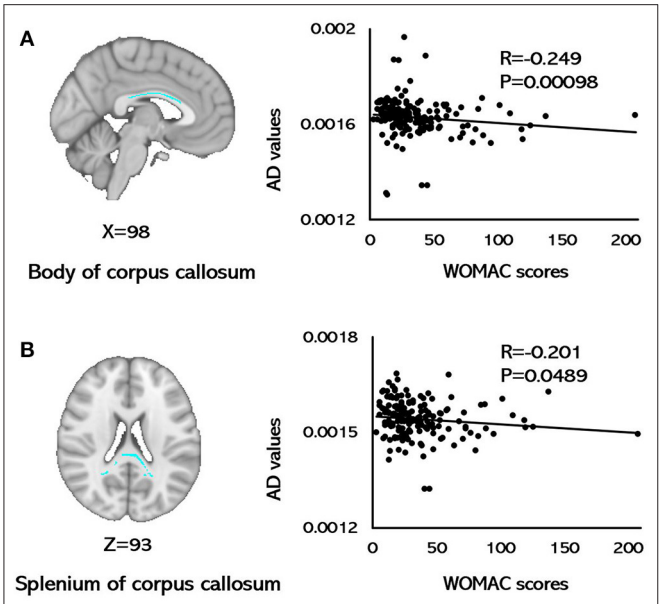

FIGURE 2 | Correlations between AD values and WOMAC scores. **(A)** A negative correlation was observed between AD values for the body of the corpus callosum and WOMAC scores. **(B)** A negative correlation was observed between the AD values for the splenium of the corpus callosum and WOMAC scores ($p < 0.05$, FDR corrected). AD, axial diffusivity; FDR, false discovery rates; WOMAC, Western Ontario and McMaster Universities Osteoarthritis Index.

and reorganization of the neurons, axons, and circuits (30, 31), further inducing the development and persistence of chronic pain (32). Furthermore, decreased gray matter volume (GMV) has been detected in the anterior cingulate cortex (ACC), orbital frontal cortex (OFC), lateral prefrontal cortex (PFC), precentral cortex, postcentral cortex, caudate nucleus, hippocampus, insula, thalamus, and amygdala of patients with OA (15, 16, 33). In this study, we found alterations in the white matter tracts of the CC, cingulum (cingulate gyrus), corona radiata, and superior longitudinal fasciculus in patients with KOA. These are all important components of the somatosensory and pain-related pathways and participate in the central integration and modulation of various peripheral perceptions, cognition, and emotion of pain (34).

The corpus callosum is the largest fiber tract and acts as a bridge for communicating perceptual, cognitive, volitional, and motor information between the two hemispheres (35, 36), and features prefrontal axons crossing the midline in the genu of the CC, somatosensory and motor axons crossing in the body of CC, and occipital and temporal axons crossing the midline in the splenium of CC (37). In the present study, we found that abnormal microstructure of the white matter spanned the length of the corpus callosum, thus suggesting alterations in the integration of cognitive, sensory, and motor information in KOA patients. Previous studies detected abnormal gray matter function and volume in the prefrontal, sensory, and cognitive regions in OA patients (12–16). Alterations in the CC connecting the sensory gyri might reflect an abnormal amount of nociceptive information entering the central nervous system from the peripheral nervous system. These alterations in motor integration may result from the evasive action evoked by KOA patients to lessen or avoid knee pain. The results of our study are in line with several other whole-brain TBSS studies which also found the abnormalities of the CC in patients with chronic pain diseases (25, 36, 38, 39). Furthermore, the AD values for the body of CC and the splenium of CC were negatively correlated with WOMAC scores in patients with KOA. Peripheral pathological pain is associated with persistent traumatic stimuli to the central nervous system and may be the microstructural basis for central sensitization, thus leading to central neuroinflammatory processes and edema (40, 41). Therefore, this correlation suggested that the integrity and neurofilament phosphorylation of axons in the CC may mediate individual variations in the clinical knee pain of patients with KOA. Abnormalities in the CC may be the specific indicator of maladaptive plastic modifications in KOA patients and CC-mediated interhemispheric connections might contribute to clinical sensory pain (42).

In the present study, we also detected an abnormal white matter microstructure in the corona radiata of patients with KOA. The corona radiata starts from the inner capsule and connects to the inferior frontal-orbital cortex and ACC, which is responsible for emotional expression and cognitive processing transmission between the brain hemispheres (43). Significant abnormalities in the corona radiata have been found in other chronic pain diseases, such as trigeminal neuralgia (39), chronic migraine (44), and chronic complex regional pain syndrome (CRPS) (45). These findings might suggest that there are abnormalities of emotional regulation in patients with chronic pain.

Increased FA values and decreased MD, AD, and RD values of the SLF were also found in patients with KOA in this study. Several previous studies have reported alterations in gray matter and abnormal functional brain activity in the insula, bilateral precentral gyrus, and frontal cortex in patients with chronic pain diseases, including chronic back pain (24), osteoarthritis (13, 14), and fibromyalgia syndrome (FMS) (25). Pain perception is mostly projected to the primary and secondary somatosensory areas, including the postcentral gyrus, paracentral lobule, precentral gyrus, and insula through the SLF (46). Furthermore, alterations in the microstructure of the white matter in the corticospinal tract were found in patients with KOA. The motor cortex may reduce the intensity of pain perception through the corticospinal tract; these represent the output pathway from cortical motor efferent to the descending pain modulatory system (47).

The cingulum is an important white matter pathway located within the limbic system (48). The midline and intralaminar thalamic nuclei (MITN) receive differing amounts of the spinothalamic tract, the pronociceptive sub-nucleus reticularis dorsalis, the parabrachial nucleus inputs, and project to the cingulate gyrus through the cingulum (49–51). In this study, microstructural alterations were mostly involved in the cingulum (cingulate gyrus) and cingulum (hippocampus). Persistent perceptive signals of

pain lead to increased connections between the cingulum-hippocampal tract and default network, thus leading to the impairments in the avoidance behaviors provoked by OA (48).

Findings from TBSS studies of patients with chronic pain diseases are controversial (38, 52–55). In patients with pediatric migraine, carpal tunnel syndrome, and neuromyelitis optica spectrum disorders with neuropathic pain, the FA values were increased (53–55). Patients with idiopathic trigeminal neuralgia were found to have a lower FA, along with an increased MD, AD, and RD, in the white matter of connecting areas (52), while patients with migraine without aura showed lower MD and AD values in multiple white matter tracts of the brain (38). In the present study, we observed increased FA values but reduced MD, AD, and RD values in several white matter tracts in patients with KOA. There are several factors that may responsible for such discordances, including different kinds of diseases and subjects, sample sizes, research methods, scanning parameters, and statistical approach. Furthermore, the intensity and persistency of pain has been proven to be related with morphological and functional brain regions in patients with OA (12, 14). In this study, the mean VAS score of KOA patients was 4.31, which may have a milder effect on white matter than patients with a high intensity of pain. Also, we should consider that changes in neural expression of the white matter of patients with KOA might be related to a longer disease duration and concomitant neuroplasticity (40, 56). In this study, the mean disease duration of KOA was about 46 months. It is possible that central nervous system plasticity may have occurred after nerve impairment (56, 57). These changes in structural plasticity help pain-related learning and memory and may further contribute to the development of chronic pain or minimize the effects of pain on the body (57). In summary, the reasons for the controversial values of FA, MD, AD, and RD in white matter tracts reported in this study may be related to abnormal axonal integrity (axonal loss or the loss of bundle coherence) (58, 59), neural regeneration, and plasticity (56, 57).

There are several limitations in this study that need to be considered. First, this was a preliminary study relating to abnormalities of the white matter in patients with KOA compared with healthy controls. Second, correlations between the injury condition of the local knee joints and white matter alternations in KOA patients has not been identified. Third, the causation between alterations in the white matter tracts and KOA has yet to be elucidated. Longitudinal observation studies on the relationships between abnormalities in the white matter tracts and KOA need to be identified in further study.

CONCLUSION

Patients with KOA showed extensive alterations in the white matter of the CC, corona radiata, longitudinal fasciculus, cingulum, and thalamic radiation. Furthermore, the AD values of the body and the splenium of CC were correlated with WOMAC scores in patients with KOA. Longitudinal observation studies on the causation between abnormalities in the white matter tracts and KOA are needed in the future.

DATA AVAILABILITY STATEMENT

The raw data supporting the conclusions of this article are available from the corresponding authors on reasonable request.

ETHICS STATEMENT

The studies involving human participants were reviewed and approved by Institutional Review Board and Ethics Committees of the First Affiliated Hospital of Chengdu University of Traditional Chinese Medicine (No. 2016KL-017). The patients/participants provided their written informed consent to participate in this study.

AUTHOR CONTRIBUTIONS

FL, ZL, and FZ participated in the conception and design of the trial. SC, XD, JZ, CT, WH, and YC acquired the data. SC, XD, JZ, and XZ collated and analyzed the data. SC, XD, and JZ participated in drafting the manuscript. All authors contributed to the article and approved the submitted version.

FUNDING

This work was supported by the National Natural Science Foundation of China (No. 81774400, 81973958, 81603708), Innovation Team and Talents Cultivation Program of National Administration of Traditional Chinese Medicine (No. ZYYCXTD-D-202003), China Postdoctoral Science Foundation (No. 2017M6100593, 2018T110954, PC2019012, 2021MD703796), and Medical Technology Project of Health Commission of Sichuan Province (No. 21PJ110).

ACKNOWLEDGMENTS

We thank all the subjects who participated in this study. We especially thank Professor *Yong Huang* and Dr. *Xuefei Qin* for their kind help in participant enrollment.

REFERENCES

1. Vos T, Flaxman AD, Naghavi M, Lozano R, Michaud C, Ezzati M, et al. Years lived with disability (YLDs) for 1160 sequelae of 289 diseases and injuries 1990-2010: a systematic analysis for the global burden of disease study 2010. *Lancet.* (2012) 380:2163–96. doi: 10.1016/s0140-6736(12)61729-2
2. Cao P, Li Y, Tang Y, Ding C, Hunter DJ. Pharmacotherapy for knee osteoarthritis: current and emerging therapies. *Expert Opin Pharmacotherapy.* (2020) 21:797–809. doi: 10.1080/14656566.2020.1732924
3. Wallace IJ, Worthington S, Felson DT, Jurmain RD, Wren KT, Maijanen H, et al. Knee osteoarthritis has doubled in prevalence since the mid-20th century. *Proc Natl Acad Sci USA.* (2017) 114:9332–36. doi: 10.1073/pnas.1703856114

4. Safiri S, Kolahi AA, Smith E, Hill C, Bettampadi D, Mansournia MA, et al. Global, regional and national burden of osteoarthritis 1990-2017: a systematic analysis of the global burden of disease study 2017. *Ann Rheumatic Dis.* (2020) 79:819–28. doi: 10.1136/annrheumdis-2019-216515
5. Munukka M, Waller B, Rantalainen T, Häkkinen A, Nieminen MT, Lammentausta E, et al. Efficacy of progressive aquatic resistance training for tibiofemoral cartilage in postmenopausal women with mild knee osteoarthritis: a randomised controlled trial. *Osteoarthr Cartilage.* (2016) 24:1708–17. doi: 10.1016/j.joca.2016.05.007
6. Felson DT. Osteoarthritis as a disease of mechanics. *Osteoarthr Cartilage.* (2013) 21:10–5. doi: 10.1016/j.joca.2012.09.012
7. Robinson WH, Lepus CM, Wang Q, Raghu H, Mao R, Lindstrom TM, et al. Low-grade inflammation as a key mediator of the pathogenesis of osteoarthritis. *Nat Rev Rheumatol.* (2016) 12:580–92. doi: 10.1038/nrrheum.2016.136
8. Boissoneault J, Penza CW, George SZ, Robinson ME, Bishop MD. Comparison of brain structure between pain-susceptible and asymptomatic individuals following experimental induction of low back pain. *Spine J.* (2020) 20:292–99. doi: 10.1016/j.spinee.2019.08.015
9. Hannan MT, Felson DT, Pincus T. Analysis of the discordance between radiographic changes and knee pain in osteoarthritis of the knee. *J Rheumatol.* (2000) 27:1513–7. doi: 10.2174/157339907779802076
10. Bedson J, Croft PR. The discordance between clinical and radiographic knee osteoarthritis: a systematic search and summary of the literature. *BMC Musculo Dis.* (2008) 9:116. doi: 10.1186/1471-2474-9-116
11. Terry EL, Tanner JJ, Cardoso JS, Sibille KT, Lai S, Deshpande H, et al. Associations of pain catastrophizing with pain-related brain structure in individuals with or at risk for knee osteoarthritis: sociodemographic considerations. *Brain Imag Behav.* (2021) 15:1769–77. doi: 10.1007/s11682-020-00372-w
12. Parks EL, Geha PY, Baliki MN, Katz J, Schnitzer TJ, Apkarian AV. Brain activity for chronic knee osteoarthritis: dissociating evoked pain from spontaneous pain. *Euro J Pain.* (2011) 15:843.e1–14. doi: 10.1016/j.ejpain.2010.12.007
13. Howard MA, Sanders D, Krause K, O'Muircheartaigh J, Fotopoulou A, Zelaya F, et al. Alterations in resting-state regional cerebral blood flow demonstrate ongoing pain in osteoarthritis: An arterial spin-labeled magnetic resonance imaging study. *Arthr Rheumatism.* (2012) 64:3936–46. doi: 10.1002/art.37685
14. Hiramatsu T, Nakanishi K, Yoshimura S, Yoshino A, Adachi N, Okamoto Y, et al. The dorsolateral prefrontal network is involved in pain perception in knee osteoarthritis patients. *Neurosci Lett.* (2014) 581:109–14. doi: 10.1016/j.neulet.2014.08.027
15. Liao X, Mao C, Wang Y, Zhang Q, Cao D, Seminowicz DA, et al. Brain gray matter alterations in Chinese patients with chronic knee osteoarthritis pain based on voxel-based morphometry. *Medicine.* (2018) 97:e0145. doi: 10.1097/md.0000000000010145
16. Mao CP, Bai ZL, Zhang XN, Zhang QJ, Zhang L. Abnormal subcortical brain morphology in patients with knee osteoarthritis: a cross-sectional study. *Front Aging Neurosci.* (2016) 8:3. doi: 10.3389/fnagi.2016.00003
17. Tournier JD, Mori S, Leemans A. Diffusion tensor imaging and beyond. *Magnetic Res Med.* (2011) 65:1532–56. doi: 10.1002/mrm.22924
18. Behrens TE, Johansen-Berg H, Woolrich MW, Smith SM, Wheeler-Kingshott CA, Boulby PA, et al. Non-invasive mapping of connections between human thalamus and cortex using diffusion imaging. *Nat Neurosci.* (2003) 6:750–7. doi: 10.1038/nn1075
19. Smith SM, Jenkinson M, Johansen-Berg H, Rueckert D, Nichols TE, Mackay CE, et al. Tract-based spatial statistics: voxelwise analysis of multi-subject diffusion data. *NeuroImage.* (2006) 31:1487–505. doi: 10.1016/j.neuroimage.2006.02.024
20. Alexander AL, Lee JE, Lazar M, Field AS. Diffusion tensor imaging of the brain. *Neurotherapeutics.* (2007) 4:316–29. doi: 10.1016/j.nurt.2007.05.011
21. Le Bihan D, Mangin JF, Poupon C, Clark CA, Pappata S, Molko N, et al. Diffusion tensor imaging: concepts and applications. *JMRI.* (2001) 13:534–46. doi: 10.1002/jmri.1076
22. Winklewski PJ, Sabisz A, Naumczyk P, Jodzio K, Szurowska E, Szarmach AJF. Understanding the physiopathology behind axial and radial diffusivity changes—what do we know? *Front Neurol.* (2018) 9:92. doi: 10.3389/fneur.2018.00092
23. Wasserthal J, Maier-Hein KH, Neher PF, Northoff G, Kubera KM, Fritze S, et al. Multiparametric mapping of white matter microstructure in catatonia. *Neuropsychopharmacology.* (2020) 45:1750–57. doi: 10.1038/s41386-020-0691-2
24. Fritz HC, McAuley JH, Wittfeld K, Hegenscheid K, Schmidt CO, Langner S, et al. Chronic back pain is associated with decreased prefrontal and anterior insular gray matter: results from a population-based cohort study. *J Pain.* (2016) 17:111–8. doi: 10.1016/j.jpain.2015.10.003
25. Sundermann B, Dehghan Nayyeri M, Pfleiderer B, Stahlberg K, Jünke L, Baie L, et al. Subtle changes of gray matter volume in fibromyalgia reflect chronic musculoskeletal pain rather than disease-specific effects. *Eur J Neurosci.* (2019) 50:3958–67. doi: 10.1111/ejn.14558
26. Altman RD. Classification of disease: osteoarthritis. *Semin Arthr Rheumatism.* (1991) 20:40–7. doi: 10.1016/0049-0172(91)90026-v
27. Kohn MD, Sassoon AA, Fernando ND. Classifications in brief: kellgren-lawrence classification of osteoarthritis. *Clin Orthopaed Rel Res.* (2016) 474:1886–93. doi: 10.1007/s11999-016-4732-4
28. Castellano A, Papinutto N, Cadioli M, Brugnara G, Iadanza A, Scigliuolo G, et al. Quantitative MRI of the spinal cord and brain in adrenomyeloneuropathy: in vivo assessment of structural changes. *Brain J Neurol.* (2016) 139:1735–46. doi: 10.1093/brain/aww068
29. Poletti S, Myint AM, Schüetze G, Bollettini I, Mazza E, Grillitsch D, et al. Kynurenine pathway and white matter microstructure in bipolar disorder. *Eur Arch Psychiatry Clin Neurosci.* (2018) 268:157–68. doi: 10.1007/s00406-016-0731-4
30. Kuner R. Central mechanisms of pathological pain. *Natu Med.* (2010) 16:1258–66. doi: 10.1038/nm.2231
31. Bushnell MC, Ceko M, Low LA. Cognitive and emotional control of pain and its disruption in chronic pain. *Nat Rev Neurosci.* (2013) 14:502–11. doi: 10.1038/nrn3516
32. Kuner R, Flor H. Structural plasticity and reorganisation in chronic pain. *Nat Rev Neurosci.* (2016) 18:20–30. doi: 10.1038/nrn.2016.162
33. Rodriguez-Raecke R, Niemeier A, Ihle K, Ruether W, May A. Brain gray matter decrease in chronic pain is the consequence and not the cause of pain. *J Neurosci.* (2009) 29:13746–50. doi: 10.1523/jneurosci.3687-09.2009
34. Malfliet A, Coppieters I, Van Wilgen P, Kregel J, De Pauw R, Dolphens M, et al. Brain changes associated with cognitive and emotional factors in chronic pain: a systematic review. *Eur J Pain.* (2017) 21:769–86. doi: 10.1002/ejp.1003
35. Fabri M, Polonara G. Functional topography of human corpus callosum: an FMRI mapping study. *Neural Plast.* (2013) 2013:251308. doi: 10.1155/2013/251308
36. Horton JE, Crawford HJ, Harrington G, Downs JH, 3rd. Increased anterior corpus callosum size associated positively with hypnotizability and the ability to control pain. *Brain J Neurol.* (2004) 127:1741–7. doi: 10.1093/brain/awh196
37. Caminiti R, Carducci F, Piervincenzi C, Battaglia-Mayer A, Confalone G, Visco-Comandini F, et al. Diameter, length, speed, and conduction delay of callosal axons in macaque monkeys and humans: comparing data from histology and magnetic resonance imaging diffusion tractography. *J Neurosci.* (2013) 33:14501–11. doi: 10.1523/jneurosci.0761-13.2013
38. Yu D, Yuan K, Qin W, Zhao L, Dong M, Liu P, et al. Axonal loss of white matter in migraine without aura: a tract-based spatial statistics study. *Cephalalgia.* (2013) 33:34–42. doi: 10.1177/0333102412466964
39. Liu J, Zhu J, Yuan F, Zhang X, Zhang Q. Abnormal brain white matter in patients with right trigeminal neuralgia: a diffusion tensor imaging study. *J Headache Pain.* (2018) 19:46. doi: 10.1186/s10194-018-0871-1
40. Ji RR, Nackley A, Huh Y, Terrando N, Maixner W. Neuroinflammation and central sensitization in chronic and widespread pain. *Anesthesiology.* (2018) 129:343–66. doi: 10.1097/aln.0000000000002130
41. Woolf CJ. Central sensitization: implications for the diagnosis and treatment of pain. *Pain.* (2011) 152:S2–15. doi: 10.1016/j.pain.2010.09.030
42. Kim DJ, Lim M, Kim JS, Son KM, Kim HA, Chung CK. Altered white matter integrity in the corpus callosum in fibromyalgia patients identified by tract-based spatial statistical analysis. *Arthr Rheumatol.* (2014) 66:3190–9. doi: 10.1002/art.38771
43. Jiang C, Yi L, Cai S, Zhang L. Ischemic stroke in pontine and corona radiata: location specific impairment of neural network investigated with resting state fMRI. *Front Neurol.* (2019) 10:575. doi: 10.3389/fneur.2019.00575

44. Coppola G, Di Renzo A, Tinelli E, Petolicchio B, Di Lorenzo C, Parisi V, et al. Patients with chronic migraine without history of medication overuse are characterized by a peculiar white matter fiber bundle profile. *J Headache Pain.* (2020) 21:92. doi: 10.1186/s10194-020-01159-6
45. Giamberardino MA. Women and visceral pain: are the reproductive organs the main protagonists? Mini-review at the occasion of the "European Week Against Pain in Women 2007". *Eur J Pain.* (2008) 12:257–60. doi: 10.1016/j.ejpain.2007.11.007
46. Makris N, Kennedy DN, McInerney S, Sorensen AG, Wang R, Caviness VS, et al. Segmentation of subcomponents within the superior longitudinal fascicle in humans: a quantitative, *in vivo*, DT-MRI study. *Cerebral Cortex.* (2005) 15:854–69. doi: 10.1093/cercor/bhh186
47. Strutton PH, Theodorou S, Catley M, McGregor AH, Davey NJ. Corticospinal excitability in patients with chronic low back pain. *J Spinal Dis Techn.* (2005) 18:420–4. doi: 10.1097/01.bsd.0000169063.84628.fe
48. Vogt BA. Pain and emotion interactions in subregions of the cingulate gyrus. *Nat Rev Neurosci.* (2005) 6:533–44. doi: 10.1038/nrn1704
49. Bester H, Bourgeais L, Villanueva L, Besson JM, Bernard JF. Differential projections to the intralaminar and gustatory thalamus from the parabrachial area: a PHA-L study in the rat. *J Comp Neurol.* (1999) 405:421–49.
50. Villanueva L, Desbois C, Le Bars D, Bernard JF. Organization of diencephalic projections from the medullary subnucleus reticularis dorsalis and the adjacent cuneate nucleus: a retrograde and anterograde tracer study in the rat. *J Comp Neurol.* (1998) 390:133–60.
51. Derbyshire SW. Exploring the pain "neuromatrix". *Curr Rev Pain.* (2000) 4:467–77. doi: 10.1007/s11916-000-0071-x
52. DeSouza DD, Hodaie M, Davis KD. Abnormal trigeminal nerve microstructure and brain white matter in idiopathic trigeminal neuralgia. *Pain.* (2014) 155:37–44. doi: 10.1016/j.pain.2013.08.029
53. Messina R, Rocca MA, Colombo B, Pagani E, Falini A, Comi G, et al. White matter microstructure abnormalities in pediatric migraine patients. *Cephalalgia.* (2015) 35:1278–86. doi: 10.1177/0333102415578428
54. Xue X, Wu JJ, Hua XY, Zheng MX, Ma J, Ma ZZ, et al. Structural white matter alterations in carpal tunnel syndrome: a modified TBSS study. *Brain Res.* (2021) 1767:147558. doi: 10.1016/j.brainres.2021.147558
55. Chen H, Lian Z, Liu J, Shi Z, Du Q, Feng H, et al. Brain changes correlate with neuropathic pain in patients with neuromyelitis optica spectrum disorders. *Mult Scl Rel Dis.* (2021) 53:103048. doi: 10.1016/j.msard.2021.103048
56. Davis KD, Taylor KS, Anastakis DJ. Nerve injury triggers changes in the brain. *Neuroscientist.* (2011) 17:407–22. doi: 10.1177/1073858410389185
57. Taylor KS, Anastakis DJ, Davis KD. Cutting your nerve changes your brain. *Brain J Neurol.* (2009) 132:3122–33. doi: 10.1093/brain/awp231
58. Benedetti F, Yeh PH, Bellani M, Radaelli D, Nicoletti MA, Poletti S, et al. Disruption of white matter integrity in bipolar depression as a possible structural marker of illness. *Biol Psychiatry.* (2011) 69:309–17. doi: 10.1016/j.biopsych.2010.07.028
59. Shu N, Wang Z, Qi Z, Li K, He Y. Multiple diffusion indices reveals white matter degeneration in Alzheimer's disease and mild cognitive impairment: a tract-based spatial statistics study. *J Alzheimer Dis.* (2011) 26(Suppl. 3):275–85. doi: 10.3233/jad-2011-0024

Conflict of Interest: The authors declare that the research was conducted in the absence of any commercial or financial relationships that could be construed as a potential conflict of interest.

Publisher's Note: All claims expressed in this article are solely those of the authors and do not necessarily represent those of their affiliated organizations, or those of the publisher, the editors and the reviewers. Any product that may be evaluated in this article, or claim that may be made by its manufacturer, is not guaranteed or endorsed by the publisher.

frontiers | Frontiers in Neurology

ORIGINAL RESEARCH
published: 02 May 2022
doi: 10.3389/fneur.2022.843815

Brain Functional Alteration at Different Stages of Neuropathic Pain With Allodynia and Emotional Disorders

Ya-Nan Zhang[1†], *Xiang-Xin Xing*[2,3†], *Liu Chen*[1], *Xin Dong*[1], *Hao-Tian Pan*[1], *Xu-Yun Hua*[3,4*] *and Ke Wang*[1*]

[1] *Acupuncture Anesthesia Clinical Research Institute, Yueyang Hospital of Integrated Traditional Chinese and Western Medicine, Shanghai University of Traditional Chinese Medicine, Shanghai, China,* [2] *Department of Rehabilitation Medicine, Yueyang Hospital of Integrated Traditional Chinese and Western Medicine, Shanghai University of Traditional Chinese Medicine, Shanghai, China,* [3] *Engineering Research Center of Traditional Chinese Medicine Intelligent Rehabilitation, Ministry of Education, Shanghai, China,* [4] *Department of Traumatology and Orthopedics, Yueyang Hospital of Integrated Traditional Chinese and Western Medicine, Shanghai University of Traditional Chinese Medicine, Shanghai, China*

OPEN ACCESS

Edited by:
Lu Liu,
Capital Medical University, China

Reviewed by:
Tao Sun,
Shandong University, China
Alireza Abed,
Kashan University of Medical Sciences, Iran
Nisar Ahmad,
University of Peshawar, Pakistan

***Correspondence:**
Xu-Yun Hua
swrhxy@126.com
Ke Wang
wangke8430@163.com

†These authors have contributed equally to this work

Specialty section:
This article was submitted to Headache and Neurogenic Pain, a section of the journal Frontiers in Neurology

Received: *27 December 2021*
Accepted: *30 March 2022*
Published: *02 May 2022*

Citation:
Zhang Y-N, Xing X-X, Chen L, Dong X, Pan H-T, Hua X-Y and Wang K (2022) Brain Functional Alteration at Different Stages of Neuropathic Pain With Allodynia and Emotional Disorders. Front. Neurol. 13:843815. doi: 10.3389/fneur.2022.843815

Neuropathic pain (NeuP), a challenging medical condition, has been suggested by neuroimaging studies to be associated with abnormalities of neural activities in some brain regions. However, aberrancies in brain functional alterations underlying the sensory-discriminative abnormalities and negative emotions in the setting of NeuP remain unexplored. Here, we aimed to investigate the functional alterations in neural activity relevant to pain as well as pain-related depressive-like and anxiety-like behaviors in NeuP by combining amplitude of low frequency fluctuation (ALFF) and degree centrality (DC) analyses methods based on resting-state functional magnetic resonance imaging (rs-fMRI). A rat model of NeuP was established *via* chronic constriction injury (CCI) of the sciatic nerve. Results revealed that the robust mechanical allodynia occurred early and persisted throughout the entire observational period. Depressive and anxiety-like behaviors did not appear until 4 weeks after injury. When the maximum allodynia was apparent early, CCI rats exhibited decreased ALFF and DC values in the left somatosensory and nucleus accumbens shell (ACbSh), respectively, as compared with sham rats. Both values were significantly positively correlated with mechanical withdrawal thresholds (MWT). At 4 weeks post-CCI, negative emotional states were apparent and CCI rats were noted to exhibit increased ALFF values in the left somatosensory and medial prefrontal cortex (mPFC) as well as increased DC values in the right motor cortex, as compared with sham rats. At 4 weeks post-CCI, ALFF values in the left somatosensory cortex and DC values in the right motor cortex were noted to negatively correlate with MWT and exhibition of anxiety-like behavior on an open-field test (OFT); values were found to positively correlate with the exhibition of depressive-like behavior on forced swimming test (FST). The mPFC ALFF values were found to negatively correlate with the exhibition of anxiety-like behavior on OFT and positively correlate with the exhibition

of depressive-like behavior on FST. Our findings detail characteristic alterations of neural activity patterns induced by chronic NeuP and underscore the important role of the left somatosensory cortex, as well as its related networks, in the mediation of subsequent emotional dysregulation due to NeuP.

Keywords: neuropathic pain, allodynia, negative emotions, functional magnetic resonance (fMRI), ALFF, DC

INTRODUCTION

Neuropathic pain (NeuP), caused by pathology of the somatosensory nervous system, is commonly seen as a chronic condition in clinical practice (1). The general prevalence of NeuP is estimated to reach 7-8% and, as such, significantly decreases the quality of life and imposes a high societal burden (2–4). In addition to hyperalgesia, allodynia, and spontaneous pain, NeuP is also accompanied by the manifestation of emotional disorders including anxiety and depression (1, 5). Notably, emotional disbalance further exacerbates NeuP (6, 7). Although NeuP has become a major worldwide public health concern (8), the mechanisms underlying its pathogenesis remain unclear, and thus its treatment remains challenging.

The brain is involved in the central regulation of pain and the generation of negative emotions (9, 10). Noxious stimulation affects multiple brain regions, including the primary somatosensory cortex (S1), the secondary somatosensory cortex (S2), anterior cingulate cortex (ACC), prefrontal cortex (PFC), thalamus, nucleus accumbens (NAc), amygdala, and periaqueductal gray (PAG) (10, 11). Most of these aforementioned brain regions similarly engage in the regulation of emotion (12–16). As such, pain induces "an unpleasant sensory and emotional experience" and provides a physiological, structural, and functional basis for multi-dimensional changes seen in the setting of chronic pain (17). Previous studies have reported that the structural and functional disorders of these relevant brain regions contributed to the generation and maintenance of allodynia and negative emotions in chronic pain (18, 19). Multiple lines of evidence have suggested that obvious pathological pain develops early and that negative emotions do not become apparent until later (20). Furthermore, a recent study reported that pathological pain resulting from different etiologies affects distinct neural circuits (21). Whether a similar sequence of alterations in distinct brain regions corresponds to the manifestation of pathological pain and negative emotions in different stages of NeuP, however, remains unknown.

Functional magnetic resonance imaging (fMRI), a non-invasive neuroimaging technique, is used to evaluate the relationship between hemodynamic response and neuronal activity (22). It reflects both physiological functions and metabolic alterations caused by local neuronal activity *via* changes in blood-oxygen-level-dependent signal (BOLD) (23). As rs-fMRI can macroscopically detect resting-state neuronal activity, it is frequently used in the study of a variety of neuropathologies (24, 25). Brain diseases are associated with abnormal local spontaneous neuronal activity (26). Many methods have been exploited to characterize local properties of

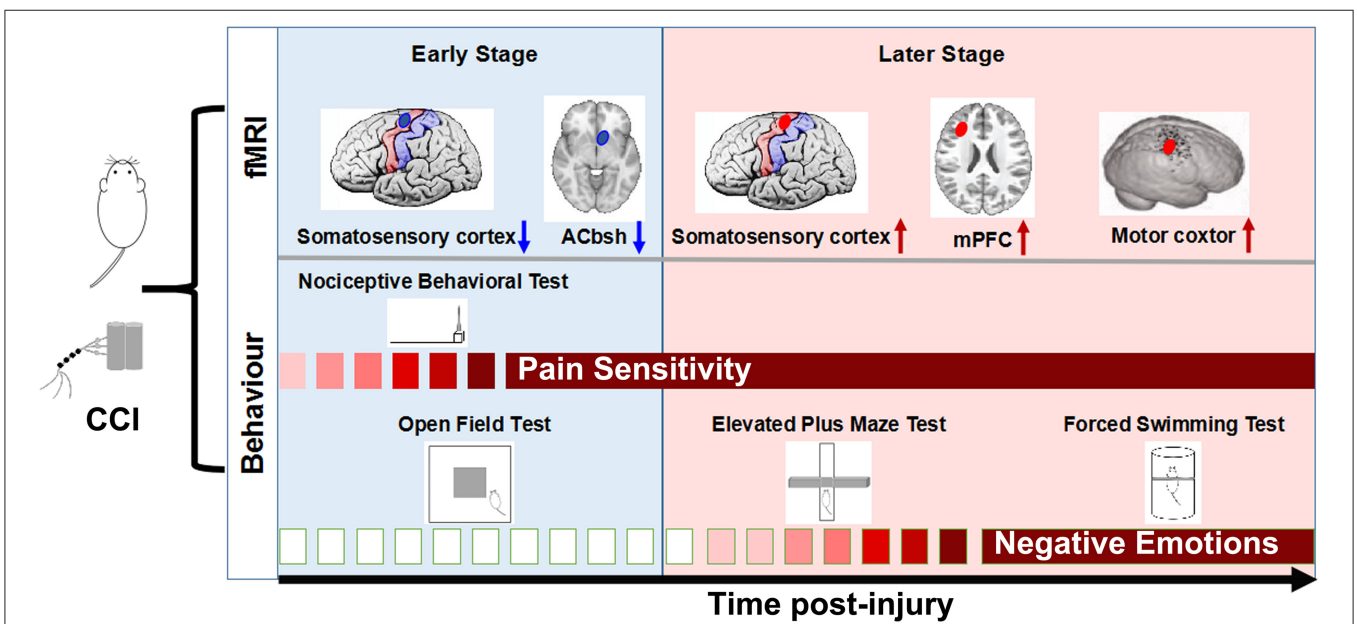

GRAPHICAL ABSTRACT | Brain functional alteration at different stages of neuropathic pain.

FIGURE 1 | Schematic of the experimental timeline.

the rs-fMRI signal, including the amplitude of low-frequency fluctuation (ALFF) and degree centrality (DC) (26, 27). ALFF is used as an indicator to characterize the intensity of neural activity at a voxel, while DC reflects the intrinsic functional connectivity between a node (voxel) and other nodes within the brain, and can be used to evaluate hub nodes (27, 28). Here, rs-fMRI was used to investigate brain abnormalities in both the early and late stages of NeuP using ALFF and DC to assess relevant central mechanisms.

MATERIALS AND METHODS

Animals

Male Sprague-Dawley (SD) rats (160-180 g) were purchased from Shanghai Slack Laboratory Animal Ltd. (Shanghai, China). The animals were kept under a 12/12 h reverse light cycle in a controlled environment at a temperature of 21 ± 1°C and relative humidity of 60–70%. Food and water were available to the rats at all times, and the animals were provided a 7-day acclimatization period to their new environment prior to experimentation. A total of 16 rats were randomly divided into sham ($n = 8$) and chronic constriction injury (CCI; $n = 8$) groups. Experimental procedures stated in the National Institutes of Health Guidelines for the Use of Laboratory Animals were approved by the Institutional Animal Care Committee of YueYang University of Traditional Chinese Medicine, Shanghai, China. All behavioral tests were performed between 8:00 am and 11:30 am. The flowchart of the experimental design is shown in **Figure 1**.

CCI Model

Rats were anesthetized *via* intraperitoneal injection with sodium pentobarbital (50 mg/kg). Left-sided CCI of the sciatic nerve was achieved as previously described by us (20). A surgical incision of one centimeter was initially made in the middle of the thigh and the left sciatic nerve was exposed after being bluntly separated from the muscle. The exposed sciatic nerve was subsequently ligated in four passes using a gut suture (3-0 silk). In sham group rats, only the left sciatic nerve was exposed without ligature. All surgical procedures were performed by the same individual to prevent potential bias. All efforts were made to minimize animal suffering, and there were no rat deaths during surgery to establish CCI.

Behavioral Tests

Nociceptive Behavioral Test

The von Frey plantar aesthesiometer (IITC, Woodland Hills, CA, USA) was used to measure mechanical withdrawal thresholds (MWT). Animals were placed separately in Plexiglas cages on a punching table for 15 min to allow acclimatization to the environment prior to testing. Each rat's left hind paw was stimulated three times at 5 min intervals during the formal examination. Paw withdrawal, flinching, or licking was regarded as positive behavior (29). Each value was recorded; MWT were represented by the mean values.

Open Field Test

The open-field test (OFT) was conducted to measure athletic ability and anxiety-like behavior (30). Rats were provided an acclimatization period of 30 min in the behavior assessment room prior to experimentation. The dimensions of the testing apparatus were 100 cm (length) × 100 cm (width) × 40 cm (height); it contained non-reflective black walls and floor. Each rat was gently placed in the central zone and allowed to freely explore the area for 10 min in a quiet environment. The central zone was defined as an area covering 40% of the total area of the box. SMART 3.0 software (Panlab, Cornella, Spain) was used to record and analyze time and distance traveled in the central zone, as well as the total distance traveled. The apparatus was cleaned after testing each rat using 75% ethanol.

Elevated Plus Maze Test

The elevated plus-maze test (EPMT) was used to measure anxiety associated with open spaces and height (31). The maze comprised two 50 × 10 cm open arms, two 50 × 10 cm closed arms, and a 10 × 10 cm central area. The closed arms were contained by boards 40 cm high. The maze was placed 80 cm above the floor in a testing room. Each rat was placed onto the central area facing one open arm and allowed to explore the maze for 10 min (20). Time spent in the arms of the maze and total distance traveled by rats was analyzed using SMART software. After testing each rat, the apparatus was cleaned as described above.

Forced Swimming Test

The forced swimming test (FST) was conducted to assess depressive behavior. Rats were placed into a glass cylinder (height 30 cm; diameter 18 cm) filled with water (23 ± 1°C) for 6 min. Immobility time throughout the 4 min of the testing session was evaluated. Immobility was defined as behavior manifesting by the rat only keeping its head above water and attempting to float with

minimal exertion (32). The experimenter was blinded to both the CCI and sham groups.

fMRI Acquisition

We performed fMRI scans at 11 and 32 days post-CCI and collected imaging data using a Bruker 7T magnetic resonance system (Bruker Corporation) with a coil. Before data acquisition, rats were anesthetized with 2.5% isoflurane and Medetomidine (0.025 mg/kg). Under continuous 1.5–2% isoflurane anesthesia, rats were fixed on the scanner with their heads immobilized. Body temperature and respiration were continuously monitored. Imaging data were obtained with the following interlayer scanning echo-plane parameters: interleaved scanning order; flip angle = 90°; slice thickness = 0.3 mm;, repetition time = 3,000 ms; 200 times points; imaging duration = 10 min; echo time = 20 ms; number of averages = 1; field of vision = 32 × 32 mm^2; matrix = 64 × 64 voxels.

fMRI Data Preprocessing

Data preprocessing was conducted using the Statistical Parametric Mapping 12 toolbox (http://www.fil.ion.ucl.ac.uk/spm/) based on the MATLAB 2014a platform. To match data to human dimensions, the first five time points were removed and images expanded by 10 × 10 × 10. This amplification procedure only modulated the dimension descriptor fields in the file header instead of changing interpolation. Manual stripping of none-brain tissue was then performed before further preprocessing. To minimize the temporal bias of slice acquisition, slice scan time correction was performed. To reverse the dislocation of voxels caused by head motion, spatial adjustment with rigid-body transformations was applied. The standard brain template in Schwarz's study was used to accomplish the normalization of common space, the voxel size for normalized images was 2.06 × 2.06 × 2 mm (33). Images were subsequently smoothed by a full width at half maximum quadruple as the voxel size (6.18 × 6.18 ×6 mm). For further preprocessing, temporal bandpass filtering (0.01–0.08 Hz) was applied to decrease the low-frequency drift based on the removal of covariates and linear trends.

ALFF Calculation

ALFF depends on the blood oxygen level (BOLD) signal of each voxel and reflects the extent of spontaneous neuronal activity (20). Here, we calculated ALFF values for the traditional low-frequency band (0.01–0.08 Hz) and divided them by the global mean ALFF value within the brain mask (28).

DC Calculation

DC represents the extent of interconnectivity between a given voxel (node) and other voxels, thus detailing the importance of the voxel or brain area. A change in the DC value of a node indicates altered connectivity; these changes were calculated during analyses (34). The DC was calculated using the REST toolbox (http://www.restfmri.net). A whole-brain functional connectivity matrix based on a REST-supported binary mask was constructed using Pearson's correlation coefficients between gray matter voxel. To improve normality and derive the Z-score matrix, the Fisher transformation was used. Regional functional connectivity strength was calculated as the sum of all the connections (*Z*-values) between voxels. Greater strength values were extracted and analyzed.

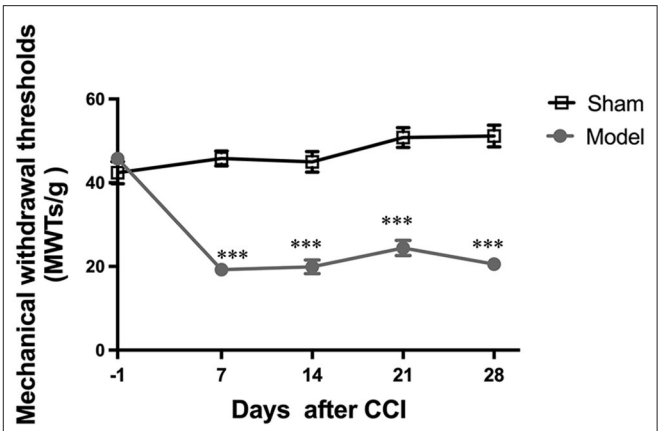

FIGURE 2 | Evaluation of mechanical withdrawal thresholds (MWT). All data are expressed as the Mean ± SEM ($n = 8$ per group). ***$p < 0.001$ vs. the sham group.

Statistical Analyses

Statistical analyses were performed using SPSS 19.0 (IBM Corp., Armonk, USA). Behavioral data were expressed as the mean ± standard error (SEM). Differences in MWT between the two groups at multiple time points were compared *via* two-way repeated measures analysis of variance (time-treatment interaction) with the *Bonferroni* test for *post-hoc* comparisons. Differences in OFT, EPMT, and FST data were analyzed using an independent-samples *t*-test. Prior to analyses, data were checked for conformance to the normal distribution using the Shapiro-Wilk normality test; when normal distribution was not supported, the Wilcoxon rank-sum test was used. A $p < 0.05$ was considered statistically significant. Sham and CCI group ALFF and DC values obtained from fMRI data were compared using two-sample *t*-tests. Results were corrected for multiple comparisons with a combined threshold of a single voxel ($p < 0.001$). AlphaSim estimation was performed using REST v2.329 (http://rfmri.org/dpabi). To decrease the possibility of false-negative results, a threshold ($p < 0.001$, cluster size >12 voxels) was applied to each cohort. Pearson correlation analysis was utilized to evaluate the correlation among behavioral test and fMRI ALFF and DC value data.

RESULTS

CCI Induced Mechanical Allodynia

A main effect of the CCI model [$F_{(1,14)} = 109.9$; $p < 0.0001$] and a significant group × time interaction [$F_{(4,56)} = 38.39$; $p < 0.0001$] were noted among the two groups. The day before CCI surgery, no significant differences in MWT among the two groups were found ($p > 0.05$). After the surgery, CCI group ipsilateral hind paw MWT values were noted to significantly decrease from days 7 to 28 as compared with sham group values

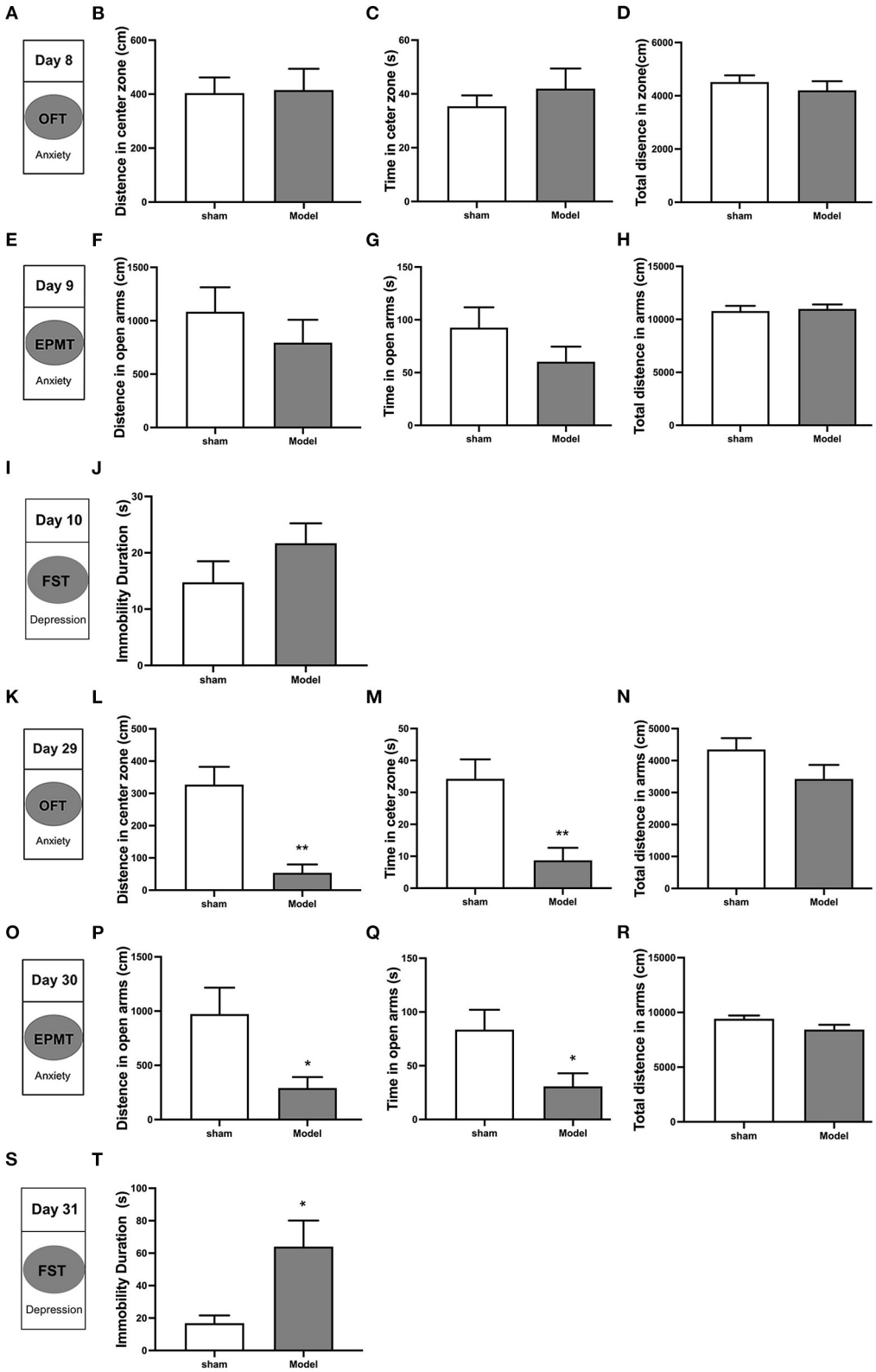

FIGURE 3 | Depressive and anxiety-like behaviors induced by CCI in rats. Anxiety-like behavior was accessed using both the open field test (OFT) **(A–D, K–N)** and the elevated plus maze test (EPMT) **(E–H, O–R)**. Depressive-like behavior was accessed using the forced swimming test (FST) **(I,J,S,T)**. **(A,K)** OFT was performed on

(Continued)

FIGURE 3 | days 8 and 29 after CCI surgery; **(B,L)** Distance traveled in the central zone on OFT; **(C,M)** Time spent in the central zone on OFT; **(D,N)** Total distance traveled on OFT; **(E,O)** EPMT was performed on days 9 and 30 after CCI surgery; **(F,P)** Distance traveled in the open arms on EPMT; **(G,Q)** Time spent in the open arms on EPMT; **(H,R)** Total distance traveled on EPMT; **(I,S)** FST was performed on days 10 and 31 after CCI surgery; **(J,T)** Immobility time on FST. All data are expressed as the Mean ± SEM ($n = 8$ per group). $^{*}p < 0.05$, $^{**}p < 0.01$ *vs.* sham group.

(all $p < 0.001$; **Figure 2**), indicating that CCI induced persistent mechanical allodynia.

CCI Induced Emotional Disorders

Behavioral tests conducted on days 8–10 after CCI revealed the following (**Figures 3A,E,I**): (1) analyses of OFT data revealed no differences in distance traveled ($p > 0.05$) and time spent ($p > 0.05$) in the central zone, as well as total distance traveled ($p > 0.05$) among CCI and sham groups (**Figures 3B–D**); (2) analyses of EPMT data revealed no differences in distance traveled ($p > 0.05$) and time spent ($p > 0.05$) in maze open arms, and total distance traveled ($p > 0.05$) among the two groups (**Figures 3F–H**); (3) analyses of FST data revealed CCI group immobility time to be similar to that of the sham group ($p > 0.05$; **Figure 3J**). Behavioral tests conducted from days 29 to 31 revealed the following: (**Figures 3K,O,S**) (1) analyses of OFT data revealed that CCI group rats traveled shorter distances ($p < 0.001$) and spent less time ($p < 0.01$) in the central zone as compared to sham group rats (**Figures 3L,M**). No differences in total distance traveled were noted between groups ($p > 0.05$; **Figure 3N**); (2) analyses of EPMT data revealed that CCI rats traveled significantly shorter distances ($p < 0.05$) and spent significantly less time ($p < 0.05$) in the open arms of the maze (**Figures 3P,Q**). The total distance in EPM did not show any difference ($p > 0.05$) in the two groups (**Figure 3R**); (3) analyses of FST data revealed that CCI rats were immobile for significantly longer as compared to sham rats ($p < 0.05$; **Figure 3T**). These findings suggest that depressive and anxiety-like behaviors induced by CCI do not appear in the early stages of pathology until approximately 4 weeks after injury.

Post-CCI Alterations in ALLF at Different Time Points

On day 11 post-CCI, experimental group rats exhibited significantly lower ALFF values in the left somatosensory cortex as compared to sham group rats (**Figure 4A** and **Table 1**). At this time point, Pearson correlation analysis revealed a positive correlation between ALFF values in the left somatosensory cortex and MWT values ($r = 0.679$, $p = 0.004$; **Figure 4B**). On day 32 post-CCI, experimental group rats were found to exhibit significantly higher ALFF values in the left somatosensory cortex and left mPFC as compared to sham group rats (**Figure 4A** and **Table 1**). Pearson correlation analysis revealed that both ALFF values in the left somatosensory cortex and left mPFC negatively correlated with MWT values ($r = -0.762$, $p = 0.001$ for the left somatosensory cortex, **Figure 4C**; $r = -0.656$, $p = 0.006$ for the left mPFC, **Figure 4D**), distance traveled in the central zone of the maze on OFT ($r = -0.647$, $p = 0.007$ for the left somatosensory cortex, **Figure 4E**; $r = -0.569$, $p = 0.02$ for the left mPFC, **Figure 4F**), and length of time spent in the central zone on OFT ($r = -0.73$, $p = 0.001$ for the left somatosensory cortex, **Figure 4G**; $r = -0.512$, $p = 0.04$ for the left mPFC, **Figure 4H**). ALFF values in the left somatosensory cortex and left mPFC, however, were both noted to positively correlate with immobility duration values on FST ($r = 0.55$, $p = 0.02$ for the left somatosensory cortex, **Figure 4I**; $r = 0.319$, $p = 0.02$ for the left mPFC, **Figure 4J**) throughout the aforementioned time period. No significant correlation between EPMT and ALFF values in the left somatosensory cortex ($r = -0.4$, $p = 0.08$ for distance traveled in the open arms; $r = -0.41$, $p = 0.1$ for time spent in the open arms) and left mPFC ($r = -0.373$, $p = 0.1$ for distance traveled in the open arms; $r = -0.406$, $p = 0.1$ for time spent in the open arms), however, was noted (**Supplementary Figure 1**).

Post-CCI Alterations in DC at Different Stages

Compared to sham rats, CCI rats were found to exhibit significantly decreased DC values in the left nucleus accumbens shell (ACbSh) on day 11 post-CCI and the right motor cortex on day 32 post-CCI (**Figure 4A** and **Table 2**). Pearson correlation analysis revealed that left ACbSh DC values positively correlated with MWT values on day 11 post-CCI ($r = 0.75$, $p = 0.001$, **Figure 5B**) and that right motor cortex DC values negatively correlated with MWT values on day 11 post-CCI ($r = -0.764$, $p = 0.001$, **Figure 5C**). Right motor cortex DC values were similarly found to negatively correlate with values of distance traveled within the central zone of the maze ($r = -0.631$, $p = 0.009$, **Figure 5D**) and time spent in the central zone ($r = -0.573$, $p = 0.02$, **Figure 5E**) on OFT, and positively correlate with immobility duration values on FST ($r = -0.542$, $p = 0.03$, **Figure 5F**). No significant correlation between right motor cortex DC values and EPMT data were noted (**Supplementary Figure 2**).

DISCUSSION

This study aimed to investigate alterations in brain functional features throughout the development and progression of NeuP. We confirmed that the robust mechanical allodynia occurred early in injury and persisted in a CCI rat model of NeuP. Pain-related negative emotions did not manifest until 4 weeks after nerve injury. ALFF and DC values were found to be significantly decreased in the left somatosensory cortex and ACbSh early in CCI rats as compared to sham controls. When anxiety- and depression-like behaviors manifested, ALFF and DC values were noted to significantly increase in the left somatosensory cortex, left mPFC, and right motor cortex among CCI rats.

As ALFF reflects the magnitude of spontaneous neuronal activity, an altered ALFF suggests abnormal regional neuronal activity. We found that neuronal activity within the somatosensory cortex of CCI group rats is suppressed early after injury yet enhanced in later stages as compared with the

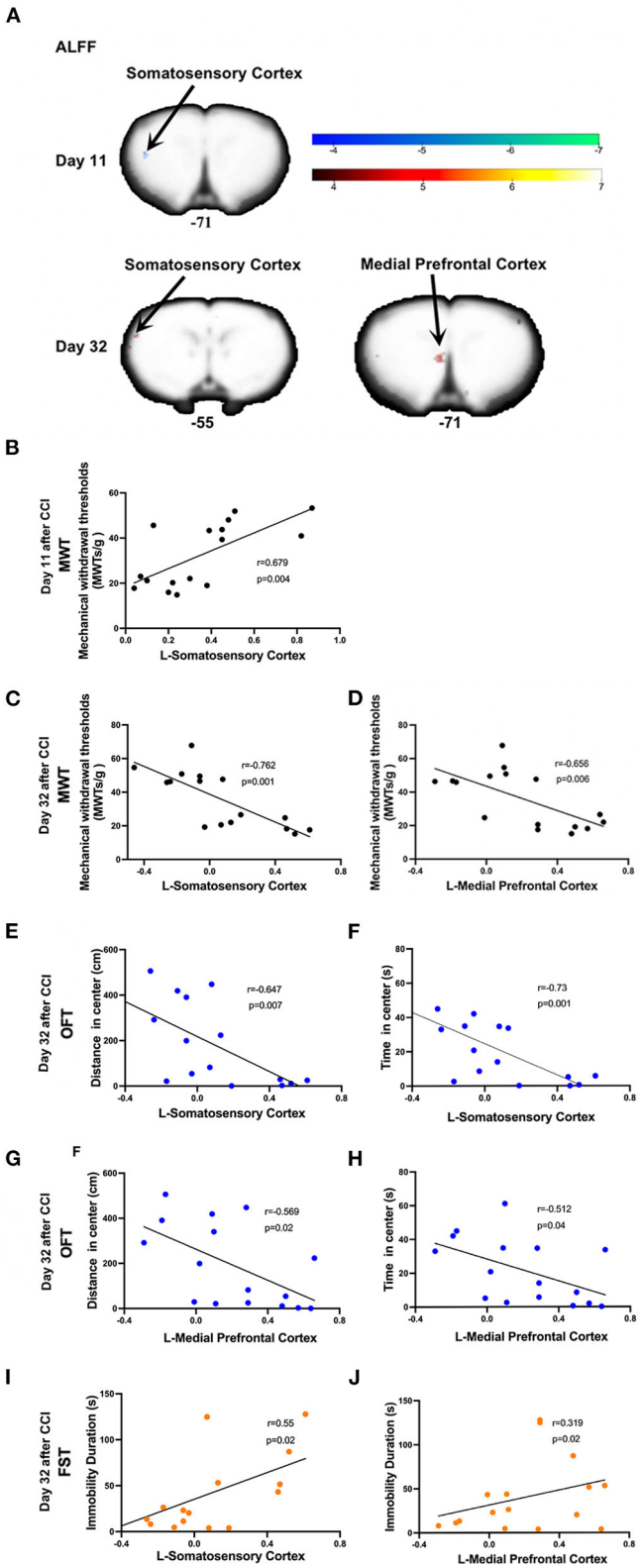

FIGURE 4 | Significant alternations in ALFF induced by CCI and correlations between ALFF values and the mechanical withdrawal thresholds (MWT) values, open field test (OFT) data, and forced swimming test (FST) data. **(A)** CCI group rats were found to exhibit significantly lower ALFF values in the left somatosensory cortex on day

(Continued)

FIGURE 4 | 11 after CCI surgery and significantly higher ALFF values in both the left somatosensory cortex and mPFC on day 32 after CCI surgery as compared to sham group rats; **(B)** ALFF values in the left somatosensory cortex (10 days after CCI surgery) positively correlated with MWT values (7 days after CCI surgery); **(C–H)** ALFF values in the left somatosensory cortex and mPFC (32 days after CCI surgery) negatively correlated with MWT (28 days after CCI surgery), distance traveled and time spent in the central zone of OFT (29 days after CCI surgery); **(I,J)** The ALFF values in the left somatosensory cortex and mPFC (32 days after CCI surgery) was positively correlated with immobility time on FST (31 days after CCI surgery).

TABLE 1 | Results of amplitude of low-frequency fluctuations (ALFF) analysis.

Contrast name				MNI-coordinates		
Time	**Region label**	**Extent**	***t*-value**	**x**	**y**	**z**
Day 11	L-Somatosensory Cortex	12	−5.324	−46	1	−71
Day 32	L-Somatosensory Cortex	24	6.063	−54	24	−37
	L-Medial Prefrontal Cortex	20	5.741	−7	−5	−69

L, left; R, right.

TABLE 2 | Differences in DC values between model and sham groups.

Contrast name				MNI-coordinates		
Time	**Region label**	**Extent**	***t*-value**	**x**	**y**	**z**
Day 11	L- nucleus accumbens shell	50	−5.281	−7	−28	−59
Day 32	R- motor cortex	45	5.030	−14	34	−63

L, left; R, right.

control group rats. The somatosensory cortex (primary (S1) and secondary (S2) somatosensory cortices) is responsible for the sensory-discriminative dimension of pain processing and receives noxious somatosensory input from the somatosensory thalamus, coding spatial, temporal, and intensive aspects of noxious somatosensory stimuli (35–38). Several clinical and experimental lines of evidence confirmed that NeuP induces changes in both morphology and plasticity within the somatosensory cortex (39–41). Patients suffering from NeuP display changes in somatosensory cortex activity and anatomy not seen in patients suffering from non-neuropathic chronic pain (42). A longitudinal study reported that lower somatosensory cortex excitability among patients in the acute stages of low back pain was associated with significantly increased odds of developing chronic pain by 6-month follow-up (43). Furthermore, activation of inhibitory neural circuits within the somatosensory cortex using electroacupuncture was reported to alleviate hyperalgesia in the setting of NeuP (44). Interestingly, somatosensory cortex functions are not restricted to pain sensation; rather, they are involved in the regulation of comorbid anxiety in the setting of persistent pain as well as aversive responses to pain (45, 46). Our results supported these concepts and suggested that changes in ipsilateral somatosensory cortex excitability play active roles in the chronification of NeuP and manifestation of negative emotions among CCI model rats with left-sided sciatic nerve ligation. Unlike the left somatosensory cortex, ALFF remained static in the left mPFC and exhibited significant increases only in the later stages of NeuP, also correlating with mechanical hyperalgesia and the manifestation of negative emotions. The mPFC has previously been extensively implicated in the affective emotional and cognitive aspects of pain and pain modulation (47, 48). A study evaluating human fMRI data that analyzed 270 participants across 18 studies found that pain representations were localized to the anterior midcingulate cortex, negative emotion representations to the ventromedial prefrontal cortex, and cognitive control representations to portions of the dorsal midcingulate cortex (49). Many studies have similarly shown that mPFC activity to be altered in the setting of chronic pain (50). Importantly, gray matter mPFC volume decreases among people suffering from chronic pain (51). Layer- and subregion-specific electrophysiological and morphological changes in the mPFC have further been reported in the setting of NeuP (52). The plasticity of serotonin transmission in the mPFC facilitates the manifestation of anxiety associated with NeuP (53). Likewise, the excitability of pyramidal mPFC neurons was noted to increase when depression manifested. Among NeuP rats; this was induced *via* nerve-sparing injury (54). As such, the mPFC plays a key role in the development of negative emotions associated with NeuP. Pain-related neural activity shifts in focus from the acute pain circuit to the emotional one, suggesting an alteration in perception to be a key consequence of NeuP (55).

The evaluation of DC reveals the importance of a neural node within connectivity networks at the voxel level (34). In this study, the left ACbSh was found to exhibit decreased DC early in NeuP. One recent fMRI study reported that patients suffering chronic pain exhibited smaller nucleus accumbens volumes and loss of power in the slow-5 frequency band (0.01–0.027 Hz) only after the onset of the chronic pain phase, highlighting a likely signature of the state of chronic pain (56). As a subregion of the nucleus accumbens, the ACbSh also plays an important role in mediating NeuP (57). Spinal nerve ligation was recently reported to decrease the relative intensity of excitatory and inhibitory synaptic inputs to medium spiny neurons within the ACbSh, resulting in a decreased the frequency of spontaneous inhibitory postsynaptic currents as well as both the frequency and amplitude of spontaneous excitatory postsynaptic currents in medium spiny neurons (58). Here, we found increased DC values in the right motor cortex later in NeuP when anxiety- and depression-like behaviors were noted. In agreement with our findings, another study reported excitability of the motor cortex to be higher in chronic pain patients and possess a significantly negative correlation with anxiety (59). A double-blind randomized study found that 40% of NeuP patients are able to achieve remission with the use of motor cortex stimulation *via* surgically implanted electrodes (60). A systematic review and meta-analysis of fMRI studies also found that the motor cortex of such patients exhibited significantly decreased activity after treatments as compared to baseline (40).

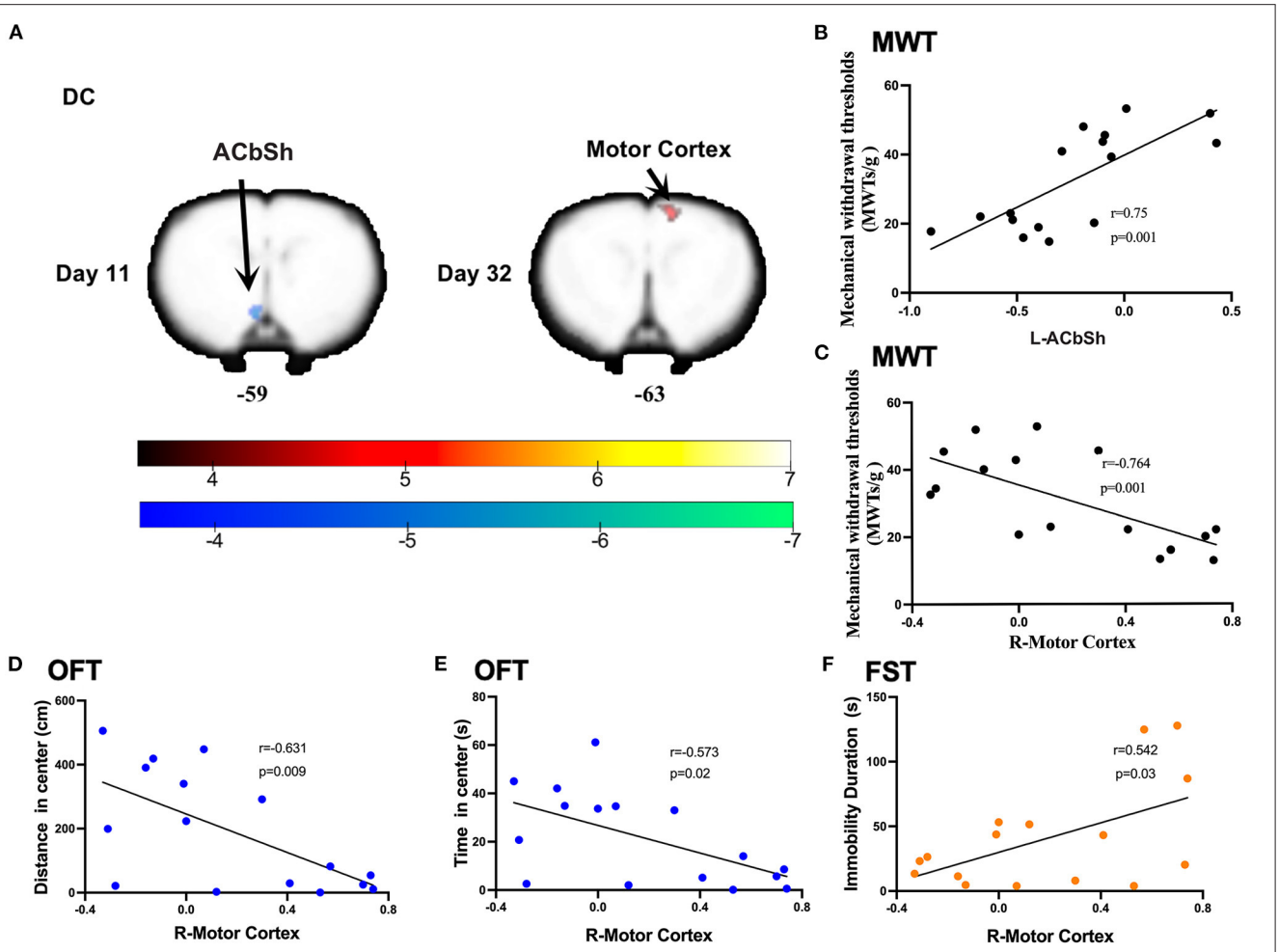

FIGURE 5 | Significant DC alternations induced by CCI and correlations between DC values and the mechanical withdrawal thresholds (MWT), open field test (OFT), and forced swimming test (FST) data. **(A)** CCI group rats exhibited significantly lower DC values in the left nucleus accumbens shell (ACbSh) on day 11 after CCI surgery and significantly higher DC values in the right motor cortex on day 32 after CCI surgery as compared to sham rats; **(B)** DC values in the ACbSh (10 days after CCI surgery) positively correlated with MWT values (7 days after CCI surgery); **(C–E)** DC values in the right motor cortex (32 days after CCI surgery) negatively correlated with MWT values (28 days after CCI surgery), distance traveled and time spent in the central zone of OFT (29 days after CCI surgery); **(F)** DC values in the right motor cortex (32 days after CCI surgery) positively correlated with the immobility time on FST (31 days after CCI surgery).

The somatosensory cortex, mPFC, nucleus accumbens, and motor cortex likely possess functional connections that participate in pain modulation. For instance, the density of perineuronal nets in the somatosensory cortex and mPFC were found to be enhanced in a mouse model of chronic inflammatory pain (61). Motor cortex stimulation was found to block the transmission of somatosensory information to the primary somatosensory cortex and alleviate chronic pain (62). Corticotropin-releasing factor neurons of the mPFC project directly to the nucleus accumbens and increased activity in these neurons in the setting of NeuP facilitates behavioral responses to morphine reward (63). Interestingly, the practice of traditional mindful breathing was found to successfully modulate functional connectivity between the prefrontal and primary somatosensory cortices and relieve pain (64).

This study was not without limitations. Here, we only focused on evaluating functional changes in brain regions as NeuP developed but did not investigate for structural abnormalities. Further studies are needed to elucidate the contribution of these brain structures to pain sensitivity and the manifestation of negative emotions. In addition, future study of changes in brain plasticity is warranted. Finally, patient sex differences were not considered in this study. A clear sexual dimorphism in NeuP is known to exist, with females reported to be more sensitive (65).

In conclusion, our study indicates that longitudinal changes in intrinsic brain activity are associated with the development of NeuP. More specifically, we found lower neuronal activity and voxel-voxel connectivity in the somatosensory cortex and ACbSh to be key in nociception and the modulation of pain processing early in NeuP when maximal allodynia was apparent. With the manifestation of depressive and anxiety-like behaviors, higher neuronal activity and voxel-voxel connectivity in the somatosensory cortex, mPFC, and motor cortex highlight the key role of these regions in the modulation of negative emotions. This study provides a basis for future investigation aiming to advance neuromodulatory intervention for NeuP.

DATA AVAILABILITY STATEMENT

The original contributions presented in the study are included in the article/**Supplementary Material**, further inquiries can be directed to the corresponding authors.

ETHICS STATEMENT

The animal study was reviewed and approved by Institutional Animal Care Committee of Yueyang Hospital of Integrated Traditional Chinese and Western Medicine, Shanghai, China's Shanghai University of Traditional Chinese Medicine.

AUTHOR CONTRIBUTIONS

KW and X-YH conceived and designed the experiments. Y-NZ and X-XX performed the experiments and analyzed the data. LC, XD, and H-TP helped with the behavior test experiments. KW, X-YH, and Y-NZ wrote and modified the manuscript. All authors discussed the results and reviewed the manuscript.

FUNDING

The project was funded by the National Natural Science Foundation of China (81973940, 81673756), Accelerating the Development of Chinese Medicine Three-Year Action Plan of Shanghai [no. ZY (2018-2020)-CCCX-2004-04], the Clinical Key Specialty Construction Foundation of Shanghai (no. shslczdzk04701), and the Shanghai Clinical Research Center for Acupuncture and Moxibustion (20MC1920500).

ACKNOWLEDGMENTS

The authors are grateful for financial support from the institutions involved in this project.

SUPPLEMENTARY MATERIAL

The Supplementary Material for this article can be found online at: https://www.frontiersin.org/articles/10.3389/fneur.2022.843815/full#supplementary-material

Supplementary Figure 1 | (A) The ALFF values in the left mPFC (32 days post-CCI surgery) negatively correlated with MWT values (28 days post-CCI surgery); **(B–E)** No significant correlations were observed between ALFF values in the left somatosensory cortex and mPFC (32 days after CCI surgery) and distance traveled and time spent in open arms on EPMT (29 days post-CCI surgery) (all $p > 0.05$).

Supplementary Figure 2 | No significant correlations were observed between DC values in the right motor cortex (32 days post-CCI surgery) and distance traveled **(A)** and time spent **(B)** in the open arms on EPMT (29 days post-CCI surgery) (all $p > 0.05$).

REFERENCES

1. Yam MF, Loh YC, Tan CS, Khadijah Adam S, Abdul Manan N, Basir R. General pathways of pain sensation and the major neurotransmitters involved in pain regulation. *Int J Mol Sci.* (2018) 19:2164. doi: 10.3390/ijms19082164
2. Bouhassira D, Attal N. Translational neuropathic pain research: a clinical perspective. *Neuroscience.* (2016) 338:27–35. doi: 10.1016/j.neuroscience.2016.03.029
3. Toth C, Lander J, Wiebe S. The prevalence and impact of chronic pain with neuropathic pain symptoms in the general population. *Pain Med.* (2009) 10:918–29. doi: 10.1111/j.1526-4637.2009.00655.x
4. Aytur SA, Ray KL, Meier SK, Campbell J, Gendron B, Waller N, et al. Neural mechanisms of acceptance and commitment therapy for chronic pain: a network-based Fmri approach. *Front Hum Neurosci.* (2021) 15:587018. doi: 10.3389/fnhum.2021.587018
5. Yalcin I, Barthas F, Barrot M. Emotional consequences of neuropathic pain: insight from preclinical studies. *Neurosci Biobehav Rev.* (2014) 47:154–64. doi: 10.1016/j.neubiorev.2014.08.002
6. Maletic V, Raison CL. Neurobiology of depression, fibromyalgia and neuropathic pain. *Front Biosci.* (2009) 14:5291–338. doi: 10.2741/3598
7. Teh WL, Liu J, Satghare P, Samari E, Mok YM, Subramaniam M. Depressive symptoms and health-related quality of life in a heterogeneous psychiatric sample: conditional indirect effects of pain severity and interference. *BMC Psychiatry.* (2021) 21:470. doi: 10.1186/s12888-021-03470-1
8. Goldberg DS, McGee SJ. Pain as a global public health priority. *BMC Public Health.* (2011) 11:770. doi: 10.1186/1471-2458-11-770
9. Zhou W, Jin Y, Meng Q, Zhu X, Bai T, Tian Y, et al. A neural circuit for comorbid depressive symptoms in chronic pain. *Nat Neurosci.* (2019) 22:1649–58. doi: 10.1038/s41593-019-0468-2
10. Saab CY. Pain-related changes in the brain: diagnostic and therapeutic potentials. *Trends Neurosci.* (2012) 35:629–37. doi: 10.1016/j.tins.2012.06.002
11. Chang PC, Centeno MV, Procissi D, Baria A, Apkarian AV. Brain activity for tactile allodynia: a longitudinal awake rat functional magnetic resonance imaging study tracking emergence of neuropathic pain. *Pain.* (2017) 158:488–97. doi: 10.1097/j.pain.0000000000000788
12. Massaly N, Copits BA, Wilson-Poe AR, Hipólito L, Markovic T, Yoon HJ, et al. Pain-Induced negative affect is mediated *via* recruitment of the nucleus accumbens kappa opioid system. *Neuron.* (2019) 102:564–73.e6. doi: 10.1016/j.neuron.2019.02.029
13. George DT, Ameli R, Koob GF. Periaqueductal gray sheds light on dark areas of psychopathology. *Trends Neurosci.* (2019) 42:349–60. doi: 10.1016/j.tins.2019.03.004
14. Jang JH, Song EM, Do YH, Ahn S, Oh JY, Hwang TY, et al. Acupuncture alleviates chronic pain and comorbid conditions in a mouse model of neuropathic pain: the involvement of DNA methylation in the prefrontal cortex. *Pain.* (2021) 162:514–30. doi: 10.1097/j.pain.0000000000002031
15. Zhuo M. Neural mechanisms underlying anxiety-chronic pain interactions. *Trends Neurosci.* (2016) 39:136–45. doi: 10.1016/j.tins.2016.01.006
16. Neugebauer V, Mazzitelli M, Cragg B, Ji G, Navratilova E, Porreca F. Amygdala, neuropeptides, and chronic pain-related affective behaviors. *Neuropharmacology.* (2020) 170:108052. doi: 10.1016/j.neuropharm.2020.108052
17. Raja SN, Carr DB, Cohen M, Finnerup NB, Flor H, Gibson S, et al. The revised international association for the study of pain definition of pain: concepts, challenges, and compromises. *Pain.* (2020) 161:1976–82. doi: 10.1097/j.pain.0000000000001939
18. Bushnell MC, Ceko M, Low LA. Cognitive and emotional control of pain and its disruption in chronic pain. *Nat Rev Neurosci.* (2013) 14:502–11. doi: 10.1038/nrn3516
19. Apkarian VA, Hashmi JA, Baliki MN. Pain and the brain: specificity and plasticity of the brain in clinical chronic pain. *Pain.* (2011) 152(3 Suppl.):S49–S64. doi: 10.1016/j.pain.2010.11.010
20. Zhang XH, Feng CC, Pei LJ, Zhang YN, Chen L, Wei XQ, et al. Electroacupuncture attenuates neuropathic pain and comorbid negative behavior: the involvement of the dopamine system in the amygdala. *Front Neurosci.* (2021) 15:657507. doi: 10.3389/fnins.2021.657507
21. Zhu X, Tang HD, Dong WY, Kang F, Liu A, Mao Y, et al. Distinct thalamocortical circuits underlie allodynia induced by tissue injury and by depression-like states. *Nat Neurosci.* (2021) 24:542–53. doi: 10.1038/s41593-021-00811-x

22. Glover GH. Overview of functional magnetic resonance imaging. *Neurosurg Clin N Am.* (2011) 22:133–9, vii. doi: 10.1016/j.nec.2010.11.001
23. Logothetis NK. What we can do and what we cannot do with Fmri. *Nature.* (2008) 453:869–78. doi: 10.1038/nature06976
24. Cagnie B, Coppieters I, Denecker S, Six J, Danneels L, Meeus M. Central sensitization in fibromyalgia? A systematic review on structural and functional brain Mri. *Semin Arthritis Rheum.* (2014) 44:68–75. doi: 10.1016/j.semarthrit.2014.01.001
25. Boyer A, Deverdun J, Duffau H, Le Bars E, Molino F, Menjot De Champfleur N, et al. Longitudinal changes in cerebellar and thalamic spontaneous neuronal activity after wide-awake surgery of brain tumors: a resting-state fmri study. *Cerebellum.* (2016) 15:451–65. doi: 10.1007/s12311-015-0709-1
26. Zang YF, He Y, Zhu CZ, Cao QJ, Sui MQ, Liang M, et al. Altered baseline brain activity in children with adhd revealed by resting-state functional Mri. *Brain Dev.* (2007) 29:83–91. doi: 10.1016/j.braindev.2006.07.002
27. Zuo XN, Ehmke R, Mennes M, Imperati D, Castellanos FX, Sporns O, et al. Network centrality in the human functional connectome. *Cereb Cortex.* (2012) 22:1862–75. doi: 10.1093/cercor/bhr269
28. Chen J, Yang J, Huang X, Wang Q, Lu C, Liu S, et al. Brain functional biomarkers distinguishing premature ejaculation from anejaculation by Alff: a resting-state Fmri study. *J Sex Med.* (2020) 17:2331–40. doi: 10.1016/j.jsxm.2020.09.002
29. He L, Xu R, Chen Y, Liu X, Pan Y, Cao S, et al. Intra-Ca1 administration of minocycline alters the expression of inflammation-related genes in hippocampus of cci rats. *Front Mol Neurosci.* (2019) 12:248. doi: 10.3389/fnmol.2019.00248
30. Prut L, Belzung C. The open field as a paradigm to measure the effects of drugs on anxiety-like behaviors: a review. *Eur J Pharmacol.* (2003) 463:3–33. doi: 10.1016/S0014-2999(03)01272-X
31. Rodgers RJ, Dalvi A. Anxiety, defence and the elevated plus-maze. *Neurosci Biobehav Rev.* (1997) 21:801–10. doi: 10.1016/S0149-7634(96)00058-9
32. Slattery DA, Cryan JF. Using the rat forced swim test to assess antidepressant-like activity in rodents. *Nat Protoc.* (2012) 7:1009–14. doi: 10.1038/nprot.2012.044
33. Schwarz AJ, Danckaert A, Reese T, Gozzi A, Paxinos G, Watson C, et al. A stereotaxic Mri template set for the rat brain with tissue class distribution maps and co-registered anatomical atlas: application to pharmacological Mri. *Neuroimage.* (2006) 32:538–50. doi: 10.1016/j.neuroimage.2006.04.214
34. Xu QH, Li QY, Yu K, Ge QM, Shi WQ, Li B, et al. Altered brain network centrality in patients with diabetic optic neuropathy: a resting-state fmri study. *Endocr Pract.* (2020) 26:1399–405. doi: 10.4158/EP-2020-0045
35. Ogino Y, Nemoto H, Goto F. Somatotopy in human primary somatosensory cortex in pain system. *Anesthesiology.* (2005) 103:821–7. doi: 10.1097/00000542-200510000-00021
36. Hofbauer RK, Rainville P, Duncan GH, Bushnell MC. Cortical representation of the sensory dimension of pain. *J Neurophysiol.* (2001) 86:402–11. doi: 10.1152/jn.2001.86.1.402
37. Lim M, Roosink M, Kim JS, Kim HW, Lee EB, Son KM, et al. Augmented pain processing in primary and secondary somatosensory cortex in fibromyalgia: a magnetoencephalography study using intra-epidermal electrical stimulation. *PLoS ONE.* (2016) 11:e0151776. doi: 10.1371/journal.pone.0151776
38. Apkarian AV, Bushnell MC, Treede RD, Zubieta JK. Human brain mechanisms of pain perception and regulation in health and disease. *Eur J Pain.* (2005) 9:463–84. doi: 10.1016/j.ejpain.2004.11.001
39. Bak MS, Park H, Kim SK. Neural plasticity in the brain during neuropathic pain. *Biomedicines.* (2021) 9:624. doi: 10.3390/biomedicines9060624
40. Kim D, Chae Y, Park HJ, Lee IS. Effects of chronic pain treatment on altered functional and metabolic activities in the brain: a systematic review and meta-analysis of functional neuroimaging studies. *Front Neurosci.* (2021) 15:684926. doi: 10.3389/fnins.2021.684926
41. Cichon J, Blanck TJJ, Gan WB, Yang G. Activation of cortical somatostatin interneurons prevents the development of neuropathic pain. *Nat Neurosci.* (2017) 20:1122–32. doi: 10.1038/nn.4595
42. Gustin SM, Peck CC, Cheney LB, Macey PM, Murray GM, Henderson LA. Pain and plasticity: is chronic pain always associated with somatosensory cortex activity and reorganization? *J Neurosci.* (2012) 32:14874–84. doi: 10.1523/JNEUROSCI.1733-12.2012
43. Jenkins LC, Chang WJ, Buscemi V, Liston M, Skippen P, Cashin AG, et al. Low somatosensory cortex excitability in the acute stage of low back pain causes chronic pain. *J Pain.* (2021) 23:289–304. doi: 10.1016/j.jpain.2021.08.003
44. Wei JA, Hu X, Zhang B, Liu L, Chen K, So KF, et al. Electroacupuncture activates inhibitory neural circuits in the somatosensory cortex to relieve neuropathic pain. *iScience.* (2021) 24:102066. doi: 10.1016/j.isci.2021.102066
45. Jin Y, Meng Q, Mei L, Zhou W, Zhu X, Mao Y, et al. A somatosensory cortex input to the caudal dorsolateral striatum controls comorbid anxiety in persistent pain. *Pain.* (2020) 161:416–28. doi: 10.1097/j.pain.0000000000001724
46. Singh A, Patel D, Li A, Hu L, Zhang Q, Liu Y, et al. Mapping cortical integration of sensory and affective pain pathways. *Curr Biol.* (2020) 30:1703–15 e5. doi: 10.1016/j.cub.2020.02.091
47. Salomons TV, Johnstone T, Backonja MM, Shackman AJ, Davidson RJ. Individual differences in the effects of perceived controllability on pain perception: critical role of the prefrontal cortex. *J Cogn Neurosci.* (2007) 19:993–1003. doi: 10.1162/jocn.2007.19.6.993
48. Etkin A, Egner T, Kalisch R. Emotional processing in anterior cingulate and medial prefrontal cortex. *Trends Cogn Sci.* (2011) 15:85–93. doi: 10.1016/j.tics.2010.11.004
49. Kragel PA, Kano M, Van Oudenhove L, Ly HG, Dupont P, Rubio A, et al. Generalizable representations of pain, cognitive control, and negative emotion in medial frontal cortex. *Nat Neurosci.* (2018) 21:283–9. doi: 10.1038/s41593-017-0051-7
50. Ong WY, Stohler CS, Herr DR. Role of the prefrontal cortex in pain processing. *Mol Neurobiol.* (2019) 56:1137–66. doi: 10.1007/s12035-018-1130-9
51. Kang D, McAuley JH, Kassem MS, Gatt JM, Gustin SM. What does the grey matter decrease in the medial prefrontal cortex reflect in people with chronic pain? *Eur J Pain.* (2019) 23:203–19. doi: 10.1002/ejp.1304
52. Mitrić M, Seewald A, Moschetti G, Sacerdote P, Ferraguti F, Kummer KK, et al. Layer- and subregion-specific electrophysiological and morphological changes of the medial prefrontal cortex in a mouse model of neuropathic pain. *Sci Rep.* (2019) 9:9479. doi: 10.1038/s41598-019-45677-z
53. Sang K, Bao C, Xin Y, Hu S, Gao X, Wang Y, et al. Plastic change of prefrontal cortex mediates anxiety-like behaviors associated with chronic pain in neuropathic rats. *Mol Pain.* (2018) 14:1744806918783931. doi: 10.1177/1744806918783931
54. Mecca CM, Chao D, Yu G, Feng Y, Segel I, Zhang Z, et al. Dynamic change of endocannabinoid signaling in the medial prefrontal cortex controls the development of depression after neuropathic pain. *J Neurosci.* (2021) 41:7492–508. doi: 10.1523/JNEUROSCI.3135-20.2021
55. Hashmi JA, Baliki MN, Huang L, Baria AT, Torbey S, Hermann KM, et al. Shape shifting pain: chronification of back pain shifts brain representation from nociceptive to emotional circuits. *Brain.* (2013) 136(Pt 9):2751–68. doi: 10.1093/brain/awt211
56. Makary MM, Polosecki P, Cecchi GA, DeAraujo IE, Barron DS, Constable TR, et al. Loss of nucleus accumbens low-frequency fluctuations is a signature of chronic pain. *Proc Natl Acad Sci USA.* (2020) 117:10015–23. doi: 10.1073/pnas.1918682117
57. Ren W, Centeno MV, Berger S, Wu Y, Na X, Liu X, et al. The indirect pathway of the nucleus accumbens shell amplifies neuropathic pain. *Nature Neuroscience.* (2016) 19:220–2. doi: 10.1038/nn.4199
58. Wu XB, Zhu Q, Gao YJ. Ccl2/Ccr2 contributes to the altered excitatory-inhibitory synaptic balance in the nucleus accumbens shell following peripheral nerve injury-induced neuropathic pain. *Neurosci Bull.* (2021) 37:921–33. doi: 10.1007/s12264-021-00697-6
59. Simis M, Imamura M, de Melo PS, Marduy A, Pacheco-Barrios K, Teixeira PEP, et al. Increased motor cortex inhibition as a marker of compensation to chronic pain in knee osteoarthritis. *Sci Rep.* (2021) 11:24011. doi: 10.1038/s41598-021-03281-0
60. Hamani C, Fonoff ET, Parravano DC, Silva VA, Galhardoni R, Monaco BA, et al. Motor cortex stimulation for chronic neuropathic pain: results of a double-blind randomized study. *Brain.* (2021) 144:2994–3004. doi: 10.1093/brain/awab189
61. Mascio G, Notartomaso S, Martinello K, Liberatore F, Bucci D, Imbriglio T, et al. A progressive build-up of perineuronal nets in the somatosensory cortex ss associated with the development of chronic pain

in mice. *J Neurosci.* (2022) 42:3037–48. doi: 10.1523/JNEUROSCI.1714-21.2022
62. Chiou RJ, Lee HY, Chang CW, Lin KH, Kuo CC. Epidural motor cortex stimulation suppresses somatosensory evoked potentials in the primary somatosensory cortex of the rat. *Brain Res.* (2012) 1463:42–50. doi: 10.1016/j.brainres.2012.04.027
63. Kai Y, Li Y, Sun T, Yin W, Mao Y, Li J, et al. A medial prefrontal cortex-nucleus acumens corticotropin-releasing factor circuitry for neuropathic pain-increased susceptibility to opioid reward. *Transl Psychiatry.* (2018) 8:100. doi: 10.1038/s41398-018-0152-4
64. Hu XS, Beard K, Sherbel MC, Nascimento TD, Petty S, Pantzlaff E, et al. Brain mechanisms of virtual reality breathing versus traditional mindful breathing in pain modulation: observational functional near-infrared spectroscopy study. *J Med Internet Res.* (2021) 23:e27298. doi: 10.2196/27298
65. Midavaine É, Côté J, Marchand S, Sarret P. Glial and neuroimmune cell choreography in sexually dimorphic pain signaling. *Neurosci Biobehav Rev.* (2021) 125:168–92. doi: 10.1016/j.neubiorev.2021.01.023

Conflict of Interest: The authors declare that the research was conducted in the absence of any commercial or financial relationships that could be construed as a potential conflict of interest.

frontiers | Frontiers in Neurology

ORIGINAL RESEARCH
published: 02 May 2022
doi: 10.3389/fneur.2022.884770

Brain Mechanism of Acupuncture Treatment of Chronic Pain: An Individual-Level Positron Emission Tomography Study

Jin Xu[1†], *Hongjun Xie*[2†], *Liying Liu*[1†], *Zhifu Shen*[3], *Lu Yang*[1], *Wei Wei*[1], *Xiaoli Guo*[1], *Fanrong Liang*[1], *Siyi Yu*[1*] and *Jie Yang*[1*]

[1] Department of Acupuncture and Tuina, Chengdu University of Traditional Chinese Medicine, Chengdu, China, [2] Department of Nuclear Medicine, Sichuan Academy of Medical Sciences and Sichuan Provincial People's Hospital, Chengdu, China, [3] Department of Traditional Chinese and Western Medicine, North Sichuan Medical College, Nanchong, China

OPEN ACCESS

Edited by:
Lingmin Jin,
Guizhou University of Traditional Chinese Medicine, China

Reviewed by:
Rui Zhao,
Xi'an Polytechnic University, China
Taipin Guo,
Yunnan University of Traditional Chinese Medicine, China

***Correspondence:**
Jie Yang
jenny_yang_jie@126.com
Siyi Yu
cdutcmysy@gmail.com

[†] These authors have contributed equally to this work

Specialty section:
This article was submitted to Headache and Neurogenic Pain, a section of the journal Frontiers in Neurology

Received: 27 February 2022
Accepted: 22 March 2022
Published: 02 May 2022

Citation:
Xu J, Xie H, Liu L, Shen Z, Yang L, Wei W, Guo X, Liang F, Yu S and Yang J (2022) Brain Mechanism of Acupuncture Treatment of Chronic Pain: An Individual-Level Positron Emission Tomography Study. Front. Neurol. 13:884770. doi: 10.3389/fneur.2022.884770

Objective: Acupuncture has been shown to be effective in the treatment of chronic pain. However, their neural mechanism underlying the effective acupuncture response to chronic pain is still unclear. We investigated whether metabolic patterns in the pain matrix network might predict acupuncture therapy responses in patients with primary dysmenorrhea (PDM) using a machine-learning-based multivariate pattern analysis (MVPA) on positron emission tomography data (PET).

Methods: Forty-two patients with PDM were selected and randomized into two groups: real acupuncture and sham acupuncture (three menstrual cycles). Brain metabolic data from the three special brain networks (the sensorimotor network (SMN), default mode network (DMN), and salience network (SN)) were extracted at the individual level by using PETSurfer in fluorine-18 fluorodeoxyglucose positron emission tomography (^{18}F-FDG-PET) data. MVPA analysis based on metabolic network features was employed to predict the pain relief after treatment in the pooled group and real acupuncture treatment, separately.

Results: Paired *t*-tests revealed significant alterations in pain intensity after real but not sham acupuncture treatment. Traditional mass-univariate correlations between brain metabolic and alterations in pain intensity were not significant. The MVPA results showed that the brain metabolic pattern in the DMN and SMN did predict the pain relief in the pooled group of patients with PDM ($R^2 = 0.25$, $p = 0.005$). In addition, the metabolic pattern in the DMN could predict the pain relief after treatment in the real acupuncture treatment group ($R^2 = 0.40$, $p = 0.01$).

Conclusion: This study indicates that the individual-level metabolic patterns in DMN is associated with real acupuncture treatment response in chronic pain. The present findings advanced the knowledge of the brain mechanism of the acupuncture treatment in chronic pain.

Keywords: acupuncture, metabolic, biomarker, primary dysmenorrhea, machine learning

INTRODUCTION

Acupuncture, a traditional Chinese medical procedure, has been widely used to alleviate diverse pains for over 2,000 years (1). The National Institutes of Health have suggested acupuncture as a potentially useful option for various chronic pain disorders, such as menstrual pain (2). Primary dysmenorrhea (PDM), a classic chronic and cyclic pain disorder, is characterized by cyclic cramping pain in the lower abdomen during menstruation and a lack of any visible pelvic pathology. PDM affects most women throughout the menstrual years, with up to 90% of adolescent females globally reported experiencing it (3). Although PDM is a common reason for work absenteeism and lower quality of life in women, the disorder is often under-diagnosed and poorly treated (4). Several randomized controlled trials (RCTs) further suggest favorable effects of acupuncture on menstrual pain intensity and other symptoms of dysmenorrhea (5–7). Moreover, our previous meta-analysis also demonstrated that acupuncture is safe and effective in PDM management (8), and real acupuncture could be more effective than placebo/sham group in pain relief (9).

Although acupuncture has been shown to be effective in pain relief in patients with PDM, the inter-individual response of different patients to acupuncture treatment varies greatly (10–12). Similarity, responses to other treatments for pain are also be affected by multidimensional individual differences (13–15). Because pain is a highly personal and subjective experience, it is not surprising that the outcome of treatment is influenced by the baseline physiological state of individuals (16, 17). Thus, the baseline brain characteristics of individuals might be a useful biomarker to predict differential responses to intervention strategies.

Neuroimaging biomarkers have recently proven promising for predicting responses to treatment and are used for elucidating the underlying brain mechanism for pain relief. For example, Reggente et al. (18) found that pre-treatment brain connectivity in the visual network and the default mode network (DMN) significantly predicted obsessive-compulsive disorder severity after treatment. Conversely, clinical pre-treatment variables did not reliably predict post-treatment outcomes, indicating that brain networks are stronger predictors than more readily obtained clinical scores. A recent study found that resting-state regional homogeneity in the temporoparietal junction was an important predictive factor of treatment effects of acupuncture in patients with cervical spondylosis neck pain (19). As such earlier studies show successful applications of brain-based biomarkers to predict therapeutic effects at the individual level, the development of quantitative, objective neuroimaging biomarkers/predictors is of increasing importance to provide optimal treatment for PDM and provides a useful approach to illustrate the broad applicability of acupuncture. In the past few years, neuroimaging studies of PDM have increasingly and collectively shown that PDM is associated with significant changes in brain anatomy, function, and metabolism (20–24). However, no study investigates the individual-level metabolic biomarker of treatment response in PDM.

In this exploratory study, we thus aimed to investigate whether individual-level brain metabolic biomarkers in a special network at baseline can predict acupuncture responses in the treatment of PDM using multivariate pattern analysis (MVPA)-based machine-learning techniques. We first acquired metabolic data from 42 individuals with PDM who underwent fluorine-18 fluorodeoxyglucose positron emission tomography (^{18}F-FDG PET-CT) at baseline. Participants were then randomized into a real group and a sham acupuncture group and treated over the course of three menstrual cycles. Lastly, MVPA was applied to explore the optimal metabolic predictors for clinical responses after treatment in subjects with PDM. To improve the analytic power and efficiency in this study, we restricted them to some special networks, such as the DMN, the sensorimotor network (SMN), and the salience network (SN), where previous studies found abnormal alterations in patients with chronic pain. We hypothesized that the individual-level metabolic patterns of these target networks can predict acupuncture responses in patients with PDM.

MATERIALS AND METHODS

Participants

A total of 42 patients with PDM were enrolled *via* advertisements and hearsay, and all participants were confirmed through telephone and face-to-face interviews. This study was approved by the affiliated Hospital of Chengdu University of Traditional Chinese Medicine Institutional Review Board. Before participation, all patients provided voluntary informed consent. The inclusion criteria for enrollment were fellows: (1) between the ages of 18 and 30; (2) a regular menstrual cycle (27–32 days); (3) more than 1 year of PDM history; (4) no hormones or centrally acting medication in the last 6 months; (5) cramping pain during menstruation at least 4 on a 0–10 visual analog scale (VAS); and (6) right-handedness. Exclusion criteria were as follows: (1) organic pelvic diseases; (2) visceral pain caused by other diseases; (3) a positive pregnancy test; (4) a history of neurological or psychiatric disorders; and (5) any contraindications to PET or MRI scanning. During the study, four cases were dropped out before the first clinical measurement and imaging scan, and five cases were dropped out before the first acupuncture treatment. Four cases did not complete all treatment sessions. Finally, 29 patients completed all clinical assessments and imaging sessions (**Figure 1**).

Clinical Assessment

In this study, we used VAS (0 = "no pain at all," 10 = "unbearable pain") as primary outcome measurement to assess menstrual pain severity (25). In addition, the Zung Self-Rating Depression Scale (SDS) and the Zung Self-Rating Anxiety Scale (SAS) were also used to access the mental state of participants (26, 27). All clinical assessments were measured at baseline and after 3 menstrual cycles' acupuncture treatments.

Acupuncture Intervention

Patients were randomly assigned to either the real or sham acupuncture groups using a computer-generated random-allocation process. All participants and clinical evaluators were unaware of the group assignment until the end of the study. Only

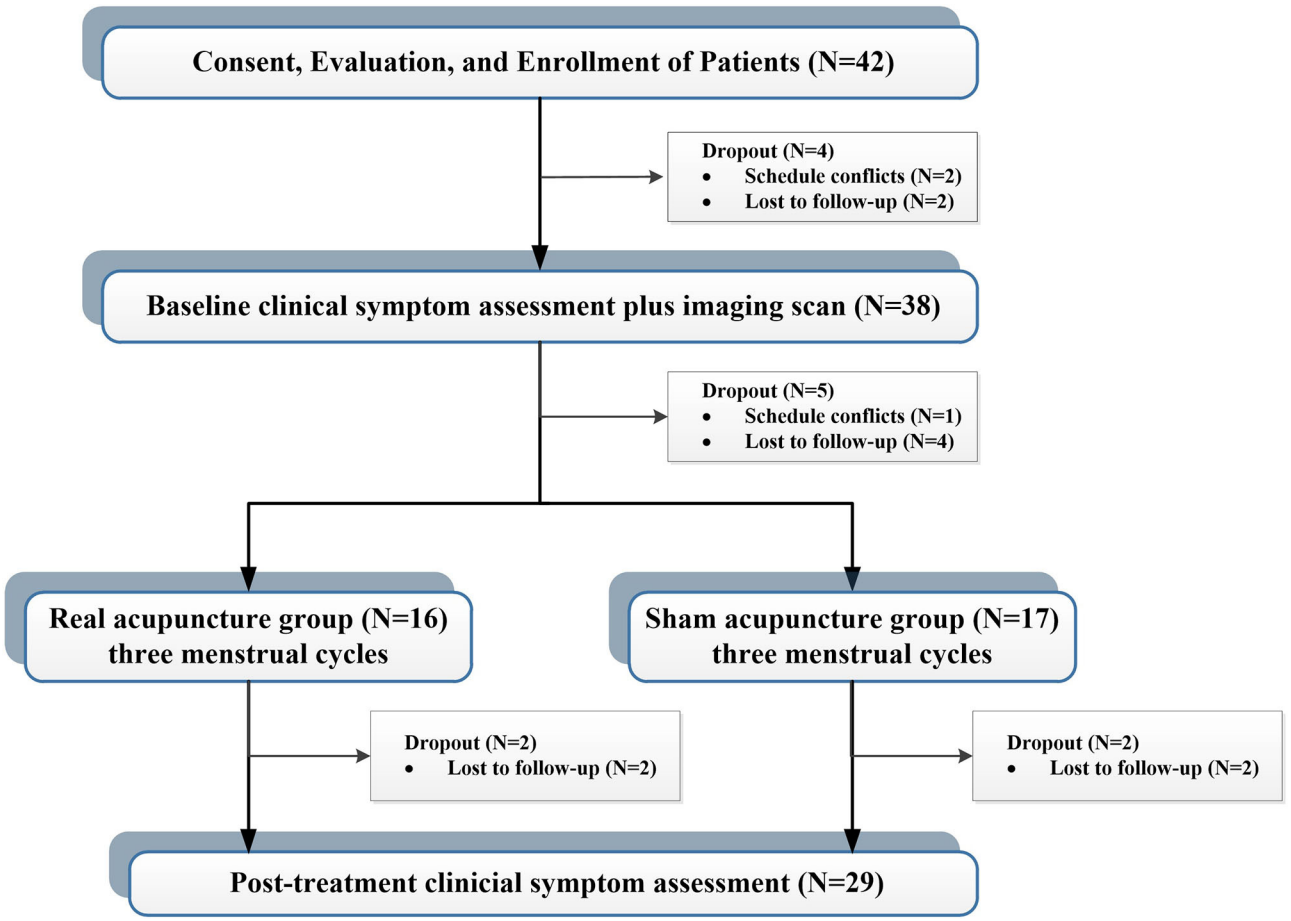

FIGURE 1 | Study design and research flow chart.

the acupuncturists were informed about the treatment allocation and accordingly delivered real or sham treatment. Two licensed acupuncturists with at least 3 years of experience performed acupuncture on two groups of PDM patients. Participants received a course of acupuncture treatment that lasted 5–7 days before menstrual onset. The treatments lasted 3 weeks.

Based on the date-driven results of previous research and expert opinions, the *Sanyinjiao* (SP6) point was chosen for the real acupuncture treatment (28). The SP6 is located on the posterior border of the tibia and 3 *cun* directly superior to the tip of the medial malleolus (29). After the skin has been cleaned with 75% alcohol, 0.25 × 40-mm stainless needles (Hwatuo, Suzhou, China) were inserted to a depth of 1.0–1.2 *cun* and gently twisted, lifted, and thrust at an even amplitude, force, and speed. "Deqi" sensation of a soreness, numbness, heaviness, and distension sensation was essential during and after the operation. A 30-s manipulation was conducted every 10 min during 30-min needling retention. For the sham group, a nearby sham acupoint was chosen at the same level as the SP6 and *Xuanzhong* (GB39), at the midpoint of the stomach and gallbladder meridians. Patients in the sham group had an acupuncture technique comparable to those in the actual acupuncture group. However, there was no manipulation following needle insertion, and the "Deqi" sensation was not required.

Statistical Analysis of Clinical Data

All statistical analyses were conducted in SPSS (SPSS statistical software, version 22.0, SPSS Inc., Chicago, IL, USA). The inner-group difference in VAS score (post-treatment minus pre-treatment) across each treatment group was tested by using paired t-test. Furthermore, a two-sample *t*-test has been used to compare the within-group difference of VAS score change (post-treatment minus pre-treatment) between the real and sham acupuncture groups. In addition, the relationships between before and after treatment clinical features were assessed with partial correlation analysis, controlling for age and treatment method. The significant level for all analyses was set at $p < 0.05$.

Imaging Acquisition

The structural MRI (sMRI) data were acquired to co-register the brain region to the PET image. A 32-channel radio-frequency head coil in a 3.0-Tesla magnetic resonance scanner was used to collect MRI data (Discovery MR750, General Electric, Milwaukee, WI, USA). To limit head motion and scanner

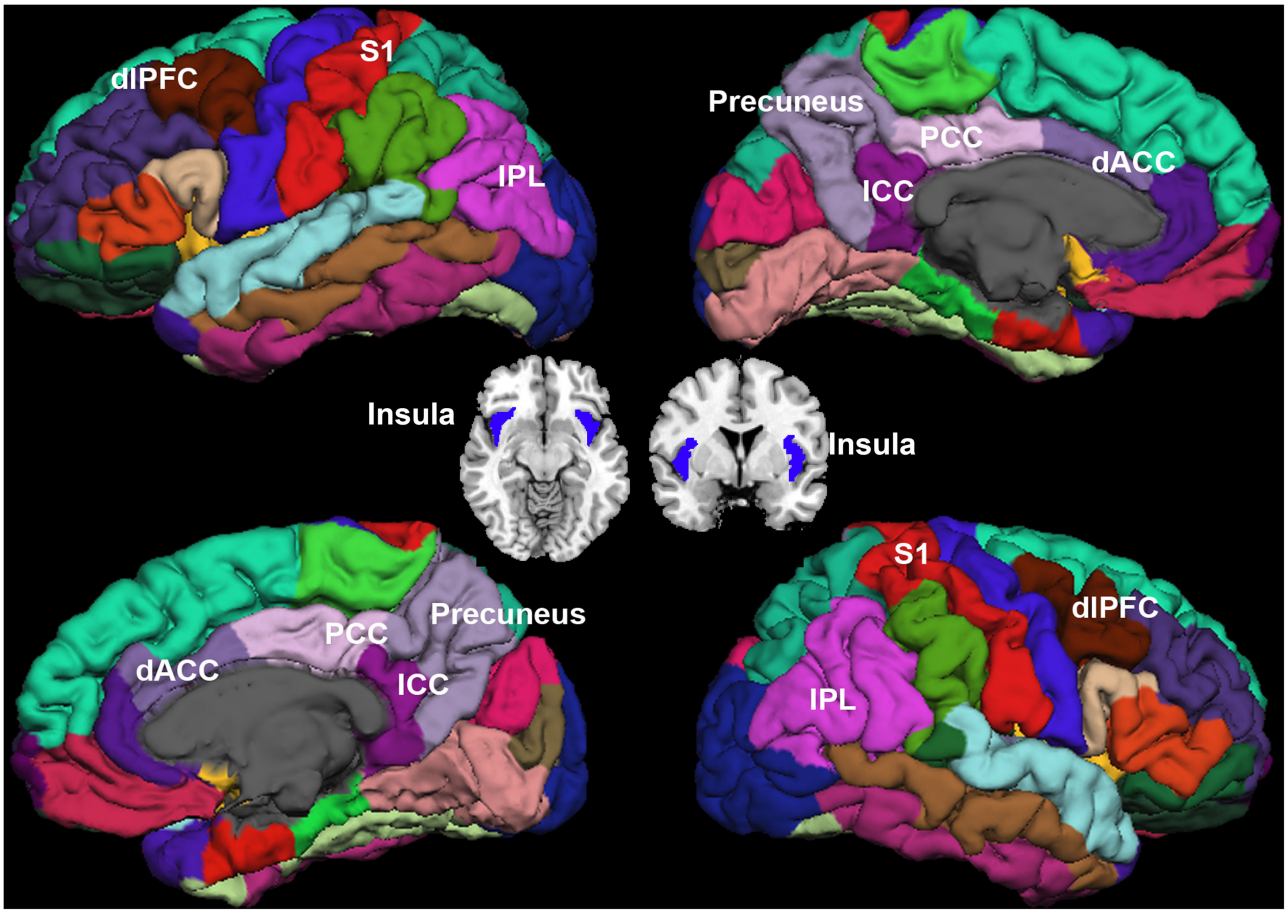

FIGURE 2 | Regions of interest. Sensorimotor network (SMN): bilateral post-central (S1), and bilateral insula. Salience network (SN): the dorsolateral prefrontal cortex (dlPFC), and bilateral dorsal anterior cingulate cortex (dACC). Default mode network (DMN): bilateral inferior parietal cortex (IPC), precuneus, isthmus cingulate cortex (ICC), and posterior cingulate cortex (PCC).

noise, earplugs and tight yet soft foam padding were used. The following parameters were used to create a high-resolution, T1-weighted structural image: repetition time = 2,530 ms, echo time = 3.39 ms, field of view = 256 mm × 256 mm, data matrix = 256 × 256; slice thickness = 1 mm, gap = 0 mm, and flip angle = 7°. Referring to our previous studies (30), ^{18}F-FDG-PET scanning was prepared at Sichuan Provincial People's Hospital using a Biograph Duo BGO scanner (Siemens, Munich, Germany). The FDG-PET image was scanned in the morning during the periovulatory phase (the middle 5 days between the two menstrual periods). After fasting for at least 12 h, patients underwent the following procedures: (1) fasting plasma glucose and resting blood pressure measurements at 8 a.m., (2) a 15–20 min peaceful rest in a darkroom, (3) an intravenous injection of fluorine-18 fluorodeoxyglucose on the back of the right hand (synthesized with a Mini Tracer accelerator at 0.11 MCi/kg dosage), (4) a 40-min rest, and (5) a PET-CT scan. Before picture capture, there was a 40-min uptake period. Patients were encouraged to stay motionless during scanning by having their heads immobilized, their ears muffled, and their eyes blinded.

Region of Interest (ROI) Selection

Sixteen ROIs in the cortical region were selected for further analysis (**Figure 2**). Four regions were identified as key regions within the SMN, the bilateral post-central (S1), and bilateral insula (31, 32), which represent the major ascending pathways of pain; four regions were selected in the SN, which represent the descending pathways that modulate pain by inhibiting nociceptive transmission, such as the bilateral caudal middle frontal gyrus (a region within the dorsolateral prefrontal cortex, dlPFC), the bilateral caudal anterior cingulate cortex (a region in the dorsal anterior cingulate cortex, dACC) (33); and eight regions were selected in the DMN, which are involved in pain rumination (34), such as the bilateral inferior parietal cortex (IPC), the precuneus, the isthmus cingulate cortex, and the posterior cingulate cortex (PCC).

Imaging Processing and Individual-Level Metabolic Extraction

The pre-processing of sMRI and metabolic data was conducted using FreeSurfer and PETSurfer toolbox (version 6.0, http://

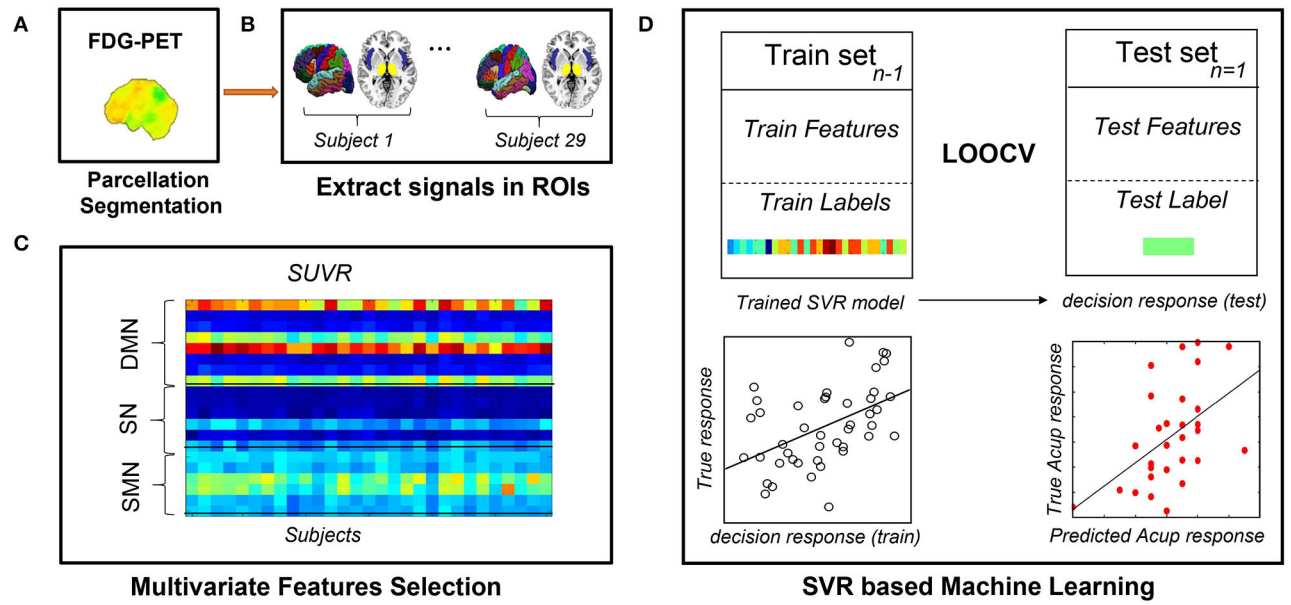

FIGURE 3 | Flowchart of the MVPA procedure. **(A)** Obtaining quantitative information from preprocessed PDG-PET scans. **(B)** Extracting metabolism data across all voxels in all ROIs. **(C)** Constructing feature matrixes of the SUVR. **(D)** Building the SVR model with LOOCV to predict each participant's response to acupuncture. FDG-PET, fluorodeoxyglucose positron emission tomography; LOOCV, leave-one-out cross-validation; ROIs, regions of interest; sMRI, structural magnetic resonance imaging; SUVR, standardized uptake value ratio; SVR, support vector regression.

surfer.nmr.harvard.edu/). First, the cortical parcellation and subcortical segmentation methods have been described in detail in our prior publications (35, 36). Second, the standardized uptake value rate (SUVR) was calculated for the metabolic state in the brain regions. The SUVR is useful for normalizing the comparison of the significant inter-individual variability in the global PET signal (37). A symmetric geometric transfer matrix (SGTM) method was used for partial volume correction (PVC) where limited scanner resolution causes the activity to appear to spill out of one region and into another (38). To perform PVC, the PET data were registered to the MRI data *via* boundary-based registration (BBR) using a six degree of freedom linear transform (39). The MRI segmentation was mapped onto the PET space in a way that accounted for the tissue fraction effect (38). The SUVR for each ROI was computed by dividing the intensity of the ROI by the intensity of the pons at the individual level (39) (FreeSurfer commands: gemseg, mri_coreg, and mri_gtmpvc). Third, the SUVR data of the 16 ROIs were extracted from the processed images at the individual level for further analysis.

Multivariate Pattern Analysis

We attempted to predict clinical symptom alterations after the treatment based on special metabolic networks. We used linear support vector regression (SVR) that was implemented with the LIBSVM toolbox (40) for model training and further prediction analysis. We used the change in pain severity (VAS change) as the dependent variable and brain metabolic network features as independent variables (predictors) while controlling for effects of age, treatment method (only in the pooled group prediction analysis, see below), and VAS score at baseline. A leave-one-out cross-validation (LOOCV) method was used to ensure a clear separation between training and test sets. LOOCV is appropriate for preliminary estimate prediction in longitudinally neuroimaging studies where sample sizes are small (41). To evaluate the predictive ability of SVR, we calculated the mean absolute error, defined as the mean discrepancy between actual and predicted values (42, 43), and the squared prediction-outcome correlation (R^2), defined as the squared correlation between the prediction and true outcome. Furthermore, we estimated the probability that random chance would predict the treatment response and SVR method (permutation test with 10,000 iterations). Because of the small sample size of the present study, we combined the real and sham groups for a pooled group MVPA analysis, where the treatment method effect was controlled as a covariate. In addition, the MVPA analysis was also conducted within each group separately. **Figure 3** illustrates the individualized prediction framework used in this investigation.

Mass-Univariate Correlation Analysis

To directly compare our multivariate SVR analysis with traditional mass-univariate correlation analyses, we tested the association between treatment responses and metabolic properties in each ROI using a traditional bivariate Pearson correlation analysis. The significance level was set at $p < 0.05$.

RESULTS

Demographic Characteristics and Clinical Results

As shown in **Table 1**, statistical analysis indicats no significant difference in age, disease duration, body mass index (BMI), baseline VAS scores, SDS scores, and SAS scores between the

TABLE 1 | Demographics and clinical characteristics of each group.

	Real ($n = 14$)		Sham ($n = 15$)		*T*	*P*
	Mean	**SD**	**Mean**	**SD**		
Age (years)	24.86	1.75	24.53	2.07	0.45	0.653
Duration (months)	90.57	36.31	97.40	34.09	−0.52	0.606
BMI	19.20	1.15	19.45	1.81	−0.44	0.664
Baseline VAS	6.07	1.07	6.00	1.20	0.17	0.867
Baseline SDS	39.68	7.28	43.42	10.07	−1.14	0.265
Baseline SAS	41.34	5.56	40.55	7.80	0.31	0.758
Post-treatment VAS	3.50	1.70	5.30	1.39	−3.14	0.004
Change VAS	−2.57	1.55	−0.70	1.62	−3.17	0.004

BMI, body mass index; VAS, visual analog scale; SAS, Self-Rating Anxiety Scale; SDS, Self-Report Depression Scale.

two treatment groups at the baseline stage (all $p > 0.05$). For intra-group comparison, the post-treatment VAS value was significantly decreased in the real acupuncture group than baseline ($T = 6.19$, $p = 3.28 \times 10^{-5}$); however, no change was detected in the sham acupuncture group throughout the trial ($T = 1.67$, $p = 0.12$). For inter-group comparison, there was a significant difference in the real acupuncture vs. sham acupuncture group in the changes of VAS value after three menstrual cycles of treatment ($T = -3.17$, $p = 0.004$). Baseline VAS scores were not significantly associated with VAS changes after treatment after controlling for age and treatment methods in the pooled group analysis ($R = -0.34$, $p = 0.07$) and the real acupuncture group ($R = -0.20$, $p = 0.51$). In addition, treatment responses did not correlate with disease duration, SAS, or SDS (all $p > 0.05$). In addition, no significant difference was found in the SUVR in all selected regions between the two groups (all $p > 0.05$), see **Table 2**.

MVPA Analysis Results

The SUVR patterns in the SMN and DMN could predict the VAS changes in the pooled group (SMN, $R^2 = 0.20$, $p = 0.01$, Mean Absolute Error = 2.64; DMN, $R^2 = 0.14$, $p = 0.04$, Mean Absolute Error = 2.51). In addition, the mixed SUVR pattern in the DMN and SMN could predict better for the VAS changes in the pooled group ($R^2 = 0.25$, $p = 0.005$, Mean Absolute Error = 2.70; **Figure 4A**). In the real acupuncture group, the SUVR pattern in the DMN could predict the VAS changes after treatment ($R^2 = 0.40$, $p = 0.01$, Mean Absolute Error = 2.71; **Figure 4B**). No other significant predictor was found in the real acupuncture or the sham acupuncture group.

Mass-Univariate Correlation Results

To directly compare the multivariate pattern machine-learning analysis with traditional mass-univariate correlation analyses, we conducted Pearson correlation analyses. The results are displayed in **Table 3**: no significant association between regional SUVR and VAS changes is found using univariate correlation analysis.

DISCUSSION

To our knowledge, this is the first study using a brain metabolic biomarker to predict the pain relief after acupuncture treatment in chronic pain disorders. MVPA-based machine-learning approach was employed to explore whether pre-treatment brain metabolism in three special networks (SMN, DMN, and SN) can predict acupuncture treatment responses in patients with PDM. The MVPA results show that mixed DMN and SMN did indeed predict the observed pain relief in patients with PDM. Specially, the DMN metabolic pattern could predict the pain relief after real acupuncture treatment in patients with PDM. These findings support the brain metabolic mechanism in the acupuncture treatment for chronic pain.

Multivariate pattern analysis is a widely used machine-learning approach in the neuroimaging research field (44). This technique has been used to investigate the pathophysiology of chronic pain conditions, such as neck pain (19), trigeminal neuralgia (45), and chronic back pain (46). The present findings illustrated that metabolic features at baseline may be a useful predictor for acupuncture treatment responses in patients with PDM. In our study, the predictive power and strength of MVPA approaches were validated in two ways. First, we found that baseline clinical or demographic features were not enough to predict outcome responses. Our results converge with previous findings of more accurate predictions from neural than readily obtained clinical information (47, 48). The MVPA analysis, where baseline VAS scores were controlled as covariates, suggests that baseline biomarkers reflect the capacity of an individual with PDM to return to normalcy (quantified by their VAS score) after acupuncture, independent of their starting symptom severity. Second, the traditional mass-univariate correlations between brain metabolic features and VAS changes were not significant. MVPA technology can increase sensitivity to subtle and spatially distributed brain differences, which may not be detected by traditional approaches (49, 50). We thus demonstrate the feasibility and reliability of MVPA models for predicting clinical symptom changes after acupuncture treatment in patients with PDM.

In our SVR models, the multivariate pattern in the SMN and DMN significantly predicted the VAS changes. The key role of the DMN and SMN in predicting responses to acupuncture is consistent with the central role of these networks in the pathophysiology of PDM. In some previous studies, brain abnormalities in areas associated with DMN and SMN have been confirmed to be related to PDM. For instance, using PET (20) and sMRI (21, 51), Tu et al. found increases in metabolism and altered gray matter volumes in brain regions within the DMN in patients with PDM vs. healthy controls. Of note, the SMN is involved in the sensory-discriminative aspects of pain. A resting-state functional MRI (fMRI) study observed a trait-related reduction of functional connectivity between the DMN and the SMN during a pain-free phase, indicating that the altered

TABLE 2 | The SUVR in all selected regions of each group.

Brain Networks	Regions	Real ($n = 14$)		Sham ($n = 15$)		*T*	*P*
		Mean	SD	Mean	SD		
Salience network	Left dACC	3.05	0.18	3.09	0.20	1.05	0.30
	Left dlPFC	2.75	0.13	2.74	0.10	0.20	0.84
	Right dACC	2.77	0.18	2.85	0.24	−1.03	0.31
	Right dlPFC	2.68	0.15	2.67	0.12	0.07	0.95
Default mode network	Left IPC	2.54	0.12	2.54	0.07	−0.22	0.83
	Left ICC	2.50	0.09	2.50	0.14	−0.10	0.92
	Left PCC	2.67	0.10	2.69	0.11	−0.45	0.66
	Left PCU	2.52	0.11	2.48	0.10	0.87	0.39
	Right IPC	2.58	0.10	2.55	0.09	0.72	0.48
	Right ICC	2.47	0.17	2.52	0.11	−0.98	0.34
	Right PCC	2.63	0.12	2.70	0.10	−1.73	0.10
	Right PCU	2.54	0.09	2.56	0.08	−0.48	0.64
Sensorimotor network	Left S1	2.17	0.08	2.17	0.09	0.03	0.98
	Left Insula	2.93	0.16	2.91	0.15	0.29	0.78
	Right S1	2.13	0.08	2.17	0.11	−0.95	0.35
	Right Insula	2.88	0.18	2.94	0.11	−0.94	0.35

dACC, dorsal anterior cingulate cortex; dlPFC, dorsolateral prefrontal cortex; IPC, inferior parietal cortex; ICC, isthmus cingulate cortex; PCC, posterior cingulate cortex; PCU, precuneus; S1, postcentral.

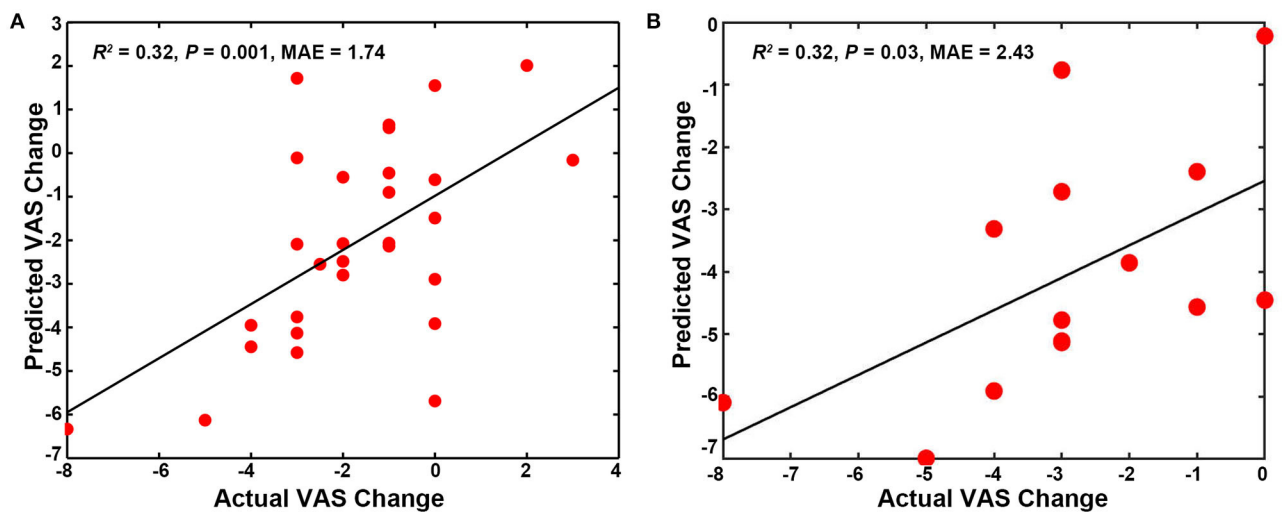

FIGURE 4 | Predicting treatment effects using baseline SUVR patterns in special networks. **(A)** SUVR pattern in the SMN and DMN as a predictor for the pooled group. **(B)** SUVR pattern in the DMN as a predictor for the real acupuncture treatment group. DMN, default mode network; SMN, sensorimotor network; SN, salience network; SUVR, standardized uptake value ratio.

DMN and SMN may be an ongoing representation of cumulative menstrual pain (52). Additionally, multiple neuroimaging studies have suggested that acupuncture may have analgesic effects by modulating the DMN and SMN (53–56), indicating that these brain networks also play an important role in mediating acupuncture effects. For example, Dhond et al. (57) demonstrated that acupuncture treatment induced hyperconnectivity of the DMN to pain, memory, and affective regions and also increased SMN connectivity to pain-related brain regions. Specially, for the real acupuncture treatment group, we also found that the metabolic in DMN, not SMN and SN, could predict the treatment response in PDM. The DMNs have been considered to be involved in pain rumination (34), and the structural, metabolic, and functional alterations in DMN have been manifested in amount of previous neuroimaging studies (21, 51). Taken together, these findings proposed that metabolic features within the DMN and SMN can be used not only to identify the pathogenesis of PDM but also to predict therapy responsiveness, especially, the DMN metabolic feature could predict the real acupuncture response for PDM.

TABLE 3 | The relationship between change of VAS and brain features by using bivariate Pearson correlation analyses.

Brain network	ROI	*R*	*P*
Default mode network	Left IPC	0.29	0.12
	Left ICC	0.26	0.18
	Left PCC	0.25	0.19
	Left PCU	0.36	0.05
	Right IPC	0.30	0.11
	Right ICC	0.37	0.05
	Right PCC	0.29	0.13
	Right PCU	0.37	0.05
Salience network	Left dACC	0.14	0.48
	Left dlPFC	0.24	0.20
	Right dACC	0.30	0.11
	Right dlPFC	0.29	0.13
Sensorimotor network	Left S1	0.29	0.13
	Left Insula	0.34	0.08
	Right S1	0.32	0.09
	Right Insula	0.32	0.09

dACC, dorsal anterior cingulate cortex; dlPFC, dorsolateral prefrontal cortex; IPC, inferior parietal cortex; ICC, isthmus cingulate cortex; PCC, posterior cingulate cortex; PCU, precuneus; S1, postcentral.

It should be emphasized that we combined the two therapy groups into a pooled group to increase statistical power in the MVPA analysis. Although we have controlled for the treatment method as a covariate, the different neural mechanisms underlying the effects observed in the real and sham acupuncture groups might have influenced the present results (10). Our analyses also identify the MVPA model as a potential predictor for treatment responses in the real acupuncture but not the sham acupuncture group. Additional studies with larger sample sizes are needed to examine further predictors for real and sham treatments in PDM. In summary, our research is in line with the growing interest in multivariate neuroimaging features and machine-learning methods for therapeutic outcome prediction and the tailoring of personalized interventions (58–60). In recent years, machine-learning-based predictive models have been successfully applied in a variety of therapies, such as transcranial magnetic stimulation (61), electroconvulsive therapy (62), and vagus nerve stimulation (63). These studies are beginning to unlock the potential and value of machine learning in the clinical practice.

It is necessary to mention the study's limitations. First, our sample size was small, and we only recruited through one single site. As the sample size is small, the cross-validation method used here may cause some instability and biased estimates. As a result, our findings should be interpreted with caution. Larger sample sizes and multiple site data are needed to verify the findings in future studies. Second, the present study used the Sanyinjiao (SP6) point for acupuncture treatment. Our previous study has manifested that the acupoint has a specific neural response (64), thus, further studies need to investigate the acupuncture neural effect with other acupoints. Third, the present study did not explore the metabolic in brain stem regions, such as the ventral tegmental area (VTA) and periaqueductal gray (PAG), as the FreeSurfer does not segment these brain stem regions. The VTA and PAG have been shown to play important roles in chronic pain and are modulated by acupuncture treatment of chronic pain (65). Future studies should include these brain regions to get a comprehensive metabolic mechanism knowledge of chronic pain and acupuncture treatment.

CONCLUSION

The present study shows that individual-level metabolic patterns of the DMN and SMN can predict the pain relief after acupuncture treatment for PDM. This preliminary study supports the potential of metabolic biomarkers and MVPA to predict therapeutic outcomes in patients with PDM. The present findings advanced the brain metabolic mechanism of the chronic pain treatment.

DATA AVAILABILITY STATEMENT

The raw data supporting the conclusions of this article will be made available by the authors, without undue reservation.

ETHICS STATEMENT

The studies involving human participants were reviewed and approved by the affiliated Hospital of Chengdu University of Traditional Chinese Medicine Institutional Review Board. The patients/participants provided their written informed consent to participate in this study.

AUTHOR CONTRIBUTIONS

JY and FL supervised the project. LL, ZS, WW, and XG enrolled the participants and acquired the data. HX performed the PET scan. JY and JX administered and conceptualized the project. SY analyzed the data. JX and SY wrote and revised the manuscript. All authors read and approved the final manuscript.

FUNDING

This work was supported by the programs of the National Natural Science Foundation of China (Nos. 81973966 and 81774440), China National Postdoctoral Program for InnovativeTalents (No. BX20190046), the Science and Technology Support Program of Nanchong (19SXHZ0100), the Doctoral Scientific Research Foundation of North Sichuan Medical College (CBY19-QD10), and Chengdu University of Traditional Chinese Medicine Xinglin Scholar Discipline Talent Research and Improvement Plan (BSH2019011).

ACKNOWLEDGMENTS

The authors thank all the participants involved in the study. The authors would like to thank Editage (www.editage.com) for English language editing.

REFERENCES

1. Zhao ZQ. Neural mechanism underlying acupuncture analgesia. *Prog Neurobiol.* (2008) 85:355–75. doi: 10.1016/j.pneurobio.2008.05.004
2. Campbell MA, McGrath PJ. Non-pharmacologic strategies used by adolescents for the management of menstrual discomfort. *Clin J Pain.* (1999) 15:313–20. doi: 10.1097/00002508-199912000-00008
3. Coco AS. Primary dysmenorrhea. *Am Fam Physician.* (1999) 60:489–96.
4. O'Connell K, Davis AR, Westhoff C. Self-treatment patterns among adolescent girls with dysmenorrhea. *J Pediatr Adolesc Gynecol.* (2006) 19:285–9. doi: 10.1016/j.jpag.2006.05.004
5. Armour M, Dahlen HG, Zhu X, Farquhar C, Smith CA. The role of treatment timing and mode of stimulation in the treatment of primary dysmenorrhea with acupuncture: An exploratory randomised controlled trial. *PLoS ONE.* (2017) 12:e0180177. doi: 10.1371/journal.pone.0180177
6. Ma YX, Ye XN, Liu CZ, Cai PY, Li ZF, Du DQ, et al. A clinical trial of acupuncture about time-varying treatment and points selection in primary dysmenorrhea. *J Ethnopharmacol.* (2013) 148:498–504. doi: 10.1016/j.jep.2013.04.045
7. Witt CM, Reinhold T, Brinkhaus B, Roll S, Jena S, Willich SN. Acupuncture in patients with dysmenorrhea: a randomized study on clinical effectiveness and cost-effectiveness in usual care. *Am J Obstet Gynecol.* (2008) 198:166.e1–8. doi: 10.1016/j.ajog.2007.07.041
8. Yu SY, Lv ZT, Zhang Q, Yang S, Wu X, Hu YP, et al. Electroacupuncture is beneficial for primary dysmenorrhea: the evidence from meta-analysis of randomized controlled trials. *Evid Based Complement Altern Med.* (2017) 2017:1791258. doi: 10.1155/2017/1791258
9. Smith CA, Zhu X, He L, Song J. Acupuncture for primary dysmenorrhoea. *Cochrane Database Syst Rev.* (2011) Cd007854. doi: 10.1002/14651858.CD007854.pub2
10. Tu Y, Ortiz A, Gollub RL, Cao J, Gerber J, Lang C, et al. Multivariate resting-state functional connectivity predicts responses to real and sham acupuncture treatment in chronic low back pain. *Neuroimage Clin.* (2019) 23:101885. doi: 10.1016/j.nicl.2019.101885
11. Liu J, Mu J, Chen T, Zhang M, Tian J. White matter tract microstructure of the mPFC-amygdala predicts interindividual differences in placebo response related to treatment in migraine patients. *Hum Brain Mapp.* (2019) 40:284–92. doi: 10.1002/hbm.24372
12. Liu J, Mu J, Liu Q, Dun W, Zhang M, Tian J. Brain structural properties predict psychologically mediated hypoalgesia in an 8-week sham acupuncture treatment for migraine. *Hum Brain Mapp.* (2017) 38:4386–97. doi: 10.1002/hbm.23667
13. Angst MS, Phillips NG, Drover DR, Tingle M, Ray A, Swan GE, et al. Pain sensitivity and opioid analgesia: a pharmacogenomic twin study. *Pain.* (2012) 153:1397–409. doi: 10.1016/j.pain.2012.02.022
14. Coghill RC, Eisenach J. Individual differences in pain sensitivity: implications for treatment decisions. *Anesthesiology.* (2003) 98:1312–4. doi: 10.1097/00000542-200306000-00003
15. Wager TD, Atlas LY, Leotti LA, Rilling JK. Predicting individual differences in placebo analgesia: contributions of brain activity during anticipation and pain experience. *J Neurosci.* (2011) 31:439–52. doi: 10.1523/JNEUROSCI.3420-10.2011
16. Wandner LD, Scipio CD, Hirsh AT, Torres CA, Robinson ME. The perception of pain in others: how gender, race, and age influence pain expectations. *J Pain.* (2012) 13:220–7. doi: 10.1016/j.jpain.2011.10.014
17. Fillingim RB. Individual differences in pain: understanding the mosaic that makes pain personal. *Pain.* (2017) 158 (Suppl 1):S11. doi: 10.1097/j.pain.0000000000000775
18. Reggente N, Moody TD, Morfini F, Sheen C, Rissman J, O'Neill J, et al. Multivariate resting-state functional connectivity predicts response to cognitive behavioral therapy in obsessive-compulsive disorder. *Proc Natl Acad Sci U S A.* (2018) 115:2222–7. doi: 10.1073/pnas.1716686115
19. Chen J, Wang Z, Tu Y, Liu X, Jorgenson K, Ye G, et al. Regional Homogeneity and multivariate pattern analysis of cervical spondylosis neck pain and the modulation effect of treatment. *Front Neurosci.* (2018) 12:900. doi: 10.3389/fnins.2018.00900
20. Tu CH, Niddam DM, Chao HT, Liu RS, Hwang RJ, Yeh TC, et al. Abnormal cerebral metabolism during menstrual pain in primary dysmenorrhea. *Neuroimage.* (2009) 47:28–35. doi: 10.1016/j.neuroimage.2009.03.080
21. Tu CH, Niddam DM, Chao HT, Chen LF, Chen YS, Wu YT, et al. Brain morphological changes associated with cyclic menstrual pain. *Pain.* (2010) 150:462–8. doi: 10.1016/j.pain.2010.05.026
22. Zhang Q, Yu S, Wang Y, Wang M, Yang Y, Wei W, et al. Abnormal reward system network in primary dysmenorrhea. *Mol Pain.* (2019) 15:1744806919862096. doi: 10.1177/1744806919862096
23. Chen T, Mu J, Xue Q, Yang L, Dun W, Zhang M, et al. Whole-brain structural magnetic resonance imaging–based classification of primary dysmenorrhea in pain-free phase: a machine learning study. *Pain.* (2019) 160:734–41. doi: 10.1097/j.pain.0000000000001428
24. Liu P, Liu Y, Wang G, Li R, Wei Y, Fan Y, et al. Changes of functional connectivity of the anterior cingulate cortex in women with primary dysmenorrhea. *Brain Imaging Behav.* (2018) 12:710–7. doi: 10.1007/s11682-017-9730-y
25. Larroy C. Comparing visual-analog and numeric scales for assessing menstrual pain. *Behav Med.* (2002) 27:179–81. doi: 10.1080/08964280209596043
26. Zung WW. A rating instrument for anxiety disorders. *Psychosomatics.* (1971) 12:371–9. doi: 10.1016/S0033-3182(71)71479-0
27. Zung WWK, Richards CB, Short MJ. Self-Rating Depression Scale in an Outpatient Clinic: Further Validation of the SDS. *Arch Gen Psychiatry.* (1965) 13:508–15. doi: 10.1001/archpsyc.1965.01730060026004
28. Yu S, Yang J, Yang M, Gao Y, Chen J, Ren Y, et al. Application of acupoints and meridians for the treatment of primary dysmenorrhea: a data mining-based literature study. *Evid Based Complemen Altern Med.* (2015) 2015:752194. doi: 10.1155/2015/752194
29. World Health Organization Western Pacific Regional Office. *WHO Standard Acupuncture Point Locations in the Western Pacific Region*. Geneva: World Health Organization (2008).
30. Zeng F, Qin W, Liang F, Liu J, Tang Y, Liu X, et al. Abnormal resting brain activity in patients with functional dyspepsia is related to symptom severity. *Gastroenterology.* (2011) 141:499–506. doi: 10.1053/j.gastro.2011.05.003
31. Tracey I, Mantyh PW. The cerebral signature for pain perception and its modulation. *Neuron.* (2007) 55:377–91. doi: 10.1016/j.neuron.2007.07.012
32. Davis KD, Flor H, Greely HT, Iannetti GD, Mackey S, Ploner M, et al. Brain imaging tests for chronic pain: medical, legal and ethical issues and recommendations. *Nat Rev Neurol.* (2017) 13:624. doi: 10.1038/nrneurol.2017.122
33. Hemington KS, Wu Q, Kucyi A, Inman RD, Davis KD. Abnormal cross-network functional connectivity in chronic pain and its association with clinical symptoms. *Brain Struct Func.* (2016) 221:4203–19. doi: 10.1007/s00429-015-1161-1
34. Kumbhare DA, Elzibak AH, Noseworthy MD. Evaluation of Chronic Pain Using Magnetic Resonance (MR) Neuroimaging Approaches. *Clin J Pain.* (2017) 33:281–90. doi: 10.1097/AJP.0000000000000415
35. Li X, Chen H, Lv Y, Chao HH, Gong L, Li CSR, et al. Diminished gray matter density mediates chemotherapy dosage-related cognitive impairment in breast cancer patients. *Sci Rep.* (2018) 8:13801. doi: 10.1038/s41598-018-32257-w
36. Yu S, Shen Z, Lai R, Feng F, Guo B, Wang Z, et al. The orbitofrontal cortex gray matter is associated with the interaction between insomnia and depression. *Front Psychiatry.* (2018) 9:651. doi: 10.3389/fpsyt.2018.00651
37. Alshikho MJ, Zürcher NR, Loggia ML, Cernasov P, Chonde DB, Garcia DI, et al. Glial activation colocalizes with structural abnormalities in amyotrophic lateral sclerosis. *Neurology.* (2016) 87:2554–61. doi: 10.1212/WNL.0000000000003427
38. Erlandsson K, Buvat I, Pretorius PH, Thomas BA, Hutton BF. A review of partial volume correction techniques for emission tomography and their applications in neurology, cardiology and oncology. *Phys Med Biol.* (2012) 57:R119. doi: 10.1088/0031-9155/57/21/R119
39. Greve DN, Salat DH, Bowen SL, Izquierdo-Garcia D, Schultz AP, Catana C, et al. Different partial volume correction methods lead to different conclusions: an 18F-FDG-PET study of aging. *Neuroimage.* (2016) 132:334–43. doi: 10.1016/j.neuroimage.2016.02.042

40. Chang CC. Lin CJ. *LIBSVM: A library for support vector machines.* (2011) 2:1–27. doi: 10.1145/1961189.1961199
41. Plitt M, Barnes KA, Wallace GL, Kenworthy L, Martin A. Resting-state functional connectivity predicts longitudinal change in autistic traits and adaptive functioning in autism. *Proc Natl Acad Sci U S A.* (2015) 112:E6699–706. doi: 10.1073/pnas.1510098112
42. Wager TD, Atlas LY, Lindquist MA, Roy M, Woo CW, Kross E. An fMRI-based neurologic signature of physical pain. *N Engl J Med.* (2013) 368:1388–97. doi: 10.1056/NEJMoa1204471
43. Lindquist MA, Krishnan A, Lopez-Sola M, Jepma M, Woo CW, Koban L, et al. Group-regularized individual prediction: theory and application to pain. *Neuroimage*, (2017) 145(Pt B):274–87. doi: 10.1016/j.neuroimage.2015.10.074
44. Yang Z, Fang F, Weng X. Recent developments in multivariate pattern analysis for functional MRI. *Neurosci Bull.* (2012) 28:399–408. doi: 10.1007/s12264-012-1253-3
45. Zhong J, Chen DQ, Hung PSP, Hayes DJ, Liang KE, Davis KD, et al. Multivariate pattern classification of brain white matter connectivity predicts classic trigeminal neuralgia. *Pain.* (2018) 159:2076–87. doi: 10.1097/j.pain.0000000000001312
46. Tu Y, Jung M, Gollub RL, Napadow V, Gerber J, Ortiz A, et al. Abnormal medial prefrontal cortex functional connectivity and its association with clinical symptoms in chronic low back pain. *Pain.* (2019) 160:1308–18. doi: 10.1097/j.pain.0000000000001507
47. Frick A, Engman J, Wahlstedt K, Gingnell M, Fredrikson M, Furmark T. Anterior cingulate cortex activity as a candidate biomarker for treatment selection in social anxiety disorder. *BJPsych Open.* (2018) 4:157–9. doi: 10.1192/bjo.2018.15
48. Whitfield-Gabrieli S, Ghosh S, Nieto-Castanon A, Saygin Z, Doehrmann O, Chai X, et al. Brain connectomics predict response to treatment in social anxiety disorder. *Mol Psychiatry.* (2016) 21:680. doi: 10.1038/mp.2015.109
49. Fan Y, Shen D, Gur RC, Gur RE, Davatzikos C, COMPARE. classification of morphological patterns using adaptive regional elements. *IEEE Trans Med Imaging.* (2006) 26:93–105. doi: 10.1109/TMI.2006.886812
50. Haxby JV. Multivariate pattern analysis of fMRI: the early beginnings. *Neuroimage.* (2012) 62:852–5. doi: 10.1016/j.neuroimage.2012.03.016
51. Tu CH, Niddam DM, Yeh TC, Lirng JF, Cheng CM, Chou CC, et al. Menstrual pain is associated with rapid structural alterations in the brain. *Pain.* (2013) 154:1718–24. doi: 10.1016/j.pain.2013.05.022
52. Wu TH, Tu CH, Chao HT, Li WC, Low I, Chuang CY, et al. Dynamic changes of functional pain connectome in women with primary dysmenorrhea. *Sci Rep.* (2016) 6:24543. doi: 10.1038/srep24543
53. Shi Y, Liu Z, Zhang S, Li Q, Guo S, Yang J, et al. Brain network response to acupuncture stimuli in experimental acute low back pain: an fMRI study. *Evid.Based Complemen Altern Med.* (2015) 2015:210120. doi: 10.1155/2015/210120
54. Lee J, Eun S, Kim J, Lee JH, Park K. Differential Influence of Acupuncture Somatosensory and Cognitive/Affective Components on Functional Brain Connectivity and Pain Reduction During Low Back Pain State. *Front Neurosci.* (2019) 13:1062. doi: 10.3389/fnins.2019.01062
55. Chen X, Spaeth RB, Freeman SG, Scarborough DM, Hashmi JA, Wey HY, et al. The modulation effect of longitudinal acupuncture on resting state functional connectivity in knee osteoarthritis patients. *Mol Pain.* (2015) 11:67. doi: 10.1186/s12990-015-0071-9
56. Zhang Y, Zhang H, Nierhaus T, Pach D, Witt CM, Yi M. Default mode network as a neural substrate of acupuncture: evidence, challenges and strategy. *Front Neurosci.* (2019) 13:100. doi: 10.3389/fnins.2019.00100
57. Dhond RP, Yeh C, Park K, Kettner N, Napadow V. Acupuncture modulates resting state connectivity in default and sensorimotor brain networks. *Pain.* (2008) 136:407–18. doi: 10.1016/j.pain.2008.01.011
58. Keshavan MS, Collin G, Guimond S, Kelly S, Prasad KM, Lizano P. Neuroimaging in Schizophrenia. *Neuroimaging Clin N Am.* (2020) 30:73–83. doi: 10.1016/j.nic.2019.09.007
59. Janssen RJ, Mourão-Miranda J, Schnack HG. Making individual prognoses in psychiatry using neuroimaging and machine learning. *Biol Psychiatry Cogn Neurosci Neuroimaging.* (2018) 3:798–808. doi: 10.1016/j.bpsc.2018.04.004
60. Gao S, Calhoun VD, Sui J. Machine learning in major depression: From classification to treatment outcome prediction. *CNS Neurosci Ther.* (2018) 24:1037–52. doi: 10.1111/cns.13048
61. Wu GR, Wang X, Baeken C. Baseline functional connectivity may predict placebo responses to accelerated rTMS treatment in major depression. *Hum Brain Mapp*. (2020) 41:632–9. doi: 10.1002/hbm.24828
62. Leaver AM, Wade B, Vasavada M, Hellemann G, Joshi SH, Espinoza R, et al. Fronto-temporal connectivity predicts ECT outcome in major depression. *Front Psychiatry.* (2018) 9:92. doi: 10.3389/fpsyt.2018.00092
63. Mithani K, Mikhail M, Morgan BR, Wong S, Weil AG, Deschenes S, et al. Connectomic profiling identifies responders to vagus nerve stimulation. *Ann Neurol.* (2019) 86:743–53. doi: 10.1002/ana.25574
64. Yang J, Zeng F, Feng Y, Fang L, Qin W, Liu X, et al. A PET-CT study on the specificity of acupoints through acupuncture treatment in migraine patients. *BMC Complement Altern Med.* (2012) 12:123. doi: 10.1186/1472-6882-12-123
65. Yu S, Ortiz A, Gollub RL, Wilson G, Gerber J, Park J, et al. Acupuncture Treatment Modulates the Connectivity of Key Regions of the Descending Pain Modulation and Reward Systems in Patients with Chronic Low Back Pain. *J Clin Med*. (2020) 9:1719. doi: 10.3390/jcm9061719

Conflict of Interest: The authors declare that the research was conducted in the absence of any commercial or financial relationships that could be construed as a potential conflict of interest.

frontiers | Frontiers in Neurology

STUDY PROTOCOL
published: 10 May 2022
doi: 10.3389/fneur.2022.890364

Effectiveness of Transcranial Direct Current Stimulation and Monoclonal Antibodies Acting on the CGRP as a Combined Treatment for Migraine (TACTIC): Protocol for a Randomized, Double-Blind, Sham-Controlled Trial

*Raffaele Ornello, Chiara Rosignoli, Valeria Caponnetto, Francesca Pistoia, Michele Ferrara, Aurora D'Atri and Simona Sacco**

Department of Biotechnological and Applied Clinical Sciences, University of L'Aquila, L'Aquila, Italy

OPEN ACCESS

Edited by:
Lei Lan,
Chengdu University of Traditional Chinese Medicine, China

Reviewed by:
Andrea Negro,
Sapienza University of Rome, Italy
Christoph Schankin,
Bern University Hospital, Switzerland

****Correspondence:***
Simona Sacco
simona.sacco@univaq.it

Specialty section:
This article was submitted to Headache and Neurogenic Pain, a section of the journal Frontiers in Neurology

Received: *05 March 2022*
Accepted: *14 April 2022*
Published: *10 May 2022*

Citation:
Ornello R, Rosignoli C, Caponnetto V, Pistoia F, Ferrara M, D'Atri A and Sacco S (2022) Effectiveness of Transcranial Direct Current Stimulation and Monoclonal Antibodies Acting on the CGRP as a Combined Treatment for Migraine (TACTIC): Protocol for a Randomized, Double-Blind, Sham-Controlled Trial. Front. Neurol. 13:890364. doi: 10.3389/fneur.2022.890364

Background: Migraine is a recurrent headache disorder that has a still unclear pathophysiology, involving several circuits of both the central and peripheral nervous system. Monoclonal antibodies acting on the calcitonin gene-related (CGRP) pathway (CGRP-MAbs) are the first drugs specifically designed for migraine; those drugs act peripherally on the trigeminal ganglion without entering the blood-brain barrier. Conversely, neuromodulation techniques such as transcranial direct current stimulation (tDCS) act centrally by increasing or decreasing the neuronal firing rate of brain cortical areas. The aim of the study will be to evaluate whether tDCS, in addition to CGRP-MAbs, is an effective add-on treatment in reducing headache frequency, intensity and acute medication use in patients with migraine. To demonstrate the biological effects of tDCS, the electroencephalographic (EEG) power changes after tDCS will be assessed.

Methods: We will include patients with migraine on treatment with CGRP-MAbs and reporting ≥8 monthly migraine days. During a prospective 28-day baseline period, patients will fill in a headache diary and questionnaires to evaluate migraine-related disability, anxiety and depressive symptoms, sleep quality, and health-related quality of life. Subjects will be randomly assigned in a 1:1 ratio to active or sham tDCS. The stimulation protocol will consist in five daily sessions, the cathodes will be applied bilaterally above the occipital areas, with the reference anode electrodes positioned above the primary motor areas. Before the first, and immediately after the last stimulation session, patients will perform a 10-min resting EEG recording. During a 28-day follow-up period following tDCS, patients will have to fill in a headache diary and questionnaires identical to those of the baseline period.

Discussion: This trial will evaluate the efficacy of an add-on treatment acting on the brain in patients with migraine, who are already treated with peripherally acting drugs,

showing how tDCS acts in restoring the dysfunctional brain networks typical of the migraine patient.

Clinical Trial Registration: NCT05161871.

Keywords: migraine treatment, transcranial direct current stimulation, electroencephalogram, monoclonal antibodies, calcitonin gene-related peptide, randomized controlled trials

INTRODUCTION

Migraine is a recurrent headache disorder representing the second cause of disability under 50 years of age and the first in young women (1). It is a central nervous system disorder whose mechanisms are poorly understood. Electrophysiology (EEG) studies have revealed abnormalities in cortical responsivity to external stimuli, in the different phases of the migraine cycle. During the days between attacks—i.e., the interictal period—, patients with migraine lack of habituation to external stimuli which normalizes in the hours that precede an attack (2). In the premonitory phase of migraine, changes in thalamocortical connectivity were observed; the presence of the so-called "thalamocortical dysrhythmia" is supported by MRI studies, before and during migraine attacks (3–5). Those studies showed altered connectivity of the cortex, thalamus, hypothalamus, brainstem and amygdala, which may be involved in the modulation of pain and sensory function (6).

Cortical spreading depression (CSD) is an event occurring in the brain which is supposed to play an important role in the genesis of migraine and to directly generate migraine aura (7). CSD consists in the diffusion of a wave of depolarization in the cerebral cortex that spreads slowly from the posterior areas of the brain; a "second phase" of neurophysiological and vascular changes ensues, characterized by a prolonged direct current potential shift that is lower in amplitude than the initial CSD wave, along with sustained vasoconstriction and reduced blood oxygenation (8). All those events lead to the activation of nociceptive centers, including a peripheral neural structure, the trigeminal ganglion (TG), which releases pain-inducing peptides and mostly calcitonin gene-related peptide (CGRP) (9, 10).

Several drug classes can be used for the prevention of migraine; they can be classified into antidepressants, antiepileptics, antihypertensives, onabotulinumtoxin A, beta-blockers, calcium agonists, and drugs that act on the calcitonin gene-related peptide (CGRP) pathway (11). Preventive drug treatment is not always viable due to potential contraindications; besides, patients may report adverse events or unsatisfactory benefit. Due to non-optimal adherence and poor tolerability to drugs, pharmacological preventive treatment can be replaced or integrated with non-pharmacological methods. Neuromodulation techniques, such as transcranial direct current stimulation (tDCS), are already used as a treatment for migraine and other chronic pain conditions (12–14), and it can be used in patients who prefer non-pharmacological management, or who cannot be adequately managed with drugs.

tDCS is a non-invasive and painless technique of brain modulation, consisting of delivering a weak current (1–2 mA) through two sponge electrodes fixed on the scalp and connected to a battery-driven stimulator; the aim of tDCS is to modulate spontaneous neuronal firing rate by the polarization of resting membrane potential (15). After-effects of the stimulation rely on the modulation of NMDA receptors and synaptic GABAergic activity (15). Anodal stimulation increases cortical excitability by depolarizing neurons in the stimulated area, while cathodal stimulation hyperpolarizes neurons with inhibitory effects (16).

Monoclonal antibodies acting on the CGRP pathway (CGRP-MAbs) are the first preventive drugs specifically designed for migraine; these drugs act by blocking the CGRP pathway, thereby inhibiting vasodilation and the transmission of pain (10). Those drugs demonstrated high efficacy in randomized controlled trials (17–19) and even more effectiveness in real-world studies (20–25). In real-life, the reduction in monthly migraine days due to CGRP-MAbs was up to 12.2 days at 6 months compared with baseline, while monthly days of acute medication consumption decreased up to 8; 50% response rates ranged from 10 to 76.5% (20–26). However, both randomized controlled trials and real-life studies showed that up to one half of patients in clinical practice do not attain a 50% reduction in monthly migraine days from baseline even with those specific treatments and need further improvements in their migraine prevention. Besides, many patients, even if reporting a significant response to those drugs, may have a high number of residual monthly headache days resulting in a substantial impact on daily activities (27). The number of residual monthly migraine days after treatment, although clinically relevant, is not reported by the available studies (28).

Due to their huge molecular dimensions, CGRP-MAbs inhibit CGRP release from the TG without crossing the blood-brain barrier (10); hence, they are not expected to interfere with the mechanisms of migraine occurring within the brain. On the contrary, tDCS acts on the central nervous system, by modulating the electrical activity of areas implied in pain modulation (29). Therefore, tDCS with CGRP-MAbs have different targets located at different levels in the nervous system; hence, we speculate that their combined administration can have a synergistic or additive effect.

OBJECTIVES

The primary aim of the present study will be to assess whether tDCS as an add-on treatment to CGRP-MAbs is effective in reducing headache frequency, intensity, and acute medication use in patients with migraine. Secondarily, we will assess the effect of tDCS add-on on migraine-related disability, quality of life, sleep disturbance, and psychological symptoms. To demonstrate and quantify the biological effects of tDCS, we will assess the electroencephalographic (EEG) power changes after tDCS.

ETHICAL ISSUES

The study was approved by the Ethics Committee for the districts of L'Aquila and Teramo with Protocol Number 272/21. All patients will sign an informed consent to participate in the study.

INCLUSION AND EXCLUSION CRITERIA

Our trial will follow the guidelines issued by the International Headache Society for neuromodulation in headaches (30). The protocol follows the SPIRIT checklist (31, 32) (**Supplementary Material 1**). The inclusion criteria will be the following:

- male or female patients, aged between 40 and 70 years, referring to the Headache Center of the University of L'Aquila;
- a diagnosis of migraine with or without aura according to the International Classification of Headache Disorders, 3rd Edition (33);
- migraine must have been present for at least 12 months;
- treated with CGRP-MAbs (erenumab, fremanezumab or galcanezumab) for 90–180 days since the first subcutaneous administration (this time range was chosen to ensure a stable CGRP pathway inhibition);
- reporting ≥8 monthly migraine days in the last 30 days of observation despite treatment with CGRP-MAbs;
- able to discriminate between migraine and tension-type headaches;
- written informed consent to participate in the study.

Treatment with CGRP-MAbs will be prescribed according to Italian reimbursement criteria, i.e., in patients reporting ≥8 monthly migraine days with a Migraine Impact and Disability Assessment Scale score ≥11 and having failed at least three preventive medication classes among beta-blockers, tricyclic antidepressants, anticonvulsants, and onabotulinumtoxinA.

Patients with other concomitant primary headache types will be included if attacks are <1 day/month and <12 days/year.

Subjects with medication overuse headache and menstrually-related migraine will be not excluded from the study but will be included in exploratory subgroup analyses. According to the clinical practice of the recruiting center, patients with medication overuse will not undergo detoxication treatments.

The exclusion criteria will be the following:

- use of any concurrent migraine preventive medication other than CGRP-MAbs;
- secondary migraine-like headache;
- epilepsy or any other neurologic condition that may be worsened by transcranial electrical stimulation;
- metallic head implants, cardiac pacemaker or any other device that could malfunction or be displaced by electrical stimulation;
- pregnancy or lactation.

Acute migraine treatment will be allowed during the study. Migraine preventive treatments other than CGRP-MAbs must be withdrawn for at least 60 days before inclusion in the trial.

TABLE 1 | Assessment schedule.

	Screening	Baseline	Stimulation	Follow-up
Informed consent	X			
Inclusion/exclusion criteria	X	X		
Clinical history	X	X		
Demographic data	X	X		
Headache diary	X*	X	X	X
mMIDAS		X		X
HIT-6		X		X
HADS		X		X
SF-36		X		X
PSQI		X		X
EEG		X	X	

*CGRP-MAbs indicates monoclonal antibodies acting on the calcitonin gene-related peptide pathway; EEG, electroencephalogram; HADS, Hospital Anxiety and Assessment Scale; HIT-6, Headache Impact Test-6; mMIDAS, modified Migraine Impact and Disability Assessment Scale; PSQI, Pittsburgh Sleep Quality Index; SF-36, Short Form Health Survey. *Retrospective assessment based upon the Headache Center diary used in clinical practice.*

VISIT SCHEDULE AND ASSESSMENT

The study includes a 90- to 180-day retrospective screening period, a 28-day baseline period, a 5-day stimulation period, and a 28-day follow-up period. The planned inclusion period of the study will be 12 months. Assessment schedule is summarized in **Table 1**.

At the beginning of the study, all subjects will be thoroughly informed about all aspects of the study, including the study treatment, visit schedule, required evaluations, diary compliance, and all regulatory requirements for informed consent. Subjects who sign an informed consent but fail to be assigned to the study treatment for any reason will be considered a screen failure. The reason for not being started on treatment will be recorded.

Subject demographic and baseline characteristic data will be collected on all subjects. This will include age, race, ethnicity, and relevant physiological and medical history. Prior headache characteristics and previous headache medication history, including information on the suitability for migraine prophylactics and prior migraine prophylactic treatment failure history, will be collected as part of screening and baseline characteristics.

RANDOMIZATION AND BLINDING

To control for placebo and nocebo effects, subjects will be randomly assigned in a 1:1 ratio to active or sham tDCS. Randomization will be performed by one of the investigators (AdA) unaware of personal data of study participants. A random allocation sequence will be generated in MATLAB environment; consecutive patients will then be allocated according to that sequence. The investigators who will administer the stimulation protocol (CR, RO), as well as the patient, will be blind as regards the type of stimulation applied (double blind). Finally, outcome

assessment will be performed by an investigator (VC) blinded to the intervention performed.

STUDY PROCEDURES

Baseline

Eligible subjects will undergo a 28-day baseline period to confirm their eligibility, by filling out a headache diary containing information about headache occurrence, its intensity on a 1–10 Numerical Rating Scale, its duration (in hours), associated symptoms (nausea, vomiting, photophobia, phonophobia), and consumption of drugs for the acute treatment. For each headache day, patients will have to rate their degree of headache-related disability as low-medium, or high (**Supplementary Material 2**).

At baseline, subjects will have to fill out questionnaires to assess migraine-related disability, quality of life, sleep disturbance and psychological aspects: the modified Migraine Disability Assessment (mMIDAS); the Headache Impact Test-6 (HIT-6); Short Form Health Survey (SF-36); Pittsburgh Sleep Quality Index (PSQI); Hospital Anxiety and Depression Scale (HADS).

Stimulation Period

tDCS will be administered by trained personnel; one of the investigators (AdA) has years of experience in the tDCS field and will train two other investigators (CR, RO). The stimulation protocol will consist in five daily sessions, each lasting 20 min. The stimulation montage will provide a bilateral cathodal stimulation on occipital areas, with the reference anodal electrodes positioned on the M1 areas. The stimulation will be applied via 4 conductive-rubber square electrodes (5 × 5 cm) placed in sponges saturated with high conductivity gel and connected to a battery-operated stimulator system (BrainSTIM, EMS medical). In the active tDCS group, a direct current with maximal intensity of 1.5 mA with be provided for 20 mins (30 s ramp-in/ramp-out); those parameters are within the range of the available randomized controlled trials (34). In the sham group, the current will be turned off after 10 s (30 s ramp-in/ramp-out) at the beginning and at the end of the 20-min interval, in order to maintain the same tingling sensation that subjects refer during the gradual increase/decrease of the current intensity at the beginning/end of the 'real' stimulation procedure. Patients will fill out the headache diary during the 5 days of tDCS.

EEG Recording

Patients will perform a 10-min resting EEG recording (5 min eyes-open, 5-min eyes-closed), immediately before the first and immediately after the last tDCS session. EEG will be performed with a 64-channel apparel (BrainAmp, Brain Products GmbH) according to the 10–10 international system.

Follow-Up

Patients will undergo a 28-day follow-up assessment period starting from the day following the last tDCS session, filling out a diary identical to those of the baseline period. At the end of the follow-up period, patients will fill out the same questionnaires as during the baseline period. To verify blindness, patients will also be asked whether they received active or sham tDCS. The study procedures are summarized in **Figure 1**.

STUDY DISCONTINUATION

The study will be discontinued under the following circumstances:

- Subject decision;
- Pregnancy;
- Failed to meet the inclusion/exclusion criteria at any time during the study;
- Any situation in which study participation might result in a safety risk to the subject;
- Any change (initiation, withdrawal, or dosing change) in concurrent medication, including preventive and abortive treatment for migraine;
- New diagnosis of diseases that may be negatively affected by tDCS, such as epilepsy.

Study subjects will be consecutively recruited until the number of subjects completing the study reaches the number of 30 (15 treated with tDCS and 15 with sham stimulation). In case of screening failure or any of the conditions listed above and leading to study discontinuation, subjects will be replaced, provided that their inclusion falls within the 12-months inclusion period.

Patients discontinuing CGRP-MAbs due to non-response or lack of tolerance, as well as patients starting oral migraine preventive treatments as add-on, will be excluded from the study due to change in their medication. To ensure that treatment with CGRP-MAbs is stable and well-tolerated and to minimize the risk of including patients who will then withdraw treatment with CGRP-MAbs or change their medication, patient screening will be performed after 90–180 days from the first MAb administration. Patients lost to follow-up, unwilling to continue the trial, or developing a contraindication to continue the trial, will be excluded from efficacy analyses; their adverse events will be monitored and reported.

STUDY OUTCOMES AND DATA ANALYSIS

Efficacy Outcomes

As we expect a short, 5-day course of tDCS to have a short-lasting effect on brain function, we will only assess short-term outcomes at 28 days after the end of tDCS.

The primary efficacy outcome will be the change in headache days from the 28-day baseline to the 28-day follow-up period.

The secondary outcomes will include the change in migraine days, headache hours, mean pain intensity (0–10 Visual Analog Scale), acute treatment consumption (doses), migraine-related disability (mMIDAS score) and impact (HIT-6 score), quality of life (SF-36 score), sleep quality (PSQI score), and anxious and depressive symptoms (HADS score) from the 28-day baseline to the 28-day follow-up period. The change in the number of days with low, medium, and high disability will also be assessed by using of a specifically designed headache diary (**Supplementary Material 2**).

The additional outcome will be the changes in spectral power and coherence in the delta (1–4 Hz), theta (5–7 Hz), alpha (8–12 Hz), and beta bands (13–30 Hz), both overall and

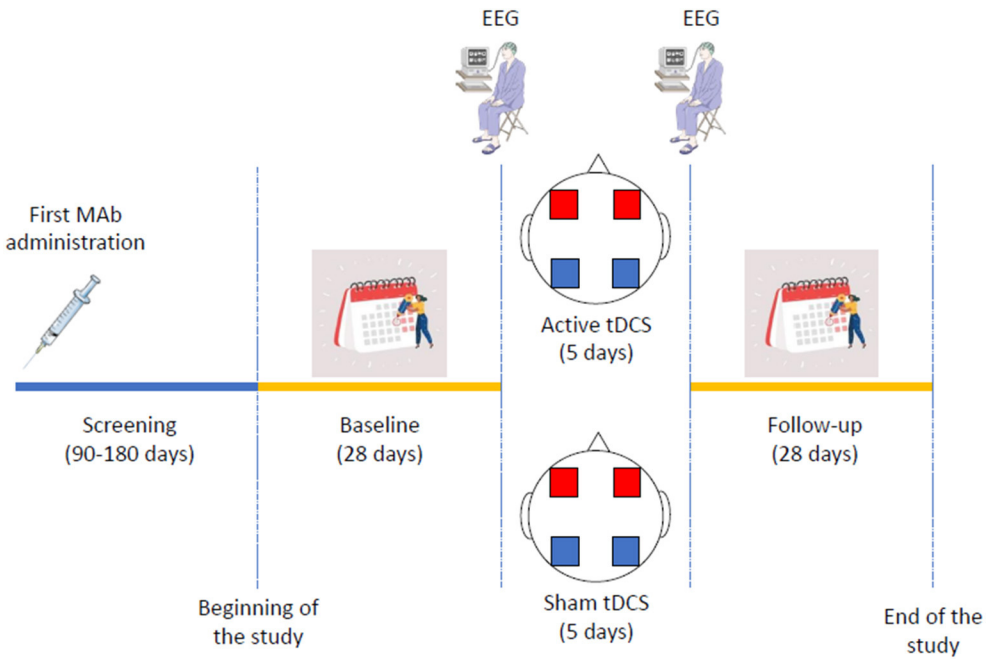

FIGURE 1 | Schematic representation of trial procedures. Mab indicates monoclonal antibody; EEG, electroencephalogram; tDCS, transcranial direct current stimulation. In the transcranial direct current stimulation figure, blue squares indicate the cathodes, while red squares indicate the anodes.

over the occipital regions, at EEG recording between the two measurements (before vs. after tDCS). The EEG power changes will be correlated with the improvement in primary and secondary outcomes. The age limit of 40–70 years was chosen to limit the variability in EEG activity generated by the inclusion of too young or old subjects, which could act as a confounder in outcome assessment.

Each outcome will be assessed in the group of active and sham tDCS; additionally, between-group comparisons will be made.

A migraine day will be defined as a day with headache lasting at least 4 h if left untreated and accompanied by typical symptoms (nausea, vomiting, photo- and/or phonophobia) or preceded by aura. All days with headache not accompanied by any of those symptoms will be considered as non-migraine headache days. The total count of headache days will include both migraine and non-migraine headache days.

Safety Outcomes

Safety assessment will include adverse event reporting. Adverse event monitoring will be performed during the tDCS stimulation sessions and during the 28-day follow-up period after tDCS. Adverse events will be detected and collected by investigators with a standard questionnaire (35) and open-ended questions. Monitoring for serious adverse events (SAEs) will be performed according to common clinical practice.

Statistical Analysis

Continuous data will be summarized by mean, standard deviation (SD), median, first and third quartiles, minimum and maximum, Categorical data will be presented by absolute and relative frequencies (n and %). Bilateral 95% confidence limit will be presented as appropriate.

Comparison between groups (active/sham) for the variables under study (headache days, days of disabling headache, intensity of pain, consumption of acute treatments, headache-related disability, and scores on questionnaires) will be performed using parametric or non-parametric statistics, depending on the data distribution.

Primary analyses will be performed on primary and secondary outcomes. Exploratory subgroup analyses will be performed on patients with a history of menstrual migraine and on patients with chronic migraine with medication overuse.

To evaluate electrophysiological changes, the dependent variable will be the variations in EEG activity after vs. before tDCS. Specifically, we will compute the spectral power *via* Fast Fourier Transform (FFT) and the coherence in cortical activity among brain areas via magnitude-squared coherence (MSC) for the artifact-free epochs in each EEG frequency band. For each group of patients (tDCS vs. sham), the power change before vs. after tDCS will be compared for each electrode and each frequency band. Given the results of a previous study (36), particular attention will be given to power in the alpha band in occipital areas. The EEG index changes will be correlated with changes in migraine parameters (headache days, migraine days, pain intensity, acute medication consumption, questionnaires score) to directly link the modifications in brain physiology to the frequency and severity of migraine episodes. Source current density of cortical generators of relevant EEG indexes will be also assessed by low-resolution electromagnetic tomography (LORETA) (37), to confirm the cortical origin of the physiological

changes induced by tDCS. Outcomes will be compared between the active and sham tDCS groups by chi-squared or t-test statistics as appropriate.

Sample Size

The sample size calculation was performed using GPower, version 3.1. According to previous literature (36), a between-groups mean difference of 3 ± 2 migraine days per month was considered significant. The computation was made with the following parameters: confidence interval (two-sided): 95%; power: 80%; ratio of sample size: 1:1; mean change in group 1: −4 days; mean change in group 2: −1 day; standard deviation: 2. The minimum sample size suggested was of 9 patients per group. In consideration of possible dropouts, we set our population size to 30 patients, 15 per group.

DISCUSSION

CGRP-MAbs have significantly changed the landscape of migraine prevention. They are an effective and well tolerated class of drugs which can substantially improve the quality of life of patients with migraine. CGRP-MAbs were proved to be effective even in patients who had failures to other preventatives. The degree of benefit of CGRP-MAbs is highly variable; in up to 10% of patients they can lead to migraine freedom (100% responders) (17, 18, 38, 39), while in all the other patients there is a residual migraine impact despite the treatment. Some patients, even if meeting criteria to be considered as responders to CGRP-MAbs, continue to experience a significant burden of migraine. In fact, in real-life studies 14.4–57% of patients received add-on treatment (21, 22, 26). It is unclear which is the optimal treatment to be associated with CGRP-MAbs. We aim to evaluate if patients, with a significant migraine burden (>8 migraine days per month) despite the use of CGRP-MAbs, may achieve further benefit by adding a non-pharmacological (tDCS) treatment targeting central mechanisms involved in migraine. The rationale to choose tDCS is its non-pharmacological nature and the central mechanism of action which may be complementary to the peripheral mechanism of action of anti-CGRP-MAbs. We will randomize patients who are on treatment with CGRP-MAbs and who still experience a significant migraine burden (>8 migraine days per month) to tDCS or placebo.

So far, several studies have already evaluated tDCS for migraine prevention proving that it is a promising treatment to prevent migraine (36, 40–50). Available RCTs included a variable number of patients (from 15 to 135 patients) with highly heterogeneous patient populations, outcomes, time schedules, and tDCS montages (34). Most of the available RCTs performed either cathodal occipital stimulation with anterior reference (40, 43, 44, 46) or anodal frontal stimulation with supraorbital reference (36, 41, 42, 45). Those montages are both justified by neurophysiology, as studies on migraine showed a hyperresponsivity of the visual cortex, while frontal stimulation reduces the excitability of the thalamus, which is responsible for pain generation (29). Results of those RCTs were overall positive in the short term, while being more controversial 12 months after tDCS (36, 48). The available RCTs are limited by the underuse of neurophysiological tests, which would improve our understanding of the effect of tDCS and how to improve it (34).

With respect to the available RCTs, our study has several differences. Firstly, we will test tDCS as an add-on to a class of drugs specifically designed to prevent migraine. Besides, our montage will be bilateral with 4 electrodes (2 anodes and 2 cathodes), while the other trials all performed unilateral stimulation. The bilateral stimulation is justified by the supposed bilateral alterations of the migraine brain (4) and will likely optimize current flow through the brain. Moreover, our montage will merge cathodal occipital stimulation and anodal frontal stimulation, by positioning the cathode over both occipital regions and the anode over both frontal regions. Those procedures are intended to maximize neuromodulation of circuits involved in migraine and pain (29). Additionally, our study will follow as closely as possible the recently issued guidelines for trials of neuromodulation in patients with migraine (30).

We will also study the cortical effect of neuromodulation by electrophysiology (EEG). Previous studies have shown that EEG activity is different between subjects with and without migraine. In detail, migraineurs showed increased slow activity between attacks compared with non-migraineurs (51, 52) and the degree of EEG slowing on the occipital areas showed a correlation with the burden of migraine (53); the increase in slow activity is coupled with decreased power of the alpha frequency. Interestingly, a trial of anodal tDCS over the frontal motor areas showed that active treatment was associated with increased alpha power over the occipital regions (36), suggesting that tDCS can mitigate the neurophysiological abnormalities of the migraineurs' brain. Quantifying EEG activity in our trial will provide a neurophysiological correlate to clinical findings and will help explaining the effect of tDCS on neural structures. The use of high-density EEG will provide accurate information on the sites of tDCS action.

The present trial has a robust double-blind, randomized approach with blinded outcome assessment. The trial complies with the most recent guidelines for neuromodulation in migraine. Besides, the tDCS montage was designed specifically for migraine prevention by reflection on the most plausible neuroanatomical targets. However, the study also has limitations. The study is single-center; besides, its sample will be sufficient to calculate the primary outcome, while subgroup analyses will be only exploratory. We will correct for low numbers by assessing the normality of variable distributions and perform conservative, non-parametric tests for non-normally distributed variables. As an add-on to highly effective migraine preventatives, we cannot exclude that the clinical effect of tDCS in the present RCT will be negative. Nevertheless, we will include patients with a high burden of migraine (≥8 monthly migraine days) to correct for this effect. Besides, a previous trial showed that active tDCS is more effective than sham even on top of topiramate (47), suggesting that tDCS could be an effective add-on migraine preventative. Besides, we will assess not only the possible clinical efficacy of tDCS, but also its effect on brain circuitry; therefore, even results that are clinically neutral will be interesting to discuss with respect to the functional effects of tDCS. Our trial

will contribute to assess the possible central, indirect effects of CGRP-MAbs by verifying whether the central circuits of migraine generation can be inhibited in addition to the action of those drugs.

CONCLUSION

In conclusion, our trial will assess the efficacy of an add-on non-pharmacological treatment acting on the brain in patients with migraine who are already treated with peripherally acting CGRP-MAbs. The trial will also allow us to better understand the pathophysiology of migraine, and to evaluate how tDCS acts in restoring the dysfunctional brain networks typical of the migraine patient.

AUTHOR CONTRIBUTIONS

RO, AD'A, and SS conceived the study and wrote the protocol draft. All other authors provided critical revision to the draft. All authors read and approved the final protocol.

FUNDING

This study will be partly funded by intramural DISCAB GRANT 2021 awarded by the Department of Biotechnological and Applied Clinical Sciences, University of L'Aquila.

ACKNOWLEDGMENTS

Figure 1 was created with pictures from Servier Medical Art (https://smart.servier.com) and Shutterstock (https://www.shutterstock.com).

SUPPLEMENTARY MATERIAL

The Supplementary Material for this article can be found online at: https://www.frontiersin.org/articles/10.3389/fneur.2022.890364/full#supplementary-material

Supplementary Material 1 | SPIRIT checklist.

Supplementary Material 2 | Headache diary.

REFERENCES

1. Steiner TJ, Stovner LJ, Jensen R, Uluduz D, Katsarava Z. Lifting the Burden: The Global Campaign Against Migraine remains second among the world's causes of disability, and first among young women: findings from GBD2019. *J Headache Pain.* (2020) 21:137. doi: 10.1186/s10194-020-01208-0
2. Goadsby PJ, Holland PR, Martins-Oliveira M, Hoffmann J, Schankin C, Akerman S. Pathophysiology of migraine: a disorder of sensory processing. *Physiol Rev.* (2017) 97:553–622. doi: 10.1152/physrev.00034.2015
3. Coppola G, Di Renzo A, Tinelli E, Di Lorenzo C, Di Lorenzo G, Parisi V, et al. Thalamo-cortical network activity during spontaneous migraine attacks. *Neurology.* (2016) 87:2154–60. doi: 10.1212/WNL.0000000000003327
4. Coppola G, Di Renzo A, Tinelli E, Lepre C, Di Lorenzo C, Di Lorenzo G, et al. Thalamo-cortical network activity between migraine attacks: Insights from MRI-based microstructural and functional resting-state network correlation analysis. *J Headache Pain.* (2016) 17:100. doi: 10.1186/s10194-016-0693-y
5. De Tommaso M, Vecchio E, Quitadamo SG, Coppola G, Di Renzo A, Parisi V, et al. Pain-related brain connectivity changes in migraine: a narrative review and proof of concept about possible novel treatments interference. *Brain Sci.* (2021) 11:234. doi: 10.3390/brainsci11020234
6. Charles A. The pathophysiology of migraine: implications for clinical management. *Lancet Neurol.* (2018) 17:174–82. doi: 10.1016/S1474-4422(17)30435-0
7. Harriott AM, Takizawa T, Chung DY, Chen SP. Spreading depression as a preclinical model of migraine. *J Headache Pain.* (2019) 20:45. doi: 10.1186/s10194-019-1001-4
8. Charles AC, Baca SM. Cortical spreading depression and migraine. *Nat Rev Neurol.* (2013) 9:637–44. doi: 10.1038/nrneurol.2013.192
9. Noseda R, Burstein R. Migraine pathophysiology: anatomy of the trigeminovascular pathway and associated neurological symptoms, CSD, sensitization and modulation of pain. *Pain.* (2013) 154 Suppl 1. doi: 10.1016/j.pain.2013.07.021
10. Edvinsson L, Haanes KA, Warfvinge K, Krause DN. CGRP as the target of new migraine therapies—successful translation from bench to clinic. *Nat Rev Neurol.* (2018) 14:338–50. doi: 10.1038/s41582-018-0003-1
11. Sacco S, Braschinsky M, Ducros A, Lampl C, Little P, Van Den Brink AM, et al. European headache federation consensus on the definition of resistant and refractory migraine: developed with the endorsement of the European Migraine and Headache Alliance (EMHA). *J Headache Pain.* (2020) 21:76. doi: 10.1186/s10194-020-01130-5
12. Knotkova H, Cruciani RA. Non-invasive transcranial direct current stimulation for the study and treatment of neuropathic pain. *Methods Mol Biol.* (2010) 617:505–15. doi: 10.1007/978-1-60327-323-7_37
13. Stilling JM, Monchi O, Amoozegar F, Debert CT. Transcranial magnetic and direct current stimulation (TMS/tDCS) for the treatment of headache: a systematic review. *Headache.* (2019) 59:339–57. doi: 10.1111/head.13479
14. Fregni F, El-Hagrassy MM, Pacheco-Barrios K, Carvalho S, Leite J, Simis M, et al. Evidence-based guidelines and secondary meta-analysis for the use of transcranial direct current stimulation in neurological and psychiatric disorders. *Int J Neuropsychopharmacol.* (2021) 24:256–313. doi: 10.1093/ijnp/pyaa051
15. Medeiros LF, De Souza IC, Vidor LP, De Souza A, Deitos A, Volz MS, et al. Neurobiological effects of transcranial direct current stimulation: a review. *Front Psychiatry.* (2012) 3:110. doi: 10.3389/fpsyt.2012.00110
16. Lefaucheur JP, Antal A, Ayache SS, Benninger DH, Brunelin J, Cogiamanian F, et al. Evidence-based guidelines on the therapeutic use of transcranial direct current stimulation (tDCS). *Clin Neurophysiol.* (2017) 128:56–92. doi: 10.1016/j.clinph.2016.10.087
17. Reuter U, Goadsby PJ, Lanteri-Minet M, Wen S, Hours-Zesiger P, Ferrari MD, et al. Efficacy and tolerability of erenumab in patients with episodic migraine in whom two-to-four previous preventive treatments were unsuccessful: a randomised, double-blind, placebo-controlled, phase 3b study. *Lancet.* (2018) 392:2280–7. doi: 10.1016/S0140-6736(18)32534-0
18. Ferrari MD, Diener HC, Ning X, Galic M, Cohen JM, Yang R, et al. Fremanezumab versus placebo for migraine prevention in patients with documented failure to up to four migraine preventive medication classes (FOCUS): a randomised, double-blind, placebo-controlled, phase 3b trial. *Lancet.* (2019) 394:1030–40. doi: 10.1016/S0140-6736(19)31946-4
19. Mulleners WM, Kim BK, Lainez MJA, Lanteri-Minet M, Pozo-Rosich P, Wang S, et al. Safety and efficacy of galcanezumab in patients for whom previous migraine preventive medication from two to four categories had failed (CONQUER): a multicentre, randomised, double-blind, placebo-controlled, phase 3b trial. *Lancet Neurol.* (2020) 19:814–25. doi: 10.1016/S1474-4422(20)30279-9
20. Lambru G, Hill B, Murphy M, Tylova I, Andreou AP. A prospective real-world analysis of erenumab in refractory chronic migraine. *J Headache Pain.* (2020) 21:61. doi: 10.1186/s10194-020-01127-0
21. Ornello R, Casalena A, Frattale I, Gabriele A, Affaitati G, Giamberardino MA, et al. Real-life data on the efficacy and safety of erenumab

in the Abruzzo region, central Italy. *J Headache Pain.* (2020) 21:32. doi: 10.1186/s10194-020-01102-9
22. Russo A, Silvestro M, Scotto Di Clemente F, Trojsi F, Bisecco A, Bonavita S, et al. Multidimensional assessment of the effects of erenumab in chronic migraine patients with previous unsuccessful preventive treatments: a comprehensive real-world experience. *J Headache Pain.* (2020) 21:69. doi: 10.1186/s10194-020-01143-0
23. De Vries Lentsch S, Verhagen IE, Van Den Hoek TC, Maassenvandenbrink A, Terwindt GM. Treatment with the monoclonal calcitonin gene-related peptide receptor antibody erenumab: a real-life study. *Eur J Neurol.* (2021) 28:4194–203. doi: 10.1111/ene.15075
24. Pensato U, Baraldi C, Favoni V, Cainazzo MM, Torelli P, Querzani P, et al. Real-life assessment of erenumab in refractory chronic migraine with medication overuse headache. *Neurol Sci.* (2021) 43:1273–80. doi: 10.1007/s10072-021-05426-5
25. Vernieri F, Altamura C, Brunelli N, Costa CM, Aurilia C, Egeo G, et al. Galcanezumab for the prevention of high frequency episodic and chronic migraine in real life in Italy: a multicenter prospective cohort study (the GARLIT study). *J Headache Pain.* (2021) 22:35. doi: 10.1186/s10194-021-01247-1
26. Raffaelli B, Kalantzis R, Mecklenburg J, Overeem LH, Neeb L, Gendolla A, et al. Erenumab in chronic migraine patients who previously failed five first-line oral prophylactics and onabotulinumtoxina: a dual-center retrospective observational study. *Front Neurol.* (2020) 11:417. doi: 10.3389/fneur.2020.00417
27. Ornello R, Baraldi C, Guerzoni S, Lambru G, Andreou AP, Raffaelli B, et al. Comparing the relative and absolute effect of erenumab: is a 50% response enough? Results from the ESTEEMen study. *J Headache Pain*. (2022) 23:1–8. doi: 10.1186/s10194-022-01408-w
28. Tfelt-Hansen P, Diener HC, Steiner TJ. Problematic presentation and use of efficacy measures in current trials of CGRP monoclonal antibodies for episodic migraine prevention: a mini-review. *Cephalalgia.* (2020) 40:122–6. doi: 10.1177/0333102419877663
29. Dasilva AF, Truong DQ, Dossantos MF, Toback RL, Datta A, Bikson M. State-of-art neuroanatomical target analysis of high-definition and conventional tDCS montages used for migraine and pain control. *Front Neuroanat.* (2015) 9:89. doi: 10.3389/fnana.2015.00089
30. Tassorelli C, Diener HC, Silberstein SD, Dodick DW, Goadsby PJ, Jensen RH, et al. Guidelines of the International Headache Society for clinical trials with neuromodulation devices for the treatment of migraine. *Cephalalgia.* (2021) 41:1135–51. doi: 10.1177/03331024211010413
31. Chan AW, Tetzlaff JM, Altman DG, Laupacis A, Gotzsche PC, Krleza-Jeric K, et al. SPIRIT 2013 statement: defining standard protocol items for clinical trials. *Ann Intern Med.* (2013) 158:200–7. doi: 10.7326/0003-4819-158-3-201302050-00583
32. Chan AW, Tetzlaff JM, Gotzsche PC, Altman DG, Mann H, Berlin JA, et al. SPIRIT 2013 explanation and elaboration: guidance for protocols of clinical trials. *BMJ.* (2013) 346:e7586. doi: 10.1136/bmj.e7586
33. Headache Classification Committee of the International Headache Society (IHS). The International Classification of Headache Disorders, 3rd edition. *Cephalalgia*. (2018) 38:1–211. doi: 10.1177/0333102417738202
34. Ornello R, Caponnetto V, Ratti S, D'aurizio G, Rosignoli C, Pistoia F, et al. Which is the best transcranial direct current stimulation protocol for migraine prevention? A systematic review and critical appraisal of randomized controlled trials. *J Headache Pain.* (2021) 22:144. doi: 10.1186/s10194-021-01361-0
35. Fertonani A, Rosini S, Cotelli M, Rossini PM, Miniussi C. Naming facilitation induced by transcranial direct current stimulation. *Behav Brain Res.* (2010) 208:311–8. doi: 10.1016/j.bbr.2009.10.030
36. De Icco R, Putorti A, De Paoli I, Ferrara E, Cremascoli R, Terzaghi M, et al. Anodal transcranial direct current stimulation in chronic migraine and medication overuse headache: A pilot double-blind randomized sham-controlled trial. *Clin Neurophysiol.* (2021) 132:126–36. doi: 10.1016/j.clinph.2020.10.014
37. Pascual-Marqui RD, Michel CM, Lehmann D. Low resolution electromagnetic tomography: a new method for localizing electrical activity in the brain. *Int J Psychophysiol.* (1994) 18:49–65. doi: 10.1016/0167-8760(84)90014-X
38. Detke HC, Goadsby PJ, Wang S, Friedman DI, Selzler KJ, Aurora SK. Galcanezumab in chronic migraine: the randomized, double-blind, placebo-controlled REGAIN study. *Neurology.* (2018) 91:e2211–21. doi: 10.1212/WNL.0000000000006640
39. Brandes JL, Diener HC, Dolezil D, Freeman MC, Mcallister PJ, Winner P, et al. The spectrum of response to erenumab in patients with chronic migraine and subgroup analysis of patients achieving >/=50%, >/=75%, and 100% response. *Cephalalgia.* (2020) 40:28–38. doi: 10.1177/0333102419894559
40. Antal A, Kriener N, Lang N, Boros K, Paulus W. Cathodal transcranial direct current stimulation of the visual cortex in the prophylactic treatment of migraine. *Cephalalgia.* (2011) 31:820–8. doi: 10.1177/0333102411399349
41. Auvichayapat P, Janyacharoen T, Rotenberg A, Tiamkao S, Krisanaprakornkit T, Sinawat S, et al. Migraine prophylaxis by anodal transcranial direct current stimulation, a randomized, placebo-controlled trial. *J Med Assoc Thai.* (2012) 95:1003–12.
42. Dasilva AF, Mendonca ME, Zaghi S, Lopes M, Dossantos MF, Spierings EL, et al. tDCS-induced analgesia and electrical fields in pain-related neural networks in chronic migraine. *Headache.* (2012) 52:1283–95. doi: 10.1111/j.1526-4610.2012.02141.x
43. Rocha S, Melo L, Boudoux C, Foerster A, Araujo D, Monte-Silva K. Transcranial direct current stimulation in the prophylactic treatment of migraine based on interictal visual cortex excitability abnormalities: a pilot randomized controlled trial. *J Neurol Sci.* (2015) 349:33–9. doi: 10.1016/j.jns.2014.12.018
44. Wickmann F, Stephani C, Czesnik D, Klinker F, Timaus C, Chaieb L, et al. Prophylactic treatment in menstrual migraine: a proof-of-concept study. *J Neurol Sci.* (2015) 354:103–9. doi: 10.1016/j.jns.2015.05.009
45. Andrade SM, De Brito Aranha REL, De Oliveira EA, De Mendonca C, Martins WKN, Alves NT, et al. Transcranial direct current stimulation over the primary motor vs prefrontal cortex in refractory chronic migraine: a pilot randomized controlled trial. *J Neurol Sci.* (2017) 378:225–32. doi: 10.1016/j.jns.2017.05.007
46. Ahdab R, Mansour AG, Khazen G, El-Khoury C, Sabbouh TM, Salem M, et al. Cathodal transcranial direct current stimulation of the occipital cortex in episodic migraine: a randomized sham-controlled crossover study. *J Clin Med.* (2019) 9:60. doi: 10.3390/jcm9010060
47. Dalla Volta G, Marceglia S, Zavarise P, Antonaci F. Cathodal tDCS guided by thermography as adjunctive therapy in chronic migraine patients: a sham-controlled pilot study. *Front Neurol.* (2020) 11:121. doi: 10.3389/fneur.2020.00121
48. Grazzi L, Usai S, Bolognini N, Grignani E, Sansone E, Tramacere I, et al. No efficacy of transcranial direct current stimulation on chronic migraine with medication overuse: a double blind, randomised clinical trial. *Cephalalgia.* (2020) 40:1202–11. doi: 10.1177/0333102420931050
49. Rahimi MD, Fadardi JS, Saeidi M, Bigdeli I, Kashiri R. Effectiveness of cathodal tDCS of the primary motor or sensory cortex in migraine: a randomized controlled trial. *Brain Stimul.* (2020) 13:675–82. doi: 10.1016/j.brs.2020.02.012
50. Pohl H, Moisa M, Jung HH, Brenner K, Aschmann J, Riederer F, et al. Long-term effects of self-administered transcranial direct current stimulation in episodic migraine prevention: results of a randomized controlled trial. *Neuromodulation.* (2021) 24:890–8. doi: 10.1111/ner.13292
51. Bjork MH, Stovner LJ, Engstrom M, Stjern M, Hagen K, Sand T. Interictal quantitative EEG in migraine: a blinded controlled study. *J Headache Pain.* (2009) 10:331–9. doi: 10.1007/s10194-009-0140-4
52. Bjork M, Stovner LJ, Hagen K, Sand T. What initiates a migraine attack? Conclusions from four longitudinal studies of quantitative EEG and steady-state visual-evoked potentials in migraineurs. *Acta Neurol Scand Suppl.* (2011) 124:56–63. doi: 10.1111/j.1600-0404.2011.01545.x
53. Bjork MH, Stovner LJ, Nilsen BM, Stjern M, Hagen K, Sand T. The occipital alpha rhythm related to the "migraine cycle" and headache burden: a blinded, controlled longitudinal study. *Clin Neurophysiol.* (2009) 120:464–71. doi: 10.1016/j.clinph.2008.11.018

Conflict of Interest: RO declares personal fees from Novartis, Teva, and Eli Lilly, and non-financial support from Novartis, Allergan/AbbVie, and Teva. SS declares personal fees and non-financial support from Allergan, Abbott, Eli Lilly, Novartis,

and Teva, personal fees from Medscape; and other from Bayer, Pfizer, Medtronic, Starmed, Bristol-Myers Squibb, and Daiichi Sankyo.

The remaining authors declare that the research was conducted in the absence of any commercial or financial relationships that could be construed as a potential conflict of interest.

Publisher's Note: All claims expressed in this article are solely those of the authors and do not necessarily represent those of their affiliated organizations, or those of the publisher, the editors and the reviewers. Any product that may be evaluated in this article, or claim that may be made by its manufacturer, is not guaranteed or endorsed by the publisher.

frontiers | Frontiers in Neurology

REVIEW
published: 19 May 2022
doi: 10.3389/fneur.2022.885020

Glymphatic System Dysfunction: A Novel Mediator of Sleep Disorders and Headaches

Ting Yi[1], *Ping Gao*[1], *Tianmin Zhu*[1]*, *Haiyan Yin*[2]* and *Shuoguo Jin*[3]*

[1] Rehabilitation and Health Preservation School, Chengdu University of TCM, Chengdu, China, [2] School of Acupuncture and Tuina, Chengdu University of TCM, Chengdu, China, [3] Hospital of Chengdu University of Traditional Chinese Medicine, Chengdu, China

Sleep contributes to the maintenance of overall health and well-being. There are a growing number of patients who have headache disorders that are significantly affected by poor sleep. This is a paradoxical relationship, whereby sleep deprivation or excess sleep leads to a worsening of headaches, yet sleep onset also alleviates ongoing headache pain. Currently, the mechanism of action remains controversial and poorly understood. The glymphatic system is a newly discovered perivascular network that encompasses the whole brain and is responsible for removing toxic proteins and waste metabolites from the brain as well as replenishing nutrition and energy. Recent studies have suggested that glymphatic dysfunction is a common underlying etiology of sleep disorders and headache pain. This study reviews the current literature on the relationship between the glymphatic system, sleep, and headaches, discusses their roles, and proposes acupuncture as a non-invasive way to focus on the glymphatic function to improve sleep quality and alleviate headache pain.

Keywords: glymphatic system, headaches, sleep, neuropathology, aquaporin 4

OPEN ACCESS

Edited by:
Lu Liu,
Capital Medical University, China

Reviewed by:
Maiken Nedergaard,
University of Rochester, United States
Feng Han,
The Pennsylvania State University (PSU), United States

***Correspondence:**
Haiyan Yin
yinhaiyan@cdutcm.edu.cn
Shuoguo Jin
jinshuoguo@cdutcm.edu.cn
Tianmin Zhu
tianminzhu@cdutcm.edu.cn

Specialty section:
This article was submitted to Headache and Neurogenic Pain, a section of the journal Frontiers in Neurology

Received: *27 February 2022*
Accepted: *13 April 2022*
Published: *19 May 2022*

Citation:
Yi T, Gao P, Zhu T, Yin H and Jin S (2022) Glymphatic System Dysfunction: A Novel Mediator of Sleep Disorders and Headaches. Front. Neurol. 13:885020. doi: 10.3389/fneur.2022.885020

INTRODUCTION

Sleep is vital to our body. Headache is a common pain complaint following poor sleep (1). Up to 70% of patients with chronic headaches also experience sleep disruption (2). Despite the common co-occurrence of these conditions, the relationship between headache and sleep is complex and poorly understood. Patients consistently report that poor sleep the previous night causes headache the next day (3), which indicates that poor sleep is a trigger for headaches and a higher frequency of headaches. However, sleep disturbances can be influenced by numerous factors. Although headache disorders have been suggested as a possible predisposing and perpetuating factor of sleep disturbances (4), the causal relationship regarding which occurs first, headache or poor sleep, remains a conundrum. To date, there have been some studies investigating the relationship, which suggests that the complex relationship between sleep and headache is bidirectional (4). However, a growing number of studies have suggested that sleep and headache share a common underlying etiology (5).

The glymphatic system (GS) is a newly discovered central nervous system (CNS) waste cleaning system that may offer a possible explanation for the relationship between sleep and headache (6). Its function is similar to the peripheral lymphatic system and relies on astrocytes; thus, the system is termed a "glia lymphatic" or "glymphatic" system, which represents a waste clearance and fluid pathway in and out of the brain (7, 8). When an individual experiences sleep disturbances,

glymphatic exchange markedly decreases, and this blocks the interstitial fluid (ISF) outflow of excitatory substances or inflammatory chemicals from interstitial space, which affects metabolic balance (9, 10). Furthermore, a variety of headaches breaks the balance of the GS, leading to the accumulation of beta-amyloid (Aβ) and metalloproteinases (11), which increase the risk of sleep disruption. Therefore, GS dysfunction may be considered a common underlying pathophysiology of headache pain and sleep problems. We propose that regulating glymphatic function is critical for alleviating headaches and sleep disorders. In this review, we highlighted important discoveries made by human and animal research regarding the role the GS plays in sleep disorders and headaches. In addition, we presented a hypothetical model network to illustrate that GS dysfunction underlies the pathophysiology of sleep disorders and various types of headaches and provides implications for current and future research.

GLYMPHATIC SYSTEM

The GS is an effective waste clearance and fluid pathway for the CNS (for a detailed review see (8)). The current network model of GS transportation is described in **Figure 1**. The pathway consists of a periarterial influx route for cerebrospinal fluid (CSF) to center the brain parenchyma and a perivenous outflux route, which allows the clearance of ISF and extracellular solutes from the brain parenchyma (8). Extensive evidence has also shown that the bulk flow of CSF-ISF into the perivascular spaces (PVS) delivers glucose (12) and transports lipids, signaling molecules (13), and apolipoprotein E (14) for brain-wide energy metabolism. Moreover, the enhanced convective bulk flow of CSF-ISF for the removal of soluble proteins, waste, and excess extracellular fluid is dependent on astrocyte aquaporin 4 (AQP4) channels (15). Therefore, the two most critical elements during the process of continuous circulation and metabolism are the capacity of the PVS for holding metabolic fluid to transport and the mediating effect of AQP4 polarization to decrease resistance-enhancing bulk flow exchange on GS.

The Main Structural Feature of the Glymphatic System

The para-arterial and para-venous spaces are collectively referred to as the PVS, which is the small tissue space that surrounds the cerebral arteries and veins. The inner wall is the vascular wall, and the outer wall comprises the basement membrane and the AQP4 expression in astrocyte endfeet, which wrap around and form the boundary of the space surrounding the blood vessel (16). The PVS is also known as the prelymphatic system and is considered an extension of the subarachnoid space, which is filled with CSF. The PVS narrows gradually at small arteries and arterial capillaries and eventually disappears. However, the outer wall of the blood vessel at the end remains surrounded by the basement membrane and astrocytes (17). The basal lamina provides low-resistance fluid space from which the CSF moves into the parenchyma through AQP4. The CSF convectively exchanges with the surrounding ISF in the brain parenchyma to expel and bind to metabolic waste and is subsequently cleared from the brain along with the surrounding space to the lymphatic system of the neck (15, 18). Thus, the key function of PVS is to enable the exchange of CSF and ISF. When PVS is constricted, it would increase resistance to convective fluid movement, suppress CSF influx, and accumulate metabolic wastes. Collectively, the loose fibrous matrix of the PVS provides an essential low-resistance pathway for the bulk flow, that is, a network of drainage channels that accelerates the flow of CSF-ISF and removes soluble proteins, toxic products, and metabolic waste within the GS from the brain.

Aquaporins are a family of water channels that are ubiquitously distributed among various tissues of the body. AQP4 is the most abundantly expressed aquaporin in the brain and participates in maintaining brain homeostasis (19). AQP4 is anchored to the dystrophin-associated protein complex *via* α-syntrophin, which is linked to laminin and agrin in the perivascular glial basement membrane by α-dystroglycan (20). Because of this complex molecular organization, AQP4 is unusually dense in the interface between the perivascular and interstitial spaces of the brain, which makes it easy to lower the resistance to aid CSF entry into the brain parenchyma and enhance CSF-ISF exchange, ultimately contributing to the exchange of solutes and metabolites in the bulk water flow (7). Research has shown that the polarization of AQP4 in healthy brains is highly distributed in the astrocyte endfeet of the outer wall of the PVS, which facilitates fluid influx into the parenchyma, fluid efflux out of the brain, and the elimination of brain metabolic waste (21, 22). When AQP4 channels are mislocalization or knockout, Iliff and colleagues found CSF influx significantly reduced relative to wild-type animals (7). As a result, we speculate that a significant reduction in the expression of AQP4 in astrocyte endfeet will lead to an impairment in the effective exchange of CSF-ISF, the accumulation of metabolic waste in the interstitium of brain tissues, and the gradual formation of plaque materials, which will eventually result in disease.

Factors That Impact the Glymphatic System

The physiological function of the GS is affected by a variety of factors; however, the exact mechanism underlying its development remains unclear. In recent years, progress in the study of the GS with animal experiments and clinical trials has increased our understanding of the GS. It is currently believed that several factors affect the GS, including (1) arterial pulsatility, which is considered an important factor that drives the flow of CSF in PVS and subsequent CSF–ISF exchange. Ligation of the internal carotid artery causes CSF influx into the brain to slow, whereas enhanced arterial pulsatility following β agonist injection leads to an increase in CSF influx (23). (2) Sleep also affects the GS, in which the arousal level appears critical for governing glymphatic dynamics of CSF-ISF. There is an association between the sleep-wake cycle, water homeostasis, and effective clearance of pathological proteins. Hablitz et al. showed that glymphatic inflow was higher during slow-wave sleep (or ketamine/xylazine anesthesia) than during wakefulness and was

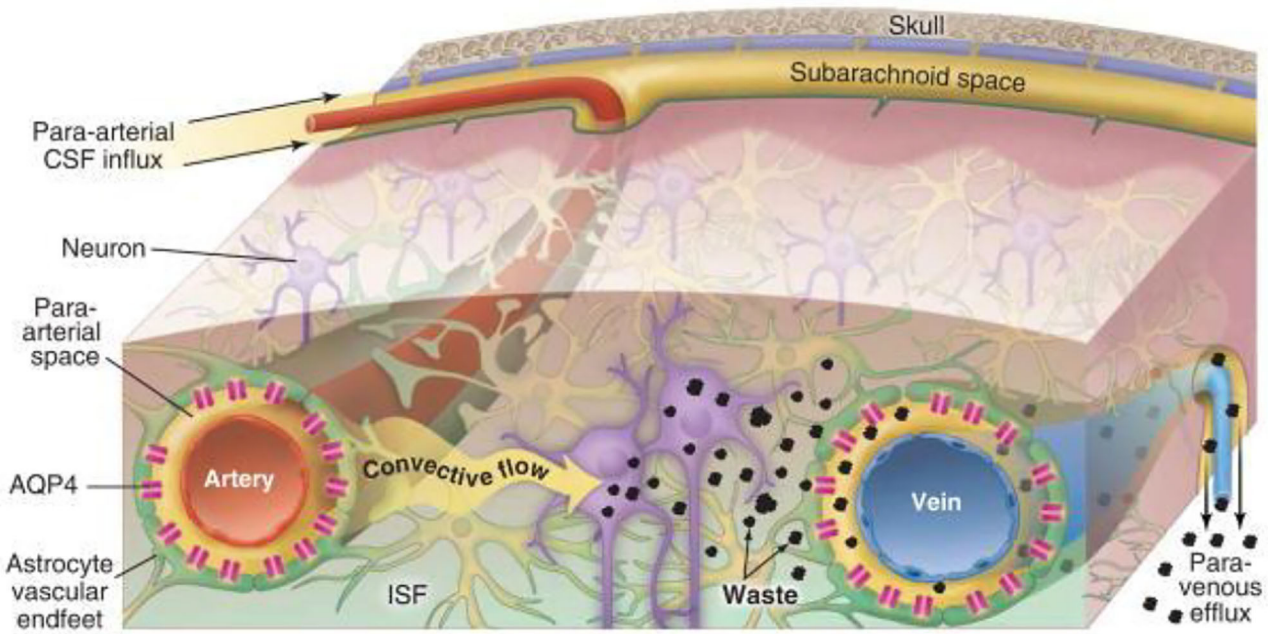

FIGURE 1 | Schematic diagram of glymphatic transport in the brain (8). Cerebrospinal fluid (CSF) influx flows through the peri-arterial space *via* pulsation of the arterial wall and is then mediated by astrocyte aquaporin 4 (AQP4) in the brain parenchyma, which drives the interstitial fluid (ISF), whereby parenchymal metabolic waste substances exchange with the CSF to efflux into the peri-venous space. Eventually, the waste is cleared into the peripheral lymphatic system of the neck by arachnoid granulations and meningeal lymphatic vessels along with cranial and spinal nerve roots.

positively correlated with delta brain waves and Aβ in the cortex (24, 25). The clearance rate of Aβ increased 2-fold, and the function of the GS increased significantly during sleep or under anesthesia (26). In order to further explore the role of sleep, the pioneering study of Fultz et al. suggested that global brain signals drive strong CSF movement associated with physiological modulations, especially during drowsiness or sleep in human (27), and global blood oxygen level-dependent (BOLD)–CSF coupling can be served as a marker for gauging glymphatic function (28). Intriguingly, this is the reason why recent studies have discovered that BOLD–CSF coupling is significantly weaker in those patients with AD (28) and PD (29) accompanying the accumulation of metabolic toxic wastes. (3) Finally, aging is a factor where brain aging has a significant impact on the function of the GS. A study compared the influx of the GS between aged and young mice and found that the influx of the CSF tracer in aged mice was 85% lower than that in young mice (10), which may be explained by meningeal lymphatic atrophy, arterial pulsatility impairment and perivascular AQP4 depolarization in the aging brain (30). In addition, other factors, such as inspiration (31) and body posture (32), have been shown to be related to the GS.

THE GLYMPHATIC SYSTEM IN VARIOUS TYPES OF HEADACHES

The Glymphatic System and Migraine

Migraine is a heterogeneous neurovascular disorder that affects people worldwide (33). Although the mechanism underlying chronic migraine is not fully understood, the trigeminovascular system has been shown to play a key role. Cortical spreading depression (CSD) and calcitonin gene-related peptide (CGRP) are recognized as key players in migraine pathophysiology (34).

Animal studies and the experience of spreading scintillations during migraine have shown that CSD, a pro-longed depolarization that spreads throughout the occipital lobe of the cortex, is the pathophysiologic mechanism underlyingly migraine aura. It is associated with transient disruption of ionic gradients, severe neuronal swelling, and neurotransmitter release, especially the local release of adenosine triphosphate, potassium, and hydrogen ions from neurons (33). A recent novel report demonstrated that CSD facilitates several minutes of the closure of PVS, a proposed exit route for ISF and solutes from the brain, which results in headaches by impairing glymphatic flow and preventing toxic substances to be cleared from the brain (**Figure 2**) (11). This study was the first to demonstrate that the GS is related to an abnormal cortical event that provokes a migraine attack. Moreover, based on the regulation of the width of the PVS by astrocytic endfeet, Rosic et al. further demonstrated that CSD is connected with the swelling of astrocytic endfeet using two-photon laser scanning microscopy in a different CSD mouse model (35). Taken together, these findings suggest that the closure of the PVS, which results in impaired clearance of excitatory and inflammatory waste along the paravascular pathways, plays a critical role in migraine pathogenesis.

The local inflammatory response is specifically triggered by CGRP, substance P, and pituitary adenylate cyclase-activating polypeptide from meningeal afferent fibers, following the

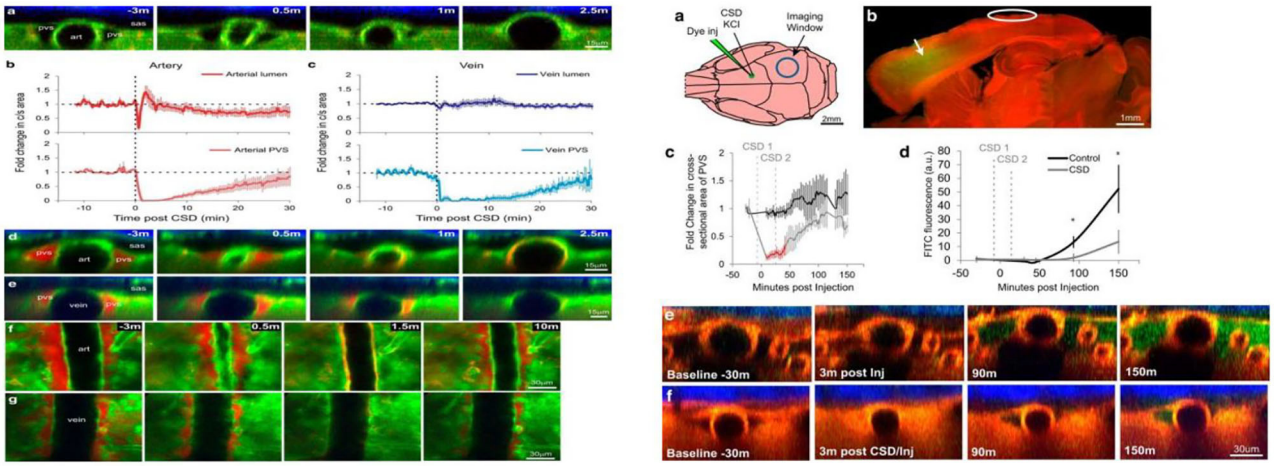

FIGURE 2 | Cortical spreading depression (CSD) closes perivascular spaces (PVS), which impairs glymphatic flow, during migraine (11). The left panel illustrates the closure of the para-arterial space and para-venous space caused by the CSD over time *in vivo* two-photon. Specifically, the para-arterial and para-venous spaces close for 6 and 16 min, respectively, and partially reopen at 30 min, which causes the impairment of glymphatic flow that is represented in the right panel. The glymphatic flow over time (green dye) in CSD mice (right f) is lower than that in controls (right e).

vasodilation and microenvironment changes that occur during migraine (36). CGRP primarily mediates neurogenic inflammation and modulates nociceptive input (37). It is a primary neuropeptide involved in headaches, particularly migraine, and is an effective vasodilatory peptide that is widely applicable to migraine treatment (37). In 1990, Goadsby et al. first reported that CGRP was elevated in the extracerebral circulation during migraine (38) and that the CGRP level obtained from the jugular vein of migraine patients is higher than individuals without migraine (39). Newer drugs that target CGRP transmission along the migraine pain pathway have recently been approved by the United States Food and Drug Administration (40). CGRP is released by the trigeminal nerve innervating meninges, pia mater, intracerebral arteries, and the central projections in the spinal trigeminal nucleus at the level of the medulla (41). The regulatory mechanism of CGRP is well-understood; however, how it is metabolized after being released from the perivascular compartment into the blood remains unclear (41). It is expressed in C- and A-delta nociceptive nerve fibers and is widely released from perivascular trigeminal afferents, yet it cannot readily cross the blood-brain barrier (42). Thus, when it is released from nerve fibers, it initially cannot reach the vessels; however, the regulatory mechanism of CGRP needs to enter the perivascular space and subsequently into the CSF of the subarachnoid space. This is the reason why research has shown that the CGRP concentration in the CSF is five times higher than that in the plasma (43). Therefore, we propose that CGRP released from nerve fibers does not enter the vessels and instead diffuses into the surrounding perivascular space, which may be a continuation of the PVS of the penetrating arteries. This process may be mediated by the GS, which promotes the exchange and flow of CSF-ISF to maintain balance and eliminates CGRP (41). Therefore, the underlying pathological mechanisms of migraine pain may involve the GS, which offers insights into potential new antimigraine targets. Further, in a separate study, Hana and colleagues found that CGRP antagonists are not only a treatment for migraine but also for AD (44), which can reduce neuroinflammation and α-synuclein aggregation indicating a new therapeutic avenue for neurological disorders. While the study does not implicate that the mechanism is related to GS, it is a meaningful direction worth further exploring the exact role.

The Glymphatic System and Post-traumatic Headache

Traumatic brain injury (TBI) is a devasting disorder that results in temporary or permanent neurological deficits and affects millions of people worldwide annually. In the past several decades, there has been an increase in the incidence of TBI globally, and this has coincided with a substantial increase in the incidence of post-traumatic headache (PTH). Globally, there are an estimated 69 million patients with TBI each year (45), whereas the 1-year prevalence for PTH is 21/100,00 (46). Moreover, PTH accounts for 4% of all headaches and is the second most common sequelae after TBI (47). The International Classification of Headache Disorders (ICHD) recently revised the diagnostic criteria for PTH in 2018 (48), although the criteria remain controversial. Nevertheless, PTH has attracted increased attention in recent years. The complex pathogenesis of TBI involves neuronal depolarization and the release of excitatory neurotransmitters, such as glutamate and aspartate, resulting in an increase in intracellular calcium, which induces dramatic changes in the metabolic state of the brain (47, 49). In addition, the accumulation of metabolic waste caused by abnormal metabolism in the brain is an important cause of PTH (50). Numerous recent studies have demonstrated the role of GS in TBI. In one study, Iliff et al. observed that the clearance of interstitial proteins and peptides from the brain parenchyma was impaired following TBI (51). Thus, it

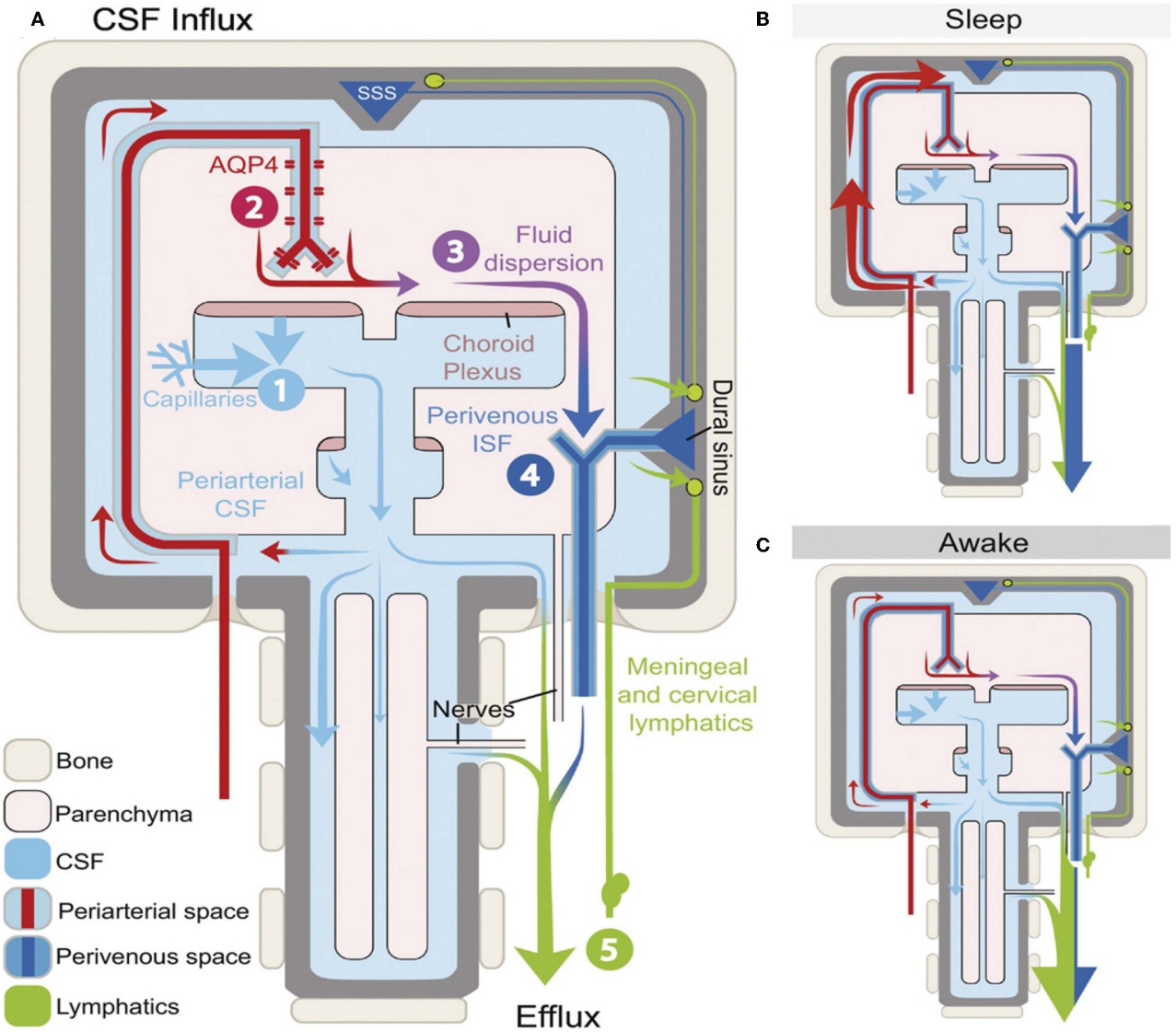

FIGURE 3 | Schematic outline of glymphatic system (GS) function during different arousal states (64). The influx and efflux of the fluid transport pathway from GS **(A)** and its function varies during different arousal states. A glymphatic clearance occurs primarily during sleep via the enlargement of the periarterial space and the perivenous space to promote the glymphatic flow **(B)**. However, function decreasing in the GS results in the accumulation of metabolic waste, which builds up in the awake brain and mostly depends on lymphatic vessels to exclude **(C)**.

has been suggested that impairment in the clearance of CGRP and interstitial proteins and peptides may also underlie PTH. Furthermore, CGRP-mediated mechanisms could play a critical role in PTH pathogenesis. This was supported by an animal study that proposed blockade of CGRP as a potential therapy for managing PTH (52). Therefore, the role of the GS is maintaining balance, and preventing the CGRP level from becoming too high may be a promising treatment for PTH. In summary, we suggest that the GS is important for PTH, and CGRP is also a significant mediator of PTH. The clearance of waste from the brain due to glymphatic dysfunction is a likely cause of PTH (50, 53).

In addition, other researchers have found that TBI induces meningeal lymphatic drainage dysfunction, accompanied by morphological changes and increased intracranial pressure (ICP) (54). Intracranial hypertension (IIH) is a debilitating disorder characterized by ICP and causes chronic headaches that reduce the quality of life. Although the pathogenesis of IIH is poorly understood, recent evidence suggests that abnormal CSF absorption as a result of GS abnormalities is the mechanism underlying IIH (55). The venous outflow pathway plays an important role in maintaining the homeostatic balance of CSF as well as ICP. The glymphatic outflow pathway may serve as a compensatory pathway to regulate fluid homeostasis when the venous outflow pathway is dysfunctional. Thus, CSF absorption anomalies cause increased ICP, which contributes to the pathophysiology of IIH. Enhancing the function of the GS to

accelerate CSF circulation may be a promising method to relieve headaches induced by IIH.

THE GLYMPHATIC SYSTEM AND SLEEP DISORDERS

Sleep is important to our bodies. Brain excitability, memory consolidation, and immune functions can become impaired following sleep disturbances (56). Rapid eye movement (REM) sleep and periods of non-REM (NREM) sleep are two metabolic and electrophysiological phases with distinct functions during sleep. The NREM sleep phase is subdivided into three stages: N1, N2, and N3. Because of the presence of slow EEG waves during N3, NREM is also called slow-wave sleep. Brain waves during REM sleep are similar to those during the awake state and are characterized by rapid eye movements. At the beginning of sleep, individuals enter the NREM sleep phase, whereby EEG exhibits slow waves, and subsequently, they enter the REM sleep phase; these phases alternate in a cyclic fashion all night (57–59).

Physiological changes in the organs and functions of the body during sleep occur as a result of changes in nervous system function. Experimental and epidemiological evidence has demonstrated a strengthening of the relationship between neurological decline and sleep problems; these conditions frequently co-occur (60). Sleep disorders have been linked to the development of neurogenerative diseases. Poor sleep impairs cognition, exacerbates depression and anxiety symptoms, and predisposes people to dementia, particularly Alzheimer's disease and Parkinson's disease (10, 61). Although the specific mechanisms underlying such effects are unknown, the involvement of the abnormal clearance of metabolic waste during sleep has been suggested (15). Our brain only weighs approximately 3 lbs, yet its high energy demand accounts for 40% of the body's total energy consumption. Moreover, cerebral oxygen consumption reduces by only 20% during sleep (5). Thus, such a high energy demand generates a higher amount of potentially toxic protein waste than that generated by other organs. However, the lack of lymphatic vasculature to remove large amounts of waste from the brain parenchyma is problematic. Further research on the GS that is focused on this issue will advance our understanding of the relationship between the GS and sleep disorders (62).

The most significant function of the GS is particularly active during sleep (63), whereby potentially toxic neural waste substances that accumulate during wakefulness are cleared *via* the GS (**Figure 3**) (24, 64). It is thought that the cell volume decreases during sleep, which expands the size of PVS, and this facilitates the influx of CSF into the peritubular space for material exchange and metabolic waste removal (10). Animal experiments using intravital 2-photon microscopy in mice showed that glymphatic clearance is decreased by 90% during wakefulness, while protein clearance in the intima of the brain doubles during sleep (24). In addition, Aβ levels in circadian-fluctuating CSF have been reported to significantly increase during wakefulness and decrease during sleep, especially during NREM sleep. To further understand the effects of sleep deprivation on Aβ clearance, a clinical trial in 20 healthy controls who underwent 31 h of sleep deprivation showed that Aβ was increased by 5% in the hippocampus, the parahippocampus, and the thalamus (65). Moreover, a recent study that tracked the REM phase in patients who experienced poor sleep found that the index of diffusion tensor imaging analysis along the perivascular space was significantly lower in patients than in healthy controls, which indicated glymphatic dysfunction (66). Thus, we speculate that the GS is intimately linked to various aspects of sleep.

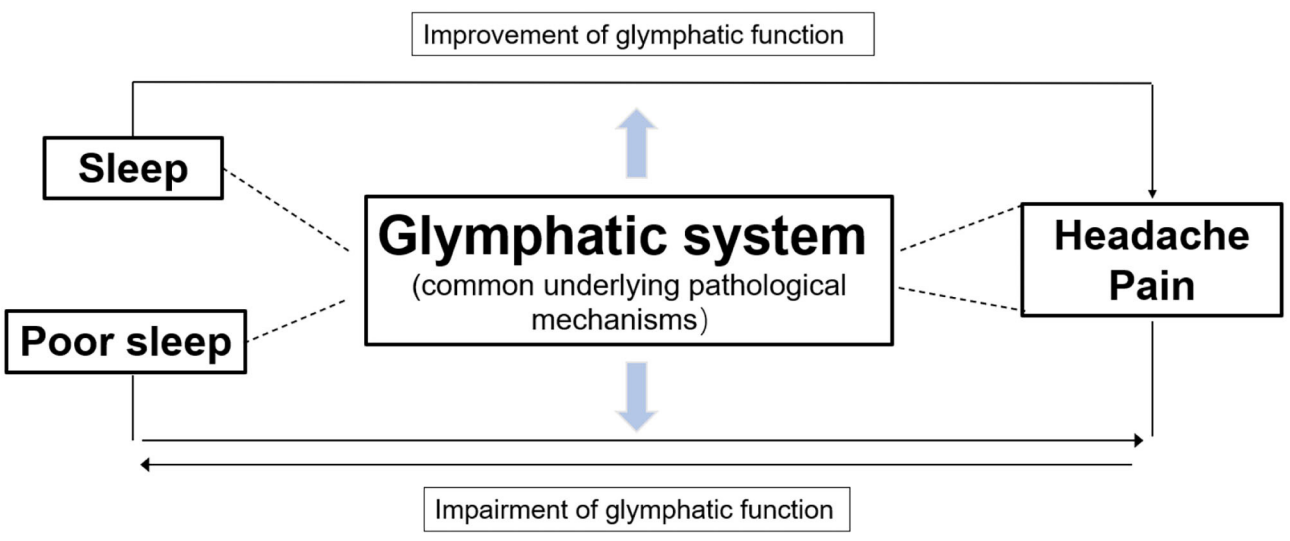

FIGURE 4 | Diagram illustrating the relationship of three parts. GS dysfunction is a common underlying pathological mechanism of sleep disturbances and headache pain. Glymphatic flow, the clearance of waste products, and nutrient transportation can be improved during sleep, which may alleviate headaches. In contrast, poor sleep and headaches affect each other and may be connected indirectly, whereby both impairing glymphatic function, which further exacerbates both conditions.

Sleep Position

Gravity can affect the flow and distribution of blood in the brain. Therefore, sleep position may be an important factor that affects the clearance of waste products from the brain. In a clinical study, Daniel et al. reported a significant association between sleeping in a supine position for more than 2 h/night and the development of neurodegenerative diseases. Interestingly, head position in a supine position during sleep can affect the clearance of neurotoxic proteins from the brain, which may trigger the development of neurodegenerative diseases (67). In another study in anesthetized rats, the transport and clearance efficiency of the GS was higher in the lateral position than in supine and prone positions, which corresponds to rats' preference for lateral decubitus behavior during rest and sleep under physiological conditions (32). Moreover, humans are also accustomed to lying in a lateral position during sleep. Thus, perhaps this is an effective way to prevent neurodegenerative diseases. Although there have not been any clinical trials investigating this idea, the potential mechanism warrants exploration.

Sleep-Wake Cycle Alterations

The suprachiasmatic nucleus of the hypothalamus controls the sleep-wake circadian rhythm (68). Abnormal circadian rhythms and altered sleep-wake patterns often coexist. Patients who have trouble falling and staying asleep at night often experience excessive daytime sleepiness. Although sleep plays an important role in glymphatic function as discussed above, research has also shown that glymphatic function depends on not only the arousal state but also the daily rhythm. This explains why glymphatic influx and interstitial fluid clearance in mice are better at noon when they are asleep (69). To further explore whether its own circadian rhythm causes the function of the GS to change or the environment change causes the light/dark cycle. Lauren et al. observed circadian behavior from constant light (LL) in mice by continuous activity monitoring, and there is no significant change in the circadian system under 10 days in LL. Subsequently, these mice were exposed to LL for 10 days. Results showed that glymphatic influx, waste clearance, and fluid drainage persisted, which supports the hypothesis that the circadian oscillations that affect the GS are endogenous, not by light cycle (70, 71).

GLYMPHATIC SYSTEM IS A POSSIBLE KEY IN THE BIDIRECTIONAL RELATIONSHIP BETWEEN SLEEP AND HEADACHES

Sleep disturbances and headaches occur throughout life. Their relationship is interdependent and often follows a vicious cycle. Headaches may occur during sleep, after sleep, or at different stages of sleep, whereas poor quality, short duration, inappropriate timing, and inappropriate sleep behaviors can also trigger headaches. Recently, the ICHD-3 described the relationship between headache and sleep disturbances, which included sleep-related headache disorders, such as migraine, cluster headache, chronic paroxysmal migraine, sleep-onset headache, and secondary headache (72). Some headache prevalence studies showed that tension-type headache (TTH) is larger than migraine worldwide, but migraine is closely linked to sleep disturbance (73). 48–74% of patients with migraine thought poor sleep is a predictor of headache, while patients with TTH only account for 26–72% (74). In patients with migraine, sleep disturbance manifested as insomnia, daytime sleepiness, obstructive sleep apnea, and parasomnia (night terrors, somnambulism) (75); Insomnia was most associated with migraine compared with other types of sleep disorders. The prevalence of insomnia in Korean patients with migraine is 25.9% (76). A prospective study has shown that patients with insomnia have higher risks of migraine after 11 years (77). The increased headache frequency in patients with migraine is associated with short sleep duration and poor sleep quality (78). Although the pathogenetic relationship between sleep and migraine is still not completely understood, they are commonly affected by potential factors such as high levels of stress, anxiety, and depression during the day, which are significant triggers of poor sleep and headache during the night. Interestingly, this is the reason why fatigue, weariness, and yawning typically precede headache attacks during the day. Thus, we concluded that headache promotes sleep disturbances, but sleep disturbances can also precede and trigger headaches.

Glymphatic dysfunction has been put forward as a common pathogenic mechanism of sleep disturbances and headaches (**Figure 4**). Sleep has been shown to play a major role in brain homeostasis and waste clearance *via* the GS (11). However, another study demonstrated that sleep deprivation reduces glycogen breakdown, which may ultimately contribute to CSD, rise the extracellular K^+ levels activating inflammatory pathways, and impair glymphatic transport causing glucose or lactate transporter deficiency; subsequently, this forms a vicious cycle in the cortex that leads to migraine pathophysiology (79). Further, norepinephrine (NE), which regulates glymphatic function, is also an important factor that affects sleep and migraine. On the one hand, NE regulates the sleep-wake cycle of glymphatic exchange and the volume of extracellular perivascular space (80). Arousal causes a burst of NE release, which turns the GS off and increases the resistance of fluid transport. On the other hand, reports have shown that rats produce headache behaviors when NE is applied to the dura mater (81), which may explain why propranolol is one of the most effective first-line medications used for migraine prophylaxis. Therefore, GS may provide a tantalizing link between sleep disturbance and headache, and glymphatic dysfunction may be a common pathogenic factor.

There are direct and indirect factors that could explain how GS affects headache and sleep. They may directly influence each other *via* the GS; for example, sleep can decline NE levels from the locus coeruleus, thereby increasing the size of the interstitial space, lowering the resistance to convective fluid movement, and promoting CSF influx and interstitial solute efflux, thus it can improve the closure of PVS by CSD to alleviate the symptoms of migraine (11, 24); pain may directly block GS function by altering neuronal function, which in turn, causes sleep disturbances. Alternatively, there may be an indirect connection, whereby sleep disruption causes the accumulation of a large amount of metabolic waste, which triggers neuroinflammation and impairment of the GS, inducing intense headache symptoms (6, 50, 53). Thus, improving sleep quality can

improve GS function by enlarging PVS, increasing CSF-ISF exchange, and promoting metabolic waste removal to relieve headaches.

Currently, effective and widely available treatments are limited for patients who experience headaches and sleep problems. Therefore, there is an urgent need to develop more effective and safe treatments. Perhaps treatments that increase CSF-ISF exchange and glymphatic clearance would improve sleep or reduce headache pain. Acupuncture is widely used clinically in patients with headaches and sleep disorders (82, 83). It is well-tolerated with little risk of serious adverse effects. Do non-pharmacological treatments, such as acupuncture, improve sleep and reduce pain? Moreover, do their effects correlate with the glymphatic function? Extensive evidence has shown that acupuncture plays an important role in reducing NE and inhibiting inflammation *via* multiple mechanisms (84, 85) and accelerating glymphatic clearance (86), which suggests that it may be an effective method for reducing the severity of headache pain while simultaneously improving sleep quality. Although this is a thought-provoking idea, validation in a larger prospective study is needed.

In conclusion, GS is a recently discovered waste clearance system for the CNS that helps remove metabolic waste products from the brain to maintain metabolic homeostasis. Impairment of the GS is observed in various neurological diseases, which include sleep and headache disorders. There is a close relationship between sleep disorders and headache disorders. Some headache disorders are significantly affected by lack of sleep; conversely, headache disorders can trigger sleep disturbances. Thus, we proposed a mechanistic model network of the glymphatic dysfunction to explain the bidirectional relationship between sleep and headache disorders and hypothesized that GS dysfunction is a common pathological mechanism of the two conditions. Although there is growing evidence to support the model, it is currently a theoretical framework, which still has some uncertain problems to be verified. For example, AQP4 is an important part of GS. When the perivascular AQP4 water channel is mislocated, it will contribute to the impairment of glymphatic flows. Recent research highlighted the role of AQP4 in human sleep-wake regulation (87). However, the trigger roles of AQP4 depolarization are still unknown when a patient is under headache attack after poor sleep. Further, sleep disturbance and headache are affected by many factors, for example, depression and anxiety are strong predictors in those with sleep and headache problems. Although depression is thought to decrease glymphatic function (88), is there any possibility that depression affects sleep and headaches by reducing GS function? Meanwhile, the brain structure (hypothalamic and brainstem) and neurotransmitters (melatonin and adenosine) have been hypothesized as an important pathological mechanism of sleep disturbance and headache, but there is a certain knowledge gap about whether these pathological mechanisms are related to GS. At last, the glymphatic system is a novel mechanism that has been recently discovered. It is still controversial and needs further exploration to pave the way for future research. In the future, we suggest identifying the key element that controls glymphatic exchange to maintain metabolic homeostasis, which would enable the development of preventive and therapeutic approaches for headaches and sleep disorders. As a non-pharmacological treatment, acupuncture may be promising as a non-invasive therapy. Furthermore, a better understanding of the pathological mechanisms underlying GS dysfunction may give rise to novel therapeutic strategies.

AUTHOR CONTRIBUTIONS

TY, SJ, and HY are responsible for the conception and design of the article, data collection and arrangement, and writing the paper. PG is responsible for the data collection. SJ, HY, and TZ are responsible for the revision, quality control, and review of the article. All authors contributed to the article and approved the submitted version.

FUNDING

National Natural Science Foundation of China Youth Science Fund Project (82004342). Chengdu University of Traditional Chinese Medicine 2021 Xinglin Scholars Disciplinary Talents Scientific Research Promotion Project (QJRC2021006). Fund of Promotion Plan of The Affiliated Hospital of Chengdu University of Traditional Chinese Medicine (21-Q24).

REFERENCES

1. Fitzcharles M, Cohen S, Clauw D, Littlejohn G, Usui C, Häuser W. Nociplastic pain: towards an understanding of prevalent pain conditions. *Lancet.* (2021) 397:2098–110. doi: 10.1016/S0140-6736(21)00392-5
2. Westergaard ML, Glümer C, Hansen EH, Jensen RH. Prevalence of chronic headache with and without medication overuse: associations with socioeconomic position and physical and mental health status. *Pain.* (2014) 155:2005–13. doi: 10.1016/j.pain.2014.07.002
3. Lovati C, Peruzzo S, Pecis M, Santus P, Pantoni L. Sleep, headache and sleep breathing disturbances: a polisomnographic study. *Neurol Sci.* (2020) 41:473–4. doi: 10.1007/s10072-020-04663-4
4. Ferini-Strambi L, Galbiati A, Combi R. Sleep disorder-related headaches. *Neurol Sci.* (2019) 40:107–13. doi: 10.1007/s10072-019-03837-z
5. Petit JM, Eren-Koçak E, Karatas H, Magistretti P, Dalkara T. Brain glycogen metabolism: a possible link between sleep disturbances, headache and depression. *Sleep Med Rev.* (2021) 59:101449. doi: 10.1016/j.smrv.2021.101449
6. Goldman N, Hablitz LM, Mori Y, Nedergaard M. The glymphatic system and pain. *Med Acupunct.* (2020) 32:373–6. doi: 10.1089/acu.2020.1489
7. Iliff JJ, Wang M, Liao Y, Plogg BA, Peng W, Gundersen GA, et al. paravascular pathway facilitates CSF flow through the brain parenchyma and the clearance of interstitial solutes, including amyloid β. *Sci Transl Med.* (2012) 4:147ra111. doi: 10.1126/scitranslmed.3003748
8. Nedergaard M. Neuroscience. *Garbage truck of the brain Science.* (2013) 340:1529–30. doi: 10.1126/science.1240514
9. Komaroff. Does sleep flush wastes from the brain? *JAMA.* (2021) 325:2153–5. doi: 10.1001/jama.2021.5631
10. Nedergaard M, Goldman SA. Glymphatic failure as a final common pathway to dementia. *Science.* (2020) 370:50–6. doi: 10.1126/science.abb8739
11. Schain AJ, Melo-Carrillo A, Strassman AM, Burstein R. Cortical spreading depression closes paravascular space and impairs glymphatic flow: implications for migraine headache. *J Neurosci.* (2017) 37:2904–15. doi: 10.1523/JNEUROSCI.3390-16.2017

12. Lundgaard I, Li B, Xie L, Kang H, Sanggaard S, Haswell JD, et al. Direct neuronal glucose uptake heralds activity-dependent increases in cerebral metabolism. *Nat Commun.* (2015) 6:6807. doi: 10.1038/ncomms7807
13. Rangroo Thrane V, Thrane AS, Plog BA, Thiyagarajan M, Iliff JJ, Deane R, et al. Paravascular microcirculation facilitates rapid lipid transport and astrocyte signaling in the brain. *Sci Rep.* (2013) 3:2582. doi: 10.1038/srep02582
14. Achariyar TM, Li B, Peng W, Verghese PB, Shi Y, McConnell E, et al. Glymphatic distribution of CSF-derived apoE into brain is isoform specific and suppressed during sleep deprivation. *Mol Neurodegener.* (2016) 11:74. doi: 10.1186/s13024-016-0138-8
15. Jessen NA, Munk AS, Lundgaard I, Nedergaard M. The glymphatic system: a beginner's guide. *Neurochem Res.* (2015) 40:2583–99. doi: 10.1007/s11064-015-1581-6
16. Wardlaw JM, Benveniste H, Nedergaard M, Zlokovic BV, Mestre H, Lee H, et al. Perivascular spaces in the brain: anatomy, physiology and pathology. *Nat Rev Neurol.* (2020) 16:137–53. doi: 10.1038/s41582-020-0312-z
17. Mestre H, Kostrikov S, Mehta RI, Nedergaard M. Perivascular spaces, glymphatic dysfunction, and small vessel disease. *Clin Sci (Lond).* (2017) 131:2257–74. doi: 10.1042/CS20160381
18. Ramirez J, Berezuk C, McNeely AA, Gao F, McLaurin J, Black SE. Imaging the perivascular space as a potential biomarker of neurovascular and neurodegenerative diseases. *Cell Mol Neurobiol.* (2016) 36:289–99. doi: 10.1007/s10571-016-0343-6
19. Rasmussen M, Mestre H, Nedergaard M. Fluid transport in the brain. *Physiol Rev.* (2021) 102:1025–151. doi: 10.1152/physrev.00031.2020
20. Nagelhus EA, Ottersen OP. Physiological roles of aquaporin-4 in brain. *Physiol Rev.* (2013) 93:1543–62. doi: 10.1152/physrev.00011.2013
21. Mader S, Brimberg L. Aquaporin-4 water channel in the brain and its implication for health and disease. *Cells.* (2019) 8:90. doi: 10.3390/cells8020090
22. Verkman AS, Smith AJ, Phuan PW, Tradtrantip L, Anderson MO. The aquaporin-4 water channel as a potential drug target in neurological disorders. *Expert Opin Ther Targets.* (2017) 21:1161–70. doi: 10.1080/14728222.2017.1398236
23. Iliff JJ, Wang M, Zeppenfeld DM, Venkataraman A, Plog BA, Liao Y, et al. Cerebral arterial pulsation drives paravascular CSF-interstitial fluid exchange in the murine brain. *J Neurosci.* (2013) 33:18190–9. doi: 10.1523/JNEUROSCI.1592-13.2013
24. Xie L, Kang H, Xu Q, Chen MJ, Liao Y, Thiyagarajan M, et al. Sleep drives metabolite clearance from the adult brain. *Science.* (2013) 342:373–7. doi: 10.1126/science.1241224
25. Hablitz LM, Vinitsky HS, Sun Q, Stæger FF, Sigurdsson B, Mortensen KN, et al. Increased glymphatic influx is correlated with high EEG delta power and low heart rate in mice under anesthesia. *Sci Adv.* (2019) 5:eaav5447. doi: 10.1126/sciadv.aav5447
26. Boespflug EL, Iliff JJ. The emerging relationship between interstitial fluid-cerebrospinal fluid exchange, amyloid-β, and sleep. *Biol Psychiatry.* (2018) 83:328–36. doi: 10.1016/j.biopsych.2017.11.031
27. Fultz NE, Bonmassar G, Setsompop K, Stickgold RA, Rosen BR, Polimeni JR, et al. Coupled electrophysiological, hemodynamic, and cerebrospinal fluid oscillations in human sleep. *Science.* (2019) 366:628–31. doi: 10.1126/science.aax5440
28. Han F, Chen J, Belkin-Rosen A, Gu Y, Luo L, Buxton OM, et al. Reduced coupling between cerebrospinal fluid flow and global brain activity is linked to Alzheimer disease-related pathology. *PLoS Biol.* (2021) 19:e3001233. doi: 10.1371/journal.pbio.3001233
29. Han F, Brown GL, Zhu Y, Belkin-Rosen AE, Lewis MM, Du G, et al. Decoupling of global brain activity and cerebrospinal fluid flow in Parkinson's disease cognitive decline. *Mov Disord.* (2021) 36:2066–76. doi: 10.1002/mds.28643
30. Kress BT, Iliff JJ, Xia M, Wang M, Wei HS, Zeppenfeld D, et al. Impairment of paravascular clearance pathways in the aging brain. *Ann Neurol.* (2014) 76:845–61. doi: 10.1002/ana.24271
31. Dreha-Kulaczewski S, Joseph AA, Merboldt KD, Ludwig HC, Gärtner J, Frahm J. Inspiration is the major regulator of human CSF flow. *J Neurosci.* (2015) 35:2485–91. doi: 10.1523/JNEUROSCI.3246-14.2015
32. Lee H, Xie L, Yu M, Kang H, Feng T, Deane R, et al. The effect of body posture on brain glymphatic transport. *J Neurosci.* (2015) 35:11034–44. doi: 10.1523/JNEUROSCI.1625-15.2015
33. Ferrari M, Goadsby P, Burstein R, Kurth T, Ayata C, Charles A, et al. Migraine. *Nat Rev Dis Prim.* (2022) 8:2. doi: 10.1038/s41572-021-00328-4
34. Close LN, Eftekhari S, Wang M, Charles AC, Russo AF. Cortical spreading depression as a site of origin for migraine: role of CGRP. *Cephalalgia.* (2019) 39:428–34. doi: 10.1177/0333102418774299
35. Rosic B, Dukefoss DB, Åbjørsbråten KS, Tang W, Jensen V, Ottersen OP, et al. Aquaporin-4-independent volume dynamics of astroglial endfeet during cortical spreading depression. *Glia.* (2019) 67:1113–21. doi: 10.1002/glia.23604
36. Chen H, Tang X, Li J, Hu B, Yang W, Zhan M, et al. IL-17 crosses the blood-brain barrier to trigger neuroinflammation: a novel mechanism in nitroglycerin-induced chronic migraine. *J Headache Pain.* (2022) 23:1. doi: 10.1186/s10194-021-01374-9
37. Russo AF. Calcitonin gene-related peptide (CGRP): a new target for migraine. *Annu Rev Pharmacol Toxicol.* (2015) 55:533–52. doi: 10.1146/annurev-pharmtox-010814-124701
38. Goadsby PJ, Edvinsson L, Ekman R. Vasoactive peptide release in the extracerebral circulation of humans during migraine headache. *Ann Neurol.* (1990) 28:183–7. doi: 10.1002/ana.410280213
39. Cernuda-Morollón E, Larrosa D, Ramón C, Vega J, Martínez-Camblor P, Pascual J. Interictal increase of CGRP levels in peripheral blood as a biomarker for chronic migraine. *Neurology.* (2013) 81:1191–6. doi: 10.1212/WNL.0b013e3182a6cb72
40. Ceriani CEJ, Wilhour DA, Silberstein SD. Novel medications for the treatment of migraine. *Headache.* (2019) 59:1597–608. doi: 10.1111/head.13661
41. Messlinger K. The big CGRP flood - sources, sinks and signalling sites in the trigeminovascular system. *J Headache Pain.* (2018) 19:22. doi: 10.1186/s10194-018-0848-0
42. Charles A, Pozo-Rosich P. Targeting calcitonin gene-related peptide: a new era in migraine therapy. *Lancet.* (2019) 394:1765–74. doi: 10.1016/S0140-6736(19)32504-8
43. Dux M, Will C, Eberhardt M, Fischer MJM, Messlinger K. Stimulation of rat cranial dura mater with potassium chloride causes CGRP release into the cerebrospinal fluid and increases medullary blood flow. *Neuropeptides.* (2017) 64:61–8. doi: 10.1016/j.npep.2017.02.080
44. Na H, Gan Q, McParland L, Yang JB, Yao H, Tian H, et al. Characterization of the effects of calcitonin gene-related peptide receptor antagonist for Alzheimer's disease. *Neuropharmacology.* (2020) 168:108017. doi: 10.1016/j.neuropharm.2020.108017
45. Dewan MC, Rattani A, Gupta S, Baticulon RE, Hung YC, Punchak M, et al. Estimating the global incidence of traumatic brain injury. *J Neurosurg.* (2018) 130:1080–97. doi: 10.3171/2017.10.JNS17352
46. Aaseth K, Grande RB, Kvaerner KJ, Gulbrandsen P, Lundqvist C, Russell MB. Prevalence of secondary chronic headaches in a population-based sample of 30–44-year-old persons. The Akershus study of chronic headache. *Cephalalgia.* (2008) 28:705–13. doi: 10.1111/j.1468-2982.2008.01577.x
47. Howard L, Schwedt TJ. Posttraumatic headache: recent progress. *Curr Opin Neurol.* (2020) 33:316–22. doi: 10.1097/WCO.0000000000000815
48. Headache Classification Committee of the International Headache Society (IHS). The international classification of headache disorders, 3rd edition. *Cephalalgia.* (2018) 38:1–211. doi: 10.1177/0333102417738202
49. Capizzi A, Woo J, Verduzco-Gutierrez M. Traumatic brain injury: an overview of epidemiology, pathophysiology, and medical management. *Med Clin North Am.* (2020) 104:213–38. doi: 10.1016/j.mcna.2019.11.001
50. Piantino J, Lim MM, Newgard CD, Iliff J. Linking traumatic brain injury, sleep disruption and post-traumatic headache: a potential role for glymphatic pathway dysfunction. *Curr Pain Headache Rep.* (2019) 23:62. doi: 10.1007/s11916-019-0799-4
51. Iliff JJ, Chen MJ, Plog BA, Zeppenfeld DM, Soltero M, Yang L, et al. Impairment of glymphatic pathway function promotes tau pathology after traumatic brain injury. *J Neurosci.* (2014) 34:16180–93. doi: 10.1523/JNEUROSCI.3020-14.2014
52. Daiutolo BV, Tyburski A, Clark SW, Elliott MB. trigeminal pain molecules, allodynia, and photosensitivity are pharmacologically and genetically modulated in a model of traumatic brain injury. *J Neurotrauma.* (2016) 33:748–60. doi: 10.1089/neu.2015.4087
53. Toriello M, González-Quintanilla V, Pérez-Pereda S, Fontanillas N, Pascual J. The potential role of the glymphatic system in headache disorders. *Pain Med.* (2021) 22:3098–100. doi: 10.1093/pm/pnab137

54. Bolte AC, Dutta AB, Hurt ME, Smirnov I, Kovacs MA, McKee CA, et al. Meningeal lymphatic dysfunction exacerbates traumatic brain injury pathogenesis. *Nat Commun.* (2020) 11:4524. doi: 10.1038/s41467-020-18113-4
55. Mondejar V, Patsalides A. The role of arachnoid granulations and the glymphatic system in the pathophysiology of idiopathic intracranial hypertension. *Curr Neurol Neurosci Rep.* (2020) 20:20. doi: 10.1007/s11910-020-01044-4
56. Cousins JN, Fernández G. The impact of sleep deprivation on declarative memory. *Prog Brain Res.* (2019) 246:27–53. doi: 10.1016/bs.pbr.2019.01.007
57. Castelnovo A, Lopez R, Proserpio P, Nobili L, Dauvilliers Y. NREM sleep parasomnias as disorders of sleep-state dissociation. *Nat Rev Neurol.* (2018) 14:470–81. doi: 10.1038/s41582-018-0030-y
58. O. Le Bon. Relationships between REM and NREM in the NREM-REM sleep cycle: a review on competing concepts. *Sleep Med.* (2020) 70:6–16. doi: 10.1016/j.sleep.2020.02.004
59. Yamazaki R, Toda H, Libourel PA, Hayashi Y, Vogt KE, Sakurai T. Evolutionary origin of distinct NREM and REM sleep. *Front Psychol.* (2020) 11:567618. doi: 10.3389/fpsyg.2020.567618
60. Bishir M, Bhat A, Essa MM, Ekpo O, Ihunwo AO, Veeraraghavan VP, et al. Sleep deprivation and neurological disorders. *Biomed Res Int.* (2020) 2020:5764017. doi: 10.1155/2020/5764017
61. Rasmussen MK, Mestre H, Nedergaard M. The glymphatic pathway in neurological disorders. *Lancet Neurol.* (2018) 17:1016–24. doi: 10.1016/S1474-4422(18)30318-1
62. Christensen J, Yamakawa GR, Shultz SR, Mychasiuk R. Is the glymphatic system the missing link between sleep impairments and neurological disorders? Examining the implications and uncertainties. *Prog Neurobiol.* (2021) 198:101917. doi: 10.1016/j.pneurobio.2020.101917
63. Chong PLH, Garic D, Shen MD, Lundgaard I, Schwichtenberg AJ. Sleep, cerebrospinal fluid, and the glymphatic system: a systematic review. *Sleep Med Rev.* (2022) 61:101572. doi: 10.1016/j.smrv.2021.101572
64. Mestre H, Mori Y, Nedergaard M. The brain's glymphatic system: current controversies. *Trends Neurosci.* (2020) 43:458–66. doi: 10.1016/j.tins.2020.04.003
65. Shokri-Kojori E, Wang GJ, Wiers CE, Demiral SB, Guo M, Kim SW, et al. β-Amyloid accumulation in the human brain after one night of sleep deprivation. *Proc Natl Acad Sci US.* (2018) 115:4483–8. doi: 10.1073/pnas.1721694115
66. Lee DA, Lee HJ, Park KM. Glymphatic dysfunction in isolated REM sleep behavior disorder. Acta Neurol Scand (2021) 145:464–70. doi: 10.1111/ane.13573
67. Levendowski DJ, Gamaldo C, St Louis EK, Ferini-Strambi L, Hamilton JM, Salat D, et al. Head position during sleep: potential implications for patients with neurodegenerative disease. *J Alzheimers Dis.* (2019) 67:631–8. doi: 10.3233/JAD-180697
68. Albrecht U, Ripperger JA. Circadian clocks and sleep: impact of rhythmic metabolism and waste clearance on the brain. *Trends Neurosci.* (2018) 41:677–88. doi: 10.1016/j.tins.2018.07.007
69. Taoka T, Jost G, Frenzel T, Naganawa S, Pietsch H. Impact of the glymphatic system on the kinetic and distribution of gadodiamide in the rat brain: observations by dynamic MRI and effect of circadian rhythm on tissue gadolinium concentrations. *Invest Radiol.* (2018) 53:529–34. doi: 10.1097/RLI.0000000000000473
70. Hablitz LM, Plá V, Giannetto M, Vinitsky HS, Stæger FF, Metcalfe T, et al. Circadian control of brain glymphatic and lymphatic fluid flow. *Nat Commun.* (2020) 11:4411. doi: 10.1038/s41467-020-18115-2
71. Cai X, Qiao J, Kulkarni P, Harding IC, Ebong E, Ferris CF. Imaging the effect of the circadian light-dark cycle on the glymphatic system in awake rats. *Proc Natl Acad Sci U S A.* (2020) 117:668–76. doi: 10.1073/pnas.1914017117
72. P.R. Holland. Headache and sleep: shared pathophysiological mechanisms. *Cephalalgia.* (2014) 34:725–44. doi: 10.1177/0333102414541687
73. Stovner L, Hagen K, Jensen R, Katsarava Z, Lipton R, Scher A, et al. The global burden of headache: a documentation of headache prevalence and disability worldwide. *Cephalalgia.* (2007) 27:193–210. doi: 10.1111/j.1468-2982.2007.01288.x
74. Fernández-de-Las-Peñas C, Fernández-Muñoz JJ, Palacios-Ceña M, Parás-Bravo P, Cigarán-Méndez M, Navarro-Pardo E. Sleep disturbances in tension-type headache and migraine. *Ther Adv Neurol Disord.* 11:5444 (2018). doi: 10.1177/1756285617745444
75. Waliszewska-Prosół M, Nowakowska-Kotas M, Chojdak-Łukasiewicz, Budrewicz S. Migraine and sleep-an unexplained association? *Int J Mol Sci.* (2021) 22:5539. doi: 10.3390/ijms22115539
76. Kim J, Cho SJ, Kim WJ, Yang KI, Yun CH, Chu MK. Impact of migraine on the clinical presentation of insomnia: a population-based study. *J Headache Pain.* (2018) 19:86. doi: 10.1186/s10194-018-0916-5
77. Odegård SS, Sand T, Engstrøm M, Stovner LJ, Zwart JA, Hagen K. The long-term effect of insomnia on primary headaches: a prospective population-based cohort study (HUNT-2 and HUNT-3). *Headache.* (2011) 51:570–80. doi: 10.1111/j.1526-4610.2011.01859.x
78. Song TJ, Yun CH, Cho SJ, Kim WJ, Yang KI, Chu MK. Short sleep duration and poor sleep quality among migraineurs: a population-based study. *Cephalalgia.* (2018) 38:855–64. doi: 10.1177/0333102417716936
79. Kilic K, Karatas H, Dönmez-Demir B, Eren-Kocak E, Gursoy-Ozdemir Y, Can A. et al. Inadequate brain glycogen or sleep increases spreading depression susceptibility. *Ann Neurol.* (2018) 83:61–73. doi: 10.1002/ana.25122
80. Van Egroo M, Koshmanova E, Vandewalle G, Jacobs HIL. Importance of the locus coeruleus-norepinephrine system in sleep-wake regulation: implications for aging and Alzheimer's disease. *Sleep Med Rev.* (2022) 62:101592. doi: 10.1016/j.smrv.2022.101592
81. Wei X, Yan J, Tillu D, Asiedu M, Weinstein N, Melemedjian O, et al. Meningeal norepinephrine produces headache behaviors in rats via actions both on dural afferents and fibroblasts. *Cephalalgia.* (2015) 35:1054–64. doi: 10.1177/0333102414566861
82. Vickers AJ, Linde K. Acupuncture for chronic pain. *JAMA.* (2014) 311:955–6. doi: 10.1001/jama.2013.285478
83. Zhao FY, Fu QQ, Kennedy GA, Conduit R, Zhang WJ, Wu WZ, et al. Can acupuncture improve objective sleep indices in patients with primary insomnia? A systematic review and meta-analysis. *Sleep Med.* (2021) 80:244–59. doi: 10.1016/j.sleep.2021.01.053
84. Liu S, Wang Z, Su Y, Qi L, Yang W, Fu MX. et al. A neuroanatomical basis for electroacupuncture to drive the vagal-adrenal axis. *Nature.* (2021) 598:641–5. doi: 10.1038/s41586-021-04001-4
85. Zhang R, Lao L, Ren K, Berman BM. Mechanisms of acupuncture-electroacupuncture on persistent pain. *Anesthesiology.* (2014) 120:482–503. doi: 10.1097/ALN.0000000000000101
86. Liang P, Li L, Zhang Y, Shen Y, Zhang L, Zhou J, et al. Electroacupuncture improves clearance of amyloid-β through the glymphatic system in the SAMP8 mouse model of Alzheimer's disease. *Neural Plast.* (2021) 2021:9960304. doi: 10.1155/2021/9960304
87. Ulv Larsen SM, Landolt HP, Berger W, Nedergaard M, Knudsen GM, Holst SC. Haplotype of the astrocytic water channel AQP4 is associated with slow wave energy regulation in human NREM sleep. *PLoS Biol.* (2020) 18:e3000623. doi: 10.1371/journal.pbio.3000623
88. Liang S, Lu Y, Li Z, Li S, Chen B, Zhang M, et al. Iron Aggravates the depressive phenotype of stressed mice by compromising the glymphatic system. *Neurosci Bull.* (2020) 36:1542–6. doi: 10.1007/s12264-020-00539-x

Conflict of Interest: The authors declare that the research was conducted in the absence of any commercial or financial relationships that could be construed as a potential conflict of interest.

frontiers | Frontiers in Neurology

ORIGINAL RESEARCH
published: 10 June 2022
doi: 10.3389/fneur.2022.899254

Temporal Grading Index of Functional Network Topology Predicts Pain Perception of Patients With Chronic Back Pain

Zhonghua Li[1†], *Leilei Zhao*[2†], *Jing Ji*[1], *Ben Ma*[3], *Zhiyong Zhao*[4], *Miao Wu*[4], *Weihao Zheng*[2] *and Zhe Zhang*[5,6*]

[1] Department of Rehabilitation Medicine, Gansu Provincial Hospital of TCM, Lanzhou, China, [2] Gansu Provincial Key Laboratory of Wearable Computing, School of Information Science and Engineering, Lanzhou University, Lanzhou, China, [3] Department of Rehabilitation Medicine, The Second Affiliated Hospital of Xi'an Jiaotong University, Xi'an, China, [4] Key Laboratory for Biomedical Engineering of Ministry of Education, College of Biomedical Engineering and Instrument Science, Zhejiang University, Hangzhou, China, [5] Institute of Brain Science, Hangzhou Normal University, Hangzhou, China, [6] School of Physics, Hangzhou Normal University, Hangzhou, China

OPEN ACCESS

Edited by:
Jixin Liu,
Xidian University, China

Reviewed by:
Gang Li,
Zhejiang Normal University, China
Chao Li,
The First Affiliated Hospital of China Medical University, China

***Correspondence:**
Zhe Zhang
zhangz@hznu.edu.cn

[†]These authors have contributed equally to this work

Specialty section:
This article was submitted to Headache and Neurogenic Pain, a section of the journal Frontiers in Neurology

Received: 18 March 2022
Accepted: 10 May 2022
Published: 10 June 2022

Citation:
Li Z, Zhao L, Ji J, Ma B, Zhao Z, Wu M, Zheng W and Zhang Z (2022) Temporal Grading Index of Functional Network Topology Predicts Pain Perception of Patients With Chronic Back Pain. Front. Neurol. 13:899254. doi: 10.3389/fneur.2022.899254

Chronic back pain (CBP) is a maladaptive health problem affecting the brain function and behavior of the patient. Accumulating evidence has shown that CBP may alter the organization of functional brain networks; however, whether the severity of CBP is associated with changes in dynamics of functional network topology remains unclear. Here, we generated dynamic functional networks based on resting-state functional magnetic resonance imaging (rs-fMRI) of 34 patients with CBP and 34 age-matched healthy controls (HC) in the OpenPain database *via* a sliding window approach, and extracted nodal degree, clustering coefficient (CC), and participation coefficient (PC) of all windows as features to characterize changes of network topology at temporal scale. A novel feature, named temporal grading index (TGI), was proposed to quantify the temporal deviation of each network property of a patient with CBP to the normal oscillation of the HCs. The TGI of the three features achieved outstanding performance in predicting pain intensity on three commonly used regression models (i.e., SVR, Lasso, and elastic net) through a 5-fold cross-validation strategy, with the minimum mean square error of 0.25 ± 0.05; and the TGI was not related to depression symptoms of the patients. Furthermore, compared to the HCs, brain regions that contributed most to prediction showed significantly higher CC and lower PC across time windows in the CBP cohort. These results highlighted spatiotemporal changes in functional network topology in patients with CBP, which might serve as a valuable biomarker for assessing the sensation of pain in the brain and may facilitate the development of CBP management/therapy approaches.

Keywords: chronic back pain (CBP), dynamic functional connectivity, temporal grading index (TGI), pain assessment, depression

INTRODUCTION

Pain and pain-related diseases are major contributors to disability (1–3). Among them, chronic back pain (CBP) is particularly prevalent with the disability rate increasing by over 54% in the last 30 years (4). CBP is known to be aroused by peripheral and central sensitization (5, 6), and alters the connectomics of the brain. Advances in neuroimaging technology have allowed researchers to characterize structural and functional alterations in the brain of patients with CBP (7–9), investigate brain signatures for predicting pain intensity (e.g., patterns of brain activation) (10–12), and identify effective methods for pain relief (13). Although these studies have painted a relatively comprehensive picture from abnormal brain alterations of CBP to its intervention, the relationship between spatiotemporal dysfunction of brain topological organization and pain intensity, a key question to the understanding of CBP, remains unclear.

The cerebral alterations of patients with CBP have been investigated in a series of studies focusing on functional connectivity (FC) established *via* functional magnetic resonance imaging (fMRI) (14–16). The large-scale functional network established by measuring pair-wise FC provides a comprehensive description of interactions among distinct brain regions, in terms of correlation, coherence, and topological organization (17–20). For example, chronic pain was associated with abnormal changes in the connectivity within the salience and central executive networks (21, 22) and altered strength of hub regions (23); and the study shows that pain would cause an increase in the shortest path length and clustering coefficient, and decreases in small-worldness (24). These alterations in inter-regional connectivity and network topology have largely affected the ability of information integration and segregation in the brain of patients with chronic pain (25, 26).

Existing evidence has suggested that the perception of pain was influenced by maladaptive neuroplastic changes over time (27, 28), and the CBP may derive from these changes in the central nervous system which could enhance nociceptive efficiency, influence normal attentional processing, and create the maladaptive perception of pain (29, 30). Since the "dynamic pain connectome" theory posits that the processing of pain in the brain is a dynamic process (31), it is necessary to investigate the CBP-related brain functional alteration from a time-varying perspective. Compared to traditional FC analysis, dynamic functional connectivity (dFC) is able to capture the alterations of intrinsic FC over time under various physiological and pathological brain conditions (32–36). For example, dynamic reconfiguration of functional brain networks was found during executive cognition by using dFC technology (37). Thus, dFC can provide additional information that may promote our understanding of the association between altered brain functions and CBP (38, 39). Recent studies have shown that dFC can reflect pain conditions at multiple timescales (e.g., short-term state and long-term trait) rather than just the current state of patients with chronic pain (40), and characterize pain pathophysiology from a dynamic perspective representing oscillations of the FC (41–43). However, previous studies have mainly focused on pain-related alterations in dFC, with few studies exploring how dynamics of functional network topology change in patients with CBP, and whether these changes can predict pain intensity has not been well explored.

The present study aims to investigate whether CBP is associated with dynamic changes in the functional network topology and to find an effective feature that could accurately predict the intensity of pain in the brain of patients with CBP. Resting-state fMRI data of 34 patients with CBP and 34 age-matched healthy controls (HC) were used to estimate the dFC through a sliding window approach along the time sequence. Degree centrality, clustering coefficient (CC), and participation coefficient (PC) of dFC network were calculated at each time window and cascaded to represent the dynamic fluctuation of network topology from the perspectives of nodal importance, local efficiency, and modular communication, respectively. Temporal grading index (TGI), a new feature that quantifies the oscillation slope of each network metric of the CBP cohort relative to the normative oscillation sequence of the HCs, was proposed and utilized to predict the pain intensity of the patients. TGI of these network metrics were submitted to three commonly used regression models (i.e., support vector regression [SVR], least absolute shrinkage and selection operator [Lasso], and elastic net), with a 5-fold cross-validation strategy, to examine the effectiveness of dynamic network topology on explaining pain intensity of patients with CBP.

MATERIALS AND METHODOLOGY

Participants

In the study, MRI data of 34 patients with CBP and 34 healthy controls (HC) who had matched age and gender in patients with CBP were downloaded from the Open Pain database (www.openpain.org). The database was collected by the OpenPain Project (OPP) for scientific investigation, teaching, or the planning of clinical research studies. All patients with CBP have completed the Short-Form of the McGill Pain Questionnaire (SF-MPQ), including a visual analog scale (VAS) ranging from 0 (painless) to 10 (maximum imaginable pain). The Beck Depression Inventory (BDI) was used to access the depression scores of all participants. Questions of SF-MPQ and BDI were finished 1 h before the brain scan.

MRI Data Acquisition

MRI data were acquired on a 3-Tesla Siemens Trio whole-body scanner using the standard radio-frequency head coil. All participants were required to close their eyes during the scan. High-resolution 3-dimensional T1-weighted data were acquired with the following parameters: voxel size $1\times1\times1$ mm^3, repetition time (TR) = 2,500 ms, echo time (TE) = 3.36 ms, flip angle = 9°, number of slices = 160, field of view = 256 mm, in-plane matrix resolution = 256×256. Resting-state fMRI (rs-fMRI) data were acquired using an echo-planar imaging (EPI) sequence at the same scanner with the following scanning parameters: repetition time (TR) = 2,500 ms, echo time (TE) = 30 ms, flip angle = 90°, number of slices = 40, slice thickness = 3 mm, in-plane resolution = 64×64, number of volumes = 245 or 305. For images

TABLE 1 | Demographic information of participants.

	CBP ($N = 30$, mean ± SD)	HC ($N = 29$, mean±SD)	p-value
Age	50.3 ± 8.1	49.2 ± 9.4	0.6519[a]
Gender (M/F)	17/13	17/12	0.6888[b]
BDI score	6.3 ± 5.6	1.3 ± 2.2	< 0.05[a]
VAS score	6.8 ± 1.7	-	-
Pain duration	15.9 ± 11.6	-	-

CBP, chronic back pain; HC, healthy control; BDI, beck depression inventory; VAS, visual analog scale; [a] denotes two-sided two-sample t-test; [b] denotes two-sided Pearson chi-square test.

that had 305 volumes, we removed the last 60 volumes to make the time point consistent (245 volumes for all images) (44, 45).

Image Preprocessing

All rs-fMRI data were preprocessed *via* the statistical parametric map 8 (SPM, https://www.fil.ion.ucl.ac.uk/spm/software/spm8) using the general pipeline. Briefly, the pipeline included the following steps: (1) removing the first 5 volumes; (2) correcting slice timing and head motion; (3) registering the functional images to the corresponding T1-weighted images, and normalizing the acquisition to Montreal Neurological Institute (MNI) space with a resampling voxel size of $3\times3\times3$ mm^3 resolution; (4) smoothing the normalized images with a 5-mm full-width at half-maximum (FWHM) Gaussian kernel spatially according to previous literature (46); (5) reducing low-frequency drift and high-frequency noise with bandpass filtering (0.01–0.1 Hz). The global signal regression was not conducted avoiding the removal of the significant neuronal signals (47, 48). Participants with poor image quality or excessive head motion [translation distances > 2 mm or rotation degree > 2° or mean framewise displacement > 0.2 mm (49, 50)] were excluded (51), leaving 30 CBP patients and 29 healthy controls for further analysis. The demographics for patients with CBP and HC are shown in **Table 1**. The human Brainnetome atlas (52) was used to parcellate the whole brain into 274 regions [246 for the cerebrum and 28 for the cerebellum derived from the Probabilistic Cerebellar Atlas (53)].

Dynamic FC Estimation

After preprocessing, a data matrix ($n\times T$) for each participant was obtained, where $T = 240$ denotes the number of time points and $n = 274$ denotes the number of brain regions. We used the DynamicBC toolbox (https://guorongwu.github.io/DynamicBC) (54) to estimate the dynamic functional connectivity (dFC) of each participant. As a key parameter in the sliding window approach, it has been proved that the method would introduce spurious correlations when window lengths $< 1/f_{\min}$, where $f_{\min}$ denotes the lowest frequency (i.e., 0.01 Hz) in preprocessing of bandpass filtering (55–57). The dFC matrices were calculated within $t = 191$ consecutive windows produced by sliding window approach with 50 TRs length of the window and 1 TR length of sliding step (58). Finally, t functional connectivity matrices $w \in \mathbb{R}^{n\times n}$, with negative- and self- connectivity removed (59), were obtained for each participant (**Figure 1A**).

Computation of TGI for Patients With CBP

We averaged the functional networks of each time window across the HCs, resulting in a series of average dFC ($W_h \in \mathbb{R}^{t\times n\times n}$) of HC subjects. The Brain Connectivity Toolbox (BCT, http://www.brain-connectivity-toolbox.net) was used to calculate the network properties of dFC matrices w of each subject across time windows, including degree, clustering coefficient (CC), and participation coefficient (PC) (**Figure 1B**). The PC was calculated based on the modular structure including Yeo's 7 cortical functional networks (i.e., visual, somatomotor, dorsal Attention, ventral attention, limbic, frontoparietal, default and subcortical networks) (60), subcortical network, and cerebellar network. The subcortical network was composed of all subcortical regions, including the amygdala (BN label 211–214), thalamus (BN label 231–246), caudate (BN label 219–220, 227–228), putamen (BN label 225–226, 229–230), globus pallidus (BN label 221–222), nucleus accumbens (BN label 223–224); and the cerebellar network was composed of all cerebellar lobules (excluding the brain stem) in the BN_274 atlas (BN label 247–274). For each network property of a participant, we concatenated this property across time windows to form a dynamic matrix $X \in \mathbb{R}^{t\times n}$.

As shown in **Figure 1B**, for the j-th brain region, we subtracted the regional network property calculated from W_h (the averaged dFC networks of the HCs) from the regional network property of each patient with CBP. Then a linear regression (equation 1) model, with the result of the subtraction as the dependent variable and the network property of average HC W_h as the independent variable, was performed to extract the temporal gradient index (TGI) of each brain region of CBP patients.

$$y - x = k_{i,j}x + b \tag{1}$$

The slope k is the TGI that represents the alteration gradient of this patient relative to the HC group at the temporal scale. For each patient with CBP, we concatenated the TGI of each network property across brain regions. In addition, the combination of all the TGI features was calculated *via* the z-score strategy.

Regression Analysis

To examine the validity of TGI in assessing the pain intensity of patients with CBP, three commonly used regression models (i.e., support vector regression [SVR], least absolute shrinkage and selection operator [Lasso], and elastic net) were applied to predict pain intensity (VAS scores) using the TGI. Five-fold cross-validation repeated ten times was performed and mean square error (MSE) was used to evaluate the regression performance.

The Linear SVR (61) we used for the prediction can approximate the actual pain intensity y with two hyperparameters $\mathcal{E}$ and o ascertain a linear regression function expressed as:

$$f(\omega, b) = \omega x + b \tag{2}$$

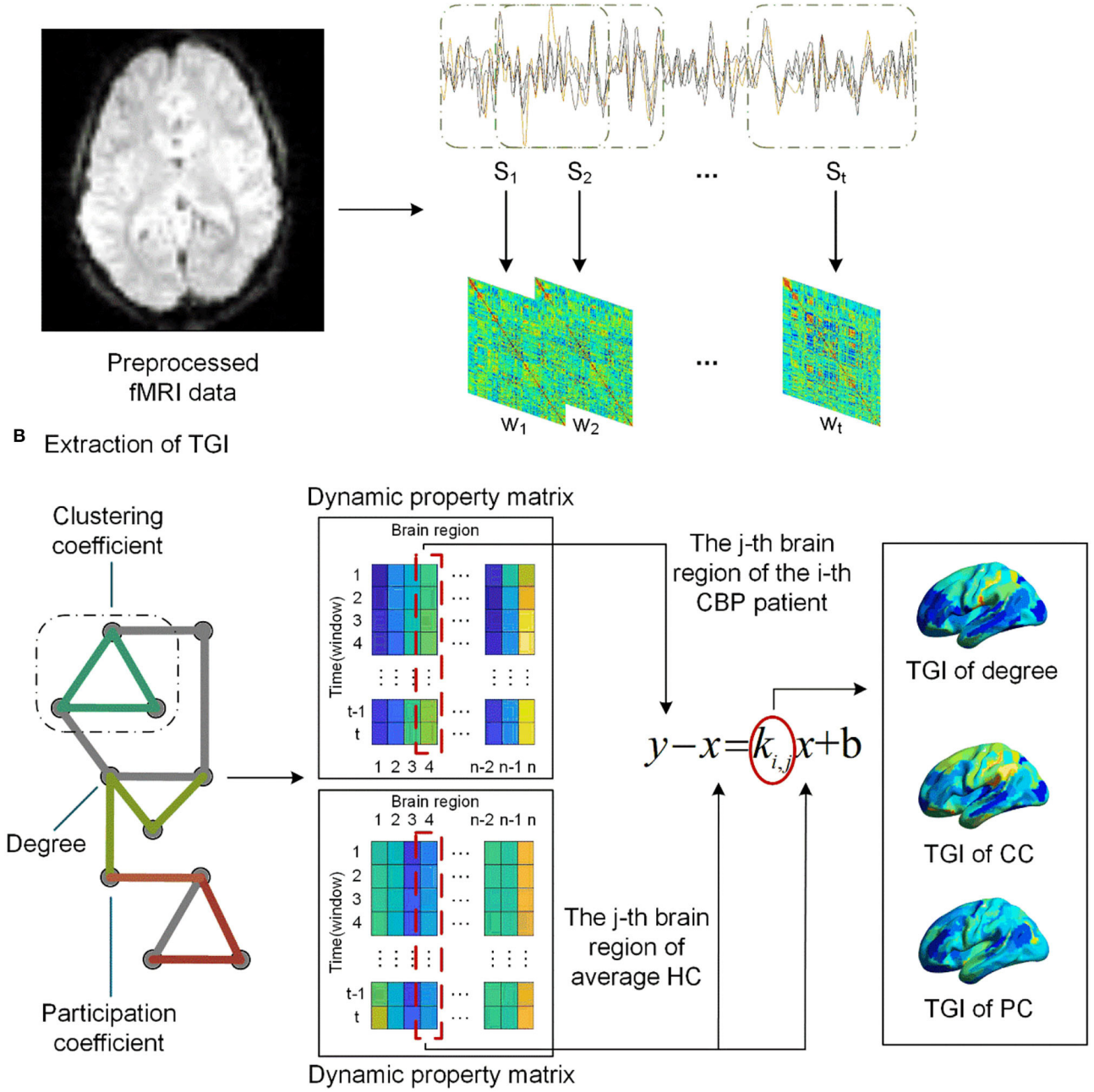

FIGURE 1 | The pipeline of TGI extraction. **(A)** We assess the dynamic functional connectivity (dFC) using the sliding window analysis with 50 TRs length for a window and 1 TR length for sliding step, resulting in t windows. **(B)** We extract dynamic property matrix (degree, clustering coefficient [CC], and participation coefficient [PC]) for the network of each CBP patient and the average network of the HCs. A linear regression model was then used to extract the TGI $K_{i,j}$ of each network property of the *j*-th brain region for *i*-th CBP subject.

where $\omega \epsilon \mathbb{R}^{1\times n}$ and b are the parameters of the function. For the prediction of the pain intensity, $x \epsilon \mathbb{R}^{n\times 1}$and the output $f(x_i)$ denoted the TGI feature of each brain region extracted from patients and the prediction result for the i-th patient, respectively.

The regression problem of Lasso (62) can be described as equation 3, where $\beta \epsilon \mathbb{R}^{n\times 1}$ is the parameter of the regression function. The L1-norm regularization was used to make the coefficients sparse so that the irrelevant predictors could be

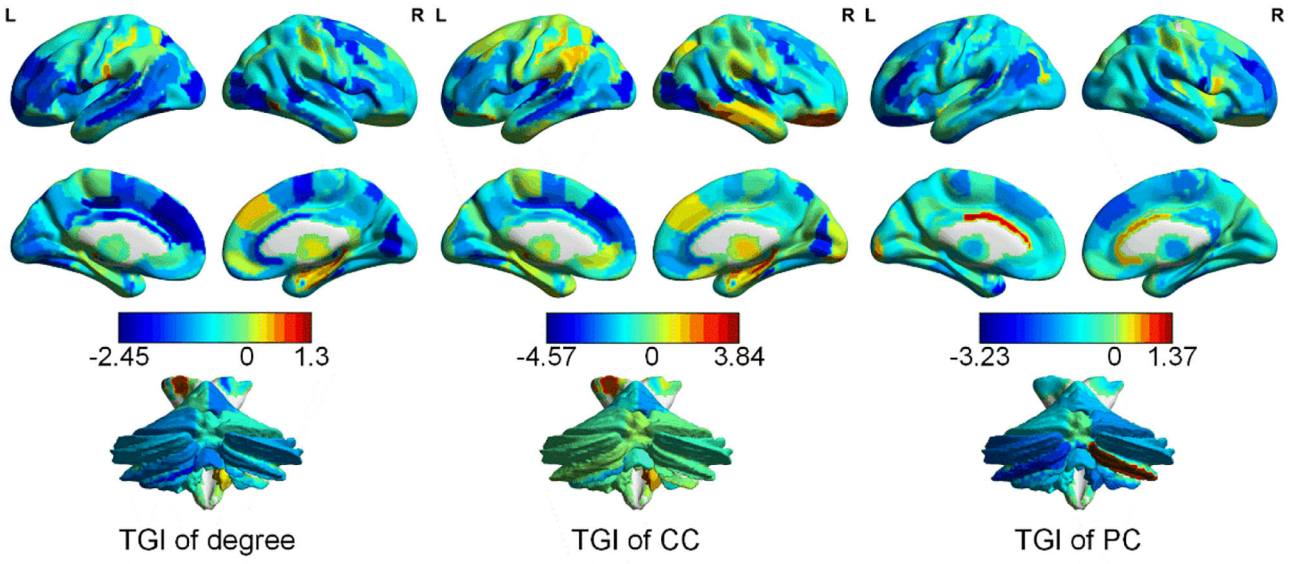

FIGURE 2 | Distribution of the TGI of different network properties [degree, clustering coefficient (CC), and participation coefficient (PC)] in cerebrum and cerebellum.

excluded (62).

$$\min_{\beta} \|y - \mathbf{X}\beta\|^2 + \lambda\|\beta\|_1 \quad (3)$$

Compared to Lasso, elastic net (63) had one more regularization term ($\beta \epsilon \mathbb{R}^{n\times 1}$) and the elastic net will turn into Lasso when setting α =0 (see equation 4). The L2-norm regularization enabled the model to select a subset rather than only one from the highly correlated features to overcome the deficit of using L1-norm regularization only.

$$\min_{\beta} \|y - \mathbf{X}\beta\|^2 + \lambda\|\beta\|_1 + \alpha\|\beta\|^2 \quad (4)$$

We used the grid search method to calibrate the λ in Lasso regression according to the previous study (64). For example, the Lasso was constructed by varying the λ in a specified range λ= {0.10,0.15,0.20,...,1} and then the optimal λ was used in the testing dataset. A two-step grid search method was applied to calibrate the parameters for both SVR and elastic net according to previous studies (65, 66). When calibrating parameters of SVR and elastic net models, we first specified a coarse grid search to determine the best region of the calibrated parameters and then conducted a finer grid search to find the optimal parameters.

We then adjusted the bias between predicted pain intensity and real pain intensity according to the bias-adjustment scheme proposed by Beheshti et al. (67). For each subject in the training set, we calculated the Δ by subtracting the real intensity from the predicted intensity of pain and then used a linear regression model of Δ against the real pain intensity to get a linear regression function with the slope μ and the intercept φ. The offset can be calculated as below:

$$offset = \mu\Omega + \varphi \quad (5)$$

where Ω denote the real pain intensity. The bias-free back pain intensity was calculated by subtracting the *offset* from individual predicted pain intensity (more information about the relation between Δ and pain intensity could be found in **Supplementary Figure S1**).

Statistical Analysis

Between-group differences in age and BDI score were estimated by using a two-sample *t*-test, and the gender difference was estimated *via* the Chi-square test. Pearson correlation analysis was performed to assess the relationship between TGI and BDI score (68) to examine whether the changes in TGI were influenced by affective factors. In addition, a two-sample *t*-test, with age, gender, and BDI score as covariates, was performed to examine the between-group differences in the network properties (i.e., nodal degree, CC and PC) in brain regions that had high prediction power. The false discovery rate (FDR) correction with $q < 0.05$ was used to correct the results for multiple comparisons.

RESULT

Spatial Distribution of the TGI of the Three Network Properties

The average TGI of each network property across patients with CBP is shown in **Figure 2**. The average TGI of degree is mainly negative values across the brain, except in the left posterior parietal thalamus (PPtha) and right ventrolateral fusiform gyrus [ventrolateral Brodmann area 37 (A37vl)] which have more positive values. Similarly, the average TGI of PC is mostly negative values except for cerebellar right lobule VIIb and left rostroventral ventral anterior cingulate cortex [rostroventral Brodmann area 24 (A24rv)]. The average TGI of CC shows more positive values relative to the other two

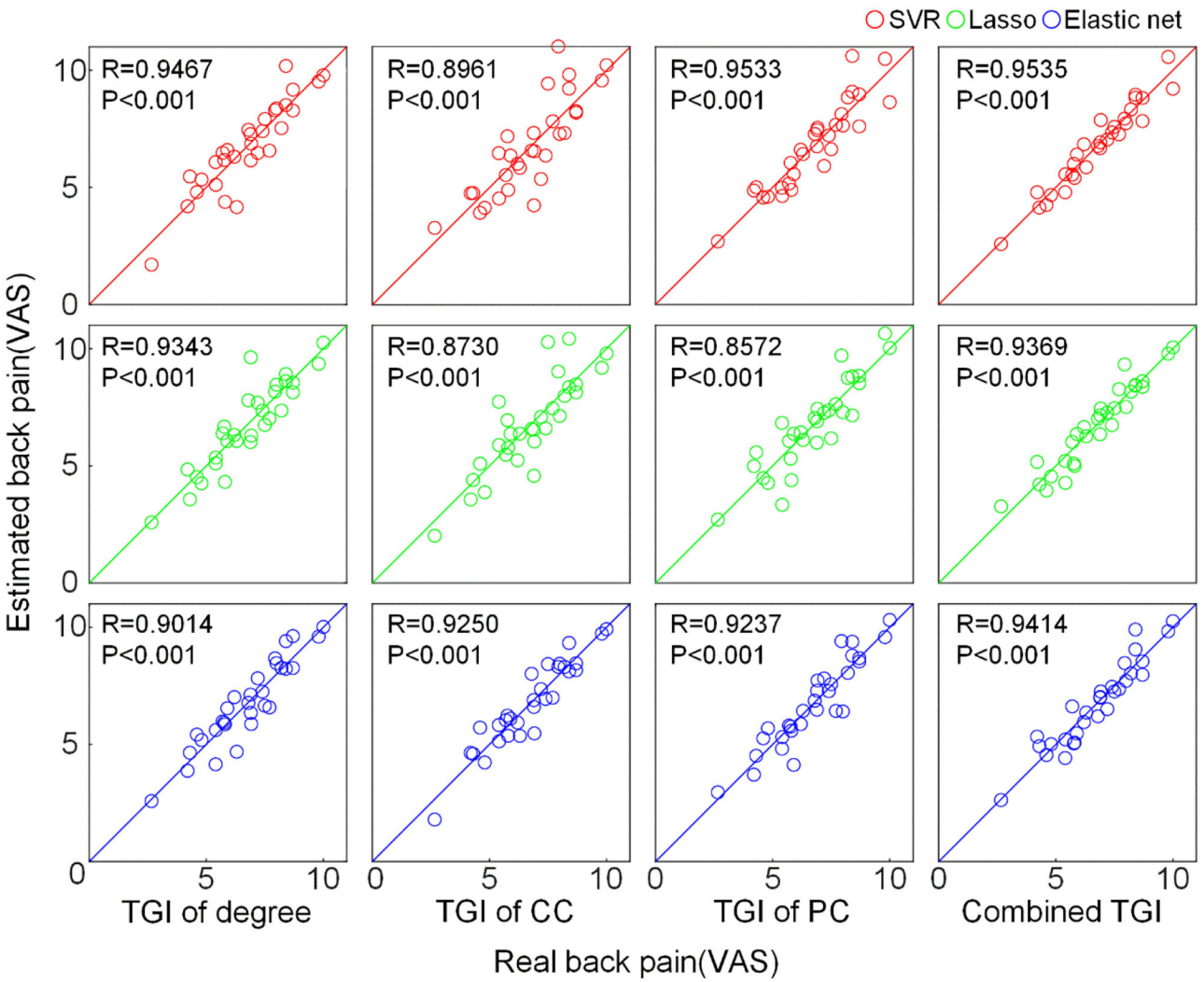

FIGURE 3 | Prediction performance of pain intensity using the TGI of different network properties. The scatter plot shows the correlation between the real VAS score and the predicted VAS score estimated by different features through different regression models. The solid lines indicate the identity line (y = x). CC, clustering coefficient; PC, participation coefficient; VAS, visual analog scale.

properties, which locates in A37vl, right rostral temporal thalamus (rTtha), and right medial pre-frontal thalamus (mPFtha), whereas the TGI of medial prefrontal and occipital cortices are highly negative. From the result (more details could be found in **Supplementary Figure S2**) of Pearson correlation analysis between TGI and BDI scores, we found no significant difference.

Prediction Performance of Pain Intensity Using the TGI Features

We used the TGI of degree, CC, PC as well as their combination as input features of SVR, Lasso, and elastic net models to predict the VAS score via a cross-validation strategy. The results are visualized in **Figure 3**. The scatter plots illustrate the correlation between estimation and the real VAS scores. The MSE of each regression task is given in **Figure 4**. For TGI of degree, SVR achieved the best prediction performance by using the parameters of $(O, \mathcal{E}) = (1,0.17)$, with the mean MSE $= 0.45 \pm 0.09$. The TGIs of CC and PC achieved the mean MSEs of 0.56 ± 0.18 and 0.54 ± 0.14, respectively, using the elastic net under the parameters $(\lambda, \alpha) = (0.08,0.28)$. The combination of all the TGI features significantly improved the regression performance of all the three models, and the Lasso achieved the minimum MSE $= 0.25 \pm 0.05$ under the parameter $\lambda = 0.65$.

Temporal Fluctuation of Network Properties of High Informative Brain Regions

The distribution of brain regions with the TGI that highly contributed to the regression process is shown in **Figure 5A** (the fluctuations of the other brain regions can be found in **Supplementary Figures S3–S5** in **Supplementary Materials**).

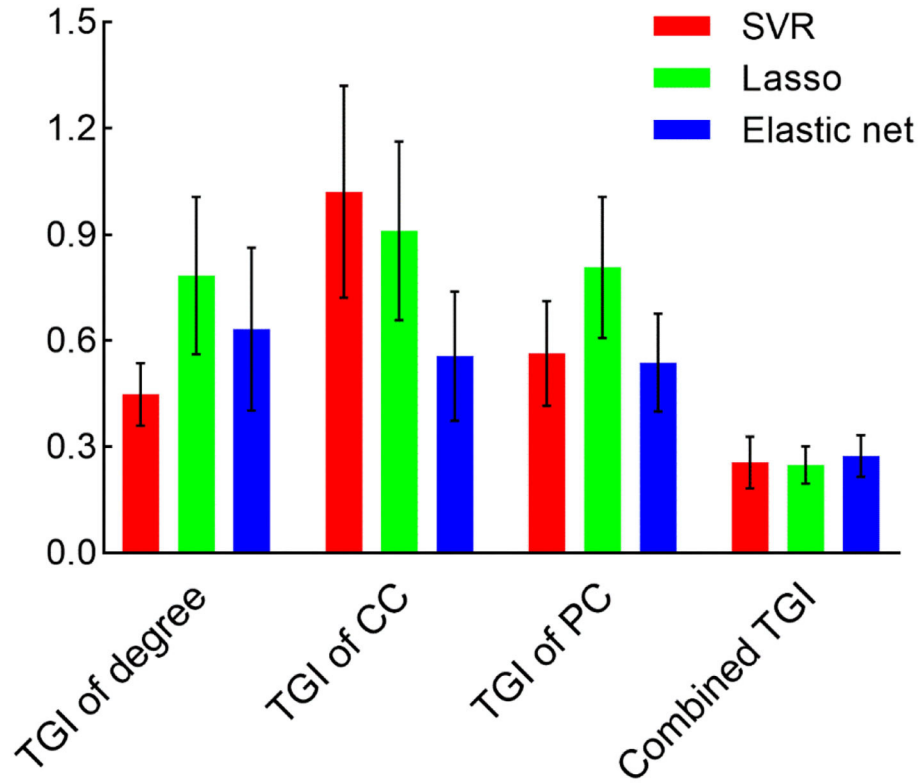

FIGURE 4 | The MSE is derived from different models and features. Bars represent the mean and SD of the MSE during the cross-validation process. CC, clustering coefficient; PC, participation coefficient.

For the TGI of degree, brian regions contributing to prediction were mainly placed in the temporal lobe, subcortical nuclei, and insular cortex, including superior temporal gyrus (STG), insular gyrus (INS), and basal ganglia (BG). For the TGI of CC, the high informative brain regions were located in the frontal and temporal lobes, including the superior frontal gyrus (SFG), superior temporal gyrus (STG), and inferior temporal gyrus (ITG). For the TGI of PC, high-weight brain regions were located across frontal, temporal, and parietal cortices, including the middle frontal gyrus (MFG), posterior superior temporal sulcus (pSTS), inferior frontal gyrus (IFG), superior temporal gyrus (STG) and superior parietal lobule (SPL). Furthermore, the cerebellum, caudoposterior superior temporal sulcus (cpSTS), and rostral somatosensory association cortex [rostral Brodmann area 7 (A7r)] highly contributed to regression tasks using each type of TGI. We also compared the fluctuations of degree, CC, and PC of five brain regions, including ventral caudate (vCa), opercular Broca's area [opercular Brodmann area 44 (A44op)], cerebellum lobule V (V), rostroventral inferior temporal gyrus [rostroventral Brodmann area 20 (A20rv)], dorsal agranular insula (dIa), cerebellum lobule VIIIa (VIIIa), dorsal dysgranular insula (dId), medial superior occipital gyrus (msOccG), caudoposterior superior temporal sulcus (cpSTS), inferior frontal junction (IFJ), rostral temporal thalamus (rTtha), cerebellum lobule Crus I (CrusI) and cerebellum lobule IX (IX), with the highest weights in pain prediction between the two groups (**Figure 5B**). Compared to the HC cohort, the CC showed higher values over time in patients with CBP in all the five brain regions, whereas, the PC in these regions showed the opposite alteration trend in the CBP cohort. In addition, the fluctuations of the nodal degree of CBP patients showed a relatively larger overlap with the HC when compared to the other two network properties.

DISCUSSION

The present study aimed to (1) investigate whether CBP is associated with altered dynamics of topological organization of functional brain networks, and (2) develop a novel kind of feature (TGI) that could better characterize pain sensation from dynamic functional networks. We found CBP significantly altered the dynamics of functional network properties, and the gradient of these dynamics of CBP patients relative to the HCs accurately predicted pain intensity. These results suggested that CBP is accompanied by abnormal alterations of functional topology at the temporal scale, which may serve as an effective biomarker for estimating pain perception in the brain.

Studies have shown that the degree gradient of patients with CBP relative to the HCs can characterize a unique neurological state of chronic pain (46, 69), such as a global randomization state of functional connectivity (46). Regarding the dynamic nature of the functional brain connectome, we speculated that the TGI extracted from the dFC networks might better depict the variations in neurological states of CBP over time than using

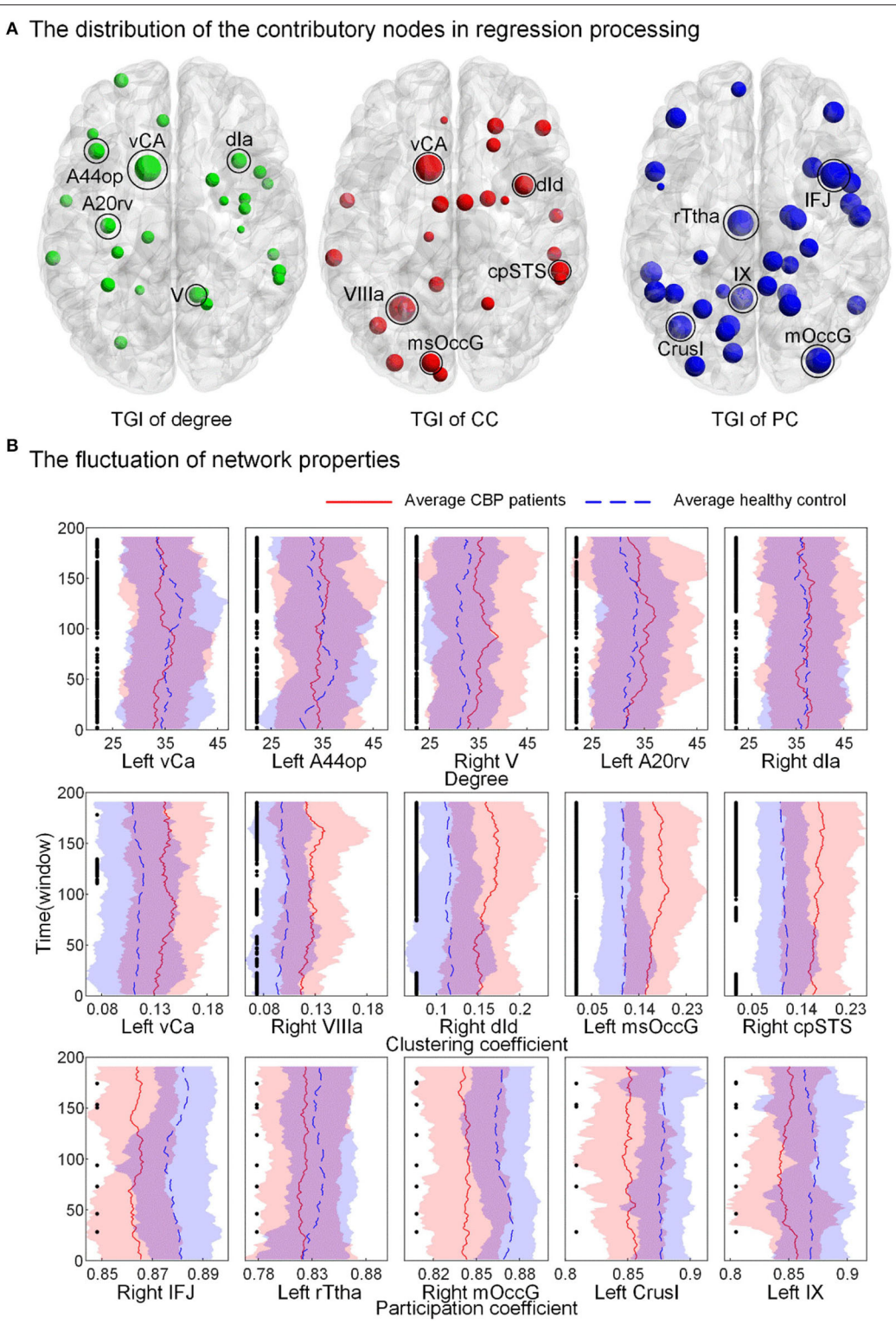

FIGURE 5 | Brain regions have high prediction power and the fluctuation of their nodal topology over time. **(A)** The weight of nodes contributed to the prediction process. Larger nodal size indicates a higher weight. **(B)** The fluctuation of network properties [nodal degree, clustering coefficient (CC), and participation coefficient (PC), not TGI] of the five nodes with the highest weights. The black point indicates a significant between-group difference ($p < 0.05$, FDR corrected). vCa, ventral caudate; A44op, opercular Broca's area (opercular Brodmann area 44); V, cerebellum lobule V; A20rv, rostroventral inferior temporal gyrus (rostroventral Brodmann area 20); dIa, dorsal agranular insula; VIIIa, cerebellum lobule VIIIa; dId, dorsal dysgranular insula; msOccG, medial superior occipital gyrus; cpSTS, caudoposterior superior temporal sulcus; IFJ, inferior frontal junction; rTtha, rostral temporal thalamus; CrusI, cerebellum lobule Crus I; IX, cerebellum lobule IX.

static functional networks. The high prediction performance of pain intensity suggested the effectiveness of the TGI feature, and no significant difference between TGI and BDI scores suggested the stabilization of the TGI feature that TGI would not be influenced by abnormal emotion (i.e., depression). Furthermore, the combination of three types of TGI significantly improved the prediction performance, suggesting the complex neural mechanism of CBP requires information from diversified domains to assess pain sensation. Nodal degree, CC and PC were indicated to represent network hubness, segregation, and integration of the brain network, respectively (59, 70, 71). Studies have reported the differences in nodal degree and PC of functional brain networks between patients with CBP and the HCs (72, 73). The CC of the insular cortex was found to be correlated with individual pain thresholds (74). Therefore, the combination of the TGI of these three network properties can comprehensively depict the alternation of brain networks of patients with CBP, which undoubtedly performed better than the TGI of a single network property in predicting the pain intensity.

Interestingly, we also found that the dynamics of CC and PC of brain regions that had TGI with high prediction power (i.e., STG, ITG, pSTS, SPL, IFG, INS, and parts of the cerebellum) showed distinct fluctuation patterns between patients with CBP and the HCs. Although previous studies have shown altered CC and PC of the static functional network in the CBP cohort (70, 75), our study moved a further step to show abnormalities in the temporal fluctuation of these two properties in patients with CBP. Since CC and PC represented the segregation and integration of the network, respectively. The altered fluctuation of them may indicate the topological reorganization of functional brain networks in patients with CBP that the network tended to be more locally connected with disruptions in inter-modular connectivity. This is in line with previous studies indicating lower efficiency of information transfer in the brain networks of patients with CBP than the HCs (42, 76). The brain regions with abnormal fluctuation of CC and PC were indicated to be extensively involved in pain processing (77–80). For example, IFG and ITG are involved in pain-related memories (81, 82), and INS plays a critical role in pain modulation (83). Furthermore, the cpSTS and the A7r of SPL showed a high contribution to pain prediction in all regression tasks using the TGI derived from different network properties (i.e., degree, CC and PC), suggesting the abnormal changes in these two brain regions were not only in local connectivity with other regions but also in the flow of information throughout the brain. These findings were supported by the previous studies indicating increased vigilance of the pain within these two brain regions (84–86). All these results supported our argument that TGI of network properties might better characterize the neurological condition of the individual with CBP in a dynamic manner.

There were several limitations in the present study. First, the sample size was limited in this study. Here, we performed a 5-fold cross-validation strategy and employed three commonly used regression models (i.e., SVR, Lasso and elastic net) that showed high generalizability across studies (87–89) to reduce the risk of overfitting, and achieved robust performance. Replications on a larger and independent dataset are still necessary to further verify the effectiveness of TGI of network topology in assessing pain intensity. Second, the dynamics of functional networks largely rely on the chosen parameters of the sliding window approach that determine the scale of the time sequence (90). In the present study, we chose the parameters according to the previous literature (55–57). Nevertheless, whether the parameters could influence the prediction power of TGI on the pain intensity need to be further explored.

CONCLUSION

We proposed a novel feature called TGI that was derived from the dFC network to represent the temporal deviation of network topology in patients with CBP relative to HCs. The TGI of network properties achieved outstanding performance in predicting the pain intensity of patients with CBP in three commonly used regression models, with a minimum MSE of 0.25 ± 0.05. Our findings suggested that the TGI can serve as a valuable biomarker for pain intensity evaluation and has potential application in CBP management/therapy.

DATA AVAILABILITY STATEMENT

The datasets presented in this study can be found in online repositories. The names of the repository/repositories and accession number(s) can be found at: https://www.openpain.org/.

ETHICS STATEMENT

The studies involving human participants were reviewed and approved by Northwestern University's Institutional Review Board Committee. The patients/participants provided their written informed consent to participate in this study. Written informed consent was obtained from the individual(s) for the publication of any potentially identifiable images or data included in this article.

AUTHOR CONTRIBUTIONS

ZL drafted the manuscript. LZ conducted data analysis. ZZ polished the manuscript. All authors provided feedback and revised the manuscript.

FUNDING

This work is supported by the Science and Technology Innovation 2030-Major Project of China (2021ZD0202002) and the China Postdoctoral Science Foundation (2020M671726).

SUPPLEMENTARY MATERIAL

The Supplementary Material for this article can be found online at: https://www.frontiersin.org/articles/10.3389/fneur.2022.899254/full#supplementary-material

REFERENCES

1. Vos T, Abajobir AA, Abate KH, Abbafati C, Abbas KM, Abd-Allah F, et al. Global, regional, and national incidence, prevalence, and years lived with disability for 328 diseases and injuries for 195 countries, 1990–2016: a systematic analysis for the global burden of disease study 2016. *Lancet.* (2017) 390:1211–59. doi: 10.1016/S0140-6736(17)32154-2
2. Steel N, Ford JA, Newton JN, Davis ACJ, Vos T, Naghavi M, et al. Changes in health in the countries of the UK and 150 english local authority areas 1990–2016: a systematic analysis for the global burden of disease study 2016. *Lancet.* (2018) 392:1647–61. doi: 10.1016/S0140-6736(18)32207-4
3. Murray CJL, Lopez AD. Measuring the global burden of disease. *N Engl J Med.* (2013) 369:448–57. doi: 10.1056/NEJMra1201534
4. Hartvigsen J, Hancock MJ, Kongsted A, Louw Q, Ferreira ML, Genevay S, et al. What low back pain is and why we need to pay attention. *Lancet.* (2018) 391:2356–67. doi: 10.1016/S0140-6736(18)30480-X
5. Latremoliere A, Woolf CJ. Central sensitization: a generator of pain hypersensitivity by central neural plasticity. *J Pain.* (2009) 10:895–926. doi: 10.1016/j.jpain.2009.06.012
6. Woolf CJ. Pain amplification—a perspective on the how, why, when, and where of central sensitization. *J Appl Biobehav Res.* (2018) 23:e12124. doi: 10.1111/jabr.12124
7. Baliki MN, Geha PY, Apkarian AV, Chialvo DR. Beyond feeling: chronic pain hurts the brain, disrupting the default-mode network dynamics. *J Neurosci Res.* (2008) 28:1398–403. doi: 10.1523/JNEUROSCI.4123-07.2008
8. Baliki MN, Baria AT, Apkarian AV. The cortical rhythms of chronic back pain. *J Neurosci.* (2011) 31:13981. doi: 10.1523/JNEUROSCI.1984-11.2011
9. Kregel J, Meeus M, Malfliet A, Dolphens M, Danneels L, Nijs J, et al., editors. Structural and functional brain abnormalities in chronic low back pain: a systematic review. *Semin Arthritis Rheum.* (2015) 42:229–37. doi: 10.1016/j.semarthrit.2015.05.002
10. Wager TD, Atlas LY, Lindquist MA, Roy M, Woo C-W, Kross E. An fmri-based neurologic signature of physical pain. *New England Journal of Medicine.* (2013) 368:1388–97. doi: 10.1056/NEJMoa1204471
11. Mayr A, Jahn P, Stankewitz A, Deak B, Winkler A, Witkovsky V, et al. Patients with chronic pain exhibit individually unique cortical signatures of pain encoding. *Hum Brain Mapp.* (2021). doi: 10.1101/2020.09.05.284117
12. Lindquist MA, Krishnan A, López-Solà M, Jepma M, Woo C-W, Koban L, et al. Group-regularized individual prediction: theory and application to pain. *Neuroimage.* (2017) 145:274–87. doi: 10.1016/j.neuroimage.2015.10.074
13. Goldstein P, Weissman-Fogel I, Shamay-Tsoory SG. The role of touch in regulating inter-partner physiological coupling during empathy for pain. *Sci Rep.* (2017) 7:1–12. doi: 10.1038/s41598-017-03627-7
14. Tagliazucchi E, Balenzuela P, Fraiman D, Chialvo DR. Brain resting state is disrupted in chronic back pain patients. *Neurosci Lett.* (2010) 485:26–31. doi: 10.1016/j.neulet.2010.08.053
15. Thorp SL, Suchy T, Vadivelu N, Helander EM, Urman RD, Kaye AD. Functional connectivity alterations: novel therapy and future implications in chronic pain management. *Pain Physician.* (2018) 21:E207–14. doi: 10.36076/ppj.2018.3.E207
16. Mao CP, Wilson G, Cao J, Meshberg N, Huang Y, Kong J. Abnormal anatomical and functional connectivity of the thalamo-sensorimotor circuit in chronic low back pain: resting-state fmri and diffusion tensor imaging study. *Neuroscience.* (2022) 487:143–54. doi: 10.1016/j.neuroscience.2022.02.001
17. Bressler SL, Menon V. Large-scale brain networks in cognition: emerging methods and principles. *Trends Cogn Sci.* (2010) 14:277–90. doi: 10.1016/j.tics.2010.04.004
18. Hutchison RM, Womelsdorf T, Allen EA, Bandettini PA, Calhoun VD, Corbetta M, et al. Dynamic functional connectivity: promise, issues, and interpretations. *Neuroimage.* (2013) 80:360–78. doi: 10.1016/j.neuroimage.2013.05.079
19. Sporns O. Structure and function of complex brain networks. *Dialogues Clin Neurosci.* (2013) 15:247–62. doi: 10.31887/DCNS.2013.15.3/osporns
20. Sporns O. Contributions and challenges for network models in cognitive neuroscience. *Nat Neurosci.* (2014) 17:652–60. doi: 10.1038/nn.3690
21. Borsook D, Edwards R, Elman I, Becerra L, Levine J. Pain and analgesia: the value of salience circuits. *Prog Neurobiol.* (2013) 104:93–105.
22. Napadow V, LaCount L, Park K, As-Sanie S, Clauw DJ, Harris RE. Intrinsic brain connectivity in fibromyalgia is associated with chronic pain intensity. *Arthritis Rheum.* (2010) 62:2545–55. doi: 10.1002/art.27497
23. Kaplan CM, Schrepf A, Vatansever D, Larkin TE, Mawla I, Ichesco E, et al. Functional and neurochemical disruptions of brain hub topology in chronic pain. *Pain.* (2019) 160:973–83. doi: 10.1097/j.pain.0000000000001480
24. Zheng W, Woo C-W, Yao Z, Goldstein P, Atlas LY, Roy M, et al. Pain-evoked reorganization in functional brain networks. *Cerebral Cortex.* (2020) 30:2804–22. doi: 10.1093/cercor/bhz276
25. Zhang Y, Liu J, Li L, Du M, Fang W, Wang D, et al. A study on small-world brain functional networks altered by postherpetic neuralgia. *Magn Reson Imaging.* (2014) 32:359–65. doi: 10.1016/j.mri.2013.12.016
26. Qi R, Ke J, Schoepf UJ, Varga-Szemes A, Milliken CM, Liu C, et al. Topological reorganization of the default mode network in irritable bowel syndrome. *Mol Neurobiol.* (2016) 53:6585–93. doi: 10.1007/s12035-015-9558-7
27. Baliki MN, Chialvo DR, Geha PY, Levy RM, Harden RN, Parrish TB, et al. Chronic pain and the emotional brain: specific brain activity associated with spontaneous fluctuations of intensity of chronic back pain. *J Neurosci.* (2006) 26:12165–73. doi: 10.1523/JNEUROSCI.3576-06.2006
28. Hashmi J, Baliki M, Huang L, Baria A, Torbey S, Hermann K, et al. Shape shifting pain: chronification of back pain shifts brain representation from nociceptive to emotional circuits. *Brain.* (2013) 136:2751–68. doi: 10.1093/brain/awt211
29. Wand BM, Parkitny L, O'Connell NE, Luomajoki H, McAuley JH, Thacker M, et al. Cortical changes in chronic low back pain: current state of the art and implications for clinical practice. *Man Ther.* (2011) 16:15–20. doi: 10.1016/j.math.2010.06.008
30. Lotze M, Moseley GL. Role of distorted body image in pain. *Curr Rheumatol Rep.* (2007) 9:488–96. doi: 10.1007/s11926-007-0079-x
31. Kucyi A, Davis KD. The dynamic pain connectome. *Trends Neurosci.* (2015) 38:86–95. doi: 10.1016/j.tins.2014.11.006
32. Du Y, Pearlson GD Yu Q, He H, Lin D, Sui J, et al. Interaction among Subsystems within default mode network diminished in schizophrenia patients: a dynamic connectivity approach. *Schizophr Res.* (2016) 170:55–65. doi: 10.1016/j.schres.2015.11.021
33. Rashid B, Damaraju E, Pearlson GD, Calhoun VD. Dynamic connectivity states estimated from resting fmri identify differences among schizophrenia, bipolar disorder, and healthy control subjects. *Front Hum Neurosci.* (2014) 8:897. doi: 10.3389/fnhum.2014.00897
34. Price T, Wee C-Y, Gao W, Shen D, editors. Multiple-network classification of childhood autism using functional connectivity dynamics. *International Conference on Medical Image Computing and Computer-Assisted Intervention.* Cham: Springer (2014).
35. Wee C-Y, Yang S, Yap P-T, Shen D. Sparse temporally dynamic resting-state functional connectivity networks for early mci identification. *Brain Imaging Behav.* (2016) 10:342–56. doi: 10.1007/s11682-015-9408-2
36. Chen X, Zhang H, Gao Y, Wee CY Li G, Shen D, et al. High-order resting-state functional connectivity network for mci classification. *Hum Brain Mapp.* (2016) 37:3282–96. doi: 10.1002/hbm.23240
37. Braun U, Schäfer A, Walter H, Erk S, Romanczuk-Seiferth N, Haddad L, et al. Dynamic reconfiguration of frontal brain networks during executive cognition in humans. *Proc Nat Acad Sci.* (2015) 112:11678–83. doi: 10.1073/pnas.1422487112
38. Jalilianhasanpour R, Ryan D, Agarwal S, Beheshtian E, Gujar SK, Pillai JJ, et al. Dynamic brain connectivity in resting state functional MR imaging. *Neuroimaging Clin.* (2021) 31:81–92. doi: 10.1016/j.nic.2020.09.004
39. Allen EA, Damaraju E, Plis SM, Erhardt EB, Eichele T, Calhoun VD. Tracking whole-brain connectivity dynamics in the resting state. *Cereb Cortex.* (2014) 24:663–76. doi: 10.1093/cercor/bhs352
40. Cheng JC, Rogachov A, Hemington KS, Kucyi A, Bosma RL, Lindquist MA, et al. Multivariate machine learning distinguishes cross-network dynamic functional connectivity patterns in state and trait neuropathic pain. *Pain.* (2018) 159:1764–76. doi: 10.1097/j.pain.0000000000001264
41. Ceko M, Shir Y, Ouellet JA, Ware MA, Stone LS, Seminowicz DA. Partial recovery of abnormal insula and dorsolateral prefrontal connectivity to cognitive networks in chronic low back pain after treatment. *Hum Brain Mapp.* (2015) 36:2075–92. doi: 10.1002/hbm.22757

42. Tu Y, Fu Z, Mao C, Falahpour M, Gollub RL, Park J, et al. Distinct Thalamocortical network dynamics are associated with the pathophysiology of chronic low back pain. *Nat Commun.* (2020) 11:3948. doi: 10.1038/s41467-020-18191-4
43. Kilpatrick LA, Kutch JJ, Tillisch K, Naliboff BD, Labus JS, Jiang Z, et al. Alterations in resting state oscillations and connectivity in sensory and motor networks in women with interstitial cystitis/painful bladder syndrome. *J Urol.* (2014) 192:947–55.
44. Fu CHY, Vythelingum GN, Brammer MJ, Williams SCR, Amaro E Jr, Andrew CM, et al. An fMRI study of verbal self-monitoring: neural correlates of auditory verbal feedback. *Cerebral Cortex.* (2006) 16:969–77. doi: 10.1093/cercor/bhj039
45. Long X-Y, Zuo X-N, Kiviniemi V, Yang Y, Zou Q-H, Zhu C-Z, et al. Default mode network as revealed with multiple methods for resting-state functional mri analysis. *J Neurosci Methods.* (2008) 171:349–55. doi: 10.1016/j.jneumeth.2008.03.021
46. Mansour A, Baria AT, Tetreault P, Vachon-Presseau E, Chang P-C, Huang L, et al. Global disruption of degree rank order: a hallmark of chronic pain. *Sci Rep.* (2016) 6:34853. doi: 10.1038/srep34853
47. Mash LE, Keehn B, Linke AC, Liu TT, Helm JL, Haist F, et al. Atypical relationships between spontaneous eeg and fMRI activity in autism. *Brain Connect.* (2020) 10:18–28. doi: 10.1089/brain.2019.0693
48. Murphy K, Birn RM, Handwerker DA, Jones TB, Bandettini PA. The impact of global signal regression on resting state correlations: are anti-correlated networks introduced? *Neuroimage.* (2009) 44:893–905. doi: 10.1016/j.neuroimage.2008.09.036
49. Jenkinson M, Bannister P, Brady M, Smith S. Improved optimization for the robust and accurate linear registration and motion correction of brain images. *Neuroimage.* (2002) 17:825–41. doi: 10.1006/nimg.2002.1132
50. Yan C-G, Cheung B, Kelly C, Colcombe S, Craddock RC, Di Martino A, et al. A comprehensive assessment of regional variation in the impact of head micromovements on functional connectomics. *Neuroimage.* (2013) 76:183–201. doi: 10.1016/j.neuroimage.2013.03.004
51. Zhao Z, Zhang Y, Chen N, Li Y, Guo H, Guo M, et al. Altered temporal reachability highlights the role of sensory perception systems in major depressive disorder. *Prog Neuropsychopharmacol Biol Psychiatry.* (2022) 112:110426. doi: 10.1016/j.pnpbp.2021.110426
52. Fan L, Li H, Zhuo J, Zhang Y, Wang J, Chen L, et al. The human brainnetome atlas: a new brain atlas based on connectional architecture. *Cerebral Cortex.* (2016) 26:3508–26. doi: 10.1093/cercor/bhw157
53. Diedrichsen J, Balsters JH, Flavell J, Cussans E, Ramnani N. A probabilistic MR atlas of the human cerebellum. *Neuroimage.* (2009) 46:39–46. doi: 10.1016/j.neuroimage.2009.01.045
54. Liao W, Wu G-R, Xu Q, Ji G-J, Zhang Z, Zang Y-F, et al. Dynamicbc: a matlab toolbox for dynamic brain connectome analysis. *Brain Connect.* (2014) 4:780–90. doi: 10.1089/brain.2014.0253
55. Leonardi N, Van De Ville D. On spurious and real fluctuations of dynamic functional connectivity during rest. *Neuroimage.* (2015) 104:430–6. doi: 10.1016/j.neuroimage.2014.09.007
56. Pedersen M, Omidvarnia A, Zalesky A, Jackson GD. On the Relationship between instantaneous phase synchrony and correlation-based sliding windows for time-resolved fmri connectivity analysis. *Neuroimage.* (2018) 181:85–94. doi: 10.1016/j.neuroimage.2018.06.020
57. Zalesky A, Breakspear M. Towards a statistical test for functional connectivity dynamics. *Neuroimage.* (2015) 114:466–70. doi: 10.1016/j.neuroimage.2015.03.047
58. Chen G, Chen P, Gong J, Jia Y, Zhong S, Chen F, et al. Shared and specific patterns of dynamic functional connectivity variability of striato-cortical circuitry in unmedicated bipolar and major depressive disorders. *Psychol Med.* (2020) 52:747–56. doi: 10.1017/S0033291720002378
59. Rubinov M, Sporns O. Complex network measures of brain connectivity: uses and interpretations. *Neuroimage.* (2010) 52:1059–69. doi: 10.1016/j.neuroimage.2009.10.003
60. Yeo BT, Krienen FM, Sepulcre J, Sabuncu MR, Lashkari D, Hollinshead M, et al. The organization of the human cerebral cortex estimated by intrinsic functional connectivity. *J Neurophysiol.* (2011) 106:1125–65. doi: 10.1152/jn.00338.2011
61. Drucker H, Burges CJ, Kaufman L, Smola A, Vapnik V. Support Vector Regression Machines. *Adv Neural Inf Process Syst*. (1996) 9:155–61.
62. Tibshirani R. Regression shrinkage and selection *via* the lasso. *J R Stat Soc.* (1996) 58:267–88. doi: 10.1111/j.2517-6161.1996.tb02080.x
63. Zou H, Hastie T. Regularization and variable selection via the elastic net. *J R Stat Soc.* (2005) 67:301–20. doi: 10.1111/j.1467-9868.2005.00503.x
64. Tang N, Mao S, Wang Y, Nelms RM. Solar power generation forecasting with a lasso-based approach. *IEEE Internet of Things Journal.* (2018) 5:1090–9. doi: 10.1109/JIOT.2018.2812155
65. Yu P-S, Chen S-T, Chang IF. Support vector regression for real-time flood stage forecasting. *J Hydrol.* (2006) 328:704–16. doi: 10.1016/j.jhydrol.2006.01.021
66. Slawski M. The structured elastic net for quantile regression and support vector classification. *Stat Comput.* (2012) 22:153–68. doi: 10.1007/s11222-010-9214-z
67. Beheshti I, Nugent S, Potvin O, Duchesne S. Bias-adjustment in neuroimaging-based brain age frameworks: a robust scheme. *NeuroImage.* (2019) 24:102063. doi: 10.1016/j.nicl.2019.102063
68. Yao Z, Fu Y, Wu J, Zhang W, Yu Y, Zhang Z, et al. Morphological changes in subregions of hippocampus and amygdala in major depressive disorder patients. *Brain Imaging Behav.* (2020) 14:653–67. doi: 10.1007/s11682-018-0003-1
69. Achard S, Delon-Martin C, Vertes PE, Renard F, Schenck M, Schneider F, et al. Hubs of brain functional networks are radically reorganized in comatose patients. *Proc Nat Acad Sci.* (2012) 109:20608–13. doi: 10.1073/pnas.1208933109
70. Huang S, Wakaizumi K, Wu B, Shen B, Wu B, Fan L, et al. Whole-brain functional network disruption in chronic pain with disk herniation. *Pain.* (2019) 160:2829–40. doi: 10.1097/j.pain.0000000000001674
71. Lenoir D, Cagnie B, Verhelst H, De Pauw R. Graph measure based connectivity in chronic pain patients: a systematic review. *Pain Physician.* (2021) 24:E1037–E58.
72. Mano H, Kotecha G, Leibnitz K, Matsubara T, Sprenger C, Nakae A, et al. Classification and characterisation of brain network changes in chronic back pain: a multicenter study. *Wellcome Open Res.* (2018) 3:19. doi: 10.12688/wellcomeopenres.14069.2
73. Balenzuela P, Chernomoretz A, Fraiman D, Cifre I, Sitges C, Montoya P, et al. Modular organization of brain resting state networks in chronic back pain patients. *Front Neuroinform*. (2010) 4:116. doi: 10.3389/fninf.2010.00116
74. Neumann L, Wulms N, Witte V, Spisak T, Zunhammer M, Bingel U, et al. Network properties and regional brain morphology of the insular cortex correlate with individual pain thresholds. *Hum Brain Mapp.* (2021) 42:4896–908. doi: 10.1002/hbm.25588
75. Liu J, Zhang F, Liu X, Zhuo Z, Wei J, Du M, et al. Altered small-world, functional brain networks in patients with lower back pain. *Science China Life Sciences*. (2018) 61:1420–4. doi: 10.1007/s11427-017-9108-6
76. Letzen JE, Boissoneault J, Sevel LS, Robinson ME. Altered mesocorticolimbic functional connectivity in chronic low back pain patients at rest and following sad mood induction. *Brain Imaging Behav.* (2020) 14:1118–29. doi: 10.1007/s11682-019-00076-w
77. Lamichhane B, Jayasekera D, Jakes R, Glasser MF, Zhang J, Yang C, et al. Multi-modal biomarkers of low back pain: a machine learning approach. *Neuroimage Clin*. (2021) 29:102530-. Epub 2020/12/08. doi: 10.1016/j.nicl.2020.102530
78. Fritz H-C, McAuley JH, Wittfeld K, Hegenscheid K, Schmidt CO, Langner S, et al. Chronic back pain is associated with decreased prefrontal and anterior insular gray matter: results from a population-based cohort study. *J Pain.* (2016) 17:111–8. doi: 10.1016/j.jpain.2015.10.003
79. Shen W, Tu Y, Gollub RL, Ortiz A, Napadow V, Yu S, et al. Visual network alterations in brain functional connectivity in chronic low back pain: a resting state functional connectivity and machine learning study. *Neuroimage Clin.* (2019) 22:101775. doi: 10.1016/j.nicl.2019.101775
80. Jensen KB, Regenbogen C, Ohse MC, Frasnelli J, Freiherr J, Lundström JN. Brain activations during pain: a neuroimaging meta-analysis of patients with pain and healthy controls. *Pain.* (2016) 157:1279–86. doi: 10.1097/j.pain.0000000000000517

81. Kelly S, Lloyd D, Nurmikko T, Roberts N. Retrieving autobiographical memories of painful events activates the anterior cingulate cortex and inferior frontal gyrus. *J Pain.* (2007) 8:307–14. doi: 10.1016/j.jpain.2006.08.010
82. Wang Y, Cao D-y, Remeniuk B, Krimmel S, Seminowicz DA, Zhang M. Altered brain structure and function associated with sensory and affective components of classic trigeminal neuralgia. *Pain.* (2017) 158:1561–70. doi: 10.1097/j.pain.0000000000000951
83. Starr CJ, Sawaki L, Wittenberg GF, Burdette JH, Oshiro Y, Quevedo AS, et al. Roles of the insular cortex in the modulation of pain: insights from brain lesions. *J Neurosci.* (2009) 29:2684–94. doi: 10.1523/JNEUROSCI.5173-08.2009
84. Vrana A, Hotz-Boendermaker S, Stämpfli P, Hänggi J, Seifritz E, Humphreys BK, et al. Differential neural processing during motor imagery of daily activities in chronic low back pain patients. *PLoS ONE.* (2015) 10:e0142391. doi: 10.1371/journal.pone.0142391
85. Ellingsen D-M, Napadow V, Protsenko E, Mawla I, Kowalski MH, Swensen D, et al. Brain mechanisms of anticipated painful movements and their modulation by manual therapy in chronic low back pain. *J Pain.* (2018) 19:1352–65. doi: 10.1016/j.jpain.2018.05.012
86. Wasan AD, Loggia ML, Chen LQ, Napadow V, Kong J, Gollub RL. Neural correlates of chronic low back pain measured by arterial spin labeling. *Anesthesiology.* (2011) 115:364–74. doi: 10.1097/ALN.0b013e318220e880
87. Bergeron C, Cheriet F, Ronsky J, Zernicke R, Labelle H. Prediction of anterior scoliotic spinal curve from trunk surface using support vector regression. *Eng Appl Artif Intell.* (2005) 18:973–83. doi: 10.1016/j.engappai.2005.03.006
88. McNeish DM. Using lasso for predictor selection and to assuage overfitting: a method long overlooked in behavioral sciences. *Multivariate Behav Res.* (2015) 50:471–84. doi: 10.1080/00273171.2015.1036965
89. VanHouten JP, Starmer JM, Lorenzi NM, Maron DJ, Lasko TA. Machine learning for risk prediction of acute coronary syndrome. *AMIA Annu Symp Proc.* (2014) 2014: 1940–9.
90. Shakil S, Lee C-H, Keilholz SD. Evaluation of sliding window correlation performance for characterizing dynamic functional connectivity and brain states. *Neuroimage.* (2016) 133:111–28. doi: 10.1016/j.neuroimage.2016.02.074

Conflict of Interest: The authors declare that the research was conducted in the absence of any commercial or financial relationships that could be construed as a potential conflict of interest.

Publisher's Note: All claims expressed in this article are solely those of the authors and do not necessarily represent those of their affiliated organizations, or those of the publisher, the editors and the reviewers. Any product that may be evaluated in this article, or claim that may be made by its manufacturer, is not guaranteed or endorsed by the publisher.

frontiers | Frontiers in Neurology

ORIGINAL RESEARCH
published: 21 June 2022
doi: 10.3389/fneur.2022.915346

fMRI Findings in Cortical Brain Networks Interactions in Migraine Following Repetitive Transcranial Magnetic Stimulation

Kirill Markin[1], Artem Trufanov[2,3], Daria Frunza[2], Igor Litvinenko[2], Dmitriy Tarumov[1], Alexander Krasichkov[4], Victoria Polyakova[5], Alexander Efimtsev[3,6] and Dmitriy Medvedev[7,8]*

[1] Psychiatry Department, Kirov Military Medical Academy, Saint Petersburg, Russia, [2] Neurology Department, Kirov Military Medical Academy, Saint Petersburg, Russia, [3] Department of Software Engineering and Computer Applications, Saint Petersburg Electrotechnical University "LETI", Saint Petersburg, Russia, [4] Radio Engineering Systems Department, Saint Petersburg Electrotechnical University "LETI", Saint Petersburg, Russia, [5] Department of Pathology, Saint-Petersburg State Pediatric Medical University, Saint Petersburg, Russia, [6] Department of Radiology, Almazov National Medical Research Centre, Saint Petersburg, Russia, [7] Federal State Unitary Enterprise, Federal Medical Biological Agency, Saint Petersburg, Russia, [8] Department of Physical Therapy and Sports Medicine, North-Western State Medical University Named After I.I. Mechnikov, Saint Petersburg, Russia

OPEN ACCESS

Edited by:
Lingmin Jin,
Guizhou University of Traditional Chinese Medicine, China

Reviewed by:
Mansoureh Togha,
Tehran University of Medical Sciences, Iran
Elcio J. Piovesan,
Federal University of Paraná, Brazil

***Correspondence:**
Kirill Markin
vmeda.work@ya.ru
orcid.org/0000-0002-6242-1279

Specialty section:
This article was submitted to Headache and Neurogenic Pain, a section of the journal Frontiers in Neurology

Received: *07 April 2022*
Accepted: *12 May 2022*
Published: *21 June 2022*

Citation:
Markin K, Trufanov A, Frunza D, Litvinenko I, Tarumov D, Krasichkov A, Polyakova V, Efimtsev A and Medvedev D (2022) fMRI Findings in Cortical Brain Networks Interactions in Migraine Following Repetitive Transcranial Magnetic Stimulation. Front. Neurol. 13:915346. doi: 10.3389/fneur.2022.915346

Background: Repetitive transcranial magnetic stimulation (rTMS) is one of the high-potential non-pharmacological methods for migraine treatment. The purpose of this study is to define the neuroimaging markers associated with rTMS therapy in patients with migraine based on data from functional MRI (fMRI).

Materials and Methods: A total of 19 patients with episodic migraine without aura underwent a 5-day course of rTMS of the fronto-temporo-parietal junction bilaterally, at 10 Hz frequency and 60% of motor threshold response of 900 pulses. Resting-state functional MRI (1.5 T) and a battery of tests were carried out for each patient to clarify their diagnosis, qualitative and quantitative characteristics of pain, and associated affective symptoms. Changes in functional connectivity (FC) in the brain's neural networks before and after the treatment were identified through independent components analysis.

Results: Over the course of therapy, we observed an increase in FC of the default mode network within it, with pain system components and with structures of the visual network. We also noted a decrease in FC of the salience network with sensorimotor and visual networks, as well as an increase in FC of the visual network. Besides, we identified 5 patients who did not have a positive response to one rTMS course after the first week of treatment according to the clinical scales results, presumably because of an increasing trend of depressive symptoms and neuroimaging criteria for depressive disorder.

Conclusions: Our results show that a 5-day course of rTMS significantly alters the connectivity of brain networks associated with pain and antinociceptive brain systems in about 70% of cases, which may shed light on the neural mechanisms underlying migraine treatment with rTMS.

Keywords: headache, neurostimulation, neuroimaging, functional connectivity, migraine

INTRODUCTION

The fact that every seventh human in the world suffers from migraine, which remains second among the causes of disability in young people, determines the importance of the subject under study (1, 2). The low efficacy of existing symptomatic therapies and high costs in view of unknown consequences after the cessation of targeted medications force us to look for new methods for treating this disease (3).

One of the high-potential alternative approach to the treatment of migraine is neurostimulation (4) and particularly repetitive transcranial magnetic stimulation (rTMS) (5). The efficacy of this method has been confirmed for acute and preventive migraine treatment (6, 7). Another significant advantage of TMS is the absence of side effects (8). The most frequently used regions for TMS are the prefrontal dorsolateral cortex and primary motor cortex, the stimulation of which resulted in a lower number of migraine attacks and increased quality of life among patients (9, 10). Yet, there still are no objective criteria for treatment efficacy, nor have its pathophysiological mechanisms been thoroughly studied. Therefore, despite showing the efficacy of rTMS in some studies, only single-pulse TMS is approved for migraine prevention.

Existing TMS techniques for treating depression (7) and secondary headaches (11) have been associated with some neuroimaging markers, particularly using functional MRI (fMRI) which is a promising tool for assessing interactions of the brain's neural networks in migraine patients (12–14). As we know, migraine is characterized by various changes in FC in the brain's neural networks, which mostly result in pain perception disorder and an inadequate response to pain (15). Therefore, combined rTMS/fMRI studies can help us better understand the mechanisms underlying this method of migraine treatment and set up objective criteria to assess the efficacy of therapy (16). To assess changes in FC during TMS treatment, we have applied independent component analysis (ICA) which is based on the registration of spontaneous low-frequency oscillations that occur in spatially separated, functionally connected, continuously communicating anatomical regions representing neural networks of the brain.

To select regions for TMS, we relied on the mechanisms underlying migraine and the effects of TMS application as reflected in fMRI studies (17). A headache in migraine, which arises through sensibilization of neurons in the trigeminal thalamocortical pathway, is characterized by an imbalance between attention to external and internal stimuli in favor of the latter (12). The network that is largely involved in these processes is the salience network, which is responsible for perceiving, processing, and switching attention between stimuli (18, 19). Its primary structure is the insular cortex lays is a portion of the cerebral cortex folded deep within the lateral sulcus. At the same time, the activity of the inferior frontal gyrus, which is a part of the frontal-temporal neural network, is closely associated with cognitive and emotional components of pain (20), and stimulating of this region by TMS can cause changes in FC of other neural networks as well (21, 22), including the default mode network, for which FC changes in migraine were described earlier (23). In view of this, for stimulation, we selected the region of the fronto-temporo-parietal junction to ensure the maximum coverage of described structures.

Aim: We presume that fMRI and subsequent analysis of changes in FC will allow assessing the brain changes associated with rTMS therapy in patients with migraine. To achieve this goal, we compared FC data before and after a 5-day course of rTMS by using independent component analysis for the brain's core neural networks.

MATERIALS AND METHODS

Sample

During one-year screening at the clinic of the Neurology Department, we selected 56 patients with newly diagnosed episodic migraine without aura according to the criteria of the International Classification of Headache Disorders, 3rd edition (24). All the patients received only acute treatment of migraine (with the exception of 2 patients who received beta-blockers at intermediate therapeutic doses due to a concomitant illness). The following criteria were applied for the inclusion in the study group: voluntary informed consent for research participation, diagnosed migraine without aura, aged 18–65, and absence of headache at the moment of screening. The criteria for exclusion: contraindications to MRI (metallic implants, claustrophobia, pacemakers, etc.) and/or TMS, major psychiatric or neurological disorders, pregnancy, antidepressant medication treatment, interruption of the 5-day TMS therapy course, invalid/unreadable MRI scans, refusal to continue participating in the study. There were 27 patients included in the study, but 8 patients were excluded in the course of research (3 patients had more than 30 invalid MRI scans after the preprocessing, 2 patients have high-movement coefficient during the scanning after the preprocessing, 2 patients refused to continue participation in the study due to the pandemic restrictions, and 1 patient refused to continue participation in the study due to unknown reasons).

Thus, this study is based on the results obtained from 19 patients (16 women, average age 39.8 $\pm$ 11.1 years) who underwent a complete TMS course and fMRI scanning before and after the course. The number of respondents was chosen to take into account the established scientific practice in this direction of research (11, 16, 25).

The illustration of the study design can be found in **Supplementary Material 1**.

All the participants received a complete description of the research and gave their informed consent in writing. The protocol was approved by the IRB/IEC, and conformed to ethical standards and principles described in the Helsinki Declaration.

Test Battery

A test battery was filled out by the patients three times–immediately prior to conducting fMRI before and after the TMS course, and after 1 month of TMS therapy. The numerical rating scale (NRS) for pain allowed to evaluate the pain intensity during the last attack before scanning, where "0"

TABLE 1 | Demographical and clinical data of patients before and after a 5-day course of rTMS and 1 month after the treatment (5 of 19 patients undergo more than one TMS therapy course).

	Before TMS ($n = 19$) (M ± S.D.)	After TMS ($n = 19$) (M ± S.D.) student's t-test; p-value (before/after)	A month after TMS ($n = 19$) (M ± S.D.) student's t-test; p-value (before/after 1 month)
Gender (male/female)		3/16	
Age		39.84 ± 7.09	
Illness duration		15.71 ± 5.24	
The numerical rating scale for pain (last episode)	7.74 ± 1.45	2.42 ± 1.57 $t = 12.68$; $p < 0.01$	1.75 ± 1.71 $t = 14.18$; $p < 0.01$
The frequency of migraine (days in month)	9.37 ± 2.91	5.95 ± 3.73 $t = 7.32$; $p < 0.01$	5.66 ± 2.42 $t = 11.83$; $p < 0.01$
the Migraine Disability Assessment Questionnaire	18.30 ± 2.52	–	8.79 ± 1.88 $t = 9.81$; $p < 0.01$
The Leeds dependency questionnaire	13.31 ± 5.08	7.05 ± 4.50 $t = 6.98$; $p < 0.01$	7.50 ± 3.52 $t = 6.43$; $p < 0.01$
Hospital anxiety scale	7.21 ± 2.84	5.58 ± 2.87 $t = 2.70$; $p = 0.015$	5.31 ± 2.49 $t = 3.06$; $p < 0.01$
Hospital depression scale	4.89 ± 2.40	4.11 ± 2.34 $t = 1.82$; $p = 0.065$	3.74 ± 2.18 $t = 3.41$; $p = 0.012$

TMS, Transcranial Magnetic Stimulation (5-day course).

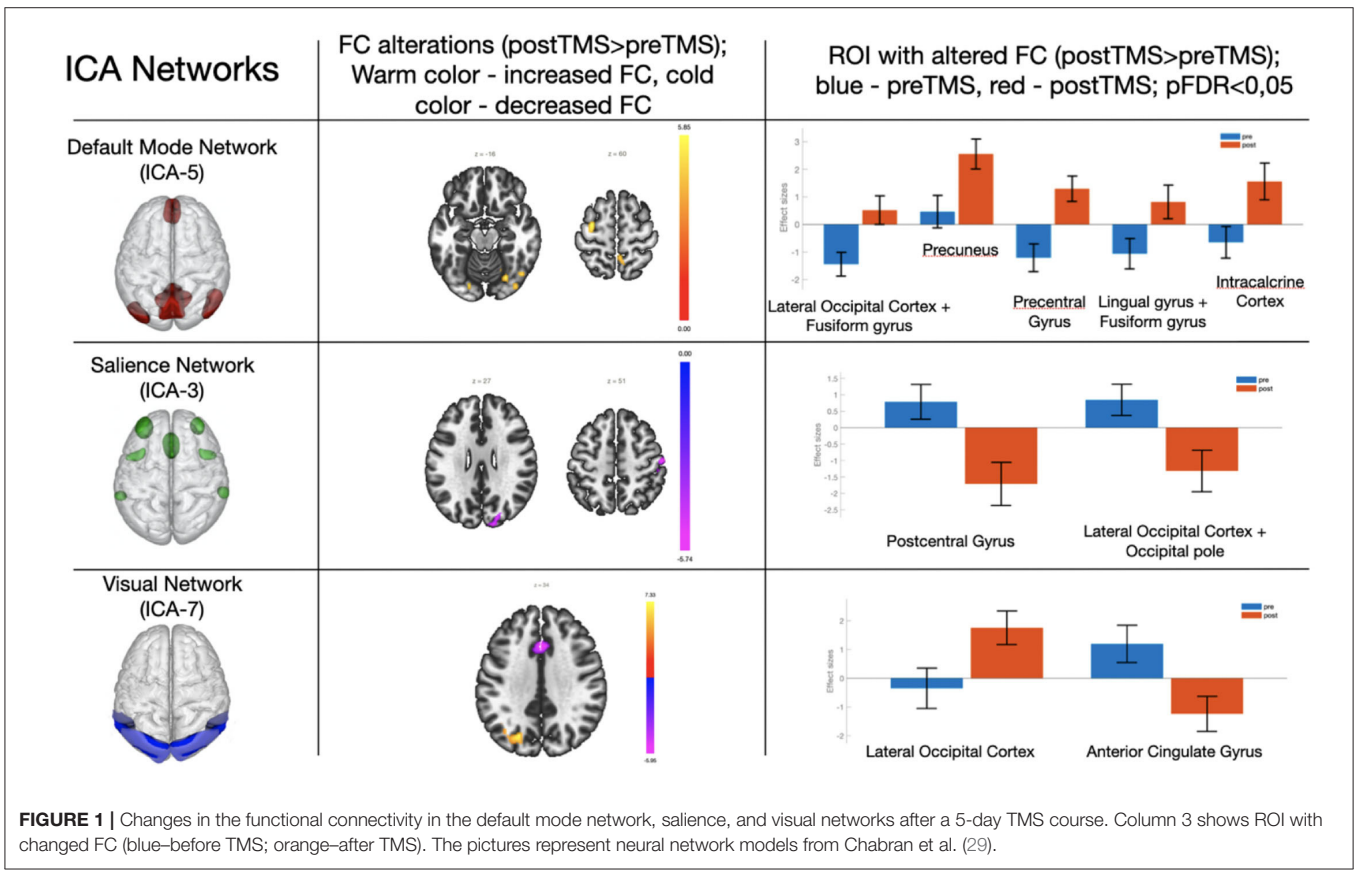

FIGURE 1 | Changes in the functional connectivity in the default mode network, salience, and visual networks after a 5-day TMS course. Column 3 shows ROI with changed FC (blue–before TMS; orange–after TMS). The pictures represent neural network models from Chabran et al. (29).

meant the absence of pain, and "10" referred to the most acute pain. The respondents filled out a standardized questionnaire in which they assessed the duration of migraine, migraine family history, number of days with headache per month; the Migraine Disability Assessment Questionnaire (MIDAS); the acute migraine preventing drugs overuse anamnesis was assessed by the Leeds Dependence Questionnaire (LDQ). In addition, the patients filled out the hospital anxiety and depression scale (HADS) for screening of associated symptoms of affective disorders.

TABLE 2 | Changes in functional connectivity in three networks with cluster names, sizes, locations according to Montreal Neurological Institute (MNI) coordinates, and validity of resulting changes with the Benjamini–Hochberg correction.

Network	MNI-space			Structure name	Cluster size (voxels)	P-FDR
	x	y	z			
Default mode network (ICA_05)	−26	−70	−18	Lateral Occipital Cortex + Fusiform gyros	125	0.000036
	+10	−54	+66	Precuneus	84	0.026138
	−30	−06	+60	Precentral gyrus	71	0.026138
	−14	−74	−02	Lingual gyrus + Fusiform gyros	70	0.033545
	+04	−74	+00	Intracalcarine Cortex	55	0.033545
Salience network (ICA_03)	+56	−14	+50	Postcentral gyrus	138	0.007110
	+18	−84	+28	Lateral Occipital Cortex + Occipital pole	81	0.022571
Visual network (ICA_07)	−22	−70	+34	Lateral Occipital Cortex	223	0.000116
	+00	+20	+34	Anterior Cingulate gyrus	124	0.003183

ICA, Independent Components Analysis.

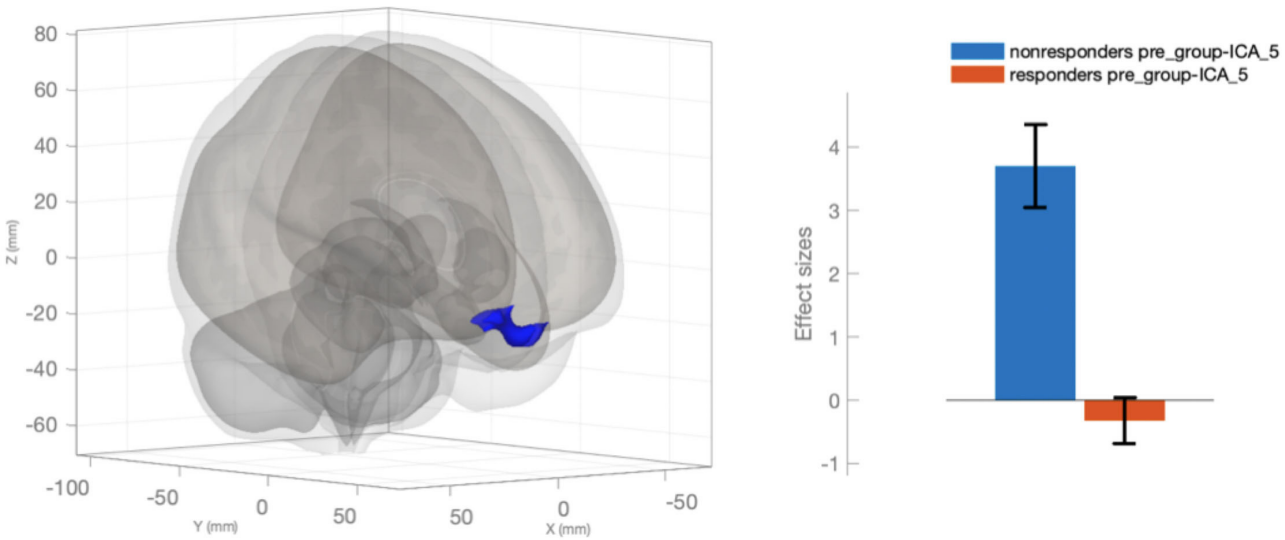

FIGURE 2 | Changed functional connectivity of the medial prefrontal cortex in the default mode network (ICA_5) in the responders in comparison with the non-responders.

Statistical Analysis of Demographic Data and Headache Characteristics

Data statistical processing was performed with the software suite SPSS 25 (SPSS Inc., USA). Data distribution normality was validated by using the Kolmogorov–Smirnov and Shapiro-Wilk tests. Ordinal scale data were analyzed by using the Mann–Whitney *U*-test, matched samples with normal distribution–by using Student's *t*-test, and non-parametric matched samples–by using the Wilcoxon signed-ranks test, differences between which had the significance levels. The results were represented with (mean ± SD) and also the median and the interquartile range for ordinal scales. Pearson and Spearman's analyses were used to assess correlations to test battery data.

According to the subjective feelings of continuing headache, NRS for actual pain (cut-off: 5-point and more of the last headache episode reduction after the first week of treatment), frequency of headaches (days in a month) (cut-off: 4-days and more reduction after the first week of treatment), and HADS-depression tests significantly different results we defined responders and non-responders.

TMS Procedures

The procedures were carried out at the TMS laboratory of the clinic of the Neurology Department. The patients did not receive antianginal therapy during the procedures. Each patient received five rTMS sessions in 5 days during the headache-free period (at least 2 h after the last attack) in the first half of the day (from 9 a.m. to 13 a.m.). Stimulations were performed with a circular coil. The stimulation field covered the lower frontal region at the temporal lobe junctions and the projection region of trigeminal nerve sensory branches. TMS was performed using a neuro-MS/D transcranial magnetic stimulator (Neurosoft, Ivanovo,

TABLE 3 | Test battery data of the responders and the non-responders to one course of TMS therapy.

	Responders ($n = 14$) (M ± S.D.)	Non-responders ($n = 5$) (M ± S.D.)
The numerical rating scale for pain (last episode)		
Before	8.14 ± 1.41	6.60 ± 0.89
After	2.36 ± 1.44	4.25 ± 0.96
Student's *t*-test; *p*-value	$t = 13.32$; $p = 0.00$	$t = 4.$; $p = 0.009$
The frequency of migraine (days in month)		
Before	8.78 ± 3.02	11.00 ±2.00
After	4.36 ± 2.65	10.40±2.51
Student's *t*-test; *p*-value	$t = 17.67$; $p = 0.00$	$t = 0.88$; $p = 0.426$
The Leeds dependency questionnaire		
Before	13.21 ± 5.67	13.60 ± 3.36
After	6.78 ± 5.03	9.80 ± 2.77
Student's *t*-test; *p*-value	$t = 5.47$; $p = 0.00$	$t = 2.49$; $p = 0.062$
Hospital anxiety scale		
Before	6.36 ± 2.38	9.60 ± 2.88
After	4.79 ± 2.61	5.20 ± 1.92
Student's *t*-test; *p*-value	$t = 1.76$; $p = 0.102$	$t = 2.24$; $p = 0.089$
Hospital depression scale		
Before	5.07 ± 2.64	7.00 ± 3.32
After	3.64 ± 1.91	5.40 ± 3.29
Student's *t*-test; *p*-value	$t = 2.46$; $p = 0.029$	$t = 0.76$; $p = 0.491$

Russia). Motor thresholds were determined by independent measurements on the primary motor cortex on both sides before the first treatment session. The motor response threshold was determined by the percentage intensity of a stimulus that generated 50 μV in the contralateral muscle abducting the thumb in 5 of 10 trials. A TMS session consisted of bilateral stimulation at 10 Hz and 60% of the motor threshold response of 900 pulses. The 10 Hz protocol was introduced as a series of 60 pulses during 6 s, followed by 20 s rest (15 trains 6.5 min for one side). The second course of TMS with the same characteristics for non-responders was conducted the next week after filling the test battery (one week after the first course).

All the patients did not receive any prophylactic therapy during the one-month follow-up to better assess the effectiveness of rTMS.

fMRI Scanning

The patients underwent fMRI scanning not earlier than a week before and not later than a week after the 5-day TMS course on a Philips Ingenia 1.5T magnetic resonance imaging scanner in the interictal period (at least 24 h after the last attack). The scanning was performed in the evening (from 5 p.m. to 8 p.m.). Patients did not eat or drink coffee at least 3 h before the scan. The protocols–T1-weighted (301 axial sections, planar resolution of 1 × 1 mm; repetition time/echo time 8.0/3.7ms; flip angle = 8) and EPI (echo-planar imaging scan) (35 axial sections; planar resolution of 3.03 × 3.03 mm; section depth of 4.0 mm; repetition time/echo time 3,000/50 ms; flip angle = 90)–were obtained for each patient with preceding instructions: "Remain lying and relaxed, with closed eyes, but do not sleep."

MRI Data Processing

Data were preprocessed using MATLAB R2019b software (MathWorks, Natick, MA) and the CONN 19c toolbox for functional connectivity analysis (26). The data processing included functional realignment and unwarp, slice-timing correction, outlier identification, direct segmentation, and normalization into standard MNI space. Functional smoothing was performed using spatial convolution with a Gaussian kernel of 8 mm full width half maximum. The default denoising pipeline combines two general steps: linear regression of potential confounding effects in the blood-oxygen-level-dependent imaging signal (BOLD) based on an anatomical component-based noise correction procedure–"aCompCor" and temporal band-pass filtering. Temporal frequencies below 0.008 Hz or above 0.09 Hz are removed from the BOLD signal to focus on low-frequency fluctuations while minimizing the influence of physiological, head-motion, and other noise sources. All the data were processed on a single MacBook (OS Catalina 10.15.5 software).

Statistical Analysis of MRI Data

Group dimensional independent component analysis was performed using the methodology of group analysis according to Calhoun (27). All the obtained data regarding functional connectivity before and after treatment were distributed into 10 components. After the spatial correlation analysis, the following components corresponding to the primary neural networks were selected: ICA_3–salience neural network, ICA_5–default mode network, ICA_7–visual neural network, and ICA_10–sensory motor network.

The subsequent comparison of FC of these networks was carried out on the basis of parametric statistics using the random field theory (28) with the clusterization threshold: $p < 0.05$, the cluster size with the Benjamini–Hochberg correction (p-FDR-corrected), and the voxel threshold: $p < 0.001$ *p*-uncorrected. We compared (1) FC of four obtained neural networks in all the patients before and after the therapy; (2) FC of obtained neural networks in responders to the therapy and FC in non-responders to the therapy; and (3) possible dependence of test results and FC changes.

RESULTS

Demography and Clinical Data

All the demographical and clinical data are presented in **Table 1**. Statistically, valid differences were observed between the results of the numerical rating scale for pain (the last episode), frequency of headaches (days in a month), and hospital anxiety scale before and after the course of treatment, and between the results of the numerical rating scale for pain (the last episode), frequency of headaches (days in a month), and hospital anxiety scale before and after the course of treatment, the Leeds dependence questionnaire, the Migraine Disability Assessment Questionnaire before the course and after 1 month of rTMS therapy.

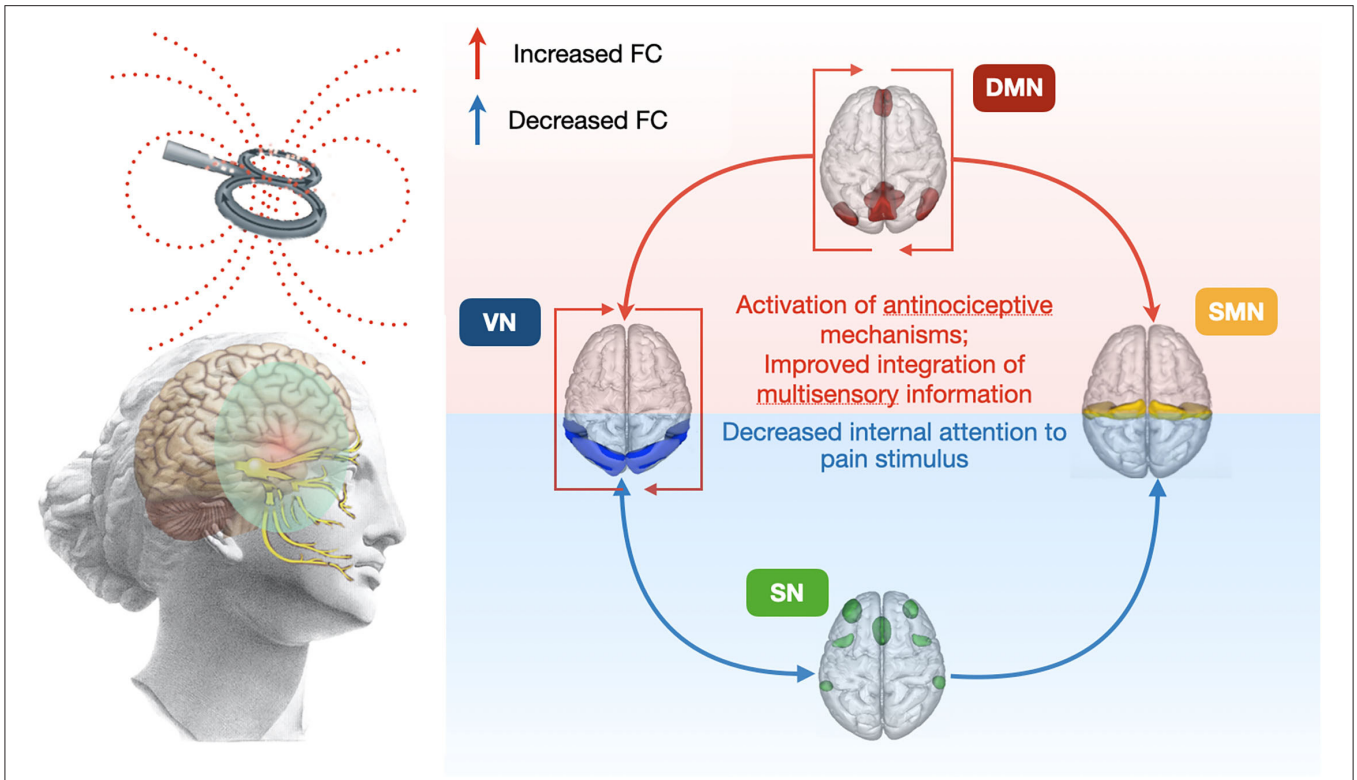

FIGURE 3 | The overall scheme of 5-day rTMS course affects changes in FC between main resting-state neural networks. FC, functional connectivity; VN, visual network; DMN, default mode network; SN, salience network; SMN, sensorimotor network.

Results of fMRI–Independent Component Analysis

According to ICA, the TMS course was followed by increased FC in the default mode network, decreased FC in the salience network, and both increase and decrease in FC in the visual network (**Figure 1** and **Table 2**).

Increased FC was observed in the region between the default mode network and lateral occipital cortex + fusiform gyros/precuneus/precentral gyrus/lingual gyrus/intracalcarine cortex. On the other hand, decreased FC was observed in the regions between the salience network and postcentral gyrus/lateral occipital cortex. FC between elements of the visual network and lateral occipital cortex was increased, while in the anterior cingulate cortex the visual network FC decreased after the TMS therapy.

Results of fMRI–Response to Therapy

We identified 14 respondents and 5 non-respondents according to the described criteria for response to therapy. We compared the selected groups to find out a reason for failure in the first week of stimulation. As a result, we revealed a significant difference in FC in the default mode network (ICA_5). In non-responders to one course of therapy, much higher dissociation of FC was observed between the medial prefrontal cortex and other regions of the default mode network, that were associated with effective alterations (**Figure 2**). It should be noted that there was a statistically valid difference in the dynamics of decreasing scores of the frequency of headaches (days in a month), The Leeds dependency questionnaire, and the hospital depression scale for responders but not for non-responders (**Table 3**).

DISCUSSION

The presented pilot study of the efficacy of stimulating the ventrolateral prefrontal cortex by repetitive TMS in patients with migraine has demonstrated certain evidence of the therapy's success based on correlations of clinical and neuroimaging data. The statistically significant differences based on the results of testing the patients before and after the applied therapy point to positive effects of TMS on patients' quality of life and amount of medication treatment. Furthermore, it should be noted that the effect of the applied TMS therapy remained evident for a month. We obtained the results of the independent component analysis which revealed FC changes in three primary neural networks of the brain.

Default Mode Network

Default Mode network is a neural network in which activity is registered (as evident from its name) in a relaxed state of rest and which is extremely important for self-referential cognitive processes, interception, and self-control (23, 30). Most authors have reported a decrease in FC both inside the default mode

network and between it and other neural networks in patients with migraine, which could point to functional disorders in that network, yet there are data to the contrary as well (23).

In the structure of the default mode network, the connectivity of the posterior cingulate gyrus with the precuneus plays a key role in antinociceptive and multisensory integration, and a decrease in FC between these structures might be a reason for the described functional disorders (31). Such contradictory findings point to a slight increase in FC between the posterior cingulate gyrus and the precuneus in patients with migraine in comparison with healthy volunteers (32). Our study has shown an increase in FC between the default mode network structure and the precuneus, which could be explained by activation of the antinociceptive system of that network and normalization of the multisensory integration function, presumably as a result of the course of therapy (33).

Reduced FC between the default mode network and precentral gyrus could reflect difficulties of multisensory information integration (34). The restoration of these connections after a TMS therapy course also allows to presume an increase in antinociceptive activity of the so-called the brain's pain system and a decrease in pain rumination (35).

Finally, increased FC with the lateral occipital cortex, lingual gyrus, and fusiform gyros could be evidence of interaction between the default mode network and the visual network whose activity changes have been observed in patients with migraine (36). Reduced FC between these two networks was a characteristic feature that distinguished patients with migraine without aura from healthy volunteers (25). Our findings provide evidence of normalized connectivity between the default mode network and the visual network after a course of TMS therapy.

Visual Network

Visual network—FC changes in the visual network are the most indicative differences between patients with migraine from healthy volunteers, presumably due to hyperexcitability of the visual cortex in migraine patients both with and without aura (33). In addition to the increase in FC with the default mode network, there was observed a decrease in connectivity between both the visual (lateral occipital cortex) and salience (anterior cingulate gyrus) networks. This observation could explain a decrease in inner attention to external and internal stimuli, which, in turn, reduces headache severity (37). Often observed photophobia in patients could also be a reason for changed FC, and therefore, its absence would lead to normalization of neural network activity (36).

Salience Network

Salience network is a neural network that is presumably involved in pain stimulus integration and subsequent switching between resting-state and active networks in migraine (18, 19). Increased FC with the postcentral gyrus and the right insular cortex was observed in migraine patients in previous studies (38). The change of FC between those regions may play an important role not only in decreasing inner attention to pain impulses, including due to an actual decrease in the number of pain stimuli but also in decreased pain rumination (35). It might also be supposed that the TMS effect results in normalizing the mechanisms of multisensory processing which are damaged in patients with migraine (33).

Finally, we found possible predictors of positive response to TMS therapy according to the described protocol. We presume that the patients' predisposition to comorbid depressive symptoms, and also their identifiable neuroimaging criteria (**Figure 3** and **Table 3**), could be a reason for the negative response to therapy. In this case, attention should be paid to their early recognition and the use of the simulation protocol for the dorsolateral prefrontal cortex or other treatment options (39).

Our study has some substantial limitations, such as the absence of placebo control in the form of sham TMS, a relatively small sample of patients, no control over medication intake, and no analysis of FC changes in subcortical structures which could be associated with the pain system. Questions also arise regarding the absence of correlation between FC changes and the clinical data.

CONCLUSION

Our results show that a 5-day course of rTMS significantly alters the connectivity of brain networks associated with pain and antinociceptive brain systems in about 70% of cases, which may shed light on the neural mechanisms underlying migraine treatment with rTMS. However, further research is required, with an extended sample and placebo control, which we intend to conduct in near future.

DATA AVAILABILITY STATEMENT

The raw data supporting the conclusions of this article will be made available by the authors, without undue reservation.

ETHICS STATEMENT

The studies involving human participants were reviewed and approved by Kirov Military Medical Academy IRB/IEC. The patients/participants provided their written informed consent to participate in this study.

AUTHOR CONTRIBUTIONS

AT performed the neurological examination of patients, analyzed and interpreted the patient data, and was a contributor in writing the manuscript. KM analyzed and interpreted the patient data, performed the neuroimage data analysis, and was a major contributor to writing the manuscript. DF performed the TMS procedures. IL was a contributor to writing the manuscript. DT and AE performed the fMRI scanning procedures. AK performed the statistical analysis of patient data. VP performed

the neurological examination of patients. DM made the translation of the manuscript. All authors read and approved the final manuscript.

FUNDING

This research was funded by the Development Program of ETU LETI within the framework of the program of Strategic Academic Leadership Priority-2030 No 075-15-2021-1318 on September 29, 2021.

SUPPLEMENTARY MATERIAL

The Supplementary Material for this article can be found online at: https://www.frontiersin.org/articles/10.3389/fneur.2022.915346/full#supplementary-material

REFERENCES

1. Steiner TJ, Stovner LJ, Jensen R, Uluduz D, Katsarava Z. Migraine remains second among the world's causes of disability, and first among young women: findings from GBD2019. *J Headache Pain.* (2020) 21:137. doi: 10.1186/s10194-020-01208-0
2. GBD 2016 Headache Collaborators. Global, regional, and national burden of migraine and tension-type headache, 1990-2016: a systematic analysis for the global burden of disease study 2016. *Lancet Neurol.* (2018) 17:954–76. doi: 10.1016/S1474-4422(18)30322-3
3. Raffaelli B, Terhart M, Overeem LH, Mecklenburg J, Neeb L, Steinicke M, et al. Migraine evolution after the cessation of CGRP(-receptor) antibody prophylaxis: a prospective, longitudinal cohort study. *Cephalalgia.* (2021) 42:326–34. doi: 10.1177/03331024211046617
4. Schwedt TJ, Vargas B. Neurostimulation for treatment of migraine and cluster headache. *Pain Med.* (2015) 16:1827–34. doi: 10.1111/pme.12792
5. Barker AT, Shields K. Transcranial magnetic stimulation: basic principles and clinical applications in migraine. *Headache.* (2017) 57:517–24. doi: 10.1111/head.13002
6. Lan L, Zhang X, Li X, Rong X, Peng Y. The efficacy of transcranial magnetic stimulation on migraine: a meta-analysis of randomized controlled trails. *J Headache Pain.* (2017) 18:86. doi: 10.1186/s10194-017-0792-4
7. Evers S. Non-invasive neurostimulation methods for acute and preventive migraine treatment-a narrative review. *J Clin Med.* (2021) 10:3302. doi: 10.3390/jcm10153302
8. Dodick DW, Schembri CT, Helmuth M, Aurora SK. Transcranial magnetic stimulation for migraine: a safety review. *Headache.* (2010) 50:1153–63. doi: 10.1111/j.1526-4610.2010.01697.x
9. Zhang B, Liu J, Bao T, Wilson G, Park J, Zhao B, et al. Locations for noninvasive brain stimulation in treating depressive disorders: a combination of meta-analysis and resting-state functional connectivity analysis. *Aust N Z J Psychiatry.* (2020) 54:582–90. doi: 10.1177/0004867420920372
10. Leung A, Shirvalkar P, Chen R, Kuluva J, Vaninetti M, Bermudes R, et al. Transcranial magnetic stimulation for pain, headache, and comorbid depression: INS-NANS expert consensus panel review and recommendation. *Neuromodulation.* (2020) 23:267–90. doi: 10.1111/ner.13094
11. Vaninetti M, Lim M, Khalaf A, Metzger-Smith V, Flowers M, Kunnel A, et al. fMRI findings in MTBI patients with headaches following rTMS. *Sci Rep.* (2021)11:9573. doi: 10.1038/s41598-021-89118-2
12. Schwedt TJ, Chiang CC, Chong CD, Dodick DW. Functional MRI of migraine. *Lancet Neurol.* (2015) 14:81–91. doi: 10.1016/S1474-4422(14)70193-0
13. Russo A, Silvestro M, Tedeschi G, Tessitore A. Physiopathology of Migraine: What Have We Learned from Functional Imaging? *Curr Neurol Neurosci Rep.* (2017) 17:95. doi: 10.1007/s11910-017-0803-5
14. Skorobogatykh K, van Hoogstraten WS, Degan D, Prischepa A, Savitskaya A, Ileen BM, et al. European Headache Federation School of Advanced Studies (EHF-SAS). Functional connectivity studies in migraine: what have we learned? *J Headache Pain.* (2019) 20:108. doi: 10.1186/s10194-019-1047-3
15. Brennan KC, Pietrobon D. A systems neuroscience approach to migraine. *Neuron.* (2018) 97:1004–21. doi: 10.1016/j.neuron.2018.01.029
16. Kumar A, Mattoo B, Bhatia R, Kumaran S, Bhatia R. Neuronavigation based 10 sessions of repetitive transcranial magnetic stimulation therapy in chronic migraine: an exploratory study. *Neurol Sci.* (2021) 42:131-9. doi: 10.1007/s10072-020-04505-3
17. Andreou AP, Holland PR, Akerman S, Summ O, Fredrick J, Goadsby PJ. Transcranial magnetic stimulation and potential cortical and trigeminothalamic mechanisms in migraine. *Brain.* (2016) 139:2002–14. doi: 10.1093/brain/aww118
18. Androulakis XM, Rorden C, Peterlin BL, Krebs K. Modulation of salience network intranetwork resting state functional connectivity in women with chronic migraine. *Cephalalgia.* (2018) 38:1731–41. doi: 10.1177/0333102417748570
19. Veréb D, Szabó N, Tuka B, Tajti J, Király A, Faragó P, et al. Temporal instability of salience network activity in migraine with aura. *Pain.* (2020) 161:856–64. doi: 10.1097/j.pain.0000000000001770
20. He Z, Zhao J, Shen J, Muhlert N, Elliott R, Zhang D. The right VLPFC and downregulation of social pain: A TMS study. *Hum Brain Mapp.* (2020) 41:1362–71. doi: 10.1002/hbm.24881
21. Freedberg M, Reeves JA, Toader AC, Hermiller MS, Kim E, Haubenberger D, et al. Optimizing Hippocampal-Cortical Network Modulation via Repetitive Transcranial Magnetic Stimulation: A Dose-Finding Study Using the Continual Reassessment Method. *Neuromodulation.* (2020) 23:366–72. doi: 10.1111/ner.13052
22. Hartwigsen G, Volz LJ. Probing rapid network reorganization of motor and language functions via neuromodulation and neuroimaging. *Neuroimage.* (2021) 224:117449. doi: 10.1016/j.neuroimage.2020.117449
23. Chong CD, Schwedt TJ, Hougaard A. Brain functional connectivity in headache disorders: A narrative review of MRI investigations. *J Cereb Blood Flow Metab.* (2019) 39:650–69. doi: 10.1177/0271678X17740794
24. Headache Classification Committee of the International Headache Society (IHS). The International Classification of Headache Disorders, 3rd edition (beta version). *Cephalalgia.* (2013) 33:629–808. doi: 10.1177/0333102413485658
25. Coppola G, Di Renzo A, Tinelli E, Lepre C, Di Lorenzo C, Di Lorenzo G, et al. Thalamo-cortical network activity between migraine attacks: Insights from MRI-based microstructural and functional resting-state network correlation analysis. *J Headache Pain.* (2016) 17:100. doi: 10.1186/s10194-016-0693-y
26. Whitfield-Gabrieli S, Nieto-Castanon A. Conn: a functional connectivity toolbox for correlated and anticorrelated brain networks. *Brain connectivity.* (2012) 2:125–41. doi: 10.1089/brain.2012.0073
27. Calhoun VD, Adali T, Pearlson GD, Pekar JJ. A method for making group inferences from functional MRI data using independent component analysis. *Hum Brain Mapp.* (2001) 14:140–51. doi: 10.1002/hbm.1048
28. Worsley KJ, Marrett S, Neelin P, Vandal AC, Friston KJ, Evans AC. A unified statistical approach for determining significant signals in images of cerebral activation. *Hum Brain Mapp.* (1996)b4:58–73. doi: 10.1002/(SICI)1097-0193(1996)4:1<58::AID-HBM4>3.0.CO;2-O
29. Chabran E, Noblet V, Loureiro de Sousa P, Demuynck C, Philippi N, Mutter C, et al. Changes in gray matter volume and functional connectivity in dementia with Lewy bodies compared to Alzheimer's disease and normal aging: implications for fluctuations. *Alzheimers Res Ther.* (2020) 12:9. doi: 10.1186/s13195-019-0575-z
30. de Tommaso M, Vecchio E, Quitadamo SG, Coppola G, Di Renzo A, Parisi V, et al. Pain-related brain connectivity changes in migraine: a narrative review and proof of concept about possible novel treatments interference. *Brain Sci.* (2021) 11:234. doi: 10.3390/brainsci11020234

31. Russo A, Silvestro M, Trojsi F, Bisecco A, De Micco R, Caiazzo G, et al. Cognitive networks disarrangement in patients with migraine predicts cutaneous allodynia. *Headache.* (2020) 60:1228–43. doi: 10.1111/head.13860
32. Zhang J, Su J, Wang M, Zhao Y, Yao Q, Zhang Q, et al. Increased default mode network connectivity and increased regional homogeneity in migraineurs without aura. *J Headache Pain.* (2016) 17:98. doi: 10.1186/s10194-016-0692-z
33. Tu Y, Zeng F, Lan L, Li Z, Maleki N, Liu B, et al. An fMRI-based neural marker for migraine without aura. *Neurology.* (2020) 94:e741–51. doi: 10.1212/WNL.0000000000008962
34. Hodkinson DJ, Veggeberg R, Kucyi A, van Dijk KR, Wilcox SL, Scrivani SJ, et al. Cortico-Cortical Connections of Primary Sensory Areas and Associated Symptoms in Migraine. *eNeuro.* (2017) 3:ENEURO.0163-16.2016. doi: 10.1523/ENEURO.0163-16.2016
35. Galambos A, Szabó E, Nagy Z, Édes AE, Kocsel N, Juhász G, et al. A systematic review of structural and functional MRI studies on pain catastrophizing. *J Pain Res.* (2019) 12:1155–78. doi: 10.2147/JPR.S192246
36. Puledda F, Fytche D, O'Daly O, Goadsby PJ. Imaging the visual network in the migraine spectrum. *Front Neurol.* (2019) 10:1325. doi: 10.3389/fneur.2019.01325
37. Niddam DM, Lai KL, Fuh JL, Chuang CY, Chen WT, Wang SJ. Reduced functional connectivity between salience and visual networks in migraine with aura. *Cephalalgia.* (2016) 36:53–66. doi: 10.1177/0333102415583144
38. Ke J, Yu Y, Zhang X, Su Y, Wang X, Hu S, et al. Functional alterations in the posterior insula and cerebellum in migraine without aura: a resting-state MRI study. *Front Behav Neurosci.* (2020) 14:567588. doi: 10.3389/fnbeh.2020.567588
39. Kumar S, Singh S, Kumar N, Verma R. The effects of repetitive transcranial magnetic stimulation at dorsolateral prefrontal cortex in the treatment of migraine comorbid with depression: a retrospective open study. *Clin Psychopharmacol Neurosci.* (2018) 16:62–6. doi: 10.9758/cpn.2018.16.1.62

Conflict of Interest: The authors declare that the research was conducted in the absence of any commercial or financial relationships that could be construed as a potential conflict of interest.

frontiers | Frontiers in Neurology

TYPE Original Research
PUBLISHED 21 September 2022
DOI 10.3389/fneur.2022.936012

OPEN ACCESS

EDITED BY
Lingmin Jin,
Guizhou University of Traditional Chinese Medicine, China

REVIEWED BY
Nathan Churchill,
St. Michael's Hospital, Canada
Jiaofen Nan,
Zhengzhou University of Light Industry, China

*CORRESPONDENCE
Huiqing Yu
yhqdyx@cqu.edu.cn
Jiuquan Zhang
zhangjq_radiol@foxmail.com

SPECIALTY SECTION
This article was submitted to Headache and Neurogenic Pain, a section of the journal Frontiers in Neurology

RECEIVED 04 May 2022
ACCEPTED 12 August 2022
PUBLISHED 21 September 2022

CITATION
Liu D, Zhou X, Tan Y, Yu H, Cao Y, Tian L, Yang L, Wang S, Liu S, Chen J, Liu J, Wang C, Yu H and Zhang J (2022) Altered brain functional activity and connectivity in bone metastasis pain of lung cancer patients: A preliminary resting-state fMRI study. *Front. Neurol.* 13:936012. doi: 10.3389/fneur.2022.936012

Altered brain functional activity and connectivity in bone metastasis pain of lung cancer patients: A preliminary resting-state fMRI study

Daihong Liu[1], Xiaoyu Zhou[1], Yong Tan[1], Hong Yu[1], Ying Cao[1], Ling Tian[2], Liejun Yang[2], Sixiong Wang[2], Shihong Liu[2], Jiao Chen[1], Jiang Liu[1], Chengfang Wang[1], Huiqing Yu[2]* and Jiuquan Zhang[1]*

[1]Department of Radiology, Chongqing University Cancer Hospital, School of Medicine, Chongqing University, Chongqing, China, [2]Department of Palliative Care and Department of Geriatric Oncology, Chongqing University Cancer Hospital, School of Medicine, Chongqing University, Chongqing, China

Bone metastasis pain (BMP) is one of the most prevalent symptoms among cancer survivors. The present study aims to explore the brain functional activity and connectivity patterns in BMP of lung cancer patients preliminarily. Thirty BMP patients and 33 healthy controls (HCs) matched for age and sex were recruited from inpatients and communities, respectively. All participants underwent fMRI data acquisition and pain assessment. Low-frequency fluctuations (ALFF) and regional homogeneity (ReHo) were applied to evaluate brain functional activity. Then, functional connectivity (FC) was calculated for the ALFF- and ReHo-identified seed brain regions. A two-sample *t*-test or Manny–Whitney *U*-test was applied to compare demographic and neuropsychological data as well as the neuroimaging indices according to the data distribution. A correlation analysis was conducted to explore the potential relationships between neuroimaging indices and pain intensity. Receiver operating characteristic curve analysis was applied to assess the classification performance of neuroimaging indices in discriminating individual subjects between the BMP patients and HCs. No significant intergroup differences in demographic and neuropsychological data were noted. BMP patients showed reduced ALFF and ReHo largely in the prefrontal cortex and increased ReHo in the bilateral thalamus and left fusiform gyrus. The lower FC was found within the prefrontal cortex. No significant correlation between the neuroimaging indices and pain intensity was observed. The neuroimaging indices showed satisfactory classification performance between the BMP patients and HCs, and the combined ALFF and ReHo showed a better accuracy rate (93.7%)

than individual indices. In conclusion, altered brain functional activity and connectivity in the prefrontal cortex, fusiform gyrus, and thalamus may be associated with the neuropathology of BMP and may represent a potential biomarker for classifying BMP patients and healthy controls.

KEYWORDS

bone metastasis pain, resting-state fMRI, low-frequency fluctuations, regional homogeneity, functional connectivity

Introduction

Pain is the most frequent symptom of cancer survivors, and this symptom has increased in prevalence (1). A previous review revealed that 64% of cancer patients reported pain (2). Bone metastasis pain (BMP) is one of the most prevalent sources of pain since common cancers, including lung, breast, and prostate cancers, have a propensity to metastasize to multiple bones (3). Existing treatments for BMP may be ineffective and fraught with side effects. Therefore, understanding the pathophysiology of BMP may guide the search for novel intervention options.

The brain is necessary for the multidimensional pain experience, and activity in multiple brain regions has been found to be associated with noxious stimuli. Therefore, brain imaging, such as functional magnetic resonance imaging (fMRI), provides valuable information. Among the fMRI indices, the amplitude of low-frequency fluctuations (ALFF) is used to evaluate brain functional activity (4), and regional homogeneity (ReHo) is used to characterize the synchronization of fluctuations of a voxel with its neighboring voxels (5). For instance, ALFF was reported to be increased in the post- and precentral gyrus, paracentral lobule, supplementary motor area, and anterior cingulate cortex, and this feature may be associated with the neuropathology of chronic low back pain (6). ReHo was decreased in the thalamus in neuropathic pain (7), and ReHo values in abnormal brain regions were associated with pain intensity in postherpetic neuralgia patients (8). In addition, functional connectivity (FC), which is used to assess brain activity synchronization between any set of brain areas, was reported to be increased in the insular cortex in our previous study on trigeminal neuralgia (9). The combination of ALFF, ReHo, and FC was also used to explore the brain activity of migraine (10), visceral pain (11), and other types of pain. However, the signature of activation may vary with the different types of nociceptive stimulation (12). The brain functional abnormalities of BMP remain unclear.

The mechanisms of BMP have been investigated in previous studies. Regarding molecular mechanisms, BMP is associated with inflammatory mediators, a highly acidic environment, and cancer invasion of peripheral nerve endings (13). Then nociceptive signals are transmitted to the cerebral cortex and subcortical structures *via* the dorsal horn of the spinal cord. Thus, the sensory, cognitive, and affective aspects of pain experience will be processed within the brain. For instance, the primary somatosensory cortex and thalamus receive nociceptive input from the spinal cord and encode the intensity of pain. In addition, nociceptive signals are sent to the brainstem, midbrain, and medullary areas, where they might modulate the perception and sensation of a noxious stimulus (14, 15). In neuroimaging studies, the cingulate cortex, prefrontal cortex, and ventral striatum showed pain-specific FC changes in a mouse model of metastatic bone cancer (16). Furthermore, prospective administration of anti-nerve growth factor treatment can prevent pain-induced FC adaptations in ascending and descending pain pathways in the same mouse model (17). Animal models of BMP provide invaluable information for pain pathophysiology; however, brain functional activity and connectivity have not been reported in the human population.

Here, we aimed to preliminarily explore the brain functional activity and connectivity patterns in BMP. ALFF and ReHo were applied to evaluate brain functional activity. Then, the FC was calculated for the ALFF- and ReHo-identified seed brain regions. Finally, the discrimination performance of neuroimaging indices was assessed to investigate whether these changes are useful for classifying BMP. The findings may advance our understanding of the mechanism of BMP and potentially provide neuroimaging biomarkers.

Materials and methods

Subjects

From August 2020 to November 2021, thirty-six lung cancer patients with BMP were recruited from inpatients, and 36 healthy controls (HCs) matched for age and sex were recruited from communities. Inclusion criteria: (1) lung cancer patients suffering from bone metastasis pain, (2) the BMP patients can tolerate the MRI scan and (3) right-handed. BMP patients were diagnosed with lung cancer according to pathology and bone metastasis according to medical imaging and/or pathology. Subjects with brain structural abnormalities, neurological or psychiatric diseases, disability, left-handedness, and contraindications to MRI examination were excluded prior to enrollment. The experiment was approved by the Medical

Research Ethics Committee of Chongqing University Cancer Hospital (Chongqing, China). All participants provided written informed consent before the experiment. All procedures were performed in accordance with the approved study protocol.

According to the head motion profile derived from subsequent MRI data processing, six BMP and three HCs with head motion >2 mm in any direction or 2° at any angle were excluded. Therefore, 30 BMP patients and 33 HCs were involved in the study. Demographic information, including age and sex, was obtained across the two groups. The intensity of real-time pain was obtained according to patients' feelings on a visual analog scale (VAS). All subjects underwent evaluation of anxiety and depression using the Self-Rating Anxiety Scale (SAS) and Self-Rating Depression Scale (SDS). Details are shown in Table 1.

MRI scan protocol

Soon after the pain evaluation, structural and functional MRI scanning were performed with a 3.0 T scanner (Magnetom Prisma; Siemens Health Care, Erlangen, Germany) using a 64-channel head-neck coil. Earplugs were used to alleviate the influence of noise and cushions to restrict head motion. Subjects stayed awake with their eyes closed and were instructed to not think about any topics during the scanning.

Conventional T2-weighted images and fluid-attenuated inversion recovery (FLAIR) images were acquired for radiological evaluation of brain structural abnormalities. Then, sagittal T1-weighted structural images were acquired using volumetric 3D magnetization prepared by a rapid-acquisition gradient-echo (MP-RAGE) sequence: repetition time/echo time = 2,100 ms/2.26 ms, flip angle = 8°, field of view = 256 × 256 mm^2, slices = 192, thickness = 1 mm, matrix = 256 × 256 and voxel size = 1 × 1 × 1 mm^3, for a total of 4 min and 53 s. Resting-state functional images were acquired transversely using an echo planar imaging (EPI) sequence: repetition time/echo time = 2,000 ms/30 ms, flip angle = 70°, field of view = 240 × 240 mm^2, slices = 36, thickness = 3 mm, matrix = 80 × 80, voxel size = 3 × 3 × 3 mm^3, and 240 volumes with a total of 8 min and 8 s.

TABLE 1 Demographic and neuropsychological data comparisons.

	BMP patients	Healthy controls	*p*-Values
Age (years)	59.57 ± 9.66	59.55 ± 9.38	0.993
Sex (male/female)	21/9	22/11	0.777[a]
Disease duration (days)	240.00 (180, 330)	NA	NA
Pain score	2 (1, 3)	NA	NA
SAS	35.70 ± 9.48	33.97 ± 6.30	0.393[b]
SDS	32.00 (25.50, 39.00)	31.00 (25.50, 39.00)	0.809[c]

Data are presented as n for proportions, means ± SD for normally distributed continuous data, and median (QR) for nonnormally distributed data.
[a]The *p* value for sex was obtained using the χ^2 test.
[b]The *p* value was obtained using the two-sample *t*-test.
[c]The *p* value was obtained using the Mann–Whitney *U*-test.
BMP, bone metastasis pain; SAS, self-rating anxiety scale; SDS, self-rating depression scale; NA, not applicable.

MRI data processing

Conventional images obtained with anatomical scans were reviewed by two radiologists with at least 5 years of experience in neuroradiology, and no subjects were excluded for brain abnormalities. The MRI data were processed with a standard protocol in DPABI V6.0 (http://rfmri.org/) (18). (1) Data in DICOM format was converted to NIfTI format. (2) For magnetization equilibrium, the first 10 volumes of individual resting-state functional images were removed. (3) Slice timing was used to correct the remaining 230 volumes due to the temporal offset between slices. (4) Realignment was performed to correct for head motion so that the brain across images was in the same position. According to the realignment parameters, a report of head motion was

TABLE 2 Brain regions with aberrant ALFF, ReHo, and FC in BMP patients.

Measurements	Brain regions	Hemisphere	BA	Peak MNI coordinates			Voxels	*t*-Values
				x	*y*	*z*		
ALFF	ACC	Left	24/32	0	12	30	294	−5.4158
	IFGoperc	Right	44	48	12	27	50	−4.5053
	PFCventmed	Right	10	6	48	−3	91	−4.8296
ReHo	THA	Left/Right	NA	−12	−18	15	98	5.2606
	FFG	Left	20	−36	−27	−18	54	5.0836
	PFCventmed	Right	10	6	45	−6	77	−5.3365
FC	Right PFCventmed (ALFF)-Right ACC	NA	11	6	39	−3	246	−6.2276
	Right PFCventmed (ReHo)-Right PFCventmed	NA	11	3	42	−3	262	−6.5679

ALFF, amplitude of low-frequency fluctuation; ReHo, regional homogeneity; FC, functional connectivity; ACC, anterior cingulate cortex; IFGoperc, inferior frontal gyrus, opercular part; PFCventmed, superior frontal gyrus, medial orbital; THA, thalamus; FFG, fusiform gyrus; BA, Brodmann area; NA, not applicable.

automatically generated for subject exclusion with head motion of >2 mm in any direction or 2° at any angle. (5) In covariate regression, the Friston 24-parameter model was applied to regress out head motion effects. Other nuisance variables including white matter signal and cerebrospinal fluid signal were regressed out by using Statistical Parametric Mapping's a priori tissue probability maps (empirical thresholds: 90% for white matter mask and 70% for cerebrospinal fluid mask). Global brain signal regression was not performed because it can cause correlation coefficient redistribution and ambiguous interpretation of negative correlations of FC. (6) To make inter-subject comparisons feasible, individual functional images were warped to standard Montreal Neurological Institute (MNI) space through spatial normalization. (7) Detrending was applied to reduce the systematic signal drift with time using a linear model. (8) Finally, to reduce the effects of very-low-frequency and high-frequency physiological noise, the data were band-filtered (0.01–0.10 Hz).

Then, ALFF and ReHo were calculated and standardized with the mean division to reduce the impact of many sources of nuisance variation and increase the test–retest reliability (19). Specifically, ALFF is calculated as the sum of amplitudes

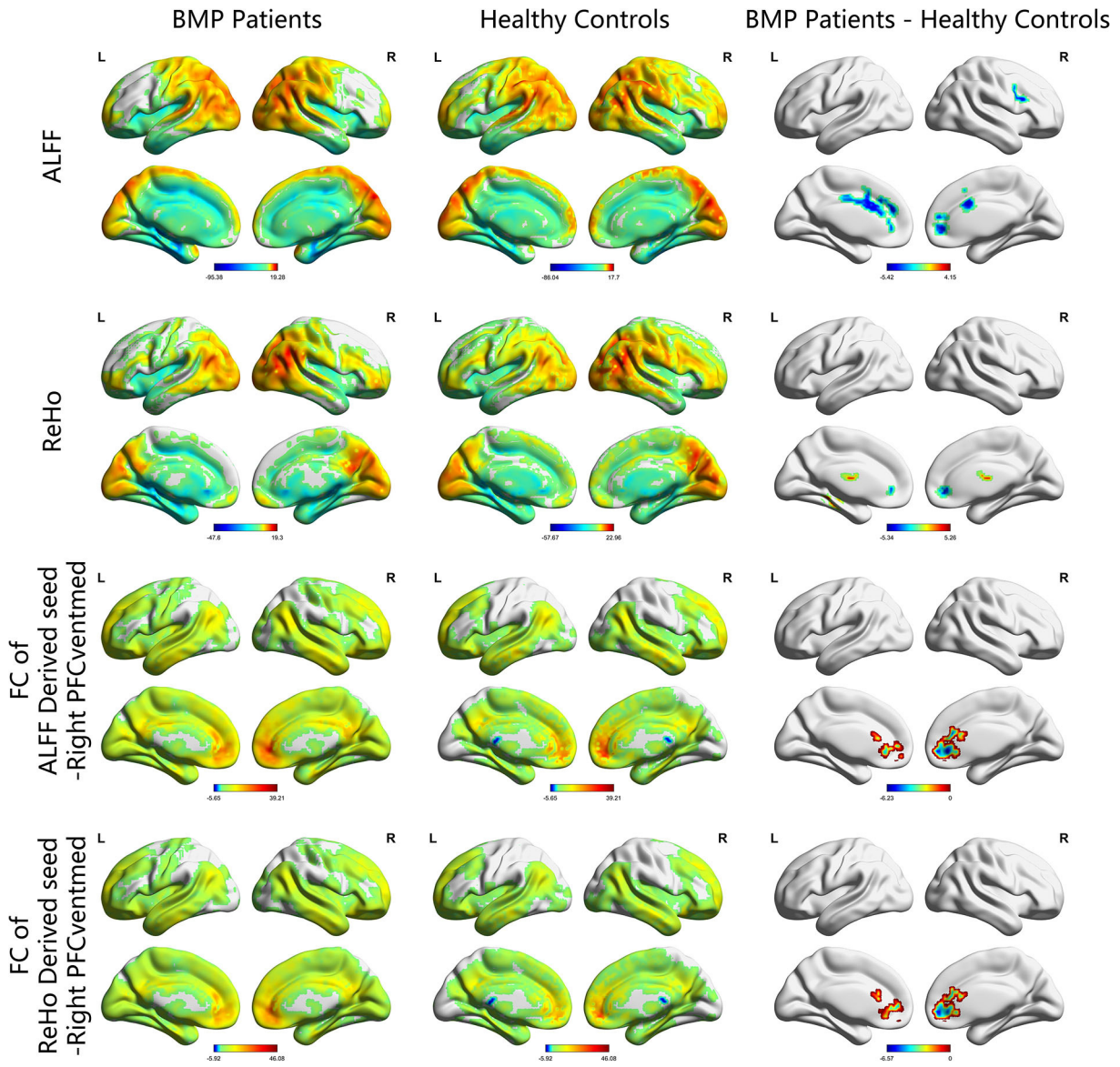

FIGURE 1
ALFF, ReHo, and FC maps of intragroup and intergroup comparisons. Corrected for multiple comparisons with Gaussian random-field theory (voxel level $p < 0.001$, cluster level $p < 0.05$). The color scale denotes the t value. ALFF, amplitude of low-frequency fluctuations; ReHo, regional homogeneity; FC, functional connectivity; PFCventmed, superior frontal gyrus, medial orbital; R, right; L, left.

within a specific low-frequency range (0.01–0.10 Hz) after transforming voxel time series frequency information into the power domain with a fast Fourier transform (4). ReHo is calculated as Kendall's coefficient of concordance (KCC) among a seed voxel and its neighbor 26 voxels (5). The widely used mean division is to calculate the mean across voxels for neuroimaging indices and divide the value at each voxel by the mean within gray matter. Smoothing (with a 6 mm full-width half-maximum isotropic Gaussian kernel) was conducted before the ALFF calculation and after the ReHo calculation. Brain regions with altered ALFF or ReHo in BMP patients were set as seeds to obtain the averaged time course, and calculate their *Pearson* correlation coefficient values for the remainder of the whole-brain voxels. Fisher's *r*-to-*z* transformation was applied to normalize the distribution correlation coefficient to obtain FC.

Statistical analysis

Demographic and neuropsychological data were analyzed with SPSS software (version 25.0; IBM Corp., Armonk, NY, USA). Two-sample *t*-tests or Mann–Whitney *U*-tests were applied to compare the data between two groups according to the distribution checked with the Kolmogorov–Smirnov test. The chi-square test was applied to intergroup comparisons of sex. Values of $p < 0.05$ were considered statistically significant.

Before the one or two-sample *t*-test, Jarque-Bera goodness-of-fit test was conducted to confirm the normal distribution of ALFF, ReHo, and FC maps (all voxels with $p > 0.05$). Subsequently, neuroimaging indices were analyzed using DPABI software. First, a one-sample *t*-test was performed to examine the functional activity and connectivity patterns in each group. Then, the *t*-statistics of group effect was analyzed after adjusting for covariates (including age, sex, and gray matter intensity and head motion parameter) with multiple linear regression. The test results were corrected for multiple comparisons with Gaussian random-field theory (GRF, voxel level $p < 0.001$, cluster level $p < 0.05$).

ALFF, ReHo values, and FC *z* scores in significantly altered brain regions were extracted for *Spearman* correlation analysis with pain intensity and neuropsychological data in BMP patients. We also explored the relationship of pain intensity with neuroimaging indices of each voxel (GRF corrected, voxel level $p < 0.001$, cluster level $p < 0.05$). The extracted values of both groups were used for receiver operating characteristic (ROC) curve analysis to evaluate their performance in discriminating individual subjects between the two groups. Leave-one-out cross-validation was performed to prevent possible inflated estimates of discriminant power and the validated AUC was obtained. Collinearity among neuroimaging indices was checked by using linear regression to avoid the loss in statistical power.

TABLE 3 Results of *Spearman* correlation between neuroimaging indices and pain scores in BMP patients.

Measurements	Brain regions	Hemisphere	ρ	p
ALFF	ACC	Left	0.112	0.557
	IFGoperc	Right	0.140	0.459
	PFCventmed	Right	0.144	0.459
ReHo	THA	Left	0.025	0.897
	THA	Right	−0.031	0.871
	FFG	Left	−0.143	0.450
	PFCventmed	Right	−0.300	0.107
FC	Right PFCventmed (ALFF)-Right ACC	NA	−0.175	0.355
	Right PFCventmed (ReHo)-Right PFCventmed	NA	−0.186	0.326

BMP, bone metastasis pain; ALFF, amplitude of low-frequency fluctuations; ReHo, regional homogeneity; FC, functional connectivity; ACC, anterior cingulate; IFGoperc, inferior frontal gyrus, opercular part; PFCventmed, superior frontal gyrus, medial orbital; THA, thalamus; FFG, fusiform gyrus; NA, not applicable.

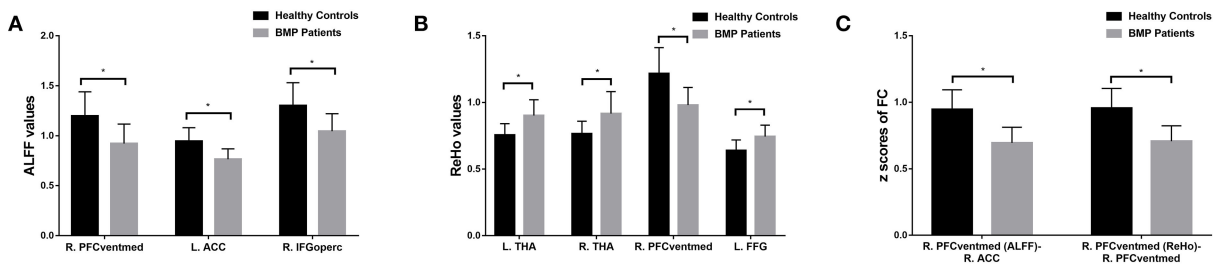

FIGURE 2
Brain regions with significant differences in ALFF **(A)**, ReHo **(B)**, and FC **(C)** between BMP patients and healthy controls. * $p < 0.05$ (corrected with Gaussian random-field theory, voxel level $p < 0.001$, cluster level $p < 0.05$). ALFF, amplitude of low-frequency fluctuations; ReHo, regional homogeneity; FC, functional connectivity; ACC, anterior cingulate cortex; IFGoperc, inferior frontal gyrus, opercular part; PFCventmed, superior frontal gyrus, medial orbital; THA, thalamus; FFG, fusiform gyrus; R, right; L, left.

TABLE 4 Classification performance of neuroimaging indices in discriminating between BMP patients and healthy controls.

Measurements	Brain regions	Hemisphere	AUC	Leave-one-out cross validated AUC	Cutoff values	Sensitivity (%)	Specificity (%)	Accuracy (%)
ALFF	ACC	Left	0.868[a]	0.866	0.8387	73.30	78.80	76.20
	IFGoperc	Right	0.804[a]	0.802	1.1565	66.70	75.80	71.40
	PFCventmed	Right	0.835[a]	0.834	1.0450	80.00	75.80	77.80
ReHo	THA	Left	0.868[a]	0.867	0.8231	73.30	84.80	79.40
	THA	Right	0.774[a]	0.773	0.8362	63.30	78.80	71.40
	FFG	Left	0.810[a]	0.811	0.6962	76.70	78.80	77.80
	PFCventmed	Right	0.848[a]	0.848	1.0708	80.00	78.80	79.40
FC	Right PFCventmed (ALFF)-Right ACC	NA	0.911[b]	0.908	0.8260	86.70	81.80	84.10
	Right PFCventmed (ReHo)-Right PFCventmed	NA	0.909[b]	0.906	0.8241	86.70	81.80	84.10
Combined ALFF and ReHo values	Brain regions with significant intergroup difference of ALFF and ReHo	NA	0.963	0.961	NA	93.30	93.90	93.70

[a]Compared with combined ALFF and ReHo values, $p < 0.05$.
[b]Compared with combined ALFF and ReHo values, $p > 0.05$.
BMP, bone metastasis pain; ALFF, amplitude of low-frequency fluctuations; ReHo, regional homogeneity; FC, functional connectivity; ACC, anterior cingulate cortex; IFGoperc, inferior frontal gyrus, opercular part; PFCventmed, superior frontal gyrus, medial orbital; THA, thalamus; FFG, fusiform gyrus; NA, not applicable.

And the probabilities of combined neuroimaging indices were obtained by using logistic regression in SPSS software and were used for the ROC curve analyses. The Delong test was applied to compare areas under ROC curves (AUCs) (20).

Results

Demographic and neuropsychological data comparisons

The BMP patients did not differ from the HCs in terms of age, sex, SAS, and SDS score ($p > 0.05$). The duration of pain in patients ranged from 20 to 2,095 days, and the pain score ranged from 1 to 7. Details are shown in Table 1.

Functional activity and connectivity analysis

According to the one-sample *t*-test, both the BMP patients and HCs showed higher ALFF and ReHo than the global mean value mainly in the parietal and occipital lobes and lower ALFF and ReHo mainly in the frontal and temporal lobes. According to the two-sample *t*-test, BMP patients showed lower ALFF and ReHo mainly in the prefrontal cortex and higher ReHo in the bilateral thalamus and left fusiform gyrus. Higher ALFF values were not observed in BMP patients.

According to the two-sample *t*-test, the brain regions with abnormal brain activity were set as the seed regions for FC calculation. In both groups, the right medial orbital of the superior frontal gyrus had higher FC than the medial frontal cortex and temporal lobes. Compared to HCs, BMP patients had lower FC of the right medial orbital of the superior frontal gyrus within the prefrontal cortex. The FC anchoring other seed regions showed no significant differences between the two groups. Details are shown in Table 2 and Figures 1, 2.

Correlation and ROC curve analysis

No significant correlations between neuroimaging indices and pain scores or neuropsychological data were noted in BMP patients ($p > 0.05$; Table 3). The extracted values of ALFF from individual brain regions showed moderate discrimination performance as well as the values of ReHo, whereas the values of FC *z* scores showed better discrimination performance than ALFF or ReHo alone. The combined ALFF and ReHo values of all brain regions were superior to individual values in ROC analysis ($p < 0.05$). FC *z* scores were not involved in the combination due to their collinearity. The combined AUC of ALFF and ReHo showed no significant difference from the AUC of FC values ($p > 0.05$; Table 4, Figures 3–6).

Discussion

We investigated the brain functional activity and connectivity differences between BMP patients and HCs. Decreased ALFF and ReHo were found mainly in the frontal cortex, and increased ReHo was

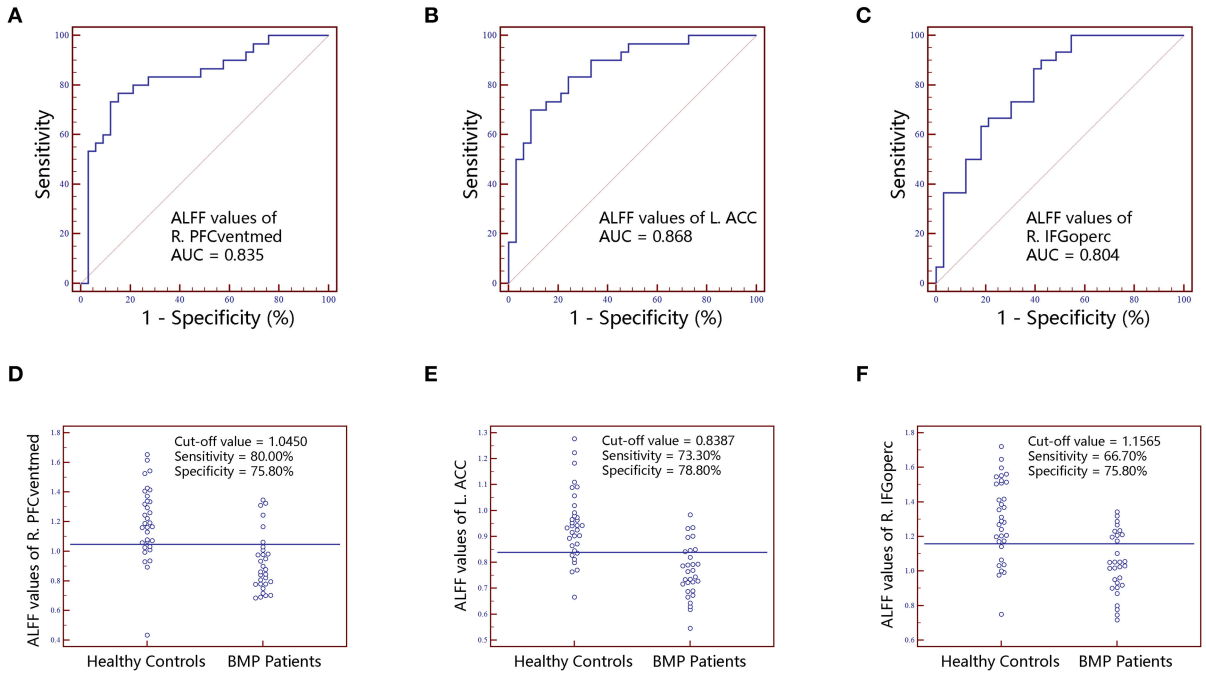

FIGURE 3
The classification performance of ALFF values extracted from individual brain regions identified by intergroup comparison. The top row are receiver operating characteristic curves for R.PFCventmed **(A)**, L.ACC **(B)** and R.IFGoperc **(C)**. The bottom row are interactive dot diagrams for R.PFCventmed **(D)**, L.ACC **(E)** and R.IFGoperc **(F)**. ALFF, amplitude of low-frequency fluctuations; ACC, anterior cingulate cortex; AUC, areas under receiver operating characteristic curve; IFGoperc, inferior frontal gyrus, opercular part; PFCventmed, superior frontal gyrus, medial orbital; R, right; L, left.

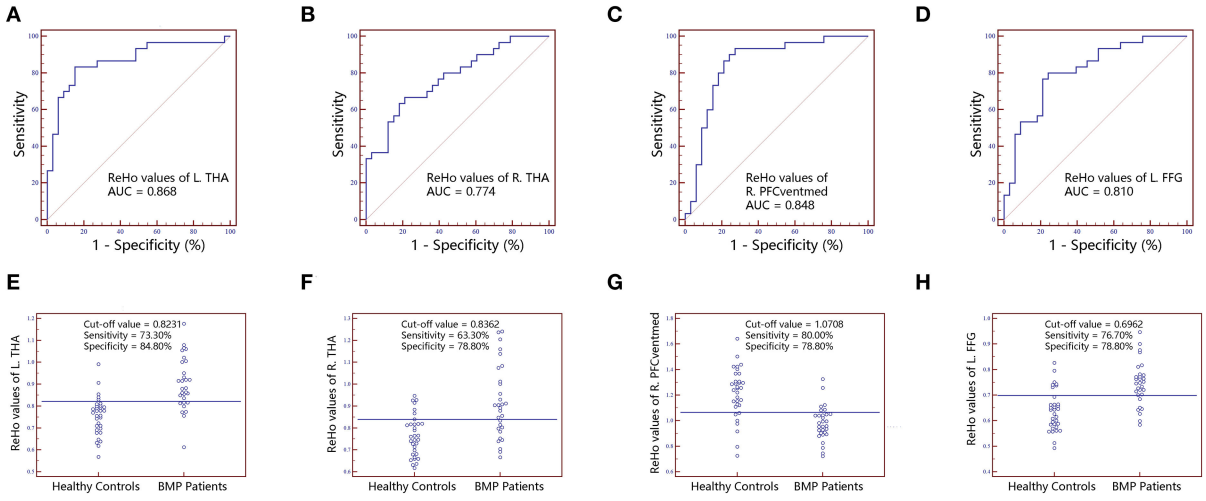

FIGURE 4
The classification performance of ReHo values extracted from individual brain regions identified by intergroup comparison. The top row are receiver operating characteristic curves for L.THA **(A)**, R.THA **(B)**, R.PFCventmed **(C)** and L.FFG **(D)**. The bottom row are interactive dot diagrams for L.THA **(E)**, R.THA **(F)**, R.PFCventmed **(G)** and L.FFG **(H)**. ReHo, regional homogeneity; AUC, areas under receiver operating characteristic curve; THA, thalamus; PFCventmed, superior frontal gyrus, medial orbital; FFG, fusiform gyrus; R, right; L, left.

found in the thalamus and fusiform gyrus in BMP patients compared with HCs. Decreased FC within the prefrontal cortex was observed in BMP patients. These neuroimaging indices showed satisfactory discriminatory performance between the two groups and may serve as neuroimaging biomarkers.

The thalamus and prefrontal cortex (including the anterior cingulate cortex) have been repeatedly reported to be associated

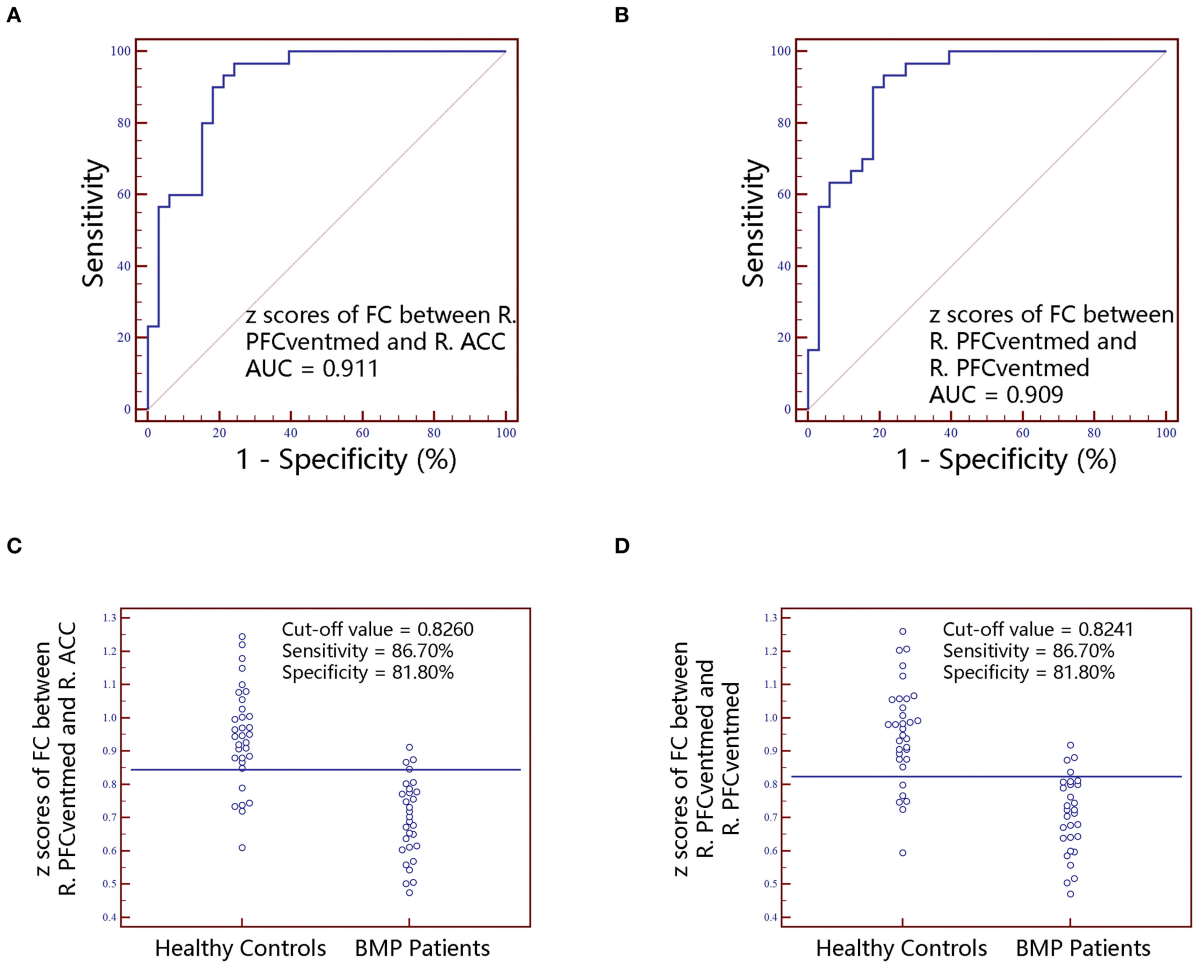

FIGURE 5
The classification performance of FC *z* scores extracted from individual brain regions identified by intergroup comparison. The top row are receiver operating characteristic curves for *z* scores of FC between R.PFCventmed and R.ACC **(A)** and *z* scores of FC between R.PFCventmed and R.PFCventmed **(B)**. The bottom row are interactive dot diagrams for *z* scores of FC between R.PFCventmed and R.ACC **(C)** and *z* scores of FC between R.PFCventmed and R.PFCventmed **(D)**. FC, functional connectivity; AUC, areas under receiver operating characteristic curve; ACC, anterior cingulate cortex; PFCventmed, superior frontal gyrus, medial orbital; R, right; L, left.

with chronic pain (21). As the relay station in ascending nociceptive inputs and descending pain modulatory pathways, the thalamus was reported to have functional and structural abnormalities in patients with migraines (22) and chronic low back pain (6). Blood oxygen level-dependent signal variability in the ascending trigeminal spinal-thalamo-cortical pathway was associated with headache severity (23). Therefore, the elevated activity of the thalamus in BMP patients may be driven by the transmission of pain information. Furthermore, the prefrontal cortex drives the cognitive modulation of the pain experience (15). Decreased pain-evoked brain activity in the prefrontal cortex was associated with reduced antinociceptive brain responses to pain in fibromyalgia patients (24). Increased prefrontal cortex activity was associated with reduced pain intensity after psychologic-based therapies in fibromyalgia patients (25). Therefore, the decreased brain activity and connectivity in the prefrontal cortex may suggest that BMP patients suffer from weakened antinociceptive cognitive modulation, which is consistent with previous studies on other types of pain.

A few studies have reported the possible role of the fusiform gyrus in pain processing. The fusiform gyrus anatomically connects the ventral visual network and is associated with facial recognition or face selection (26). Heightened activity in the fusiform gyrus was found to be a robust biomarker of pain intensity in experimental pain and chronic low back pain (27). The fusiform gyrus may be involved in the affective component of pain processing occurring in the amygdala

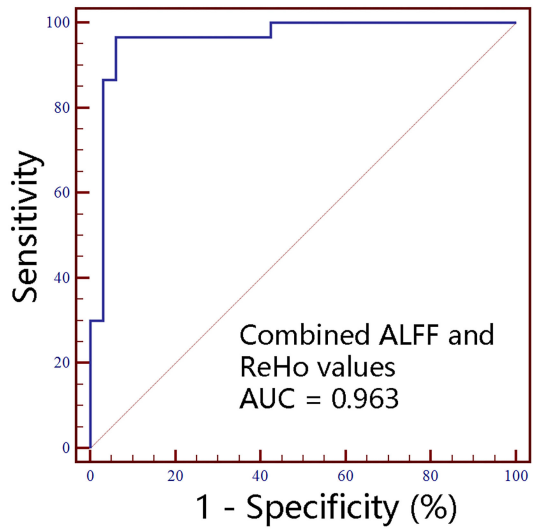

FIGURE 6
The classification performance of combined ALFF and ReHo values extracted from individual brain regions identified by intergroup comparison. ALFF, amplitude of low-frequency fluctuations; ReHo, regional homogeneity; AUC, areas under receiver operating characteristic curve; R, right; L, left.

and hippocampus by outputting the visualization of painful experiences (28). The present study's findings of increased activity in fusiform are consistent with previous studies and suggest the potential involvement of affective processing in BMP patients.

Neuroimaging indices have been used as biomarkers to discriminate between pain patients and controls. ALFF maps were used to classify chronic low back pain patients and controls with a moderate discriminate performance (accuracy rate >70%) (29). In addition, ReHo maps showed poor performance in classifying the more resilient chronic pain patients from the less resilient chronic pain patients (accuracy rate = 55%); however, the accuracy rate of combined ReHo and fractional ALFF achieved 79% (30). In the present study, the combined ALFF and ReHo showed satisfactory classification performance (accuracy rate = 93.7%) between BMP patients and HCs, which is comparable with the classification performance of FC maps. And the classification performance of FC maps was not significantly different from the combined ALFF and ReHo maps. Hence, ALFF, ReHo, and FC maps may serve as neuroimaging biomarkers for classifying BMP patients and HCs. However, the discriminant power of ROC may be overestimated by entering the values extracted from previously-identified significant brain regions, which can be inferred from the similarity between the original AUCs and leave-one-out cross-validated AUCs. Therefore, the classification performance in the present study should be interpreted with caution. In addition, the disadvantages of these neuroimaging indices are not negligible, including respiratory carbon dioxide influence on ALFF (31), the impact of neighborhood voxel size on ReHo (32), and the potential transitivity problem, controversial anti-correlations, and unsatisfactory reliability of FC (29, 33).

Of note, no correlation between brain activity or connectivity was found with pain intensity in the present study. The dissociation between the magnitude of the response in the brain and the persistence of pain may be due to the habituation of repetitive noxious stimuli (12). For instance, brain activity was significantly related to stimulus intensity rather than pain intensity in healthy participants during experimental tonic noxious heat stimulation (34). Moreover, a recent study suggests that fMRI may not be a reliable measure of reported pain intensity (35). Other confounding factors should also be taken into consideration, including pain caused directly by the tumor and treatment. On one hand, the tumor can release pain-modulating agents and their growth can erode into normal tissue, resulting in pain. On the other hand, surgical insult contributes to chronic post-surgical pain and chemotherapy and monoclonal antibodies can induce neuropathy which is associated with pain (36). In addition, the individual amplitude of pain may be facilitated by negative emotions (37), even though no significant differences in SAS and SDS scores were noted between BMP patients and HCs.

Some limitations should be acknowledged. First, the sample size is relatively small. The findings should be further validated in other datasets with larger sample sizes. Second, patients suffering from severe intensities of pain are impractical to be involved with potential evident head movement and only those with mild and moderate intensities were included. Therefore, bias is not avoidable. Third, we cannot exclude the confounding effects of analgesics, lung cancer, and its treatment. Fourth, the MRI data processing should be taken into consideration since there is no definite standard procedure. For instance, though the effects of variables of interest have remained largely after standardization (19), we must acknowledge that the choice of whether to conduct standardization may have an impact on the results. Despite these limitations, the preliminary positive findings warrant further investigation.

In conclusion, it is necessary to better understand cancer pain. Our findings suggested a decrease in brain functional activity mainly in the frontal cortex and an increase in the thalamus and fusiform gyrus in BMP. Moreover, a decrease in functional connectivity within the frontal cortex was observed. These abnormalities may be associated with the neuropathology of BMP and hold the potential to classify BMP patients and HCs. However, we should note that the present preliminary findings should be verified in future elaborate study designs.

Data availability statement

The raw data supporting the conclusions of this article will be made available by the authors, without undue reservation.

Ethics statement

The studies involving human participants were reviewed and approved by Medical Research Ethics Committee of Chongqing University Cancer Hospital. The patients/participants provided their written informed consent to participate in this study.

Author contributions

DL contributed to the experiments, statistical analysis, and the writing of the manuscript. XZ contributed to the MRI data analysis. YT, HY, YC, LT, LY, SW, SL, JC, JL, and CW contributed to MRI and clinical data collection. HYQ and JZ are the guarantors of this study and had complete access to all the data in the study. All authors contributed to the article and approved the submitted version.

Funding

The study was supported by the National Natural Science Foundation of China (82071883), Chongqing Medical Research Project of Combination of Science and Medicine (2021MSXM035), Graduate Research and Innovation Foundation of Chongqing, China (CYS21071), 2020 SKY Imaging Research Fund of the Chinese International Medical Foundation (Z-2014-07-2003-24), and Chongqing Natural Science Foundation (cstc2021jcyj-msxmX0319 and cstc2021jcyj-msxmX0313).

Acknowledgments

The authors thank all the volunteers who participated in the study for their kind collaboration.

Conflict of interest

The authors declare that the research was conducted in the absence of any commercial or financial relationships that could be construed as a potential conflict of interest.

Publisher's note

References

1. Bennett MI, Kaasa S, Barke A, Korwisi B, Rief W, Treede RD. The IASP classification of chronic pain for ICD-11: chronic cancer-related pain. *Pain.* (2019) 160:38–44. doi: 10.1097/j.pain.0000000000001363

2. Scarborough BM, Smith CB. Optimal pain management for patients with cancer in the modern era. *CA Cancer J Clin.* (2018) 68:182–96. doi: 10.3322/caac.21453

3. Aielli F, Ponzetti M, Rucci N. Bone metastasis pain, from the bench to the bedside. *Int J Mol Sci.* (2019) 20:280. doi: 10.3390/ijms20020280

4. Zang YF, He Y, Zhu CZ, Cao QJ, Sui MQ, Liang M, et al. Altered baseline brain activity in children with ADHD revealed by resting-state functional MRI. *Brain Dev.* (2007) 29:83–91. doi: 10.1016/j.braindev.2006.07.002

5. Zang Y, Jiang T, Lu Y, He Y, Tian L. Regional homogeneity approach to fMRI data analysis. *Neuroimage.* (2004) 22:394–400. doi: 10.1016/j.neuroimage.2003.12.030

6. Zhang B, Jung M, Tu Y, Gollub R, Lang C, Ortiz A, et al. Identifying brain regions associated with the neuropathology of chronic low back pain: a resting-state amplitude of low-frequency fluctuation study. *Br J Anaesth.* (2019) 123:e303–11. doi: 10.1016/j.bja.2019.02.021

7. Wang Z, Huang S, Yu X, Li L, Yang M, Liang S, et al. Altered thalamic neurotransmitters metabolism and functional connectivity during the development of chronic constriction injury induced neuropathic pain. *Biol Res.* (2020) 53:36. doi: 10.1186/s40659-020-00303-5

8. Cao S, Song G, Zhang Y, Xie P, Tu Y, Li Y, et al. Abnormal local brain activity beyond the pain matrix in postherpetic neuralgia patients: a resting-state functional MRI study. *Pain Physician.* (2017) 20:E303–14. doi: 10.36076/ppj.2017.E314

9. Yin J, Sun H, Wang Z, Ni H, Shen W, Sun PZ. Diffusion kurtosis imaging of acute infarction: comparison with routine diffusion and follow-up MR imaging. *Radiology.* (2018) 287:651–7. doi: 10.1148/radiol.2017170553

10. Wei HL, Li J, Guo X, Zhou GP, Wang JJ, Chen YC, et al. Functional connectivity of the visual cortex differentiates anxiety comorbidity from episodic migraineurs without aura. *J Headache Pain.* (2021) 22:40. doi: 10.1186/s10194-021-01259-x

11. Nan J, Yang W, Meng P, Huang W, Zheng Q, Xia Y, et al. Changes of the postcentral cortex in irritable bowel syndrome patients. *Brain Imaging Behav.* (2020) 14:1566–76. doi: 10.1007/s11682-019-00087-7

12. Legrain V, Iannetti GD, Plaghki L, Mouraux A. The pain matrix reloaded: a salience detection system for the body. *Prog Neurobiol.* (2011) 93:111–24. doi: 10.1016/j.pneurobio.2010.10.005

13. Kane CM, Hoskin P, Bennett MI. Cancer induced bone pain. *BMJ.* (2015) 350:h315. doi: 10.1136/bmj.h315

14. Ji RR. Recent progress in understanding the mechanisms of pain and itch: the second special issue. *Neurosci Bull.* (2018) 34:1–3. doi: 10.1007/s12264-018-0204-z

15. Martucci KT, Mackey SC. Neuroimaging of pain: human evidence and clinical relevance of central nervous system processes and modulation. *Anesthesiology.* (2018) 128:1241–54. doi: 10.1097/ALN.0000000000002137

16. Buehlmann D, Grandjean J, Xandry J, Rudin M. Longitudinal resting-state functional magnetic resonance imaging in a mouse model of metastatic bone cancer reveals distinct functional reorganizations along a developing chronic pain state. *Pain.* (2018) 159:719–27. doi: 10.1097/j.pain.0000000000001148

17. Buehlmann D, Ielacqua GD, Xandry J, Rudin M. Prospective administration of anti-nerve growth factor treatment effectively suppresses functional connectivity alterations after cancer-induced bone pain in mice. *Pain.* (2019) 160:151–9. doi: 10.1097/j.pain.0000000000001388

18. Yan C-G, Wang X-D, Zuo X-N, Zang Y-F. DPABI: data processing & analysis for (resting-state) brain imaging. *Neuroinformatics.* (2016) 14:339–51. doi: 10.1007/s12021-016-9299-4

19. Yan CG, Craddock RC, Zuo XN, Zang YF, Milham MP. Standardizing the intrinsic brain: towards robust measurement of inter-individual variation in 1000 functional connectomes. *Neuroimage.* (2013) 80:246–62. doi: 10.1016/j.neuroimage.2013.04.081

20. Delong ER, Delong DM, Clarke-Pearson DL. Comparing the areas under two or more correlated receiver operating characteristic curves: a nonparametric approach. *Biometrics.* (1988) 44:837–45. doi: 10.2307/2531595

21. Tu Y, Cao J, Bi Y, Hu L. Magnetic resonance imaging for chronic pain: diagnosis, manipulation, and biomarkers. *Sci China Life Sci.* (2021) 64:879–96. doi: 10.1007/s11427-020-1822-4

22. Amin FM, Hougaard A, Magon S, Sprenger T, Wolfram F, Rostrup E, et al. Altered thalamic connectivity during spontaneous attacks of migraine without aura: a resting-state fMRI study. *Cephalalgia.* (2018) 38:1237–44. doi: 10.1177/0333102417729113

23. Lim M, Jassar H, Kim DJ, Nascimento TD, Dasilva AF. Differential alteration of fMRI signal variability in the ascending trigeminal somatosensory and pain modulatory pathways in migraine. *J Headache Pain.* (2021) 22:4. doi: 10.1186/s10194-020-01210-6

24. Schrepf A, Harper DE, Harte SE, Wang H, Ichesco E, Hampson JP, et al. Endogenous opioidergic dysregulation of pain in fibromyalgia: a PET and fMRI study. *Pain.* (2016) 157:2217–25. doi: 10.1097/j.pain.0000000000000633

25. Jensen KB, Kosek E, Wicksell R, Kemani M, Olsson G, Merle JV, et al. Cognitive Behavioral Therapy increases pain-evoked activation of the prefrontal cortex in patients with fibromyalgia. *Pain.* (2012) 153:1495–503. doi: 10.1016/j.pain.2012.04.010

26. Kravitz DJ, Saleem KS, Baker CI, Ungerleider LG, Mishkin M. The ventral visual pathway: an expanded neural framework for the processing of object quality. *Trends Cogn Sci.* (2013) 17:26–49. doi: 10.1016/j.tics.2012.10.011

27. Lee JJ, Kim HJ, Ceko M, Park BY, Lee SA, Park H, et al. A neuroimaging biomarker for sustained experimental and clinical pain. *Nat Med.* (2021) 27:174–82. doi: 10.1038/s41591-020-1142-7

28. Shimo K, Ueno T, Younger J, Nishihara M, Inoue S, Ikemoto T, et al. Visualization of painful experiences believed to trigger the activation of affective and emotional brain regions in subjects with low back pain. *PLoS ONE.* (2011) 6:e26681. doi: 10.1371/journal.pone.0026681

29. Baran TM, Lin FV, Geha P. Functional brain mapping in patients with chronic back pain shows age-related differences. *Pain.* (2021) 163:e917–26. doi: 10.1097/j.pain.0000000000002534

30. You B, Wen H, Jackson T. Identifying resting state differences salient for resilience to chronic pain based on machine learning multivariate pattern analysis. *Psychophysiology.* (2021) 58:e13921. doi: 10.1111/psyp.13921

31. Golestani AM, Kwinta JB, Strother SC, Khatamian YB, Chen JJ. The association between cerebrovascular reactivity and resting-state fMRI functional connectivity in healthy adults: the influence of basal carbon dioxide. *Neuroimage.* (2016) 132:301–13. doi: 10.1016/j.neuroimage.2016.02.051

32. Li Z, Kadivar A, Pluta J, Dunlop J, Wang Z. Test-retest stability analysis of resting brain activity revealed by blood oxygen level-dependent functional MRI. *J Magn Reson Imaging.* (2012) 36:344–54. doi: 10.1002/jmri.23670

33. Noble S, Scheinost D, Finn ES, Shen X, Papademetris X, Mcewen SC, et al. Multisite reliability of MR-based functional connectivity. *Neuroimage.* (2017) 146:959–70. doi: 10.1016/j.neuroimage.2016.10.020

34. Nickel MM, May ES, Tiemann L, Postorino M, Ta Dinh S, Ploner M. Autonomic responses to tonic pain are more closely related to stimulus intensity than to pain intensity. *Pain.* (2017) 158:2129–36. doi: 10.1097/j.pain.0000000000001010

35. Hoeppli ME, Nahman-Averbuch H, Hinkle WA, Leon E, Peugh J, Lopez-Sola M, et al. Dissociation between individual differences in self-reported pain intensity and underlying fMRI brain activation. *Nat Commun.* (2022) 13:3569. doi: 10.1038/s41467-022-31039-3

36. Brown M, Farquhar-Smith P. Pain in cancer survivors; filling in the gaps. *Br J Anaesth.* (2017) 119:723–36. doi: 10.1093/bja/aex202

37. Gandhi W, Rosenek NR, Harrison R, Salomons TV. Functional connectivity of the amygdala is linked to individual differences in emotional pain facilitation. *Pain.* (2020) 161:300–7. doi: 10.1097/j.pain.0000000000001714

frontiers | Frontiers in Neurology

TYPE Original Research
PUBLISHED 26 September 2022
DOI 10.3389/fneur.2022.948024

OPEN ACCESS

EDITED BY
Simona Sacco,
University of L'Aquila, Italy

REVIEWED BY
Yohannes W. Woldeamanuel,
Stanford University, United States
Hongyi Zhu,
Shanghai Jiao Tong University, China

*CORRESPONDENCE
Pingliang Yang
pingliangyang@163.com
Ling Ye
zerodq_hx@163.com

†These authors have contributed equally to this work and share first authorship

SPECIALTY SECTION
This article was submitted to Headache and Neurogenic Pain, a section of the journal Frontiers in Neurology

RECEIVED 19 May 2022
ACCEPTED 02 September 2022
PUBLISHED 26 September 2022

CITATION
Chen L, Qing A, Zhu T, Yang P and Ye L (2022) Effect and safety of extracorporeal shockwave therapy for postherpetic neuralgia: A randomized single-blind clinical study. *Front. Neurol.* 13:948024. doi: 10.3389/fneur.2022.948024

Effect and safety of extracorporeal shockwave therapy for postherpetic neuralgia: A randomized single-blind clinical study

Lu Chen[1†], Ailing Qing[2†], Tao Zhu[3], Pingliang Yang[4*] and Ling Ye[1*]

[1]Department of Pain Management, West China Hospital, Sichuan University, Chengdu, China, [2]Department of Anesthesiology, West China School of Public Health and West China Fourth Hospital, Sichuan University, Chengdu, China, [3]Department of Anesthesiology, West China Hospital of Sichuan University, Chengdu, China, [4]Department of Anesthesiology, The First Affiliated Hospital of Chengdu Medical College, Xindu, China

Objective: To evaluate the efficacy and safety of extracorporeal shockwave therapy (ESWT) for postherpetic neuralgia.

Design: Randomized single-blind clinical study.

Patients: Patients with postherpetic neuralgia.

Methods: Patients were randomly divided into the control group and the ESWT group. The control group received conventional treatment while the ESWT group received conventional treatment and ESWT. The primary outcome is pain degree as assessed by the numeric rating scale (NRS), and secondary outcomes include brief pain inventory (BPI), Self-rating Anxiety Scale (SAS), Self-rating Depression Scale (SDS), and Pittsburgh Sleep Quality Index (PSQI). Data were collected at baseline and at weeks 1, 4, and 12. Linear mixed-effects models were applied to repeated measurement data.

Results: The scores on the NRS, BPI, SAS, SDS, and PSQI decreased over time in both groups. The NRS and SDS scores of the ESWT group were statistically lower than the control group. There was no time × group interaction in the mixed model analysis. Baseline age was correlated with NRS scores and BPI scores, and invasive treatment was related to PSQI scores, with no interaction effect for baseline confounders observed. No adverse events were observed during the process of this trial.

Conclusion: Extracorporeal shockwave therapy combined with conventional treatment could relieve pain and improve the psychological state in patients with postherpetic neuralgia without serious adverse effects.

KEYWORDS

extracorporeal shockwave therapy, postherpetic neuralgia, neuropathic pain, chronic pain, quality of life

Introduction

Postherpetic neuralgia (PHN) is defined as persistent pain lasting more than 3 months after the onset of shingles (1), which is the most common complication of herpes zoster occurring in 20–30% of patients (2–5). As a type of neuropathic pain, PHN is related to peripheral-nerve damage and characterized by burning, itching, lightning, and sharp pain, some with allodynia or hyperalgesia, which seriously affect patients' life quality, sleep quality, and mental state (3). The current common treatment for PHN includes medication and interventional therapy. First-line medication therapy includes pregabalin, gabapentin, and tricyclic antidepressants, while interventional therapy includes subcutaneous injection, electrical nerve stimulation, nerve block, pulsed radiofrequency, and spinal cord stimulation (6). Despite multiple treatments, there are still adverse effects, such as nausea, vomiting, and constipation caused by medication, as well as infection, bleeding, and nerve injury related to interventional therapy. Therefore, it is necessary to find an effective and non-invasive treatment for PHN.

A shockwave is a type of transient pressure fluctuation generated by electromagnetic, electrohydraulic, or piezoelectric devices (7). As an effective and safe treatment, extracorporeal shockwave therapy (ESWT) is widely used in urinary disease and musculoskeletal disorders (8–10). The main biological mechanism of ESWT includes wound healing, tissue regeneration, bone remodeling, angiogenesis, and anti-inflammation (11). In recent studies, ESWT has been reported to improve neuropathic pain, such as Morton's neuroma, primary trigeminal neuralgia, and diabetic neuropathy (12–15). In addition, a pilot study that includes 13 patients suggested that ESWT could significantly reduce symptoms of PHN (16). However, a randomized controlled trial with a larger sample size and longer follow-up is lacking. The objective of this study is to evaluate the effect and safety of ESWT on patients with PHN in short and middle term.

Materials and methods

Design

This study design is a single-center, single-blind, randomized controlled trial, which was approved by the Ethics Committee of West China Hospital, Sichuan University, Chengdu, China (No. 2019[814], date of approval: 30 December 2019) and registered at ChiCTR.org.cn (Identifier: ChiCTR1900025828, date of registration: 10 September 2019). The initial version of the protocol was published (17). Consolidated Standards of Reporting Trials (CONSORT) were followed.

Participants

Patients were recruited from September 2019 to September 2020 in the pain department of West China Hospital. After being informed of the procedures and possible complications of the study, they decided whether to participate in this study. Then, more detailed information was collected to assess the eligibility. The inclusion criteria included adults diagnosed with PHN according to the Consensus of Chinese experts on PHN (18); had an NRS score $\geq$4 points; had described symptoms objectively; had not received ESWT previously; and had not participated in other clinical trials within 3 months. The exclusion criteria included patients who had a history of allergy to coupling agent; tumor; liver or kidney dysfunction; thrombosis or abnormal coagulation; with a cardiac pacemaker; infectious; pregnant; fracture or severe osteoporosis; and mental disorders.

Randomization and blinding

After signing the informed consent, the participants were allocated into the control group or the ESWT group (1:1). In this process, a researcher was in charge of preparing the sealed opaque envelopes, which contained random numbers generated by EXCEL table. Another researcher was responsible for assigning the envelope to participants randomly, and then a shockwave therapist decided whether to perform shockwave therapy according to the random numbers in envelopes. The assessors and statisticians were blinded to randomization and did not participate in the treatment.

Treatment and outcomes

The control group received conventional treatment, such as medication and invasive interventional therapy, while the ESWT group received conventional treatment and extracorporeal shockwave therapy. Conventional treatment remained stable during the study period in patients receiving ESWT. The detailed therapeutic schedule is shown in Table 1. The schedule of drugs was adjusted based on the patients' symptoms, while the selection of invasive interventional therapy depended on the painful area and course of disease.

Extracorporeal shockwave therapy was performed by a skilled therapist with a radial extracorporeal shockwave generator (MASTERPULS MP100; Storz Medical AG, Switzerland). As shown in Figure 1, the patients could be in different positions (prone, lateral, or seated position) depending on the location of skin lesions. After applying the coupling agent to the skin, a R15 probe (radius of 15 mm) was moved along the nerve. The energy could gradually increase according to the patients' reaction. The primary outcome is pain intensity assessed by the numeric rating scale (NRS), and

TABLE 1 Therapeutic schedule.

Therapy			Schedule
Conventional treatment	Medication	Gabapentin	0.3 g qd on day 1
			0.3 g bid on day 2
			0.3 g tid on day 3 and maintained
		Pregabalin	75 mg bid
		Oxycodone and acetaminophen	0.5 tablet tid
		Mecobalamin	0.5 mg tid
	Invasive interventional therapy	Epidural nerve block	2 ml 2% Lidocaine
			1 ml compound Betamethasone
			2 ml Mecobalamin for injection
			5 ml normal saline
		Radiofrequency modulation	42°C 65 V, 15 min
		Radiofrequency thermocoagulation	65°C, 30 s; 70°C, 30 s
			75°C, 1 min; 80°C, 2 min; 85°C, 2 min
Extracorporeal shockwave therapy			10 Hz; 1–4 bar; 4000–7000 pulses
			performed every 3–5 days
			3–5 sessions consist a course

qd, once a day; bid, two times a day; tid, three times a day.

secondary outcomes include quality of life assessed by brief pain inventory (BPI), psychological state assessed by the Self-rating Anxiety Scale (SAS) and the self-rating Depression Scale (SDS), and sleep quality assessed by the Pittsburgh Sleep Quality Index (PSQI). Assessors collected data by telephone interviews at baseline and at weeks 1, 4, and 12. Adverse reactions related to ESWT were recorded to evaluate the safety.

Statistical analysis

The sample size was estimated with the superiority test ($\alpha = 0.05$ and $\beta = 0.2$). According to a previous study (19), we calculated that 76 participants were required. Demographic and baseline characteristics included age, sex, BMI, nerve segments of PHN, PHN duration, medication, invasive therapy, and per capital invasive therapy course. In the analysis of baseline data, quantitative data with normal distribution were presented as mean ± standard deviation (SD) and analyzed by the independent-samples *T*-test, while data that did not conform with normal distribution were presented as median (the upper and lower quartiles) and analyzed by the Mann–Whitney *U*-test. Categorical data were presented as frequency (percentage) and compared by the χ^2 test. In the analysis of repeated measurement data, intention-to-treat (ITT) analysis was conducted with the missing data replaced by using the last observation carried forward (LOCF) imputation method. Linear mixed-effects models were applied to longitudinal data, and restricted maximum likelihood (REML) with an unstructured covariance matrix was used. In the 2 groups (ESWT vs. control), 4 time points (baseline, weeks 1, 4, and 12), and the time × group interaction were considered as fixed effects, while baseline confounders, such as age, sex, body mass index (BMI), invasive treatment, and PHN nerve segments as covariates. IBM SPSS Statistics 26 was used for statistical analysis. All tests were two-sided, with $p < 0.05$ indicating statistical significance.

Results

Patient flow

In this study, 109 patients were recruited and assessed for eligibility and a total of 100 patients were included. After being randomized in a 1:1 ratio to the two groups, they received their allocated treatment. At week 1, 4 patients were lost to follow-up, 15 patients were lost to follow-up at week 4, and 31 patients were lost to follow-up at week 12. Finally, 69 patients finished 12-week follow-up. The data of all participates were included in the ITT analysis (Figure 2).

Demographic and baseline characteristics

There were no significant differences between the ESWT group and the control group in age, gender, body mass index (BMI), PHN localization, PHN duration, medication therapy, and invasive therapy, suggesting that the baselines were comparable (Table 2).

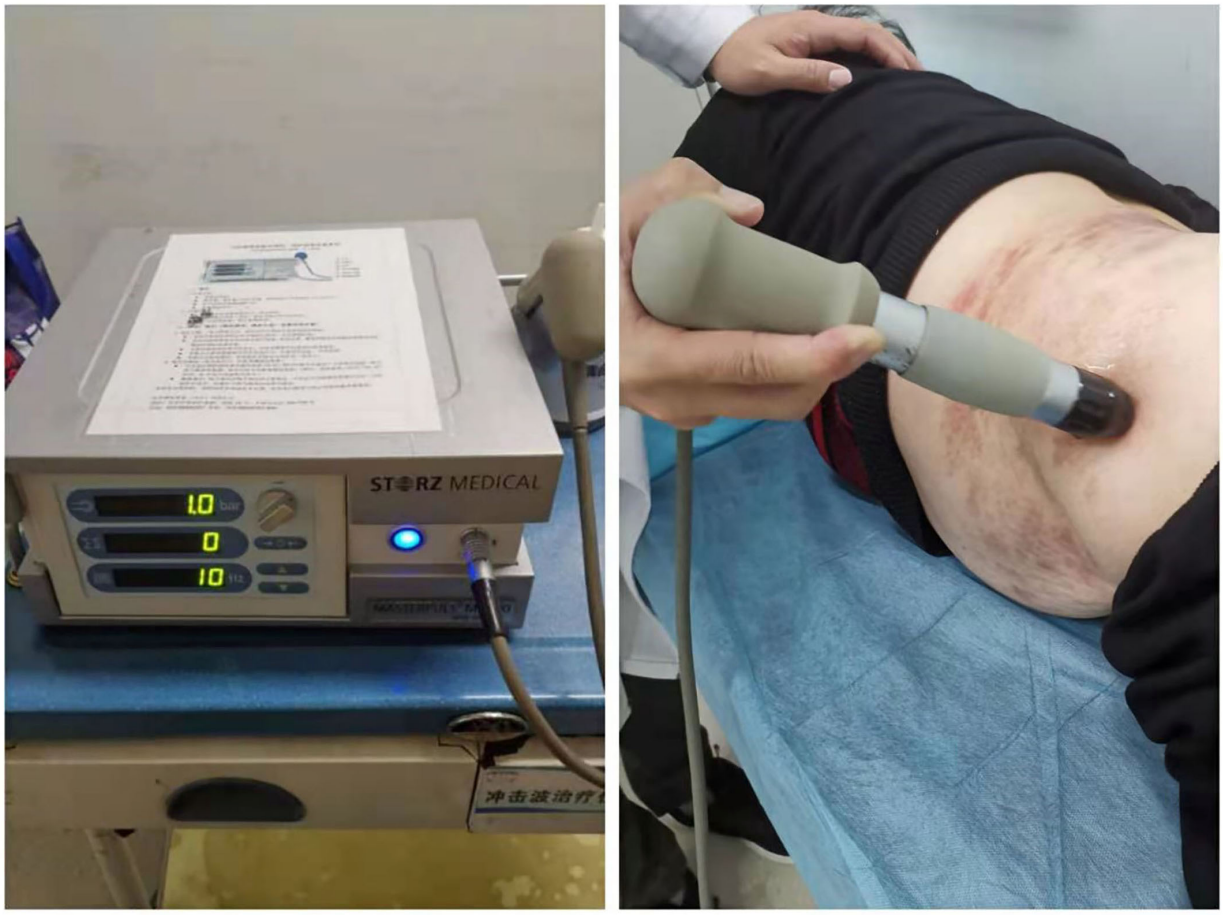

FIGURE 1
Extracorporeal shockwave therapy (ESWT) for postherpetic neuralgia (PHN). The patient was treated by a radial extracorporeal shockwave generator (MASTERPULS MP100; Storz Medical AG, Switzerland) in a lateral position.

A total of 31 participants were lost to follow-up because nobody answered the phone. The demographic and baseline characteristics of lost patients indicated that they were significantly older ($p < 0.001$) with lower BMI ($p = 0.026$) than patients who finished follow-up, while there was no significant difference in sex, PHN nerve segments, PHN duration, medication therapy, invasive therapy, and per capital invasive therapy course (Table 2).

Of the 31 patients who lost to the follow-up, 16 patients were in the treatment group while 15 patients were in the control group. There was a statistical difference in sex ($p = 0.044$) and BMI ($p = 0.031$) between the two groups. In 69 patients who finished 12-week follow-up, there were no significant difference in demographic and baseline characteristics between the ESWT group and the control group (Table 2).

Primary outcome

The scores and trends of baseline and post-treatment NRS scores are shown in Table 3 and Figure 3. The analysis of interaction effects for baseline confounders suggested that age was correlated with the NRS score but there was no interaction effect. A time × group interaction term was added in the mixed model, which indicated that the NRS scores in the ESWT group and the control group followed similar trends over time ($p > 0.05$), then the model was refitted without the time × group interaction term (Table 4). The final model showed that NRS scores was statistically associated with group ($p = 0.027$) and time ($p < 0.001$). The NRS scores decreased over time, and the NRS scores of the ESWT group were statistically lower than the control group.

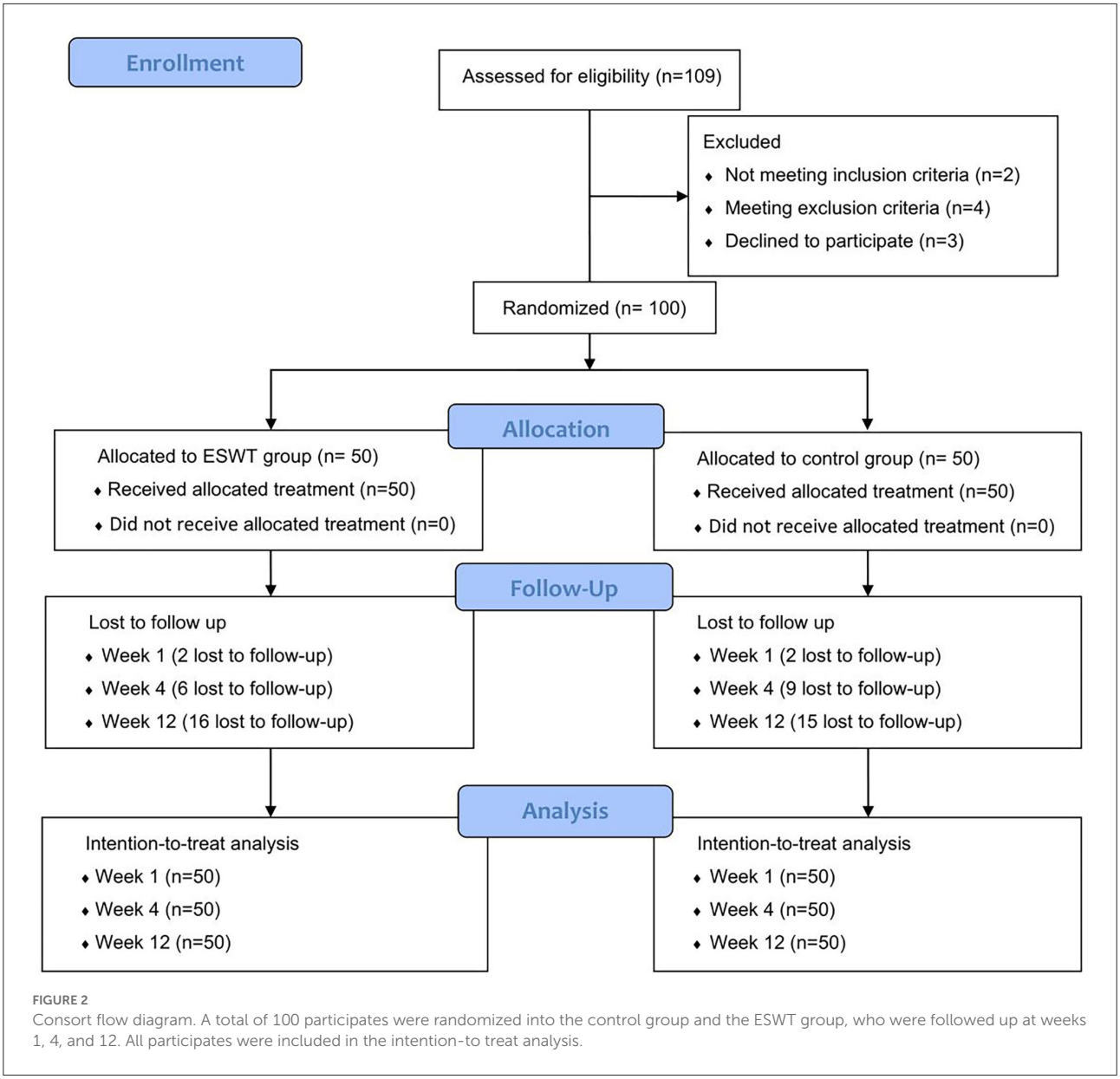

FIGURE 2
Consort flow diagram. A total of 100 participates were randomized into the control group and the ESWT group, who were followed up at weeks 1, 4, and 12. All participates were included in the intention-to treat analysis.

Secondary outcome

The scores and trends of baseline and post-treatment BPI, SAS, SDS, and PSQI scores are shown in Table 3 and Figure 4. In the analysis of interaction effects for baseline confounders, age was associated with BPI scores while invasive treatment was related to PSQI scores. There was no interaction effect of confounders in this study.

The analysis of time × group interaction showed that the BPI, SAS, SDS, and PSQI scores changed similarly in both groups over time ($p > 0.05$). After readjusting the model without the time × group interaction term, the final model showed that SDS scores were statistically associated with group ($p = 0.003$) and the BPI, SAS, SDS, and PSQI scores were statistically associated with time ($p < 0.001$; Table 4). The BPI, SAS, SDS, and PSQI scores decreased over time while SDS scores in the ESWT group were statistically lower than the control group.

Adverse reactions

There were no patient complaints about adverse reactions related to ESWT in either group through the follow-up period, such as skin swelling, allergy, fever, pain aggravation, paresthesia, tissue edema, and other adverse effects.

TABLE 2 Demographic and baseline characteristics of participates.

Variable	All ($n = 100$)			Finished follow-up ($n = 69$)			Lost follow-up ($n = 31$)			All ($n = 100$)		
	ESWT ($n = 50$)	Control ($n = 50$)	*P*	ESWT ($n = 34$)	Control ($n = 35$)	*P*	ESWT ($n = 16$)	Control ($n = 15$)	*P*	Finished ($n = 69$)	Lost ($n = 31$)	*P*
Age, years	67.9 ± 10.8	67.4 ± 11.2	0.84	64.15 ± 8.89	65.71 ± 11.96	0.540	75.75 ± 10.35	71.33 ± 8.24	0.201	64.94 ± 10.51	73.61 ± 9.50	**<0.001**
Male sex, *n* (%)	23 (46%)	23 (46%)	1	20 (58.8%)	15 (42.86%)	0.185	3 (18.8%)	8 (53.3%)	**0.044**	35 (50.7%)	11 (35.4%)	0.157
BMI (kg/m^2)	23.16 ± 3.12	23.40 ± 3.36	0.705	24.10 ± 2.92	23.43 ± 3.61	0.398	21.15 ± 2.59	23.34 ± 2.79	**0.031**	23.76 ± 3.28	22.21 ± 2.87	**0.026**
PHN segment, *n* (%)												
Cervical-facial segment	12 (24%)	10 (20%)	0.59	8 (23.5%)	6 (17.1%)	0.248	4 (25%)	4 (26.7%)	0.562	14 (20.3%)	8 (25.8%)	0.644
Thoracic segment	34 (68%)	38 (76%)		22 (64.7%)	28 (80%)		12 (75%)	10 (66.6%)		50 (72.5%)	22 (71.0%)	
Sacral-lumbar segment	4 (8%)	2 (4%)		4 (11.8%)	1 (2.9%)		0 (0%)	1 (6.7%)		5 (7.2%)	1 (3.2%)	
PHN duration, months	2 (1–3.25)	2 (1–6)	0.2	2 (1–3.25)	2 (1–6)	0.546	2 (1–5.25)	3 (2–7)	0.175	2 (1–5)	2 (1–6)	0.269
Medication									/			
Gabapentin g/d	0.9 (0.9–1.125)	0.9 (0.9–0.9)	0.981	0.9 (0.9–1.125)	0.9 (0.9–1.125)	0.886	/	0.9 (0.9–0.9)	0.110	0.9 (0.9–0.9)	0.9 (0.9–0.9)	0.728
Pregabalin mg/d	150 (150–225)	150 (150–225)	0.856	150 (150–225)	150 (225–300)	0.290	150 (150–225)	150 (150–150)		150 (150–225)	150 (150–150)	0.169
Invasive therapy, *n* (%)												
Epidural nerve block	3 (6%)	6 (12%)	0.657	3 (8.8%)	5 (14.3%)	0.773	0 (0%)	1 (6.7%)	0.151	8 (11.6%)	1 (3.2%)	0.576
Radiofrequency modulation	25 (50%)	22 (44%)		16 (47.1%)	15 (42.9%)		9 (56.3%)	7 (46.7%)		31 (44.9%)	16 (51.6%)	
Radiofrequency thermocoagulation	14 (28%)	16 (32%)		9 (26.5%)	11 (31.4%)		5 (31.2%)	5 (33.3%)		20 (29.0%)	10 (32.3%)	
Combined therapy	8 (16%)	6 (12%)		6 (17.6%)	4 (11.4%)		2 (12.5%)	2 (13.3%)		10 (14.5%)	4 (12.9%)	
Per capital invasive therapy course, times	2 (1∼3)	2 (2∼3)	0.61	2 (2–3)	2 (2–3)	0.630	3 (2–3.75)	2 (2–3)	0.748	2 (2–3)	2 (2–3)	0.279

PHN, postherpetic neuralgia; BMI, body mass index; ESWT, extracorporeal shockwave therapy.

10.3389/fneur.2022.948024

TABLE 3 Baseline and post-treatment outcome scores.

	NRS	BPI	SAS	SDS	PSQI
Baseline					
Control	7.62 ± 1.35	37.88 ± 9.18	40.48 ± 6.64	41.96 ± 7.76	15.76 ± 4.80
ESWT	7.18 ± 1.35	41.36 ± 12.35	42.52 ± 6.76	38.76 ± 7.41	18.04 ± 5.71
Week 1					
Control	4.36 ± 1.84	25.14 ± 11.30	36.42 ± 7.16	35.96 ± 8.16	14.62 ± 5.15
ESWT	3.54 ± 1.87	20.62 ± 13.22	31.00 ± 4.06	29.06 ± 3.99	9.82 ± 5.45
Week 4					
Control	4.30 ± 1.87	24.56 ± 11.41	35.98 ± 7.03	34.88 ± 7.49	14.20 ± 5.03
ESWT	3.60 ± 2.16	18.90 ± 13.29	30.28 ± 4.45	28.52 ± 3.61	9.62 ± 6.07
Week 12					
Control	4.28 ± 2.01	24.04 ± 12.34	35.62 ± 7.49	34.04 ± 7.67	14.40 ± 5.57
ESWT	3.54 ± 2.36	18.28 ± 13.50	29.62 ± 4.32	28.24 ± 3.60	9.50 ± 6.03

ESWT, extracorporeal shockwave therapy; NRS, numeric rating scales; BPI, brief pain inventory; SAS, self-rating anxiety scale; SDS, self-rating depression scale; PSQI, Pittsburgh sleep quality index.

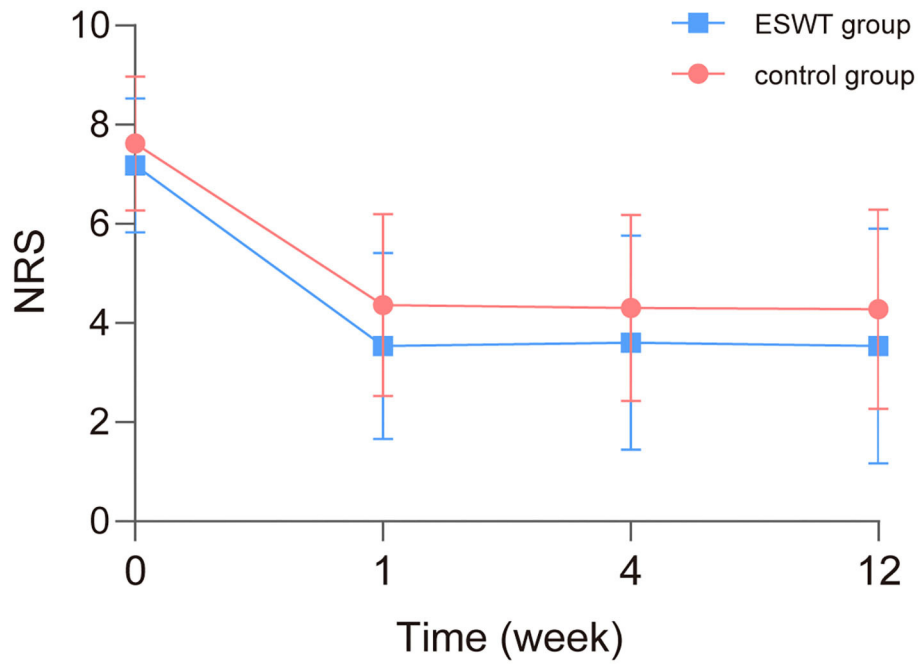

FIGURE 3
Baseline and post-treatment numeric rating scale (NRS) scores. The NRS scores in the ESWT group and control group decreased over time similarly. NRS scores of the ESWT group were statistically lower than the control group.

Discussion

To our knowledge, ectopic activity, central sensitization, and inflammatory mediators might contribute to the pathophysiological mechanisms of neuropathic pain (20, 21). As a common type of neuropathic pain, PHN is related to varicella zoster virus, which remains dormant in the nerve after the primary infection and causes local rash and skin pain after reaction because of weakened immunity (22). The injury of the nerve could lead to the activation and migration of macrophages, release of proinflammatory cytokines, such as tumor necrosis factor α (TNF-α), which might contribute to hyperalgesia (20). In a previous study, ESWT may reduce the plasma levels of TNF-α and substance *P* (23). Therefore, the

TABLE 4 Longitudinal change in scores for intervention related to the control group from baseline through 12 weeks.

Parameter	NRS			BPI			SAS			SDS			PSQI		
	β(SE)	*t*	*P*	*β*(SE)	*t*	*P*	*β*(SE)	*t*	*P*	*β*(SE)	*t*	*P*	*β*(SE)	*t*	*P*
Group															
control	Ref			Ref			Ref			Ref			Ref		
ESWT	−0.589 (0.262)	−2.245	**0.027**	−0.057 (2.002)	−0.028	0.977	−0.485 (1.55)	−0.313	0.755	−5.07 (1.632)	−3.107	**0.003**	−1.153 (0.933)	−1.236	0.220
Time	−0.268 (0.056)	−4.825	**<0.001**	−2.111 (0.317)	−6.653	**<0.001**	−2.542 (0.599)	−4.247	**<0.001**	−1.528 (0.454)	−3.366	**0.001**	−0.632 (0.14)	−4.514	**<0.001**
Sex															
Female	Ref			Ref			Ref			Ref			Ref		
Male	−0.071 (0.268)	−0.265	0.792	0.198 (2.041)	0.097	0.923	−0.102 (1.58)	−0.065	0.948	−0.595 (1.664)	−0.358	0.722	−1.545 (0.951)	−1.624	0.108
PHN nerve segment															
Lumbar segment	Ref			Ref			Ref			Ref			Ref		
Sacral segment	−0.976 (1.086)	−0.898	0.371	2.043 (8.286)	0.247	0.806	7.338 (6.413)	1.144	0.256	−4.484 (6.755)	−0.664	0.508	2.297 (3.862)	0.595	0.554
Cervical segment	−0.21 (0.805)	−0.262	0.794	−3.507 (6.138)	−0.571	0.569	−1.109 (4.751)	−0.233	0.816	−5.756 (5.004)	−1.150	0.253	−2.354 (2.861)	−0.823	0.413
Thoracic segment	−0.568 (0.784)	−0.725	0.470	−2.687 (5.979)	−0.449	0.654	−0.599 (4.627)	−0.129	0.897	−6.648 (4.874)	−1.364	0.176	−2.936 (2.786)	−1.054	0.295
Age	0.032 (0.013)	2.553	**0.012**	0.252 (0.097)	2.600	**0.011**	−0.026 (0.075)	−0.352	0.726	−0.064 (0.079)	−0.804	0.423	0.059 (0.045)	1.313	0.192
BMI	0.009 (0.042)	0.218	0.828	−0.091 (0.319)	−0.284	0.777	−0.046 (0.247)	−0.187	0.852	0.406 (0.26)	1.562	0.122	−0.044 (0.149)	−0.296	0.768
Invasive treatment	0.08 (0.139)	0.572	0.569	0.034 (1.061)	0.032	0.974	−0.564 (0.822)	−0.686	0.494	0.065 (0.865)	0.075	0.941	1.309 (0.495)	2.647	**0.010**

PHN, postherpetic neuralgia; BMI, body mass index; ESWT, extracorporeal shockwave therapy; NRS, numeric rating scale; BPI, brief pain inventory; SAS, self-rating anxiety scale; SDS, self-rating depression scale; PSQI, pittsburgh sleep quality index.

10.3389/fneur.2022.948024

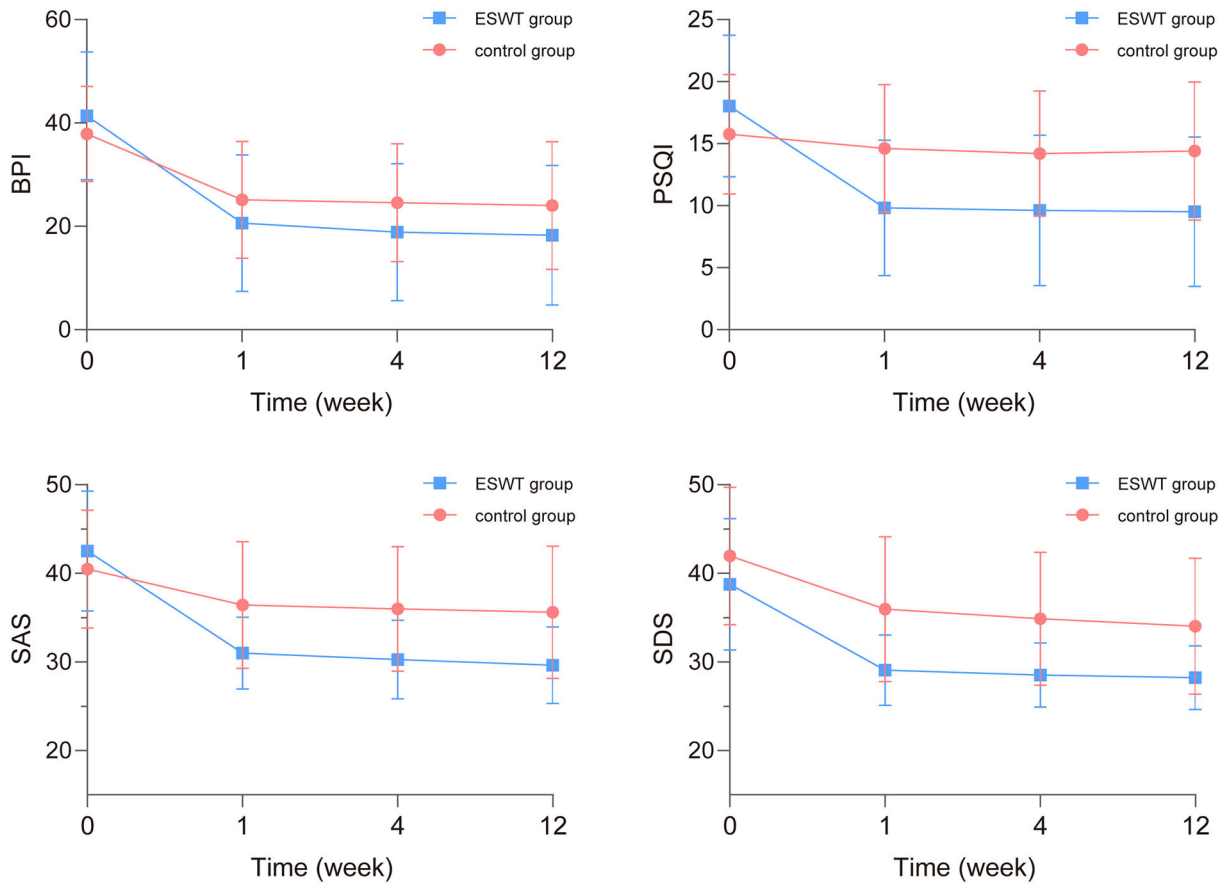

FIGURE 4
The baseline and post-treatment brief pain inventory (BPI), self-rating anxiety scale (SAS), self-rating depression scale (SDS), and pittsburgh sleep quality index (PSQI) scores. The BPI, SAS, SDS, and PSQI scores in the ESWT group and the control group decreased over time while SDS scores in the ESWT group were statistically lower than the control group.

researchers designed this study to confirm the efficacy of ESWT for PHN based on the immune regulation and analgesic effect of ESWT.

In terms of demographic and baseline characteristics, the mean age of the patients was 67.9 (10.8) years in the ESWT group and 67.4 (11.2) years in the control group. Similarly, a previous study suggested that the risk of PHN rose sharply between 50 and 79 years (24). Advanced age was suggested to be a risk factor associated with PHN (4), which may be related to decreased immunity and weakened self-repair ability of the elderly, and the effect of age may differ in gender (25). Furthermore, female patients (54%) were more than male patients (46%) in our study and the risk of PHN was suggested higher in female patients (24). However, another study suggested that there was no significant difference in gender in the development of PHN in patients with Herpes zoster (HZ) (26). The correlation between gender and PHN was still controversial and more evidence is needed. In addition, the most commonly PHN localization was thoracic in our result, which was similar to another study (25).

The reason for patients' being lost to follow-up was that nobody answered the phone. The demographic and baseline characteristics of lost patients indicated that they were significantly older (73.61 years) than patients who finished follow-up (64.94 years). Patients who did not answer the phone might be related to the low smartphone adoption and unskilled use of smartphone in Chinese elderly people (27).

Considering that pain is an emotional experience and sense is the gold standard of pain (28), the researchers selected the NRS score as the primary outcome. In addition to pain, psychological disorders, such as anxiety and depression are common symptoms of patients with PHN, which could worsen pain, cause disability, and effect quality of life and sleep (29, 30). As a result, life quality, psychological state, and sleep quality were assessed as secondary outcomes to evaluate the efficacy of ESWT. The result indicated that there was no time × group interaction in the NRS, BPI, SAS, SDS, and PSQI scores, which indicated that these outcomes in the ESWT group and the control group followed similar trends over time. The NRS,

BPI, SAS, SDS, and PSQI scores were statistically decreased with time in both groups. The NRS scores of the ESWT group were statistically lower than the control group, which may be related to lower sensory nerve conduction velocities, which result in altered peripheral pain perception after ESWT (31). In addition, the molecular neurobiology of chronic pain-induced depression contains genetic modifications, epigenetic modifications, transcription factors, and neurotransmitters (32). The reduced SDS scores and improved depression state in the ESWT group compared with the control group may be associated with analgesic effects and neuroinflammatory alterations caused by ESWT, such as TNF-α, which could be explored in further study. Although the BPI, SAS, PSQI scores in the ESWT group were lower than the control group, the difference was not significant, which might because both groups improved well over time, making the difference unobvious. In this study, we assessed durability of ESWT by evaluating participants during a 12-week follow-up and the result indicated that ESWT could relieve pain and improve depression state. In another study (33), ESWT relieved pain for Morton's neuroma at a 12-week follow-up, which was similar to this study. In addition, durability could be assessed by more measurement methods, such as recurrence rate at the longer follow-up visit, which could be improved in future studies.

Interaction effects for baseline confounders, such as age, sex, BMI, invasive treatment, and PHN nerve segments were explored in this study, and no interaction effect for baseline confounders was observed. PHN duration was not added into this analysis because of some outliers. The result indicated that the age was correlated with the NRS and BPI scores. Hyperalgesia is more common in elderly population, as well as prolonged pain development and less effective medication, which might influence the quality of life (34). Furthermore, the result suggested that invasive treatment was related to PSQI scores. In some studies, pulse-modulated radio frequency affects brain physiology, which might explain the correlation between the invasive treatment and sleep quality (35).

In a systematic review, 20.7% of patients developed transient pain, swelling, petechiae, and other side effect after ESWT (36), which was related to high-dose ESWT, constant energy level, and radial shockwave therapy (36). In our study, ESWT was performed by a skilled therapist to ensure a low dose of energy (1–4 bar) gradually increasing according to patients' reaction, which might be the potential reason of no adverse reactions in this study. The result suggested that ESWT could be a non-invasive and safe treatment if under administration of low-dose, gradually progressively energy.

There are some limitations. Further studies with objective measurement and therapeutic mechanism are needed. Furthermore, a high proportion (31%) of patients were lost to follow-up, which could introduce potential bias. Some old patients had difficulty in telephone use and were lost to follow-up. Optimizing follow-up protocol and extending follow-up may be necessary in the future. In addition, the single-blind method may have the risk of bias. More double-blind and multicenter studies would be needed to confirm the result.

In conclusion, ESWT combined with conventional treatment could relieve pain and improve the psychological state of patients with PHN without serious adverse effects. Further randomized clinical studies are needed to confirm these results, so that ESWT could be used as a safe and effective complementary treatment for PHN.

Data availability statement

The raw data supporting the conclusions of this article will be made available by the authors, without undue reservation.

Ethics statement

The studies involving human participants were reviewed and approved by the Ethics Committee of West China Hospital, Sichuan University, Chengdu, China (No. 2019[814], date of approval: 30th December 2019). The patients/participants provided their written informed consent to participate in this study.

Author contributions

LC designed this randomized controlled trial, collected the data, and wrote the article. PY and LY performed the statistical analysis, revised the manuscript, and provided final approval to the version of the study. AQ performed treatment in this study. TZ revised the manuscript and gave final approval to the version of the study. All authors discussed the results and commented on the manuscript.

Funding

This study is supported by grant 2019HXFH069 from the 1·3·5 project for disciplines of excellence—Clinical Research Incubation Project, West China Hospital, Sichuan University, the grant 2018JY0105 from the Science and Technology Department of Sichuan Province, CYTD17-05 Innovation grant of the Chengdu Medical College and CYFY-GQ01 Startup foundation for Distinguished Scholars of the First Affiliated Hospital of Chengdu Medical College, and 1·3·5 project for disciplines of excellence (ZYJC21008), West China Hospital, Sichuan University (to TZ). These projects will not participate in

any aspect of the trial, including design, data collection, analysis, or interpretation.

Conflict of interest

The authors declare that the research was conducted in the absence of any commercial or financial relationships that could be construed as a potential conflict of interest.

Publisher's note

References

1. Hadley GR, Gayle JA, Ripoll J, Jones MR, Argoff CE, Kaye RJ, et al. Post-herpetic neuralgia: a review. *Curr Pain Headache Rep.* (2016) 20:17. doi: 10.1007/s11916-016-0548-x

2. Saguil A, Kane S, Mercado M, Lauters R. Herpes zoster and postherpetic neuralgia: prevention and management. *Am Fam Phys.* (2017) 96:656–63.

3. Johnson RW, Rice AS. Clinical practice. Postherpetic neuralgia. *N Engl J Med.* (2014) 371:1526–33. doi: 10.1056/NEJMcp1403062

4. Wei S, Li X, Wang H, Liu Q, Shao L. Analysis of the risk factors for postherpetic neuralgia. *Dermatology.* (2019) 235:426–33. doi: 10.1159/000500482

5. Forbes HJ, Thomas SL, Smeeth L, Clayton T, Farmer R, Bhaskaran K, et al. A systematic review and meta-analysis of risk factors for postherpetic neuralgia. *Pain.* (2016) 157:30–54. doi: 10.1097/j.pain.0000000000000307

6. Lin CS, Lin YC, Lao HC, Chen CC. Interventional treatments for postherpetic neuralgia: a systematic review. *Pain Phys.* (2019) 22:209–28. doi: 10.36076/ppj/2019.22.209

7. An S, Li J, Xie W, Yin N, Li Y, Hu Y. Extracorporeal shockwave treatment in knee osteoarthritis: therapeutic effects and possible mechanism. *Biosci Rep.* (2020) 40:BSR20200926. doi: 10.1042/BSR20200926

8. Moen MH, Rayer S, Schipper M, Schmikli S, Weir A, Tol JL, et al. Shockwave treatment for medial tibial stress syndrome in athletes; a prospective controlled study. *Br J Sports Med.* (2012) 46:253–7. doi: 10.1136/bjsm.2010.081992

9. Pinitkwamdee S, Laohajaroensombat S, Orapin J, Woratanarat P. Effectiveness of extracorporeal shockwave therapy in the treatment of chronic insertional achilles tendinopathy. *Foot Ankle Int.* (2020) 41:403–10. doi: 10.1177/1071100719898461

10. Lu Z, Lin G, Reed-Maldonado A, Wang C, Lee YC, Lue TF. Low-intensity extracorporeal shock wave treatment improves erectile function: a systematic review and meta-analysis. *Eur Urol.* (2017) 71:223–33. doi: 10.1016/j.eururo.2016.05.050

11. Cheng JH, Wang CJ. Biological mechanism of shockwave in bone. *Int J Surg.* (2015) 24(Pt B):143–6. doi: 10.1016/j.ijsu.2015.06.059

12. Seok H, Kim SH, Lee SY, Park SW. Extracorporeal shockwave therapy in patients with morton's neuroma a randomized, placebo-controlled trial. *J Am Podiatr Med Assoc.* (2016) 106:93–9. doi: 10.7547/14-131

13. Zhang D, Meng Y, Hai H, Yu XT, Ma YW. Radial extracorporeal shock wave therapy in an individual with primary trigeminal neuralgia: a case report and literature review. *Am J Phys Med Rehabil.* (2018) 97:e42–e5. doi: 10.1097/PHM.0000000000000831

14. Chen YL, Chen KH, Yin TC, Huang TH, Yuen CM, Chung SY, et al. Extracorporeal shock wave therapy effectively prevented diabetic neuropathy. *Am J Transl Res.* (2015) 7:2543–60.

15. Chen KH, Yang CH, Wallace CG, Lin CR, Liu CK, Yin TC, et al. Combination therapy with extracorporeal shock wave and melatonin markedly attenuated neuropathic pain in rat. *Am J Transl Res.* (2017) 9:4593–606.

16. Lee SH Ryu KH, Kim PO, Lee HW, Cho EA, Ahn JH, et al. Efficacy of extracorporeal shockwave therapy in the treatment of postherpetic neuralgia: a pilot study. *Medicine.* (2020) 99:e19516. doi: 10.1097/MD.0000000000019516

17. Chen L, Zhou R, Sun F, Weng Y, Ye L, Yang P. Efficacy and safety of the extracorporeal shockwave therapy in patients with postherpetic neuralgia: study protocol of a randomized controlled trial. *Trials.* (2020) 21:630. doi: 10.1186/s13063-020-04564-z

18. Shengyuan Y, You W, Qi W, Ke M, Jiashuang W, Zhenhe L, et al. Chinese expert consensus on the diagnosis and treatment of postherpetic neuralgia. *Chin J Pain Med.* (2016) 22:161–7.

19. Sun Q, Ye S, Guo C, Zou J. Clinical study of radial shock wave therapy for different types of postherpetic neuralgia. *Chin J Pain Med.* (2020) 26:463–6.

20. Baron R, Binder A, Wasner G. Neuropathic pain: diagnosis, pathophysiological mechanisms, and treatment. *Lancet Neurol.* (2010) 9:807–19. doi: 10.1016/S1474-4422(10)70143-5

21. Sommer C, Leinders M, Üçeyler N. Inflammation in the pathophysiology of neuropathic pain. *Pain.* (2018) 159:595–602. doi: 10.1097/j.pain.0000000000001122

22. Le P, Rothberg M. Herpes zoster infection. *BMJ.* (2019) 364:k5095. doi: 10.1136/bmj.k5095

23. Wang CJ, Huang CC, Yip HK, Yang YJ. Dosage effects of extracorporeal shockwave therapy in early hip necrosis. *Int J Surg.* (2016) 35:179–86. doi: 10.1016/j.ijsu.2016.09.013

24. Forbes HJ, Bhaskaran K, Thomas SL, Smeeth L, Clayton T, Mansfield K, et al. Quantification of risk factors for postherpetic neuralgia in herpes zoster patients: a cohort study. *Neurology.* (2016) 87:94–102. doi: 10.1212/WNL.0000000000002808

25. Amicizia D, Domnich A, Arata L, Zoli D, Zotti CM, Cacello E, et al. The role of age-sex interaction in the development of post-herpetic neuralgia. *Hum Vaccin Immunother.* (2017) 13:376–8. doi: 10.1080/21645515.2017.1264799

26. Wang XX, Zhang Y, Fan BF. Predicting postherpetic neuralgia in patients with herpes zoster by machine learning: a retrospective study. *Pain Ther.* (2020) 9:627–35. doi: 10.1007/s40122-020-00196-y

27. Qi S, Sun Y, Yin P, Zhang H, Wang Z. Mobile phone use and cognitive impairment among elderly Chinese: a national cross-sectional survey study. *Int J Environ Res Public Health.* (2021) 18:5695. doi: 10.3390/ijerph18115695

28. Fillingim RB, Loeser JD, Baron R, Edwards RR. Assessment of chronic pain: domains, methods, and mechanisms. *J Pain.* (2016) 17:T10–20. doi: 10.1016/j.jpain.2015.08.010

29. Du J, Sun G, Ma H, Xiang P, Guo Y, Deng Y, et al. Prevalence and risk factors of anxiety and depression in patients with postherpetic neuralgia: a retrospective study. *Dermatology.* (2020) 2020:1–5. doi: 10.1159/000512190

30. Lerman SF, Rudich Z, Brill S, Shalev H, Shahar G. Longitudinal associations between depression, anxiety, pain, and pain-related disability in chronic pain patients. *Psychosom Med.* (2015) 77:333–41. doi: 10.1097/PSY.0000000000000158

31. Bolt DM, Burba DJ, Hubert JD, Strain GM, Hosgood GL, Henk WG, et al. Determination of functional and morphologic changes in palmar digital nerves after nonfocused extracorporeal shock wave treatment in horses. *Am J Vet Res.* (2004) 65:1714–8. doi: 10.2460/ajvr.2004.65.1714

32. Humo M, Lu H, Yalcin I. The molecular neurobiology of chronic pain-induced depression. *Cell Tissue Res.* (2019) 377:21–43. doi: 10.1007/s00441-019-03003-z

33. Fridman R, Cain JD, Weil L. Extracorporeal shockwave therapy for interdigital neuroma: a randomized, placebo-controlled, double-blind trial. *J Am Podiatr Med Assoc.* (2009) 99:191–3. doi: 10.7547/0980191

34. Tinnirello A, Mazzoleni S, Santi C. Chronic pain in the elderly: mechanisms and distinctive features. *Biomolecules.* (2021) 11:1256. doi: 10.3390/biom11081256

35. Schmid MR, Murbach M, Lustenberger C, Maire M, Kuster N, Achermann P, et al. Sleep EEG alterations: effects of pulsed magnetic fields vs. pulse-modulated radio frequency electromagnetic fields. *J Sleep Res.* (2012) 21:620–9. doi: 10.1111/j.1365-2869.2012.01025.x

36. Roerdink RL, Dietvorst M, van der Zwaard B, van der Worp H, Zwerver J. Complications of extracorporeal shockwave therapy in plantar fasciitis: systematic review. *Int J Surg.* (2017) 46:133–45. doi: 10.1016/j.ijsu.2017.08.587

frontiers | Frontiers in Neurology

TYPE Review
PUBLISHED 01 December 2022
DOI 10.3389/fneur.2022.982223

OPEN ACCESS

EDITED BY
Jixin Liu,
Xidian University, China

REVIEWED BY
Paola Sandroni,
Mayo Clinic, United States
Jun Zhong,
Shanghai Jiao Tong University, China

*CORRESPONDENCE
Xiaoli Feng
363379246@qq.com
Hui Bian
24606341@qq.com

SPECIALTY SECTION
This article was submitted to Headache and Neurogenic Pain, a section of the journal Frontiers in Neurology

RECEIVED 30 June 2022
ACCEPTED 10 November 2022
PUBLISHED 01 December 2022

CITATION
Li S, Feng X and Bian H (2022) Optogenetics: Emerging strategies for neuropathic pain treatment. *Front. Neurol.* 13:982223. doi: 10.3389/fneur.2022.982223

Optogenetics: Emerging strategies for neuropathic pain treatment

Siyu Li[1], Xiaoli Feng[1,2]* and Hui Bian[1]*

[1]Department of Physiology, Faculty of Basic Medical Science, Kunming Medical University, Kunming, Yunnan, China, [2]Key Laboratory of Animal Models and Human Disease Mechanisms of the Chinese Academy of Sciences and Yunnan Province, Kunming Institute of Zoology, Chinese Academy of Sciences, Kunming, Yunnan, China

Neuropathic pain (NP) is a chronic health condition that presents a significant burden on patients, society, and even healthcare systems. However, in recent years, an emerging field in the treatment of neuropathic pain – optogenetic technology has dawned, heralding a new era in the field of medicine, and which has brought with it unlimited possibilities for studying the mechanism of NP and the treatment of research. Optogenetics is a new and growing field that uses the combination of light and molecular genetics for the first time ever. This rare combination is used to control the activity of living cells by expressing photosensitive proteins to visualize signaling events and manipulate cell activity. The treatments for NP are limited and have hardly achieved the desirable efficacy. NP differs from other types of pain, such as nociceptive pain, in that the treatments for NP are far more complex and highly challenging for clinical practice. This review presents the background of optogenetics, current applications in various fields, and the findings of optogenetics in NP. It also elaborates on the basic concepts of neuropathy, therapeutic applications, and the potential of optogenetics from the bench to the bedside in the near future.

KEYWORDS

neuropathic pain, optogenetics, treatment, neuromechanism, potential

Introduction

Neuropathic pain (NP) is defined by the International Association for the Study of Pain (IASP) as the "pain caused by a lesion or disease of the somatosensory nervous system" (1, 2). The definition of NP is very broad based owing to the complexities it presents and should also include in its fold several characteristics and traits of NP (3). However, many definitions put forth to describe NP are still inadequate and even missing appropriate words. NP is caused by neuronal lesions, and treatment methods to bring about an effective cure for this disease are very limited. The prevalence of chronic pain in patients with neuropathological characteristics, according to large-scale epidemiological

findings, is ∼7–10% (4). In recent years, as the growing trend of the global population is toward aging, and as their survival rate has prolonged after the treatment of various diseases, the prevalence of NP too has increased further. Studies have shown that patients with NP often experience anxiety, depression, sleep disorders, and other symptoms (5). These debilitating symptoms seriously affect their quality of life when compared to patients who experience other types of chronic pain, such as: inflammatory pain, fibromyalgia, non-specific low back pain, etc. NP has numerous causes and complex neuromechanisms, so far, that these neuromechanisms of NP have not been fully understood and even remain to be elucidated. This review describes a few common neuromechanism views of NP.

Furthermore, the treatment of NP that is being given to these NP patients still presents a great challenge for clinical practice, as the clinicians have to face a plethora of problems while engaging and handling such patients. Pharmacotherapy is the main and important treatment method to bring about a drastic cure in these patients, but the current treatment only produces limited remission (30–50%) that too only for a portion of patients (6). Pharmacotherapy also brings along with it the problem of drug dose and side effects which could also affect these patients. Non-pharmacological treatments have small side effects, but some treatments lack clinically reliable evidences, while in some cases, the combination of multiple drugs or treatments can achieve better results. In recent years, an emerging field of neurogenic pain treatment – optogenetics is the newest and most recent treatment method for the treatment of NP and has started making its imprint in treating NP patients, and there is so much unlimited untapped potential for the treatment of NP it offers to treat patients. Thanks to the development of photogenetics, researchers can now control the treatment-related activities in defined neuronal populations and projections, while examining their effects on behavior and physiology. Unlike pharmacology and disease-based intervention, optogenetics also opens up causal investigation and specificity for the rapid time scale of natural nervous system communication (7, 8).

The results of many research works corroborate the role of optogenetics and have also put forth a certain affirmation of the role of optogenetics. In this review, we provide an overview of the basic concepts of optogenetics and the active application of optogenetic techniques in the treatment of NP in recent years.

Neuromechanism for NP

Neuropathic pain (NP), which is triggered by the impaired somatosensory system, attributes its origin to various health-related causes. These causes are diverse, arising from a wide gamut of diseases, such as diabetes, metabolic diseases, tumors, spinal cord injury, etc. After a nerve injury takes place, the nerve fibers change at multiple levels, resulting in disturbances during transmission to the brain and spinal cord, and involves issues such as altered pain thresholds and signal effects (9). There are several points regarding the pathogenesis of NP that merit our attention and need to be studied in depth.

Neuronal activity

Abnormalities in neuronal activity

Changes in nerve fiber secretions are closely associated with pain. As regards to neurons, a popular view was held to express the fact that nociceptive afferents inhibit the flow of harmful information from the spinal cord into the brain by activating spinal inhibitory neurons and that the imbalance between excitatory and inhibitory neurotransmission serves as the source of ectopic pain (10). The hypothesis has been confirmed by many studies in recent decades, with increasing evidence suggesting that the balance between excitation and inhibition in spinal circuits is disrupted in NP (11). This reasoning was corroborated further by experimental studies, which were conducted to prove that the transplantation of GABAergic precursor cells into the dorsal spinal horn reduced neurological mechanical pain (12). At present, the research dynamics of the mechanism of neurons in neuronal circuits are relatively active, and the results of the research works are relatively rich in values and data. However, it has not been explained accurately in which neuronal circuits do the neurons participate.

Ion channels

Transient receptor potential (TRP) family of ion channels and other ion channels, such as acid-sensing ion channels adenosine triphosphate (ATP)-gated purine channel [ATP-PRX (peroxiredoxin)], has highly specific involvement in various types of nociceptive stimulations. At this time, different types of sodium channels play a significant role, by magnifying the point of the receptor, so as to trigger the depolarization of the action potential. Notably, these ion channels are all not only strongly regulated by post-translational modifications and transcriptional levels, but can also be deregulated upon nerve damage. However, the present study does not prove the main connection of TRP channels with NP syndrome, but pharmacologically related studies prove that blocking TRP channels in rodent models relieves neuropathic allergy (13). Studies have shown that knockout mouse sodium channels in root ganglion neurons effectively slow down pain (14, 15). This suggests that there is a connection between NP and ion channels and that NP is strongly associated with ion channels. For instance, several studies have shown that downregulation of potassium channels was observed in the experimental animal models of NP (16). Overexpression or downregulation of sodium channels is closely related to threshold and ectopic activity, which also provides a huge therapeutic space for subsequent intervention of sodium channel blockers.

Immune cells

Here, we focus on some of the most recent studies related to NP. T cells in immune cells have a very important role to play, and studies have shown that mice lacking T cells completely lack the ability to produce neuropathic abnormal pain after a nerve injury (17). Furthermore, other studies have demonstrated that angiotensin 2 mediates the attenuation of neurological ectopic pain in the expression of invading macrophages at the site of nerve injury (18). These studies suggest a great therapeutic potential of immune cells in targeting NP and warrant further exploration.

Mitochondrial factors

Notably, the dysfunction of mitochondrial function in peripheral neurons can manifest in various NP types in different animal models (19, 20), and this reasoning reflects the important role of mitochondria in NP. Mitochondria are closely related to the production of reactive oxygen species (ROS), and any mitochondrial dysfunction leads to an energy deficiency, triggering off many potential crises. Mitochondria and reactive oxygen species (ROS) have only recently emerged in the field of NP and have aroused the widespread interest of researchers in their direction. Studies have shown that drugs that cause a nitrite breakdown also serve the function to reduce neuropathic ectopic pain during chemotherapy for cancer patients (21). Passakorn et al. (22) demonstrated an additional benefit by supplementing coenzyme Q10 (CoQ10) on pain relief in patients with pregabalin-treated fibromyalgia, which may be achieved by improving mitochondrial function, reducing inflammation, and reducing brain activity. In conclusion, mitochondria have a potential therapeutic space for the treatment of interventional NP, but their more precise mechanism needs more intensive investigation.

We describe several neural mechanisms associated with NP that are currently well recognized. Actually, the neuromechanisms underlying NP remain unexplored, because of its diverse etiology and numerous systems involved. Moreover, the transmission of pain signals is regulated by complex large neural networks, making it more difficult to carry out research on neural mechanisms. Of course, the views discussed previously also bring a direction toward new therapy in the treatment of NP, because optogenetics can also help with research into NP pathways.

General treatment of neuropathic pain

At present, the treatment approach of NP is mainly divided into pharmacotherapy and non-pharmacotherapy types, and both the treatment methods have their own inherent advantages and disadvantages. A broad consensus has been reached on the drug treatment to be administered to the patient (23), as this drug treatment is mostly based on the urgency and severity of the patient's condition and the specific course of the disease. Hence, generally drugs are divided into three echelons. However, either tricyclic antidepressants or opioid analgesics, as the first choice of drugs (24), or the third-line drugs, such as cetin, NMDA (N-methyl-D-aspartate) receptor antagonists, and local capsaicin (25, 26), have been greatly restricted in their usage due to the clinical side effects caused by them, and the clinical response is general. With regard to the non-pharmacotherapy type, whether it is traditional acupuncture (27, 28), physical therapy (29, 30), transcutaneous electrical nerve stimulation (31–33) or the virtual reality (VR) (34), spinal cord stimulation (35, 36) and other treatment methods, although its side effects have been greatly reduced (37, 38)and some results have even been achieved by pharmacotherapy, the effect of its clinical treatment has not yet brought the effect of the much-desired ideal treatment to patients. However, the clinical efficacy of some therapeutic methods still needs clarity (39), and even the relevant therapeutic mechanism also needs to be explicit (40). In a word, the therapeutic mechanism and efficacy of these non-pharmacotherapy options in the field of neuropathic pain still need to be corroborated by a large number of basic experiments and clinical experiments.

As we all know, optogenetics has become a new technology in recent years, which is helpful to explore the mechanism of most diseases. We notice that this technology still has huge untapped potential and offers scope for utilizing the unlimited prospects in the application of neurological diseases and other diseases in the future.

Background in optogenetics

Optogenetics is an emerging field, which boasts of a hitherto unknown, amazing combination of optics and genetics. Optogenetics mainly acts on the corresponding proteins by currents that are generated by transfer to photosensitive proteins (41, 42). Optogenetic activators, such as channelrhodopsin, halorhodopsin (halogenated rhodopsin), and archaerhodopsin (Arch)., are used to control neurons, and the monitoring of neuronal activity is performed through genetically encoded ions (e.g., calcium) or membrane voltage sensors. The effectors in this system are light, with the advantage of working at high spatial and temporal resolution at multiple wavelengths and locations (43, 44). The first step in the development of optogenetic techniques was started way back in 1971 when Oesterhelt and Stoeckenius discovered that the bacterium rhodopsin, a purulentin from the halogen violet membrane of Halogen bacillus, could pump protons under light (45). Later, Sugiyama and Mukohata identified another member of the opsin family in 1984 – halogenated rhodopsin (46), while Nagel et al.

identified channelrhodopsin purpurulite in 2002 (47). A major breakthrough was made in the field of optogenetics after the discovery that neurons respond to light when microbial opsin genes were introduced without any other component (48).

Optogenetics includes three main optogenetic tools, including (1) photoactivated proteins; (2) light; (3) delivery mode, virus-mediated gene delivery system is currently one of the most commonly used methods. When applying optogenetic techniques, we benefit from a number of advantages. A significant advantage one can derive from optogenetics is that rapid activation and silencing of expressed proteins can be achieved without the use of chemicals (41, 49). Optogenetic techniques are currently receiving widespread attention from researchers and are actively being applied in various fields. Photogenetics is the result of the fruitful combination of optics and genetic engineering, which maximizes the advantages of each discipline to the fullest extent possible. These advantages are multifold such as optical control by manipulating the wavelength and light intensity on the millisecond time scale, as well as specific gene expression and gene product transport with subcellular accuracy. It is not possible to realize this kind of fine adjustment by traditional methods. Therefore, optogenetics technology has brought about a revolution to neuroscience (50).

Applications of optogenetics

Optogenetics has been vigorously developing in recent years, such as giving light, facility to be controlled in real time, and becoming closer to the natural environment (51, 52). One branch of medicine that has benefited the most in the field of medicine from optogenetics is ophthalmology. In vision studies, optogenetics makes it possible to impart and infuse light sensitivity to different retinal cell types, thus providing a new perspective on vision restoration in various inherited retinal degenerative diseases. Bi et al. (53) first showed that after complete photoreceptor degeneration, light sensitivity can be restored by the expression of channel rhodopsin-2 (ChR2) in retinal ganglion cells, and a number of other studies have since proven this scientific advancement (54–57). Optogenetics has also been widely used in the treatment of neurological diseases in recent years. Alzheimer's disease (AD) is characterized by the presence of amyloid β (Aβ) plaques and neurofiber tau tangles (58), Lim et al. (59) developed fluorescently labeled optogenetically activated Aβ peptides that can oligomerize *in vitro* during light exposure. Kaur et al. (60) had used a similar method to produce Aβ aggregations *in vivo*. There are also studies that suggest that optogenetic inhibition of pyramidal cells (PCs) in the CA1 region of the dorsal side of the hippocampus (61) or by deinsuppression of somatostatin-positive (SST) cells (62) reversibly disrupts memory acquisition. In the field of neuroscience, scientists have found that optogenetic techniques reduce circuit noise associated with schizophrenia to enhance the performance of cortical circuit (63, 64). Optogenetics shows great potential in various fields, and of course, NP is no exception.

The combination of optogenetics and electrophysiology has also brought about sweeping reforms in the field of neuroscience. Traditional *in vivo* electrophysiology is also difficult to relate to specific cell types defined by genetics or connectivity, so it serves as an important and universal technology integration to combine *in vivo* electrophysiological recording with optogenetics. It is reported that using this method, the activation of the basolateral amygdala (BLA) stimulates the nucleus accumbens (NAc) to drive reward seeking (65). The activation of GABAergic cells from the extended amygdala inhibits the lateral hypothalamic neurons, leading to an increased food consumption. In addition, the medial prefrontal cortex (mPFC) requires ventral hippocampus input to encode the target position (66) and the aversion (open) and safety (closed) spaces (67) in the elevated maze. Similar neurological events can occur across circuits; for instance, the bed nucleus of the stria terminalis (BNST) uses the BLA input to code the enclosed space in the same maze (68). The combination of electrophysiology and photogenetics has unlimited potential in the field of neuroscience. However, neuropathic pain is an extremely complex disease, with complex symptoms and causes. The mechanism and treatment of neuropathic pain still merit a lot of work to be done by researchers to explore their unknown potential.

Optogenetics in neuropathic pain

Recently, optogenetic combination with NP has also been developing increasingly. When compared to conventional electrical stimulation, optogenetics eliminates the critical step of placing electrodes in the brain with a relatively homogeneous group of neurons (69). But the millisecond-level time accuracy of electrical stimulation displayed by optogenetic techniques stands unmatched. The application of optogenetics in the field of neuropathy has shown us the great potential of utilizing optogenetics in the treatment of NP and the exploration of mechanisms.

In recent years, a large number of studies have combined this technique of optogenetics in the field of NP and have brought to light various novel features and potential of optogenetics in NP treatment by way of new methods for pain relief. For example: in an earlier study, Daou et al. (70) demonstrated the role of optogenetics in suppressing pain using a binary genetic approach, delivering ChR2 channels to peripheral nociceptors in the Nav1.8-Cre transgenic mouse line. Notably, in their experiments, the free-moving small pains were caused to move in a non-invasive and remote manner. In the two other studies, in the NP model, *in vivo* stimulation of the halogenated rhodopsin (eNpHR3.0) channel of the yellow photosensitive

third-generation chloride pump successfully prevented pain (71, 72), thus highlighting the therapeutic potential of optogenetics. In studies of neuropathic pain-like behaviors controlled by the parabrachial nucleus circuit, optogenetic activation of glutamatergic or inhibition of γ-aminobutyric acid (GABA)-capable lateral parabrachial nucleus (LPBN) neurons induced neuropathic pain-like behavior in young mice (73). The medial prefrontal cortex (mPFC) is a region of the brain that is involved in the emotional component of pain that undergoes plasticity during the development of chronic pain. Dopamine (DA) is the key neuromodulator in the middle cortical circuit that regulates working memory and loathing. In this study on brain pathways, the results demonstrated that phase activation of DA input from the ventral cover area (VTA) to mPFC reduced mechanical hypersensitivity in NP states (74). The central amygdala (CeA) in the brain is also an important area for mood control, and the results of Hua et al. show that the optogenetic activation of CeA effectively inhibits the reflex and self-healing behaviors caused by pain in sensory patterns and eliminates the mechanical (high) sensitivity induced by NP (75). Similar results were obtained in another study of this region (amygdala), where optogenetic manipulation of adrenocorticotropic hormone-releasing factor (central amygdala corticotropin-releasing factor (CeA-CRF)) neurons in CeA modulates NP and controls pain and anxiety-like behavior in rats (76). Gadotti et al. (77) confirmed that optogenetic techniques could also be operated through modulation of the medial prefrontal cortex function to treat NP. Xiong et al. (78) have found that altering neuronal properties and normalizing their cortical excitability relieves pain. Stimulation of the anterior cingulate cortex enhances excitatory synaptic transmission of the spinal cord and leads to pain hypersensitivity responses. Studies have demonstrated that inhibition of this type by optogenetic methods can produce an anti-injury effect and can also reduce nerve damage caused by synaptic enhancement (79). Recently, there have been many reports of successful control of pain in animal models mediated by optogenetic techniques (80–83). These experimental studies suggest the infinite potential of optogenetics in NP treatment. Optogenetic precision, being controllable, and deliberate selectivity are its advantages (84).

The real challenge of optogenetics is to target the mechanisms of NP, pinpoint its damaged nociceptive neurons, understand nociceptors (as the main subset of units of pain, with receptors and ion channels that can detect stimuli for potential damage) and circuits. Optogenetics involves inducing neuronal expression of light-activated membrane proteins, the activation of which can directly turn on or off neurons by depolarization (e.g., channel rhodopsin-2, ChR2) or hyperpolarization (e.g., haloopeopreum purpurulite), respectively, and opening a cascade of G protein-coupled receptor (GPCR) signals (85). Therefore, it is necessary to understand the genetics of pathological neurons compared with normal functional neural circuits. The complete transcriptome of trigeminal ganglia (TG) and dorsal root ganglia (DRG) in adult mice was analyzed to gain insight into the expression of ion channels and G-protein-coupled receptors (GPCRs) under physiological and pathophysiological conditions. This analysis suggests that given the complex etiologies of ganglion pathological changes, conventional strategies to inhibit individual ion channels or inflammatory processes are less useful (86–88).

All in all, optogenetics presents both an opportunity and a challenge. For example, optogenetics is currently restricted to experiments on animals only, so how can it be extended to experiments conducted on human beings? Optogenetic technology can be effectively implemented in rodents most of the time, but it has been difficult to effectively implement this optogenetic technology in primates for many years now. The reason for this difficulty is attributed to the all-time flexibility of primates, which makes it even more difficult to translate experiments into clinical practice. There are also limitations regarding the way photosensitive proteins are entered and the length of optogenetics to be maintained. Is there a way to make the effect longer or even permanent? There is no denying the fact that addressing these questions presents great challenges, and this also requires further in-depth investigation of optogenetics. It is worth noting that optogenetic techniques are crucial in terms of both the pathways, mechanisms, and treatment of NP. Identifying pain nociceptors through the spatiotemporality of optogenetic techniques and identifying damaged neurons is a breakthrough step in understanding the mechanism by which God carries out pain, and provides a crucial role for later treatment.

Conclusion and outlook

Neuropathic pain is a complex, comprehensive disorder that is extremely challenging to treat clinically, owing to the complexities that surface during NP treatment. The treatments of NP are a major challenge for effective clinical practice. Pharmacotherapy is a common clinical method to relieve pain in patients, but we cannot ignore the side effects of the drug treatment, and its efficacy has not achieved the ideal effect. Non-pharmacological treatments have small side effects, but most of their efficacy lacks reliable clinical evidence. The combination of treatment methods may be a good way to improve the efficacy, as the patients stand to benefit from the cumulative effect of both these treatment methods. It has been clinically confirmed that drug treatment with some traditional treatments can not only increase the efficacy, but also reduce the side effects. It can be further explored in the combination of multiple treatment methods.

In summary, there are uncertainties in both pharmacological and non-pharmacological treatments, and although the efficacy of some treatment methods is clinically affirmed, further research is still needed. Optogenetics, as an emerging field

of NP, has unlimited potential in terms of the mechanism pathways and treatment of NP. Through the spatiotemporality of optogenetic techniques, the identification and localization of pain receptors, damaged neurons, which helps us to further explore pain transmission pathways. In addition, optogenetic techniques are now widely used in various fields, including the treatment of NP. According to the previous description, optogenetic techniques have been affirmed for their efficacy in relieving pain, but there are still issues that need to be further explored. For example, optogenetics is currently limited to animal experiments, so how can it be applied to human beings? How is the light-sensitive protein entered? The length of optogenetics to be maintained is also a limitation. Is there a way to make the effect longer or even permanent? There is no denying the fact that addressing these questions presents great challenges, and this also requires further investigation of optogenetics.

Generally, before performing clinical experiments on human beings, we usually conduct experiments first on non-human primates that bear closeness to humans both in evolution and in development. The implementation of optogenetic technology is good and successful in rodents, but we face tough challenges while applying this technology to primates, which also signifies the application of optogenetic technology to clinical practice. Second, optogenetic techniques may be used in combination with other fields (such as slice electrophysiology (89)), to investigate the mechanisms of neuropathic pain further. Examples include changes in the network of connections in brain regions related to NP, and pain pathways involved in nerve pain. The combination of optogenetic techniques with other techniques is going to work wonders and is thus likely to help explore the underlying mechanisms of NP even further. At the same time, this technology also has great potential in exploring the potential targets of NP treatment and the development and efficacy of potential drugs. If this technique can identify its damaged pain neurons, it provides a potential therapeutic target and it marks a breakthrough in neuroscience. Optogenetics technology is going to be of immense help to medical fraternity and patients by being able to judge the positioning of drugs after they enter the body through their spatial advantages. This in turn helps to pave the way to explore the mechanism of action of drugs and the possible mechanism of their own diseases, and then to judge the efficacy of their drugs. The application of this technology also reduces the side effects consequent to the use of many clinical drugs, and the above conditions are possible research directions in NP optogenetics in the future and have great potential.

In a word, optogenetics brings with it a reliable promise for the treatment of NP. After analyzing the various advantages of optogenetics for the treatment of NP, we can emphatically state that the therapeutic prospects of optogenetic technology for NP are certain and deserve promotion and exploration for extensive experimental research.

Author contributions

SL, XF, and HB have participated sufficiently to accept responsibility for the content of the manuscript. SL wrote the draft of the article. XF and HB played a critical role in article revision. All authors contributed to the article and approved the submitted version.

Funding

This work was supported by the Kunming Medical Joint Project-Key Project (202101AY070001-001), Kunming Medical University 100 Young and Middle-Aged Academic and Technical Backbone Training Program (J13326055), and Yunnan Province Ten Thousand Talents Program Young Top Talent Special Project (YUWR-QNBJ-2019-043).

Conflict of interest

The authors declare that the research was conducted in the absence of any commercial or financial relationships that could be construed as a potential conflict of interest.

Publisher's note

References

1. Jensen TS, Baron R, Haanpää M, Kalso E, Loeser JD, Rice AS, et al. A new definition of neuropathic pain. *Pain.* (2011) 152:2204–5. doi: 10.1016/j.pain.2011.06.017

2. Bouhassira D. Neuropathic pain: definition, assessment, and epidemiology. *Rev Neurol.* (2019) 175(1-2):16–25. doi: 10.1016/j.neurol.2018.09.016

3. National Institute of Neurological Disorders and Stroke (NINDS). *Wiley Encyclopedia of Clinical Trials*. American: American Cancer Society (2008).

4. St John Smith E. Advances in understanding nociception and neuropathic pain. *J Neurol.* (2018) 265:231–8. doi: 10.1007/s00415-017-8641-6

5. Akram MJ, Malik AN. Frequency of chronic neuropathic pain and its association with depression in the elderly in Pakistan. *J Pak Med Assoc.* (2019) 69:1907–9. doi: 10.5455/JPMA.302642229

6. Finnerup NB, Attal N, Haroutounian S, McNicol E, Baron R, Dworkin RH, et al. Pharmacotherapy for neuropathic pain in adults: a systematic review and meta-analysis. *Lancet Neurol.* (2015) 14:162–73. doi: 10.1016/S1474-4422(14)70251-0

7. Deisseroth K. Optogenetics: 10 years of microbial opsins in neuroscience. *Nat Neurosci.* (2015) 18:1213–25. doi: 10.1038/nn.4091

8. Grosenick L, Marshel JH, Deisseroth K. Closed-loop and activity-guided optogenetic control. *Neuron.* (2015) 86:106–39. doi: 10.1016/j.neuron.2015.03.034

9. Meacham K, Shepherd A, Mohapatra DP, Haroutounian S. Neuropathic pain: central vs. peripheral mechanisms. *Curr Pain Headache Rep.* (2017) 21:28. doi: 10.1007/s11916-017-0629-5

10. Melzack R, Wall PD. Pain mechanisms: a new theory. *Science.* (1965) 150:971–9. doi: 10.1126/science.150.3699.971

11. Laird JM, Bennett GJ. An electrophysiological study of dorsal horn neurons in the spinal cord of rats with an experimental peripheral neuropathy. *J Neurophysiol.* (1993) 69:2072–85. doi: 10.1152/jn.1993.69.6.2072

12. Bráz JM, Sharif-Naeini R, Vogt D, Kriegstein A, Alvarez-Buylla A, Rubenstein JL, et al. Forebrain GABAergic neuron precursors integrate into adult spinal cord and reduce injury-induced neuropathic pain. *Neuron.* (2012) 74:663–75. doi: 10.1016/j.neuron.2012.02.033

13. Basso L, Altier C. Transient Receptor Potential Channels in neuropathic pain. *Curr Opin Pharmacol.* (2017) 32:9–15. doi: 10.1016/j.coph.2016.10.002

14. Li Y, North RY, Rhines LD, Tatsui CE, Rao G, Edwards DD, et al. DRG voltage-gated sodium channel 17 is upregulated in paclitaxel-induced neuropathy in rats and in humans with neuropathic pain. *J Neurosci.* (2018) 38:1124–36. doi: 10.1523/JNEUROSCI.0899-17.2017

15. Hameed S. Na(v)1.7 and Na(v)1.8: Role in the pathophysiology of pain. *Mol Pain.* (2019) 15:1744806919858801. doi: 10.1177/1744806919858801

16. Abd-Elsayed A, Jackson M, Gu SL, Fiala K, Gu J. Neuropathic pain and Kv7 voltage-gated potassium channels: the potential role of Kv7 activators in the treatment of neuropathic pain. *Mol Pain.* (2019) 15:1744806919864256. doi: 10.1177/1744806919864256

17. Vicuña L, Strochlic DE, Latremoliere A, Bali KK, Simonetti M, Husainie D, et al. The serine protease inhibitor SerpinA3N attenuates neuropathic pain by inhibiting T cell-derived leukocyte elastase. *Nat Med.* (2015) 21:518–23. doi: 10.1038/nm.3852

18. Shepherd AJ, Mickle AD, Golden JP, Mack MR, Halabi CM, De Kloet AD, et al. Macrophage angiotensin II type 2 receptor triggers neuropathic pain. *Proc Natl Acad Sci U S A.* (2018) 115:E8057–e8066. doi: 10.1073/pnas.1721815115

19. Bennett GJ, Doyle T, Salvemini D. Mitotoxicity in distal symmetrical sensory peripheral neuropathies. *Nat Rev Neurol.* (2014) 10:326–36. doi: 10.1038/nrneurol.2014.77

20. Trevisan G, Materazzi S, Fusi C, Altomare A, Aldini G, Lodovici M, et al. Novel therapeutic strategy to prevent chemotherapy-induced persistent sensory neuropathy by TRPA1 blockade. *Cancer Res.* (2013) 73:3120–31. doi: 10.1158/0008-5472.CAN-12-4370

21. Janes K, Doyle T, Bryant L, Esposito E, Cuzzocrea S, Ryerse J, et al. Bioenergetic deficits in peripheral nerve sensory axons during chemotherapy-induced neuropathic pain resulting from peroxynitrite-mediated post-translational nitration of mitochondrial superoxide dismutase. *Pain.* (2013) 154:2432–40. doi: 10.1016/j.pain.2013.07.032

22. Sawaddiruk P, Apaijai N, Paiboonworachat S, Kaewchur T, Kasitanon N, Jaiwongkam T, et al. Coenzyme Q10 supplementation alleviates pain in pregabalin-treated fibromyalgia patients via reducing brain activity and mitochondrial dysfunction. *Free Radic Res.* (2019) 53:901–9. doi: 10.1080/10715762.2019.1645955

23. Deng Y, Luo L, Hu Y, Fang K, Liu J. Clinical practice guidelines for the management of neuropathic pain: a systematic review. *BMC Anesthesiol.* (2016) 16:12. doi: 10.1186/s12871-015-0150-5

24. Vranken JH. Elucidation of pathophysiology and treatment of neuropathic pain. *Cent Nerv Syst Agents Med Chem.* (2012) 12:304–14. doi: 10.2174/187152412803760645

25. Centre for Clinical Practice at N National Institute for Health and Care Excellence. Clinical Guidelines In *Neuropathic Pain: The Pharmacological Management of Neuropathic Pain in Adults in Non-specialist Settings*. London: National Institute for Health and Care Excellence. (2013).

26. Dworkin RH. O'connor AB, Backonja M, Farrar JT, Finnerup NB, Jensen TS, et al. Pharmacologic management of neuropathic pain: evidence-based recommendations. *Pain.* (2007) 132:237–51. doi: 10.1016/j.pain.2007.08.033

27. Choi DC, Lee JY, Lim EJ, Baik HH, Oh TH, Yune TY. Inhibition of ROS-induced p38MAPK and ERK activation in microglia by acupuncture relieves neuropathic pain after spinal cord injury in rats. *Exp Neurol.* (2012) 236:268–82. doi: 10.1016/j.expneurol.2012.05.014

28. Lee JY, Choi DC, Oh TH, Yune TY. Analgesic effect of acupuncture is mediated via inhibition of JNK activation in astrocytes after spinal cord injury. *PLoS ONE.* (2013) 8:e73948. doi: 10.1371/journal.pone.0073948

29. Nijs J, Apeldoorn A, Hallegraeff H, Clark J, Smeets R, Malfliet A, et al. Low back pain: guidelines for the clinical classification of predominant neuropathic, nociceptive, or central sensitization pain. *Pain Physician.* (2015) 18:E333–46. doi: 10.36076/ppj.2015/18/E333

30. Ostelo RW. Physiotherapy management of sciatica. *J Physiother.* (2020) 66:83–8. doi: 10.1016/j.jphys.2020.03.005

31. DeSantana JM, Da Silva LF, De Resende MA, Sluka KA. Transcutaneous electrical nerve stimulation at both high and low frequencies activates ventrolateral periaqueductal grey to decrease mechanical hyperalgesia in arthritic rats. *Neuroscience.* (2009) 163:1233–41. doi: 10.1016/j.neuroscience.2009.06.056

32. Kalra A, Urban MO, Sluka KA. Blockade of opioid receptors in rostral ventral medulla prevents antihyperalgesia produced by transcutaneous electrical nerve stimulation (TENS). *J Pharmacol Exp Ther.* (2001) 298:257–63. doi: 10.1002/tox.22084

33. Sluka KA, Deacon M, Stibal A, Strissel S, Terpstra A. Spinal blockade of opioid receptors prevents the analgesia produced by TENS in arthritic rats. *J Pharmacol Exp Ther.* (1999) 289:840–6.

34. Chi B, Chau B, Yeo E, Ta P. Virtual reality for spinal cord injury-associated neuropathic pain: systematic review. *Ann Phys Rehabil Med.* (2019) 62:49–57. doi: 10.1016/j.rehab.2018.09.006

35. Kapural L, Yu C, Doust MW, Gliner BE, Vallejo R. Sitzman BT,et al. Novel 10-kHz high-frequency therapy (HF10 Therapy) is superior to traditional low-frequency spinal cord stimulation for the treatment of chronic back and leg pain: the SENZA-RCT randomized controlled trial. *Anesthesiology.* (2015) 123:851–60. doi: 10.1097/ALN.0000000000000774

36. Kapural L, Yu C, Doust MW, Gliner BE, Vallejo R, Sitzman BT, et al. Comparison of 10-kHz high-frequency and traditional low-frequency spinal cord stimulation for the treatment of chronic back and leg pain: 24-month results from a multicenter, randomized, controlled pivotal trial. *Neurosurgery.* (2016) 79:667–77. doi: 10.1227/NEU.0000000000001418

37. Gwak YS, Kim HY, Lee BH, Yang CH. Combined approaches for the relief of spinal cord injury-induced neuropathic pain. *Complement Ther Med.* (2016) 25:27–33. doi: 10.1016/j.ctim.2015.12.021

38. Li Y, Yin C, Li X, Liu B, Wang J, Zheng X, et al. Electroacupuncture alleviates paclitaxel-induced peripheral neuropathic pain in rats via suppressing TLR4 signaling and TRPV1 upregulation in sensory neurons. *Int J Mol Sci.* (2019) 20:5917. doi: 10.3390/ijms20235917

39. Sdrulla AD, Guan Y, SRaja SN. Spinal cord stimulation: clinical efficacy and potential mechanisms. *Pain Pract.* (2018) 18:1048–67. doi: 10.1111/papr.12692

40. Guy SD, Mehta S, Casalino A, Côté I, Kras-Dupuis A, Moulin DE, et al. The Canpain SCI clinical practice guidelines for rehabilitation management of neuropathic pain after spinal cord: recommendations for treatment. *Spinal Cord.* (2016) 54 Suppl 1:S14–23. doi: 10.1038/sc.2016.90

41. Berndt A, Lee SY, Wietek J, Ramakrishnan C, Steinberg EE, Rashid AJ, et al. Structural foundations of optogenetics: determinants of channelrhodopsin ion selectivity. *Proc Natl Acad Sci U S A.* (2016) 113:822–9. doi: 10.1073/pnas.1523341113

42. Boyden ES. Optogenetics and the future of neuroscience. *Nat Neurosci.* (2015) 18:1200–1. doi: 10.1038/nn.4094

43. Häusser M. Optogenetics: the age of light. *Nat Methods.* (2014) 11:1012–4. doi: 10.1038/nmeth.3111

44. Duebel JK, Marazova, Sahel A. *Optogenetics Curr Opin Ophthalmol.* (2015) 26:226–32. doi: 10.1097/ICU.0000000000000140

45. Oesterhelt D, Stoeckenius W. Rhodopsin-like protein from the purple membrane of Halobacterium halobium. *Nat New Biol.* (1971) 233:149–52. doi: 10.1038/newbio233149a0

46. Sugiyama Y, Mukohata Y. Isolation and characterization of halorhodopsin from Halobacterium halobium. *J Biochem.* (1984) 96:413–20. doi: 10.1093/oxfordjournals.jbchem.a134852

47. Nagel G, Ollig D, Fuhrmann M, Kateriya S, Musti AM, Bamberg E, et al. Channelrhodopsin-1: a light-gated proton channel in green algae. *Science.* (2002) 296:2395–8. doi: 10.1126/science.1072068

48. Boyden ES, Zhang F, Bamberg E, Nagel G, Deisseroth K, et al. Millisecond-timescale, genetically targeted optical control

of neural activity. *Nat Neurosci.* (2005) 8:1263–8. doi: 10.1038/nn1525

49. Rost BR, Schneider-Warme F, Schmitz D. Hegemann P. Optogenetic tools for subcellular applications in neuroscience. *Neuron.* (2017) 96:572–603. doi: 10.1016/j.neuron.2017.09.047

50. Shirai F, Hayashi-Takagi A. Optogenetics: applications in psychiatric research. *Psychiatry Clin Neurosci.* (2017) 71:363–72. doi: 10.1111/pcn.12516

51. Szabo V, Ventalon C, De Sars V, Bradley J, Emiliani V. Spatially selective holographic photoactivation and functional fluorescence imaging in freely behaving mice with a fiberscope. *Neuron.* (2014) 84:1157–69. doi: 10.1016/j.neuron.2014.11.005

52. Gagnon-Turcotte G, LeChasseur Y, Bories C, Messaddeq Y, De Koninck Y, Gosselin B, et al. Wireless headstage for combined optogenetics and multichannel electrophysiological recording. *IEEE Trans Biomed Circuits Syst.* (2017) 11:1–14. doi: 10.1109/TBCAS.2016.2547864

53. Bi A, Cui J, Ma YP, Olshevskaya E, Pu M, Dizhoor AM, et al. Ectopic expression of a microbial-type rhodopsin restores visual responses in mice with photoreceptor degeneration. *Neuron.* (2006) 50:23–33. doi: 10.1016/j.neuron.2006.02.026

54. Zhang Y, Ivanova E, Bi A, Pan ZH. Ectopic expression of multiple microbial rhodopsins restores ON and OFF light responses in retinas with photoreceptor degeneration. *J Neurosci.* (2009) 29:9186–96. doi: 10.1523/JNEUROSCI.0184-09.2009

55. Tomita H, Sugano E, Yawo H, Ishizuka T, Isago H, Narikawa S, et al. Restoration of visual response in aged dystrophic RCS rats using AAV-mediated channelopsin-2 gene transfer. *Invest Ophthalmol Vis Sci.* (2007) 48:3821–6. doi: 10.1167/iovs.06-1501

56. Tomita H, Sugano E, Isago H, Hiroi T, Wang Z, Ohta E, et al. Channelrhodopsin-2 gene transduced into retinal ganglion cells restores functional vision in genetically blind rats. *Exp Eye Res.* (2010) 90:429–36. doi: 10.1016/j.exer.2009.12.006

57. Greenberg KP, Pham A, Werblin FS. Differential targeting of optical neuromodulators to ganglion cell soma and dendrites allows dynamic control of center-surround antagonism. *Neuron.* (2011) 69:713–20. doi: 10.1016/j.neuron.2011.01.024

58. Regland B, McCaddon A. Alzheimer's Amyloidopathy: An Alternative Aspect. *J Alzheimers Dis.* (2019) 68:483–8. doi: 10.3233/JAD-181007

59. Lim CH, Kaur P, Teo E, Lam VY, Zhu F, Kibat C, et al. Application of optogenetic Amyloid-β distinguishes between metabolic and physical damages in neurodegeneration. *Elife.* (2020) 9:sa2. doi: 10.7554/eLife.52589.sa2

60. Kaur P, Kibat C, Teo E, Gruber J, Mathuru A, Tolwinski NS. Use of optogenetic amyloid-β to monitor protein aggregation in drosophila melanogaster, danio rerio and caenorhabditis elegans. *Bio Protoc.* (2020) 10:e3856. doi: 10.21769/BioProtoc.3856

61. Goshen I, Brodsky M, Prakash R, Wallace J, Gradinaru V, Ramakrishnan C, et al. Dynamics of retrieval strategies for remote memories. *Cell.* (2011) 147:678–89. doi: 10.1016/j.cell.2011.09.033

62. Lovett-Barron M, Kaifosh P, Kheirbek MA, Danielson N, Zaremba JD, Reardon TR, et al. Dendritic inhibition in the hippocampus supports fear learning. *Science.* (2014) 343:857–63. doi: 10.1126/science.1247485

63. Sohal VS, Zhang F, Yizhar O, Deisseroth K. Parvalbumin neurons and gamma rhythms enhance cortical circuit performance. *Nature.* (2009) 459:698–702. doi: 10.1038/nature07991

64. Cardin JA, Carlén M, Meletis K, Knoblich U, Zhang F, Deisseroth K, et al. Driving fast-spiking cells induces gamma rhythm and controls sensory responses. *Nature.* (2009) 459:663–7. doi: 10.1038/nature08002

65. Stuber GD, Sparta DR, Stamatakis AM, van Leeuwen WA, Hardjoprajitno JE, Cho S, et al. Excitatory transmission from the amygdala to nucleus accumbens facilitates reward seeking. *Nature.* (2011). 475:377–80. doi: 10.1038/nature10194

66. Spellman T, Rigotti M, Ahmari SE, Fusi S, Gogos JA, Gordon JA. Hippocampal-prefrontal input supports spatial encoding in working memory. *Nature.* (2015) 522:309–14. doi: 10.1038/nature14445

67. Padilla-Coreano N, Bolkan SS, Pierce GM, Blackman DR, Hardin WD, Garcia-Garcia AL, et al. Direct ventral hippocampal-prefrontal input is required for anxiety-related neural activity and behavior. *Neuron.* (2016) 89:857–66. doi: 10.1016/j.neuron.2016.01.011

68. Kim SY, Adhikari A, Lee SY, Marshel JH, Kim CK, Mallory CS, et al. Diverging neural pathways assemble a behavioural state from separable features in anxiety. *Nature.* (2013) 496:219–23. doi: 10.1038/nature12018

69. Gu L, Uhelski ML, Anand S, Romero-Ortega M, Kim YT, Fuchs PN, et al. Pain inhibition by optogenetic activation of specific anterior cingulate cortical neurons. *PLoS One.* (2015) 10:e0117746. doi: 10.1371/journal.pone.0117746

70. Daou I, Tuttle AH, Longo G, Wieskopf JS, Bonin RP, Ase AR, et al. Remote optogenetic activation and sensitization of pain pathways in freely moving mice. *J Neurosci.* (2013) 33:18631–40. doi: 10.1523/JNEUROSCI.2424-13.2013

71. Towne C, Pertin M, Beggah AT, Aebischer P, Decosterd I. Recombinant adeno-associated virus serotype 6 (rAAV2/6)-mediated gene transfer to nociceptive neurons through different routes of delivery. *Mol Pain.* (2009) 5:52. doi: 10.1186/1744-8069-5-52

72. Iyer SM, Vesuna S, Ramakrishnan C, Huynh K, Young S, Berndt A, et al. Optogenetic and chemogenetic strategies for sustained inhibition of pain. *Sci Rep.* (2016) 6:30570. doi: 10.1038/srep30570

73. Sun L, Liu R, Guo F, Wen MQ, Ma XL Li KY, et al. Parabrachial nucleus circuit governs neuropathic pain-like behavior. *Nat Commun.* (2020) 11:5974. doi: 10.1038/s41467-020-19767-w

74. Huang S, Zhang Z, Gambeta E, Xu SC, Thomas C, Godfrey N, et al. Dopamine inputs from the ventral tegmental area into the medial prefrontal cortex modulate neuropathic pain-associated behaviors in mice. *Cell Rep.* (2020) 31:107812. doi: 10.1016/j.celrep.2020.107812

75. Hua T, Chen B, Lu D, Sakurai K, Zhao S, Han BX, et al. General anesthetics activate a potent central pain-suppression circuit in the amygdala. *Nat Neurosci.* (2020) 23:854–68. doi: 10.1038/s41593-020-0632-8

76. Mazzitelli M, Yakhnitsa V, Neugebauer B, Neugebauer V. Optogenetic manipulations of CeA-CRF neurons modulate pain- and anxiety-like behaviors in neuropathic pain and control rats. *Neuropharmacology.* (2022) 210:109031. doi: 10.1016/j.neuropharm.2022.109031

77. Gadotti VM, Zhang Z, Huang J, Zamponi GW. Analgesic effects of optogenetic inhibition of basolateral amygdala inputs into the prefrontal cortex in nerve injured female mice. *Mol Brain.* (2019) 12:105. doi: 10.1186/s13041-019-0529-1

78. Xiong W, Ping X, Ripsch MS, Chavez GS, Hannon HE, Jiang K, et al. Enhancing excitatory activity of somatosensory cortex alleviates neuropathic pain through regulating homeostatic plasticity. *Sci Rep.* (2017) 7:12743. doi: 10.1038/s41598-017-12972-6

79. Chen T, Taniguchi W, Chen QY, Tozaki-Saitoh H, Song Q, Liu RH, et al. Top-down descending facilitation of spinal sensory excitatory transmission from the anterior cingulate cortex. *Nat Commun.* (2018) 9:1886. doi: 10.1038/s41467-018-04309-2

80. Elina KC, Islam J, Kim S, Kim HK, Park YS. Pain relief in a trigeminal neuralgia model via optogenetic inhibition on trigeminal ganglion itself with flexible optic fiber cannula. *Front Cell Neurosci.* (2022) 16:880369. doi: 10.3389/fncel.2022.880369

81. Wei X, Centeno MV, Ren W, Borruto AM, Procissi D, Xu T, et al. Activation of the dorsal, but not the ventral, hippocampus relieves neuropathic pain in rodents. *Pain.* (2021) 162:2865–80. doi: 10.1097/j.pain.0000000000002279

82. Elina KC, Moon HC, Islam J, Kim HK, Park YS. The effect of optogenetic inhibition of the anterior cingulate cortex in neuropathic pain following sciatic nerve injury. *J Mol Neurosci.* (2021) 71:638–50. doi: 10.1007/s12031-020-01685-7

83. Zhuang X, Huang L, Gu Y, Wang L, Zhang R, Zhang M, et al. The anterior cingulate cortex projection to the dorsomedial striatum modulates hyperalgesia in a chronic constriction injury mouse model. *Arch Med Sci.* (2021) 17:1388–99. doi: 10.5114/aoms.2019.85202

84. Liu K, Wang L. Optogenetics: therapeutic spark in neuropathic pain. *Bosn J Basic Med Sci.* (2019) 19:321–7. doi: 10.17305/bjbms.2019.4114

85. Czapiński J, Kiełbus M, Kałafut J, Kos M, Stepulak A, Rivero-Müller A. How to train a cell-cutting-edge molecular tools. *Front Chem.* (2017) 5:12. doi: 10.3389/fchem.2017.00012

86. Manteniotis S, Lehmann R, Flegel C, Vogel F, Hofreuter A, Schreiner BS, et al. Comprehensive RNA-Seq expression analysis of sensory ganglia with a focus on ion channels and GPCRs in Trigeminal ganglia. *PLoS ONE.* (2013) 8:e79523. doi: 10.1371/journal.pone.0079523

87. Dawes JM, Antunes-Martins A, Perkins JR, Paterson KJ, Sisignano M, Schmid R, et al. Genome-wide transcriptional profiling of skin and dorsal root ganglia after ultraviolet-B-induced inflammation. *PLoS ONE.* (2014) 9:e93338. doi: 10.1371/journal.pone.0093338

88. Perkins JR, Antunes-Martins A, Calvo M, Grist J, Rust W, Schmid R, et al. A comparison of RNA-seq and exon arrays for whole genome transcription profiling of the L5 spinal nerve transection model of neuropathic pain in the rat. *Mol Pain.* (2014) 10:7. doi: 10.1186/1744-8069-10-7

89. Zhang Z, Zamponi GW. Protocol for detecting plastic changes in defined neuronal populations in neuropathic mice. *STAR Protoc.* (2021) 2:100698. doi: 10.1016/j.xpro.2021.100698

Frontiers in Neurology

Explores neurological illness to improve patient care

The third most-cited clinical neurology journal explores the diagnosis, causes, treatment, and public health aspects of neurological illnesses. Its ultimate aim is to inform improvements in patient care.

Discover the latest Research Topics

See more →

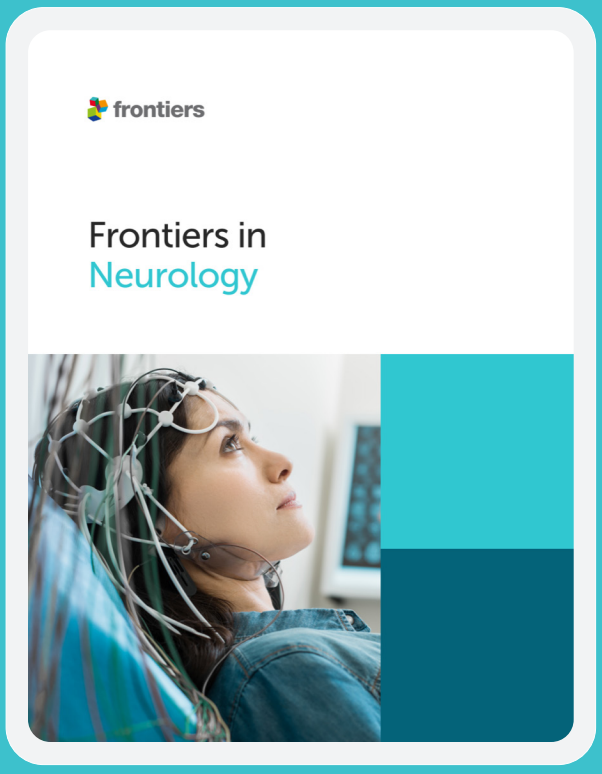

Frontiers

Avenue du Tribunal-Fédéral 34
1005 Lausanne, Switzerland
frontiersin.org

Contact us

+41 (0)21 510 17 00
frontiersin.org/about/contact